ABSTRACT

Title of Dissertation: DEVELOPMENT OF A COMPACT HEAT EXCHANGER WITH BIFURCATED BARE TUBES

Zhiwei Huang, Doctor of Philosophy, 2017

Dissertation directed by: Reinhard Radermacher, Professor
Department of Mechanical Engineering

Heat transfer enhancement of air-to-fluid heat exchangers by novel surface or geometry design and optimization is a major research topic. The traditional way of reducing airside thermal resistance is to extend airside heat transfer area by adding fins and the conventional method of reducing fluid side thermal resistance is to use enhanced inner surfaces. These approaches have limitations in further reducing the thermal resistance.

Small diameter (4 and 5 mm) fin-and-tube heat exchangers, louvered fin mini-channel heat exchangers (MCHX), newly studied round bare tube heat exchangers (BTHX) and shape optimized bare tube heat exchangers (sBTHX) with diameter of 0.8~1.0 mm were experimentally investigated using air and water to gain the fundamental understanding of heat transfer and the current technology limitations. Correlations of air-side heat transfer coefficient and pressure drop were then developed for BTHX and sBTHX.

To improve current technologies, a novel bifurcated bare tube heat exchanger (referred as bBTHX, hereafter) was proposed in this study. It was numerically investigated and optimized using Parameterized Parallel Computational Fluid Dynamics (PPCFD) and Approximation Assisted Optimization (AAO) techniques. The most unique feature of bBTHX is the addition of bifurcation, which enhances airside heat transfer by creating 3D flow and waterside heat transfer by boundary layer interruption and redevelopment. The airside and waterside pressure drop can also be reduced by proper design and optimization, resulting in smaller fan and pumping power. Compared to MCHX with similar capacity and frontal area, the optimal bBTHX design has 38% lower total power and 83% smaller volume and 87% smaller material volume. Compared to BTHX with similar capacity and frontal area, the optimal design has 28% lower total power and 11% smaller volume and 10% smaller material volume.

The bBTHX design can be widely applied in industry such as automotive radiators, oil coolers, condenser and evaporator. Two applications of this heat exchanger were discussed in detail: car radiator and indoor coil for Hybrid Variable Refrigerant Flow (HVRF) system. The bBTHX car radiator has 30% lower pumping power, 68% smaller heat exchanger volume and 67% less water weight than those of baseline. Moreover, refrigerant charge of HVRF systems with bBTHX is reduced by 40~70%.

DEVELOPMENT OF A COMPACT HEAT EXCHANGER WITH
BIFURCATED BARE TUBES

by

ZHIWEI HUANG

Dissertation submitted to the Faculty of the Graduate School of the
University of Maryland, College Park, in partial fulfillment
of the requirements for the degree of
Doctor of Philosophy
2017

Advisory Committee:
  Professor Reinhard Radermacher, Chair
  Professor Peter B. Sunderland (Dean's Representative)
  Research Professor Yunho Hwang
  Professor Marino diMarzo
  Professor Bao Yang
  Professor Gary A. Pertmer
  Associate Research Scientist Vikrant Aute

Dedication

To everyone who believed in me:
My family, mentors and friends

Acknowledgements

The work presented in this dissertation was carried out during the years of 2013 to 2017 at the Center for Environmental Energy Engineering (CEEE), University of Maryland. I owe my deepest gratitude to my supervisor Professor Reinhard Radermacher. I feel extremely lucky to be given the opportunity to work with my mentor. This work could hardly have been completed without his support, guidance and continuous encouragement. I would also like to express my warmest gratitude to my dissertation committee members, Dr. Peter B. Sunderland, Dr. Yunho Hwang, Dr. Marino diMarzo, Dr. Bao Yang, Dr. Gary A. Pertmer and Dr. Vikrant Aute for their efforts, advice and time.

I am deeply grateful to my advisor, Dr. Yunho Hwang. His enthusiasm, optimism, support and detailed guidance led me through the darkest days in my research. My sincere appreciation also goes to Dr. Vikrant Aute for supporting and guiding me using his programming, mathematical and optimization expertise. I would like to extend my gratitude to Mr. Jan Muehlbauer for training me in the lab, helping me with my experimental testing and inspiring me with his unlimited wonderful ideas. I also owe a great debt of gratitude to Dr. Jiazhen Ling for instructing and influencing me in both research and life.

It is a magnificent pleasure to acknowledge my sincere thanks to every colleague in CEEE, especially Dr. Daniel Baceller, James Tancabel, Lei Gao and Zhenning Li who have been working with me on the project and related publications. These great minds provided an intellectual atmosphere and an enjoyable work

Table of Contents

List of Tables

List of Figures

Nomenclature

A	area (m^2)
A_f	minimum free flow area (m^2)
A_f	surface area of fin (m^2)
A_0	total air side heat transfer area (m^2)
$A_{p,i}$	inside surface area of tubes (m^2)
$A_{p,o}$	outside surface area of tubes (m2)
b_p'	slope of a straight line between the outside and inside tube wall temperature (J/kgK)
b_r'	slope of the air saturation curved at the mean coolant temperature and the inside wall temperature (J/kgK)
$b_{w,m}'$	slope of the air saturation curve at the water film temperature of the fin surface (J/kgK)
$b_{w,p}'$	slope of the air saturation curve at the water film temperature of the tube wall surface (J/kgK)
C_0, C_1	constant
C_p	specific heat capacity at constant pressure (J/kgK)
D_c	tube outside diameter (include collar) (m)
D_i	tube inside diameter (m)
EB	energy balance (%)
EES	Engineering Equation Solver
f	friction factor
f_i	in-tube friction factors of water
F	log mean temperature difference correction factor
G	mass flux (kg/m^{2}s)
G_{max}	maximum mass velocity based on minimum flow area (kg·m^2)
h	convective heat transfer coefficient (W/m^{2}K)
$h_{c,o}$	sensible capacity transfer coefficient (W/m^{2}K)
$h_{d,o}$	mass transfer coefficient (W/m^{2}K)
h_i	inside heat transfer coefficient (W/m^{2}K)
$h_{o,w}$	total heat transfer coefficient for wet external fin (W/m^{2}K)
HVAC&R	heating, ventilation, air-conditioning and refrigeration
I_0	modified Bessel function solution of the first kind, order 0
I_1	modified Bessel function solution of the first kind, order 1
i	enthalpy (kJ/kg)
i_a	air enthalpy (kJ/kg)
$i_{a,in}$	inlet air enthalpy (kJ/kg)
$i_{a,m}$	mean air enthalpy (kJ/kg)
$i_{a,out}$	outlet air enthalpy (kJ/kg)
i_g	saturated water vapor enthalpy (kJ/kg)
i_m	mean enthalpy (kJ/kg)
$i_{r,in}$	saturated air enthalpy at the inlet water temperature (kJ/kg)
$i_{r,m}$	mean saturated air enthalpy at the mean water temperature (kJ/kg)
$i_{r,out}$	saturated air enthalpy at the outlet water temperature (kJ/kg)
$i_{s,fm}$	saturated air enthalpy at the fin mean temperature (kJ/kg)

$i_{s,fb}$	saturated air enthalpy at the fin base temperature (kJ/kg)
$i_{s,p,i,m}$	mean saturated air enthalpy at the mean inside tube wall temperature (kJ/kg)
$i_{s,p,o,m}$	mean saturated air enthalpy at the mean outside tube wall temperature (kJ/kg)
$i_{s,w}$	saturated air enthalpy at the water film temperature (kJ/kg)
$i_{s,w,m}$	mean saturated air enthalpy at the mean water film temperature of the fin surface (kJ/kg)
j_h	Chilton-Coburn j-factor of the heat transfer
j_m	Chilton-Coburn j-factor of the mass transfer
K_0	modified Bessel function solution of the second kind, order 0
K_1	modified Bessel function solution of the second kind, order 1
k	thermal conductivity (W/mK)
k_f	thermal conductivity of fin (W/mK)
k_i	thermal conductivity of water (W/mK)
k_p	thermal conductivity of tube (W/mK)
k_w	thermal conductivity of water film (W/mK)
L_p	tube length (m)
Le	Lewis number
$\dot{m}$	mass flow rate (g/s)
NTU	number of transfer unit
Nu	Nusselt number
OD	outer diameter (m)
P	pressure (Pa)
ΔP	pressure difference (Pa)
P_l	longitudinal tube pitch (m)
Pr	Prandtl number
P_t	transverse tube pitch (m)
$\dot{Q}$	heat transfer rate (W)
Re	Reynolds number
Re_{Di}	Reynolds number based on inside diameter
R_{eq}	equivalent radius for circular fin
R_{ov}	overall thermal resistance (K/W)
r	tube inside radius (m)
r_i	distance from the center of the tube to the fin base (m)
r_o	distance from the center of the tube to the fin tip (m)
Sc	Schmidt number
T	temperature (K)
$T_{w,m}$	mean temperature of the water film (K)
$T_{p,i,m}$	mean temperature of the inner tube wall (K)
$T_{p,o,m}$	mean temperature of the outer tube wall (K)
$T_{r,m}$	mean temperature of water (K)
ΔT	temperature difference (K)
ΔT_{lm}	log mean temperature difference for counter-flow (K)
t	Fin thickness (m)
U	overall heat transfer coefficient (W/m^{2}K)
$U_{o,w}$	wet surface heat transfer coefficient, based on enthalpy difference (kg/m^{2}s)
VFR	volume flow rate (m^3/s)
W_a	humidity ratio of moist air (kg/kg)

$W_{a,m}$	mean air humidity ratio (kg/kg)
$W_{s,p,o,m}$	mean saturated air humidity ratio at the mean outside tube wall temperature (kg/kg)
$W_{s,w}$	saturated air humidity ratio at the water film temperature (kg/kg)
$W_{s,w,m}$	mean saturated air humidity ratio at the mean water film temperature of the fin surface (kg/kg)
X_L	geometric parameter (m)
X_M	geometric parameter (m)
y_w	Thickness of condensate water film (m)

Greek symbols

ρ	density (kg/m^3)
ε	fin factor
σ	contraction ratio
η_0	surface effectiveness
η	fin efficiency
δ_f	fin thickness
μ	dynamic viscosity (Ns/m^2)

Subscripts

a	air side
i	inlet
m	mean
n	exponent
o	outlet
tw	tube wall
w	wet
fr	frontal
r	refrigerant

Chapter 1: Motivations

1.1. _Motivations_

Air-to-fluid Heat eXchanger (HX) is widely used in industry as automotive radiator, oil cooler, water and glycol cooler, condenser, evaporator and indoor coil for chiller system. The heat exchange efficiency of the heat exchanger has a considerable influence on total energy usage.

As the economy develops and population grows, the demand for energy, material, space and other resources increases dramatically, calling for better energy, material and space usage. Compact heat exchanger that has less material, less envelope volume than traditional heat exchanger is the next generation heat exchanger.

The work presented here is motivated by the need of innovative designs and advanced geometries to improve heat exchanger performance. Heat transfer enhancement has been studied for decades and the traditional way to maximize the overall HX conductance (hA) is to increase surface area by employing extended surfaces, for instance fins, to airside to reduce airside thermal resistance because it accounts for 75~90% of total thermal resistance. However, fin surfaces have lower heat transfer coefficients compared with primary heat transfer surfaces (tube surface) because of the boundary layer development. Moreover, additional fins inevitably result in more material consumption. Thus, conventional fin-and-tube heat exchanger designs have intrinsic limitation of further improving heat transfer performance giving certain amount of volume and material volume.

1.2. *Literature Review*

1.2.1. Airside heat transfer enhancement

Air-to-fluid heat exchangers in applications are mainly fin-and-tube heat exchangers, including round tube heat exchangers, flat tube heat exchangers and microchannel heat exchangers. A large amount of literature can be found in enhancing heat transfer of these conventional designs. Over 9500 literatures on Heat Transfer Enhancement (HTE) are published per Webb and Kim (2005). Webb and Kim (2005) categorized the heat transfer enhancement techniques into passive methods and active methods, as shown in Table 1. Compound enhancement and combinations of two or more passive and/or active techniques are also found. Passive techniques are the most sought (70.9%) with emphasis on extended surfaces (Manglik and Bergles, 2004).

The ultimate objective of enhancing heat exchanger performance is to increase the total UA value, which can result in: (a) size reduction usually reflecting cost and weight reduction, (b) increase in heat duty, (c) LMTD reduction leading to better thermodynamic efficiency or (d) pumping power reduction which can be translated into the operating cost reduction. UA can be increased by increasing U, A or both. Since air thermal resistance accounts for 75%~95% of the overall HX thermal resistance, efforts to improve air-to-fluid heat exchanger performance mainly focus on air side.

Table 1 Classification of Various HTE Techniques
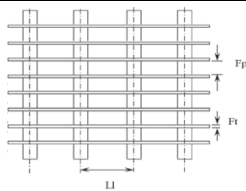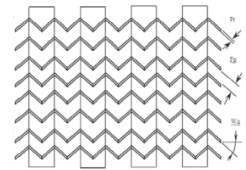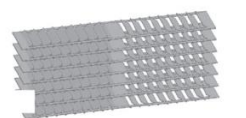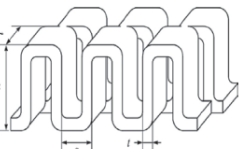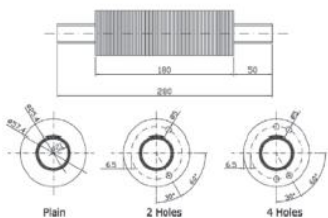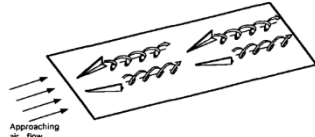
Passive Techniques	Active Techniques
Surface coating	Mechanical aids
Rough surfaces	Surface vibration
Extended surfaces	Fluid vibration
Displaced inserts	Electrostatic fields
Swirl Flow	Injection
Coiled tubes	Suction
Surface tension	Jet impingement
Additives for liquids	
Additives for gases	

Round tube-and-fin heat exchangers (RTHX) with various configurations were proposed and studied in the past decades. RTHX has become a universally used air-to-fluid heat exchanger type. Such heat exchanger consists of mechanically or hydraulically expanded equally spaced parallel tube bundles in staggered or in-lined pattern with continuous various configured fins on the outside of the tube array to improve heat transfer coefficient on airside. Usually liquid heat transfer medium such as water, oil, or refrigerant is forced to flow through the tube bundles while gas heat transfer medium, such as air, flows across the tubes through the fins. Different fins types have been studied comprehensively including plain fins, wavy fins or corrugated fins, louvered fins, offset strip fins, and perforated fins. The shapes of tubes are mostly round or oval. The fundamental characteristics of different fin types are summarized in a recent review paper (Bhuiyan and Islam, 2016) by numerically comparing heat transfer and pressure drop performance of different fin-and-tube heat exchangers under different conditions. Two basic concepts are extensively used for such extended surfaces: (i) special channel shapes, such as wavy channels, which provide mixing due to the boundary layer separation within the channel; (ii) repeated growth and wake destruction of boundary layers, such as offset strip fin, louvered fin and perforated fin (Bhuiyan and Islam, 2016). Another method to enhance heat transfer is vortex generator which not

only interrupts the development of thermal boundary layer but also generates longitudinal vertices and causes flow destabilization and it can be combined with all previous enhanced fin types. Jacobi and Shah (1995) reviewed the vortex generators in detail. Fundamentally heat transfer enhancement comes with pressure drop penalty. These different surfaces discussed above are summarized in Table 2.

Flat tube or mini- and micro- channel heat exchangers (MCHX) are standard heat exchangers for automobile radiators. They are also widely applied as air conditioning evaporators and condensers for residential, industrial and automotive use. Typical flat tube heat exchangers and microchannel heat exchangers are usually designed with multi-louvered fins of which the heat transfer enhancement mechanism was explained previously. The flat tube shape is also beneficial compared with RTHX regarding airside pressure drop. A typical MCHX comprises of a flat tube with multiple small sized ports. The advantage of MCHX over round fin-and-tube heat exchanger and flat tube heat exchanger is on the liquid side. By reducing the tube size, a factor of 10 in the heat dissipation of integrated chips using a microchannel heat exchanger was reported by Tuckerman and Pease (1981). Smaller liquid flow passages lead to higher surface area to volume ratio, higher thermal transport, smaller envelope volume, smaller overall refrigerant charge and higher system efficiency. Specially, the usage of headers simplifies the refrigerant circuitry and reduces the total flow path, resulting in reduced pressure drop.

Table 2 Fin types and HTE mechanism

Fin type	Picture	HTE mechanism
Plain fin-and-tube HX (Kays and London, 1984)		• Extended heat transfer area
Wavy fin-and-tube HX (Kays and London, 1984)		• Extended heat transfer area • Lengthened flow path • Improved airflow mixing • Boundary layer interruption and redevelopment at corrugations
Corrugated louvered fin-and-tube HX (Bhuiyan and Islam, 2016)		• Extended heat transfer area • Boundary layer is interruption and redevelopment at louvers • Improved flow mixing
Offset strip fin-and-tube HX (Bhuiyan and Islam, 2016)		• Extended heat transfer area • Boundary layer interruption and redevelopment at strips • Improved flow mixing
Perforated fin-and-tube HX (Bhuiyan and Islam, 2016)		• Boundary layer dissipation in the wake region formed by holes • Improved flow mixing
Vortex generator (Jacobi and Shah, 1995)		• Boundary layer interruption and redevelopment • Generate longitudinal vortices • Cause flow destabilization

Recently, small diameter (<5 mm) finless heat exchangers have been proposed and investigated. Bacellar (2014) numerically investigated bare tube heat exchangers and plain fin-and-tube heat exchangers with diameter of 2 ~ 5 mm and developed correlations based on CFD simulation results. Paitoonsurikarn et al. (2000) numerically found that bare tube heat exchanger can achieve a much larger air-side heat transfer coefficient (300 W/m^{2}K) with the air velocity range of 1 ~ 6 m/s by reducing tube diameter to 0.3 ~ 0.5 mm. Thus, finless designs using bare tubes with hydraulic diameter less than 1 mm can exceed the air-side heat transfer performance of conventional heat exchangers.

5

1.2.2. Heat transfer and friction characteristics of water flow in macro and micro-tubes (<4 mm)

In current study, water is used as the in-tube side fluid and single-phase heat transfer and friction characteristics are analyzed. As it is the first time to investigate the performance of the novel geometry, the single-phase characteristics are needed as 'building block' (Brognaux et al., 1997) for the development of the needed two-phase heat transfer mechanisms and correlations. So here the heat transfer enhancement approaches for in-tube side of bare tube are briefly summarized and the heat transfer and friction characteristics of water flow in macro and micro-tubes are analyzed. .

Although the airside heat transfer enhancement is significant, tube side heat transfer performance enhancement is also a major topic. Similar to the airside, there are also passive and active heat transfer enhancement methods. Passive heat transfer enhancement methods include enhanced inner surfaces (micro-fin tubes, inner grooved tubes) and inserts (coils, twisted tape). Enhanced inner surfaces are commonly used in air-cooled compact heat exchanger designs because they can produce enhanced tube side heat transfer coefficient with a small pressure drop penalty. Enhanced surfaces promote turbulence and reduce the thickness of the boundary layer, leading to higher local heat transfer coefficient.

Brognaux et al. (1997) investigated heat transfer and friction characteristics for single-phase flow in single-grooved and cross grooved micro-fin tubes with outer diameter of 15.987 mm. It was found that micro-fin tubes had enhanced heat transfer coefficient as high as 1.8 times that of smooth tubes. There is also research on two-phase flow in micro-fin tube with even smaller diameter (4~7 mm) (Hu et al., 2008, Mancin et al., 2016).

6

However, in current study, the diameter range is below 4 mm. As far as the author knows, there is no available microgroove or micro-fin tubes within this diameter range, especially for diameter that is less than 1 mm. Thus, one main task of current research is to find a way to enhance heat transfer in macro and micro tubes (Kandlikar, 2002).

Conventional forced convection heat transfer and friction correlations which were derived from tubes with diameter much larger than micro-tubes were examined by many researchers. Here is a summary:

Friction factors

Yang et al. (2003) measured the friction factors of water flow in tubes with diameter ranging from 0.5 to 4 mm. They found that there is no significant discrepancy for water flow in small diameter tubes compared with large diameter tubes. Yang and Lin (2007) also found that for tubes diameter ranging from 100 to 1100 μm, the test results agree very well with the conventional Poiseuille ($f = 16/Re_d$) and Blasius ($f = 0.079Re_d^{-0.25}$) equations in laminar and turbulent regime, respectively. Comparable results were reported by Lelea et al. (2004) for diameter range of 0.1~0.5 mm, Li et al. (2003) for dimeter of 79.9 to 205.3 μm and Celata et al. (2002) for diameter of 130 μm. So, the conventional theories are applicable for flow in the size range of current study (0.5~4 mm). This is the theoretical basis of baseline bare tube heat exchanger CFD simulation results verification for pressure drop.

Fully developed heat transfer

Yu et al. (3) found the Nusselt numbers for water cooling in turbulent regime were considerably larger than those would be predicted for larger tubes, suggesting the Reynolds analogy does not apply for micro tube flow. Yen et al, (9) measured heat transfer performance of

laminar refrigerant R-123 in 0.3 mm diameter tube and found the results were in reasonable agreement with the analytical laminar constant heat flux value (Nu=4.36). However, in these experiments, the temperature was measured by direct attaching K-type thermocouple on the tube wall. Yang and Lin (2007) pointed out that the measurement accuracy of micro-tube wall temperature is significant because the diameter of the sensors for measuring micro-tube surface temperature is comparable to the size of the micro-tube itself. This may result in inaccurate temperature measurement because of sensor wire thermal shunt. A non-contacted liquid crystal thermography (LCT) method was proposed to measure the surface temperature of micro-tubes to avoid the thermal shunt and thermocouple contact problems. Samples with diameter of 123 to 962 μm were tested. They found the conventional heat transfer correlations for laminar and turbulent flow can be well applied for predicting the fully developed heat transfer performance in micro-tubes. The transition occurs at Reynolds number from 2300 to 3000, which is the same range as that for conventional tubes. Correlations examined for turbulent flow include Dittus and Boelter (1930) correlation, Petukhov and Popov (1963) correlation and Gnielinski (1976) correlation. Thus, we can conclude there is no significant size effect for water flow in tubes within the diameter range in current study (0.5~4 mm). This serves as the theoretical basis of baseline bare tube heat exchanger CFD simulation results verification for heat transfer.

1.2.3. Nature inspired heat exchangers

Nature has inspired many scientists and engineers to solve problems through observation and mimicry. One such example is heat transfer enhancement. The enormous natural heat and mass transfer phenomena have led engineers to seek solutions to heat transfer enhancement problems from nature. Fractal geometries are found in respiratory and vascular systems of plants and animals, such as blood vessels, human lungs, leaves, coastlines, etc. Inspired by this, fractal heat exchangers

8

have been developed and are found to have intrinsic advantage of minimized flow resistance and strong heat transfer capability.

Significant amount of research has been conducted on the theory of fractals (Murray, 1926; Sherman, 1981; Mandelbrot, 1982; West, 1997; Bejan et al., 2008; Bejan and Lorente, 2006, 2007, 2011; Bejan, 1997, 2002, 2003; Xu and Yu, 2006), and the main findings are summarized in Table 3.

Table 3 Fractal theory development

Researchers	Major findings
Murray, 1926	Developed Murray's law: The cube of the radius of a parent branch equals the sum of the cubes of the radii of daughter branches.
Sherman, 1981	Found when Murray's law was obeyed a functional relationship exists between channel diameters and various flow characteristics such as wall shear stress, velocity profile, and pressure gradient.
Mandelbrot, 1982	Described fractal structure from nature: coastlines, leaves and clouds.
West, 1997	Developed scaling laws for a bulk fluid transport problem to minimize the flow work.
Bejan et al., 2008; Bejan and Lorente, 2006, 2007, 2011; Bejan, 1997, 2002, 2003	Developed Constructal Theory: For a finite-size flow system to persist in time (to survive) its configuration must evolve in such a way that it provides an easier access to the currents that flow through it.
Xu and Yu, 2006	Analyzed the transport properties including electrical conductivity, heat conduction, convective heat transfer, laminar flow, and turbulent flow in the networks and derived the scaling exponents of the transport properties in the networks.

For application, the fractal channels (FC) are mainly used for electronic cooling. Thus, most research focuses on comparing its performance with traditional serpentine channel (SC) and parallel channel (PC). The major findings are summarized in Table 4. Even though there are various application of fractal channels, including heat sink (as shown in Table 2), fuel cell (Senn and Poulikakos, 2004), microreactor (Chen et al., 2011; Chen et al., 2015) distributor (Tondeur and Luo, 2004; Luo et al. 2007; Guo et al., 2014), collector (Guo et al., 2014), tube and shell heat exchanger (Guo et al., 2014), spindle (Xia et al., 2015), Si/Ge nanocomposite (Chen et al., 2015), etc. However, most of the research focus on heat sink for electronic cooling due to the inherent advantage of temperature uniformity of fractal structure. For fluid types, research cover liquid-to-liquid (Tondeur and Luo, 2004; Luo et al., 2007; Guo et al., 2014), solid-to-liquid (as shown in Table 2), solid-to-two phase (Daniels et al. 2011; Daniels et al., 2007; Zhang et al., 2011), solid-to-gas (Chen et al., 2014; Chen et al., 2011; Chen et al., 2015), and solid-to-solid (Chen et al.,

2015) heat exchangers; however, no research has been done to liquid-to-gas heat exchangers, which is a research gap and should be investigated.

Table 4 Summary of major findings in research on fractal heat sinks

Ref.	Major findings
Pence, 2002	Compared with parallel channels (PC) with equal surface area, fractal channels (FC) has: 1. 60% lower pressure drop for the same total flow rate and 30°C lower wall temperature under identical pumping power condition. 2. 50% lower density with similar maximum wall temperature and pressure drop.
Chen and Cheng, 2002	Compared with PC with equal surface area, FC has: 1. Higher total heat transfer rate; 2. Lower total pressure drop; 3. Larger fractal dimension or a larger total number of branch levels will result in a stronger heat transfer capability with a smaller pumping power.
Senn and Poulikakos, 2004	1. Compared with SC with same heat transfer area and same rectangular area, FC has larger heat transfer capability and 50% lower pressure drop; 2. Pressure drop from bifurcation is substantial and not negligible; 3. Lower pressure results from the not fully developed flow in higher branch level; 4. Secondary flow motions initiates at bifurcations; 5. Transverse vortices create recirculation at bifurcations that result in hot spots at the inner corners of bifurcations; 6. Longitudinal vortices result in enhanced thermal mixing and a decrease in the required flow rate for heat transfer; 7. Laminar mixing by secondary flow motions improves local Nusselt number.
Alharbi et al., 2003	Compared with Pence's 1-D model, the 3D model: 1. Predicts a 20% lower total pressure drop for fractal channels but similar for straight one, this is due to pressure recovery at bifurcations that results from an increase in flow area; 2. Predicts pressure drop 17% higher for SC when using temperature dependent properties, but similar for FC; 3. Has the reinitiating assumption, which seems to provide plausible trends in pressure distribution.
Alharbi et al., 2004	1. FC has 75% lower temperature variation and a 10% pressure-drop penalty compared with the PC; 2. The assumption of constant properties is not suitable for high heat flux condition.
Enfield et al., 2004	1. Developed a 2D model for predicting concentration profiles and degree of mixing (DoM); 2. Developed a non-dimension number and a design guideline to determine the optimal number of branch levels to minimize pressure drop and maximize DoM for a fixed initial parent channel width, total path length, and channel depth.
Wang et al., 2006	Compare FC with PC and SC, FC has: 1. The best temperature uniformity; 2. Lower pressure drop than SC but higher pressure drop than PC; 3. Reduced risk of accidental blockage of channel segments; 4. Reduced potential of thermal damage due to the reduced risk of blockage; 5. Increased number of parent channels and branch levels resulted in increased temperature uniformity.
Wang et al., 2007	1. Pressure drop increases as bifurcation angle increases with a decreasing increasing rate and 30° is the optimal angle; 2. Channels with bifurcation angle of 180°+180° has a lower pressure drop compared with PC due to pressure recovery at bifurcation; 3. Increasing angle also increases the risk of appearance of hotspot near the bifurcation; 4. More uniform distribution of the outlet mass flow can be achieved with increased bifurcation angles, but the gradient is reduced with increasing angles.
Hong et al., 2007	1. A modified structure was proposed to address the hotspot issue (by adding serpentine channel structure at the end of highest branches); 2. Hotspot appears at the highest branch (4th) due to assumption of conjugate heat transfer; 3. Effect of bifurcation on pressure drop becomes more obvious for higher flow rate, resulting in a non-linear relationship between pressure drop and mass flow rate, unlike the linear one for PC; 4. The modified FC is much better than that of PC with respect to pressure drop, thermal resistance and temperature uniformity; and this advantage is much more obvious when the flow rate or the pressure drop is low, which is favored because high pressure drop is not recommended in practice for the design of microsystems.
Chen et al., 2010	1. FC has considerable advantages over SC in both heat transfer and pressure drop; 2. FC has inherent advantage of uniform temperature on the heating surface than SC. 3. The local pressure loss due to confluence flow is found to be larger than that due to difluence flow.
Wang et al., 2010	1. Leaf-like flow networks has lower pressure drop and higher heat transfer coefficient than symmetric tree-like ones.
Yu et al., 2012	1. FC has a much higher heat transfer coefficient at the cost of a much higher pump power compared with PC with the same heat transfer area. 2. AR (aspect ratio=height/width) of microchannel plays a very important role when considering pressure loss, heat transfer coefficient, and COP; 3. FC with lowest AR has highest COP, but the one with highest AR has the highest ratio of COP over COP of PC.
Zhang et al., 2013	1. Small aspect ratio is preferred for a smaller pressure drop and a larger heat transfer rate; 2. A high branch level produced a high pressure drop and a large heat transfer rate; 2. The bends with fillets for the fractal-like microchannel reduce the local minor pressure losses, compared with that with the 90° bends, resulting in a lower overall pressure drop.

Zhang et al., 2015	1. Both the flow rate and the AR have large influences on the evolution of the vortices, which promote the fluid mixing and enhance the efficiency of heat transfer; 2. FC with a smaller AR of 0.333 was verified to have lower pressure drop and better heat transfer performance within all the other microchannel networks under investigation in the study; 3. Observed transverse and longitudinal vorticities, secondary flow and recirculation flow motions; 4. Confluence flow has a larger pressure drop than diffluent flow, but not much difference.

1.2.4. Numerical study of compact heat exchangers

The design and sizing of heat exchangers involve many complex procedures and calculations. The convective heat transfer coefficients between fluids and walls are key variables in the design procedure. Heat transfer coefficients are functions of flow velocity, fluid properties, internal tube geometry and dimension, external tube geometry and dimension. For simple geometries, heat transfer coefficients are available in literature for single-phase flow at laminar, turbulent or transitional conditions (Sunden, 2007). However, for complex heat exchanger geometries or novel heat exchangers, analytical solutions and correlations in literature are no longer applicable. As a numerical solution methodology of governing equations for mass conservation, momentum, heat transfer and other transport process, Computational fluid dynamics (CFD) or computational heat transfer (CHT) or numerical heat transfer (NHT) has become a powerful tool for HX design nowadays (Sunden, 2007). In Sunden's review, the CFD can be applied to HX simulation in two ways: (i) entire heat exchanger or (ii) unitary cell. In the first way, the entire heat exchanger or the heat transferring surface is modeled by using large scale or coarse computational meshes or by applying a local averaging or porous medium approach. However, when applying this method, several assumptions including physical properties and characteristics should be known beforehand which is not practical for prediction. The advantage is the computational cost is relatively low. Another way is to identify modules or group of modules that repeat themselves in a periodic or cyclic manner in the main flow direction. This method enables accurate calculations by including more details in the model. Patankar et al. (1980) first introduced

stream wise periodic flow and heat transfer which becomes a common method for HX research, especially for prediction of novel surfaces and complex geometry. The CFD model should be validated using experimental data to demonstrate the validity of the computation. Abdelaziz et al. (2010) reported uncertainty of ±10% in airside capacity against experimental data for a novel HX. Xiaoping et al. (2010) also reported ±10% uncertainty for airside heat transfer coefficient predication against experimental data for a louvered fin microchannel heat exchanger. In Chen et al. (2016)'s study of a printed circuit heat exchanger, the largest deviation for prediction of Nusselt number is found to be 6.5% and that for capacity is 6.14%. CFD has also been applied to investigate the airside flow maldistribution (Yaïci et al., 2016).

1.2.5. Heat exchanger design optimization

Design optimization involving CFD calculation is a major research topic, especially in novel heat exchanger design. To do optimization, the first step is to automate CFD calculation to make it easier to explore the design space. The reasons are, first although commercial software allows one to build model and mesh, it is hard to change the topology and second, the calculation time can be reduced by taking advantage of parallel calculation.

Hilbert et al. (2006) and Abdelaziz et al. (2009, 2010) both introduced such automated method and Abdelaziz named it Parallel Parameterized CFD (PPCFD). This PPCFD method relies on the commercial software Gambit (2017) for geometry and mesh generation and FLUENT® (2017) for solving the flow and energy equations. It has four steps:

- Generate profile for design variables and parameters
- Generate journal files for both Gambit and FLUENT®

- Execute Gambit and FLUENT® using the journal files to generate geometry, generate mesh and run simulation in FLUENT®

- Post process output data to obtain thermal-hydraulic performance

A batch file generated alongside executes these four steps. Depending upon the number of processors available, different cases can be run in parallel. It is reported that this automation technique saves more than 90% engineering time compared to conventional CFD modeling (Abdelaziz et al., 2010).

Even though the PPCFD technique can help reduce the computational time by automating the simulation procedure and using parallel computation, it may still result in huge computational cost when implementing this method into heat exchanger optimization problem. Therefore approximation-assisted optimization (AAO) has been applied for optimization using numerical simulations. Huang et al. (2015) summarized the optimization methods into five categories as shown in Table 5.

Table 5 Summary of HX optimization methods (adapted from Huang et al. 2015)

Methodology	Expertise	Relative Computational Cost
Exhaustive Search	Low	10,000,000
Random Search	Low	1,000,000
Parametric Analysis	Low	100,000
Gradient-Based Methods	Medium	10,000
Heuristic Methods (e.g. GA's, MOGA, etc.)	Medium	10,000
Approximation Assisted Optimization (offline)	High	100-1000
Approximation Assisted Optimization (online)	High	100

One key procedure in approximation assisted optimization (AAO) is metamodeling. Metamodels are statistical approximations that are used to replace the actual models with acceptable estimation errors to significantly reduce the computation amount. Metamodeling

involves three steps (Simpson et al., 2001): (a) choose an experimental design for generating data, (b) choose a model to represent the data, and then (c) fit the model to the observed data. There are several options for each of these steps, as shown in Figure 1. First, AAO requires an initial set of sample points in the design space. It is recommended to use Design of Experiments (DoE). Classical designs tend to allocate points on or near the design space boundaries and leave a few points in the center, including full and fractional factorial designs, central composite designs and Box-Behnken designs. However, a good DoE should fill the entire design space instead of focusing only on the boundaries or at the center (Sacks et al., 1989, Jin et al., 2001), thus space filling designs should be applied, including Latin Hypercubes (LHC) (McKay, 1979), mean squared error (Jin et al., 2002), integrated mean squared error (Sacks et al., 1989), maximin distance approach (Johnson et al., 1990), orthogonal arrays (Taguchi, 1987; Owen, 1992), Hammersley sequences (Kalagnanam and Diwekar, 1997). Various metamodeling approaches in engineering optimization have been reported, including response surface techniques (Otto et al., 1996; Sobieski et al., 1998), Kriging (Jones et al., 1998), artificial neural networks (ANNs) (Fonseca et al., 2003), and inductive learning (Langley and Simon, 1995). Simpson et al. (2001) reviewed several of these techniques in detail.

Among them, Kriging meta-model technique is most widely used for heat exchangers because of its flexibility and suitability (Jones et al., 1998). The approximation can be done in both offline and online manners. In offline mode, the metamodeling procedure is carried out before any optimization is conducted, while in online approximation, an existing metamodel is updated during optimization with new points sampled in intermediate stages based on the progress of the optimizer. Recent air-refrigerant heat exchanger optimization research using AAO techniques are summarized in Table 6.
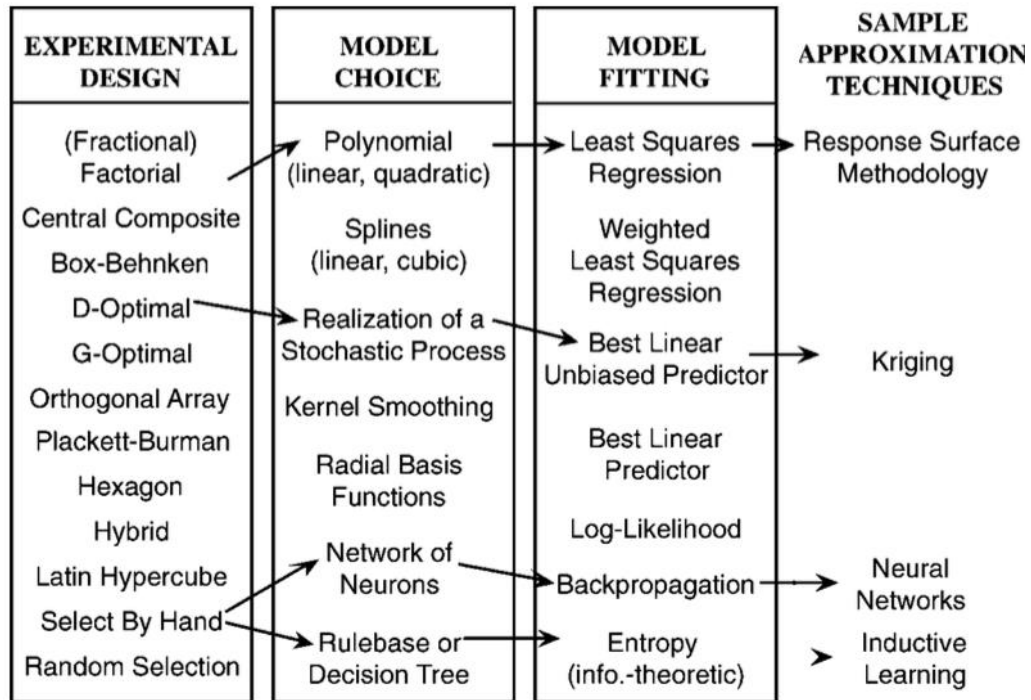
Figure 1 Techniques for metamodeling
(Simpson et al., 2001)

Table 6 Summary of air-refrigerant heat exchanger optimization using AAO techniques

Authors	Experimental design	Meta-model	Objectives
Aute (2008)	Space-Filling Cross-Validation Tradeoff (SFCVT)	Kriging	Multi-objective: Min: ADP, V
Abdelaziz (2009)	MED	Kriging	Single objective: Max: heat transfer capacity per frontal area, per heat exchanger volume, and per material.
Khaled et al. (2010)	Space-Filling Cross-Validation Tradeoff (SFCVT)	Kriging	Single-objective: Min: ADP Max: AHTC
Baceller (2016)	Latin Hypercube Sampling (LHS)	Kriging	Multi-objective: Min: ADP, V

1.2.6. Research gaps

Based on the literature review, the main gaps are as follows:

- Air-side heat transfer coefficient of air-to-fluid heat exchanger still has the potential to be improved, and so is the fluid side. Which means the air-to-fluid heat exchanger still has the potential to have less pressure drop, less volume and less material volume when delivering the same capacity.

- Air flow is limited to be two dimensional on primary heat transfer surface (tube surface) for bare tube heat exchangers. There is no bare tube heat exchanger design that utilizes 3D flow on primary heat transfer surface.

- Nature inspired heat exchange devices haven't been systematically reviewed and there lacks design guideline for nature inspired thermal device design.

- Though numerical studied, small diameter fin-and-tube heat exchangers and bare tube heat exchangers have not been widely experimentally investigated.

1.3. *Objectives*

There are three main objectives of current research: (1) experimentally investigate the performance of state-of-the-art heat exchangers to gain the heat exchanger design fundamentals, including traditional louvered finned mini-channel heat exchangers, small diameter fin-and-tube heat exchanger (4~5 mm), newly studied round and shape optimized bare tube heat exchanger (0.8~1mm); (2) invent, simulate and optimize a novel heat exchanger that has improved thermal and hydraulic performance as compared to baselines on both airside and fluid side and validate the novel heat exchanger performance against experimental data, (3) analyze the applicability of the

novel heat exchanger; and discuss its applicability as automotive radiator and indoor coil for hybrid variable flow system in detail.

Investigation of the state-of-the-art heat exchangers performance encompasses: (a) design and construct an ASHRAE standardized air-to-water/Ref. test facility for heat exchanger capacity ranging from 1 to 10 kW with uncertainty of less than ±5%; (b) experimentally investigate the single-phase transfer using water and air for mini-channel heat exchangers, small diameter fin-and-tube heat exchanger (4~5 mm) and bare tube heat exchanger (0.8~1 mm); (c) experimentally investigate the two-phase heat transfer using refrigerant (R410A) and air for fin-and-tube heat exchangers; (d) develop air-side heat transfer coefficient and pressure drop correlations for bare tube heat exchangers (0.8~1 mm) which have been rarely investigated in literature; (e) analyze the thermal and hydraulic mechanisms of distinct fins and tube shapes to gain the fundamental understanding of heat transfer and address potentials and limitations of compact air-to-fluid heat exchanger design.

Novel air-to-fluid heat exchanger design optimization includes: (a) review nature inspired heat exchange devices comprehensively and develop a design guideline for nature-inspired heat exchangers; (b) invent a heat exchanger with newly defined geometry; (b) conduct numerical simulation and parametric study on both airside and waterside using Computational Fluid Dynamics (CFD) software; (c) conduct experimental tests to validate CFD simulation; (d) explore thermal and hydraulic characteristics of the novel air-to-refrigerant heat exchanger on both airside and waterside; (d) develop Parallel Parameterized CFD (PPCFD) technique in ANSYS® Workbench™ and couple it with Approximation Assisted Optimization (AAO) technique; (e) optimize current heat exchanger so that it has 30% lower total pumping power, 30% less volume and 30% less material volume than those of baseline louvered fin mini-channel heat exchanger

with similar capacity, same or smaller frontal area, similar aspect ratio and same working condition; (f) optimize current heat exchanger so that it has 10% lower total pumping power, 10% less volume and 10% less material volume than those of baseline bare tube heat exchanger with similar capacity, same or smaller frontal area, similar aspect ratio and same working condition.

Applicability analysis of the novel heat exchanger includes: (a) design an air-to-water automotive radiator that has 30% lower total pumping power, 30% less volume and 30% less material volume than those of baseline which is the widely used louvered fin and flat tube heat exchanger that has been tested; (b) model a Hybrid Variable Refrigerant Flow (HVRF) system numerically with current heat exchanger design as indoor coil that has 30% less charge than those of baseline Refrigerant Flow (VRF) system; and, investigate the performance of HVRF system with different refrigerants, including R410A, R290 and R600a.

1.4. *Dissertation organization*

This dissertation is organized so that the research motivation, literature review and research objectives are presented in Chapter 1. Chapter 2 summarizes the research approaches including experimental study, CFD simulation, approximation techniques and multi-scale optimization. Chapter 3 discusses the test results of all baseline heat exchangers that were tested using water and air under both dry and dehumidifying conditions. The novel bifurcated bare tube heat exchanger (bBTHX) is presented in Chapter 4, 5 and 6. In Chapter 4, the bBTHX design concept is shown and parametric study results are discussed for both airside and waterside. The thermal and hydraulic mechanisms are discussed in detail to demonstrate the advantages. In Chapter 5, the metamodel and bBTHX solver are explained and the optimization results are discussed. Two optimization cases are studied. In Chapter 6, two applications of current design are described.

Chapter 7 draws the main conclusions, summarizes the contributions and related publications and provides recommendations for future work. Test facility pictures, HX blockage test results, HX experimental data, Grid Convergence Index (GCI) calculation data, meta-model data and optimization results are listed in the appendices.

Chapter 2: Research Approach

This chapter gives a detailed description of research approaches of experimental test, Computational Fluid Dynamics (CFD) simulation and optimization.

2.1. *Experimental Study*

2.1.1. Test facility

The experimental setup (shown in Figure 2) consists of a closed-loop wind tunnel, a water system, a refrigerant pumped system and a data acquisition system, which is capable of testing heat exchangers from 100 W to 10 kW capacity under a wide range of operating conditions.

The closed-loop wind tunnel was designed and constructed based on the ASHRAE standard 41.2 (ASHRAE, 1987). It included three parts: (1) a test section with two different duct sizes to test heat exchangers with cross section area as large as 0.66×0.66 m, (2) a flow measurement chamber with nozzle grid to measure air-side mass flow rate and (3) an air return duct with three air handling coils with hot water, cold water and glycol water and a humidifier to control the inlet air temperature and humidity. A variable speed fan was installed to allow different air velocities through the wind tunnel.

Two ducts were built independently as test sections with the cross-section area of 0.33×0.33 m and 0.66×0.66 m, respectively. Both the test sections have the same length of 2.5 m. There is no difference in construction materials and instrumentations between the small and large ducts except for the cross-section area. During a heat exchanger test, one test section is selected based on heat exchanger size, and the other is blocked meanwhile. Both test sections were built using 9.53 mm polypropylene plates with a thermal conductivity of 0.5 W/mK and insulated from the

inside using 50.8 mm thick polystyrene foams with a thermal conductivity of 0.12 W/mK, to prevent heat loss from or into the duct.

The heat exchanger prototype was placed inside the smaller test section. The gaps between the heat exchanger and the section were completely blocked with plates to avoid bypass flow, with leading edge in the air flow direction. Two sampling trees which were branch structure made of thin copper tubes with uniform sampling holes distributed over cross section area were installed at the upstream and downstream of heat exchanger. Sample air was drawn from the sampling tree by a blower mounted outside the duct and supplied back into the duct to ensure same amount of air flow. Air flow rate inside the sampling tree was only 1 L/min through a moisture resistant tube with an inner diameter of 3.2 mm thus the power consumption of blower is too small to cause any significant temperature increase of the air. Along the sampling air tube, there was a 4-wire Class 1/10DIN RTD sensor and a chilled mirror hygrometer chamber to measure the temperature and dew point temperature of sample air. Two sets of mixers and settling means were installed before and after sampling devices to ensure the uniformity of air stream.
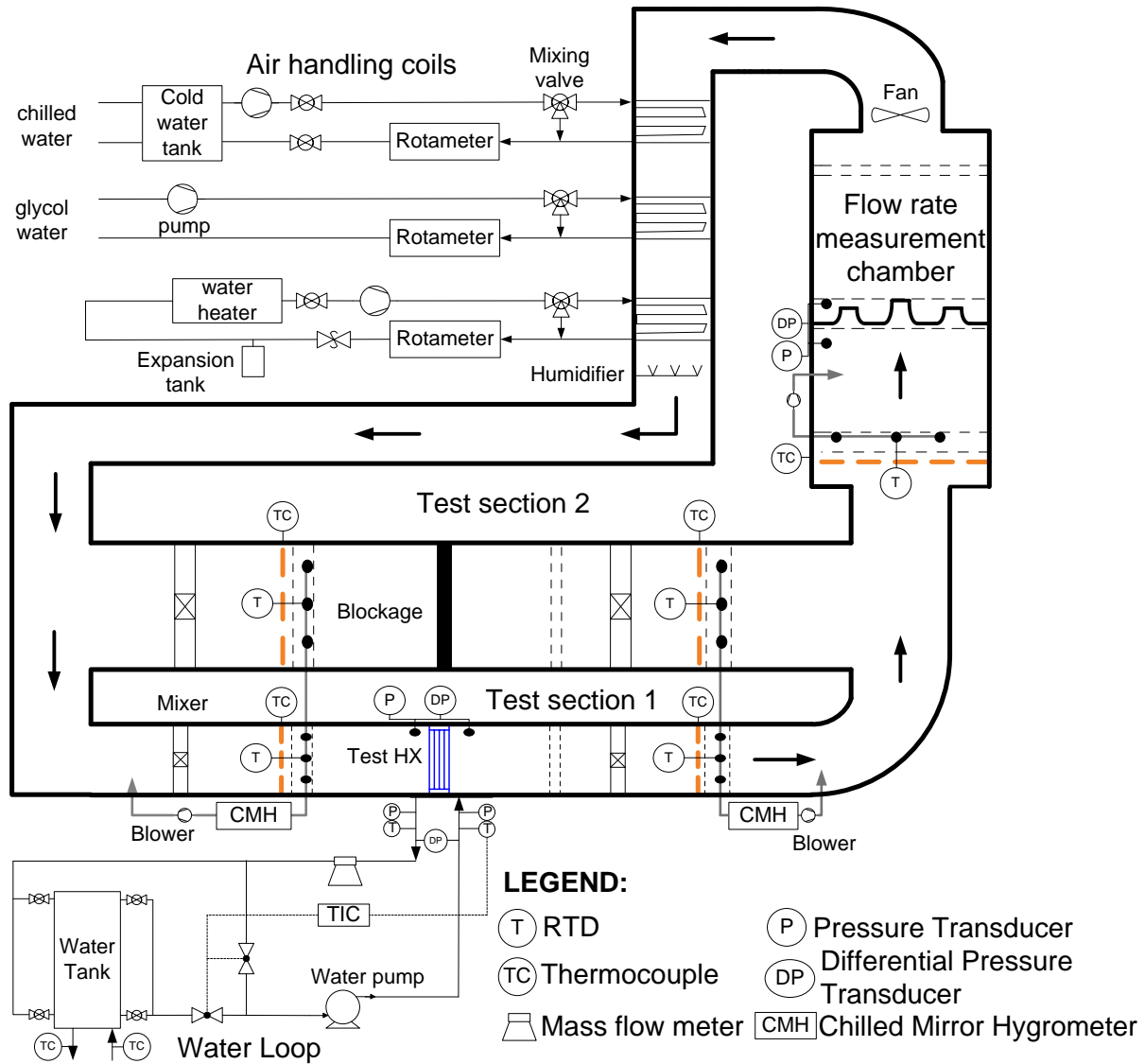
Figure 2 Heat exchanger test facility – wind tunnel and water loop

Settling means are two layers of metal mesh with 51% open area each which also functions as supporting structure of sampling trees and thermal couple grids with six and nine T-type thermocouples for small and big test sections, respectively. Readings of thermocouples were used as a supplement of RTD for temperature measurement and as a mean of air uniformity check. RTD readings was used in the data reduction due to its high accuracy. Both barometric and differential

pressure transducers were installed with ASHRAE standard pressure tap to measure absolute pressure before heat exchanger and pressure drop across heat exchanger.

Air flow measurement chamber is in the downstream of heat exchanger testing section. A nozzle grid of seven ASHRAE-standard nozzles with diameter of 0.051, 0.076, 0.076, 0.127, 0.127, 0.178 and 0.178 m were installed in the middle of this chamber to cover the volume flow rate range of 0.03 to 1.65 m³/s. Nozzles are plugged when not in use. Two sets of settling means were installed before and after the nozzle grid to straighten the flow. A sampling tree integrated with a four-wire-class 1/10DIN RTD sensor was installed in the upstream of nozzle grid to measure the air temperature of nozzle. Both barometric and differential pressure transducers were connected to the standard pressure tap ring to measure the absolute pressure before nozzle and pressure drop across nozzle. Nozzles were calibrated under the procedure described in ASHRAE standard 41.2 (AHRAE, 1987). This procedure is based on energy conservation, which means heat output from electric heater should be equal to heat input into the air inside the duct. Electric heaters with capacities of 0.5, 4, 7 and 9 kW were used to ensure the air temperature rise to be no less than 10˚C to reduce uncertainty. Watt meter with a high accuracy of $\pm$ 0.2% of reading was used to measure the heater's actual power ($\dot{Q}_{wattmeter}$). This should equal the heating capacity of the air which was calculated using air flow rate and air temperature difference, as shown in Equation (1). Air flow rate was measured by nozzle and was calculated by using equations from ASHRAE standard 41.2 (ASHRAE, 1987) without correction factor.

$$\dot{Q}_{nozzle} = \rho VFR_{nozzle} C_{p,a} \Delta T \tag{1}$$

Comparison between the actual heater output (with an uncertainty of $\leq$ 3%) and heating capacity measured by nozzle (with an uncertainty of $\leq$ 1%) are shown in Figure 3. The differences

for all flow rates are within ±4.8%, indicating that no correction factor is needed for this nozzle grid.

Air return duct is a metal duct with outside insulation to reduce heat loss. Three coils were installed to control the air inlet temperature. A tankless gas water heater with the highest outlet temperature of 185°F heated the hot water loop. A chiller with the lowest outlet temperature of 5°C and -11°C cools the cold-water loop and glycol water loop respectively. Three mixing valves are located on each water line to regulate the temperature of each coil thus to control the temperature of inlet air of test heat exchanger. Cold water and glycol water lines are also used to dehumidify the air while an electric steam humidifier is used to increase the humidity.

The water loop of the heat exchanger test facility consists of (1) a variable speed gear pump to provide different steady water flow rates, (2) two 4-wire Class 1/10 DIN RTD sensors and two absolute pressure transducers installed at the inlet and outlet of heat exchangers, (3) a differential pressure transducer to measure the pressure drop across the heat exchanger, (4) a Coriolis mass flow meter to measure mass flow rate and density of water, (5) a water buffer tank to eliminate small fluctuations of water temperature and (6) a plate heat exchanger that exchangers heat from a tankless gas water heater to water inside the water tank.
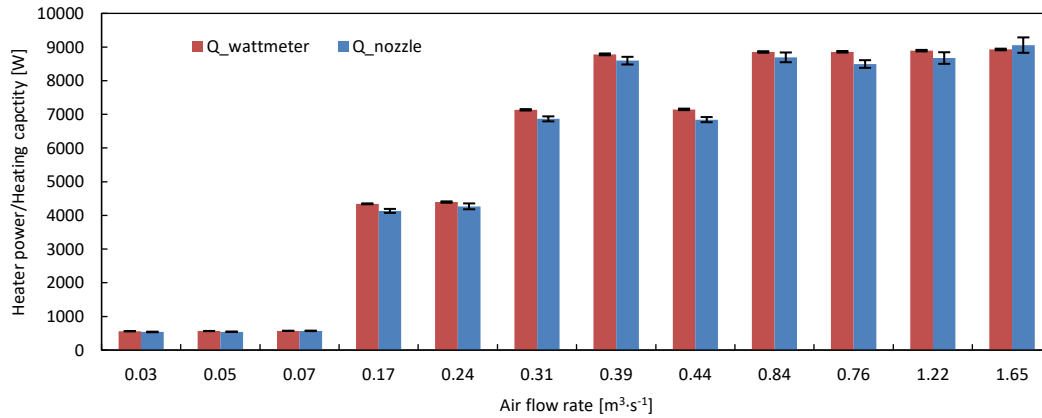
Figure 3 Comparison of air flow rate measured by wattmeter and nozzles
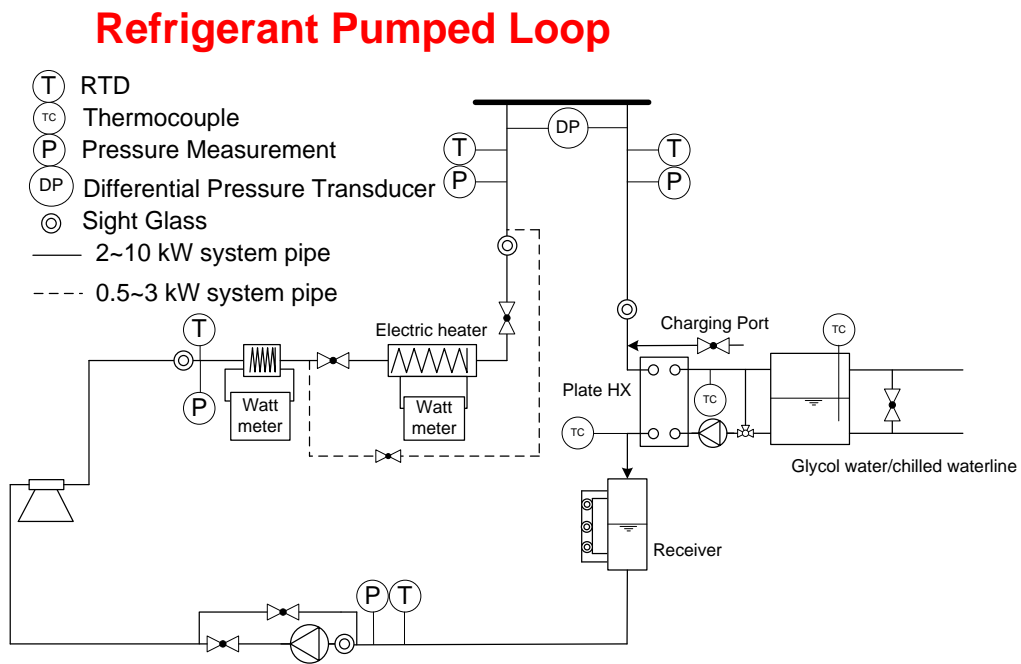
Figure 4 Heat exchanger test facility – refrigerant pumped loop

Besides water loop, a refrigerant pumped loop was built as well to conduct two-phase testing. The refrigerant pumped loop consists of (1) a variable speed gear pump to provide different refrigerant flow rates, (2) four 4-wire Class 1/10 DIN RTD sensors and two absolute pressure transducers installed at the inlet and outlet of heat exchangers, (3) a differential pressure transducer

to measure the pressure drop across the heat exchanger, (4) a Coriolis mass flow meter to measure mass flow rate and density of refrigerant, (5) one 5 kW electric heater and one 10 kW electric heater to heat refrigerant and watt meters to measure power consumption in order to back calculate inlet quality, (6) a receiver, (7) a plate heat exchanger to balance heat transfer, and (8) a glycol water/chilled water tank connected to plate heat exchanger to control the temperature. This refrigerant loop can handle refrigerant like R410A, R134a etc.

All data were recorded after steady state was reached for each test. All data signals of instrumentation were collected by a data acquisition system (DAQ) and transmitted to a computer.

2.1.2. Instrumentation and data acquisition system

Table 7 summarizes the instruments installed in the test facility and the corresponding uncertainties. National Instrument's compact field point models were installed as the data acquisition (DAQ) systems. All the measured signals were collected using LabVIEW program. In addition to receiving signals, the program also provided signals output to system so that a proportional-integral-derivative (PID) control was used to control temperatures, mass flow rates and pressures.

Table 7 Measurement instrument

Instrument	Type	Manufacturer	Model	Range	Systematic Uncertainty
Mass Flow Meter	Coriolis	Micro Motion	2700	0~500 g/s	0.1%
RTD	Resistance	Omega	PR-25AP	-200~800 °C	0.03~0.07 °C
Thermocouple	T	Omega	Tt-T-24-100	-250°~350 °C	0.5 °C
Dew point sensor	Chilled mirror hygrometer	EdgeTech	DewTrak II Chilled Mirror Transmitter	-40~60 °C	± 0.2 °C dew/frost point
Barometric	Strain	Setra	2781600MA1B2BT1	60~110 kPa	±100~±200Pa
Differential	Strain	Setra	2641001WD11T1F	0 to 1" W.C.	(+/-0.25%FS) ± 0.62Pa
			2641005WD11T1F	0 to 0.5" W.C.	(+/-0.25%FS) ± 3Pa
Watt meter	Suspended coil torsion	Ohio Semitronics Int	GH-020D	0~4 kW	±0.2% of reading

2.1.3. Energy balance

For each test, the capacity was measured from both air side and water/refrigerant side. Per ASHARE standard 33, the difference between these two capacities, which is defined as energy balance, should be less than $\pm 5\%$. The definition of energy balance is shown in Equation (2).

$$EB = \frac{\dot{Q}_a - \dot{Q}_{w/ref}}{\dot{Q}_a + \dot{Q}_{w/ref}} \times 2 \times 100\% \tag{2}$$

2.1.4. Uncertainty analysis

Total uncertainty is the summation of systematic uncertainty and random uncertainty. Systematic uncertainty is caused by measurement and instrumentation which is defined as the difference between the true value and the value that instrument can measure. Systematic uncertainty sources include imperfect calibration of instruments, changes in the environment and imperfect methods of observation. Random uncertainty is caused by predictable fluctuation in reading which is usually represented by standard deviation. Random uncertainty sources include lack of sensitivity, random noises and statistical processes.

Data could be classified into directly measured data (e.g. temperature T) and calculated data (e.g. heating capacity $\dot{Q}$). For directly measured data, uncertainty sources include instrument systematic error and random error which is represented as the standard deviation of data series. Total uncertainty of calculated parameter is determined by uncertainty propagation with total uncertainties of directly measured parameters. Pythagorean summation is used for uncertainty propagation. For a calculated value f, which is calculated using measured value $x_1, x_2, \cdots, x_n$ as shown in Equation (3), the total uncertainty of f, is then calculated as in Equation (4). Equation (5) and (6) is an example of uncertainty propagation for enthalpy. In current study, the uncertainty propagation is conducted using software Engineering Equation Solver (EES). Experimental uncertainties of the key parameters are summarized in Table 8. Uncertainty was evaluated for each test in current study.

$$f = f(x_1, x_2, \cdots, x_n) \tag{3}$$

$$\omega_f = \sqrt{\left(\frac{\partial f}{\partial x_1}\omega_{x_1}\right)^2 + \left(\frac{\partial f}{\partial x_2}\omega_{x_2}\right)^2 + \cdots + \left(\frac{\partial f}{\partial x_n}\omega_{x_n}\right)^2} \tag{4}$$

$$h = f(P, T) \tag{5}$$

$$\omega_h = \sqrt{\left(\frac{\partial f}{\partial P}\omega_P\right)^2 + \left(\frac{\partial f}{\partial T}\omega_T\right)^2} \tag{6}$$

Table 8 Total uncertainty in key parameters

	Air	Water
Temperature	±0.18K	±0.14K
Flow rate	±0.8~1.7%	±0.2~0.3%
Pressure drop	±1.5~2.1%	±1.4~2.5%
Capacity	±1.2~2.1%	±1.6~3.1%

2.1.5. Data reduction

For heat exchanger, both dry and wet condition tests were conducted, thus here the data reduction method are explained separately.

28

Dry condition

The heat exchanger capacities under dry conditions were calculated for air-side and water-side using Equation (7) and (8), respectively,

$$\dot{Q}_a = C_{p,a}\dot{m}_a\left(T_{a,o} - T_{a,i}\right) \tag{7}$$

$$\dot{Q}_r = C_{p,r}\dot{m}_r\left(T_{r,i} - T_{r,o}\right) \tag{8}$$

For further data reduction, the arithmetic average of air-side capacity $\dot{Q}_a$ and water-side capacity $\dot{Q}_r$ are used as the heat exchanger capacity, $\dot{Q}$, represented by Equation (9).

$$\dot{Q} = \frac{\dot{Q}_a + \dot{Q}_r}{2} \tag{9}$$

To calculate the air heat transfer coefficient, Wilson plot method was used. The Wilson plot method was first proposed by Wilson (Wilson, 1915), and is a widely-used method to determine the convective HTC using experimental data (Fernández-Seara, 2007). In this case, Wilson plot method was used to find the air-side HTCs for different flow rates. The overall thermal resistance could be expressed as the summation of water-side convective thermal resistance, R_w, tube wall thermal resistance R_{tw} and air-side convective thermal resistance R_a. Thermal resistance due to fluid fouling was neglected. Thus, the overall thermal resistance could be written as Equation (10).

$$R_{ov} = R_a + R_{tw} + R_r \tag{10}$$

Based on experimental data, overall thermal resistance (R_{ov}) could be evaluated using either ε-NTU method or LMTD method. LMTD method was chosen for this study because the inlet and outlet temperatures of both fluids are known. For a cross-flow heat exchanger, we could evaluate the heating capacity as Equation (11).

$$\dot{Q} = UAF\Delta T_{lm} \tag{11}$$

Where ΔT_{lm} is the log mean temperature difference for counter-flow configuration, and F is the log mean temperature difference correction factor for the cross-flow heat exchanger, then F is determined by temperature effectiveness, heat capacity rate ratio. Thus, overall thermal resistance could be expressed as Equation (12).

$$R_{ov} = \frac{1}{UA} = \frac{F\Delta T_{lm}}{\dot{Q}} \tag{12}$$

We kept the air-side HTC, the air flow rate constant while water flow rate was varied. Wilson (1915) theorized that if the mass flow of the water was modified, then the change in the overall thermal resistance would mainly be due to the variation of the air-side HTC (while the remaining thermal resistances remained nearly constant). Since air inlet temperature and water inlet temperature were constant, we could assume the thermal resistance of air-side and tube wall to be a constant number. Air-side convective thermal resistance R_a and tube wall thermal resistance R_{tw} could be expressed as Equation (13).

$$R_{tw} + R_a = C_1 \tag{13}$$

The convective HTC of water was proportional to a power of the velocity as written as Equation (14).

$$h_r = C_2 v_r^n \tag{14}$$

Here the coefficient C_2 and exponent of water velocity n are unknowns. By combining Equation (12), (13) and (14), the regression form is derived as Equation (15).

$$R_{ov} = \frac{1}{C_2 A_w} * \frac{1}{v_w^n} + C_1 \tag{15}$$

Thus, a linear regression was applied to obtain the values of C_1, C_2 and best curve fitting was used to find n. Then the air-side thermal resistance R_a could be calculated using Equation (13).

For heat exchanger with fins, the air-side thermal resistance can be represented as Equation (16). Thus, to find air-side heat transfer coefficient, iteration must be conducted to determine fin efficiency using Equation (17) to (22).

$$R_a = \frac{1}{\eta_0 h A_0} \tag{16}$$

The η_0 here is the surface effectiveness, and is related to the fin surface area, total surface area and fin efficiency by Schmidt (1949) equation.

$$\eta_0 = 1 - \frac{A_f}{A_0}(1 - \eta) \tag{17}$$

where

$$\eta = \frac{\tanh(mr\phi)}{mr\phi} \tag{18}$$

$$m = \sqrt{\frac{2h}{k_f \delta_f}} \tag{19}$$

$$\phi = \left(\frac{R_{eq}}{r} - 1\right)[1 + 0.35\ln(R_{eq}/r)] \tag{20}$$

$$R_{eq} = 1.27\frac{X_M}{r}\left(\frac{X_L}{X_M} - 0.3\right)^{1/2} \text{ for staggered tube layout} \tag{21}$$

31

$$R_{eq} = 1.28 \frac{X_M}{r} \left(\frac{X_L}{X_M} - 0.2 \right)^{1/2} \text{ for single row coil and inline layout} \tag{22}$$

For finless heat exchangers, $\eta_0 = 1$, thus h can be directly calculated using Equation (16).

The Chilton-Colburn j factor and f factor is expressed as follows:

$$j_a = \frac{h_a}{G_{max} C_{p,a}} \text{Pr}^{2/3} \tag{23}$$

$$f_a = \frac{A_c}{A} \frac{\rho_m}{\rho_{a,i}} \left[\frac{2\Delta P \rho_{a,i}}{G_{max}^2} - (1 + \sigma^2)(\frac{\rho_{a,i}}{\rho_{a,o}} - 1) \right] \tag{24}$$

Wet condition

Data reduction for wet condition is more complicated. Basically, the present reduction method is based on the Threlkeld (1970) method. The main steps are to calculate overall wet heat transfer coefficient $h_{o,w}$ and sensible capacity transfer coefficient $h_{c,o}$ first and then calculate mass transfer coefficient $h_{d,o}$. Details are as below.

The total heat transfer rate for air side is shown in Equation (25). The water side heat transfer rate is the same as shown in Equation (8).

$$\dot{Q}_{a,w} = \dot{m}_a (i_{a,o} - i_{a,i}) \tag{25}$$

The overall heat transfer coefficient, based on the enthalpy potential is given as follows:

$$\dot{Q}_w = U_{o,w} A_o \Delta i_m F \tag{26}$$

where Δi_m is the mean enthalpy difference for counter flow coil,

$$\Delta i_m = i_{a,m} - i_{r,m} \tag{27}$$

The mean enthalpy difference for the counter flow configuration is listed in Equation (28) and (29) according to Bump (1963) and Myers (1967).

$$i_{a,m} = i_{a,in} + \frac{i_{a,in} - i_{a,out}}{\ln(\frac{i_{a,in} - i_{r,out}}{i_{a,out} - i_{r,in}})} - \frac{(i_{a,in} - i_{a,out})(i_{a,in} - i_{r,out})}{(i_{a,in} - i_{r,out}) - (i_{a,out} - i_{r,in})} \tag{28}$$

$$i_{r,m} = i_{r,out} + \frac{i_{r,out} - i_{r,in}}{\ln(\frac{i_{a,in} - i_{r,out}}{i_{a,out} - i_{r,in}})} - \frac{(i_{r,out} - i_{r,in})(i_{a,in} - i_{r,out})}{(i_{a,in} - i_{r,out}) - (i_{a,out} - i_{r,in})} \tag{29}$$

The overall heat transfer coefficient is related to the individual heat transfer resistance (Myers, 1967) as follows:

$$\frac{1}{U_{o,w}} = \frac{b'_r A_0}{h_i A_{p,i}} + \frac{b'_r A_0 \ln(\frac{D_c}{D_i})}{2\pi k_p L_p} + \frac{1}{h_{o,w}(\frac{A_{p,o}}{b'_{w,p} A_0} + \frac{A_f \eta_{f,w}}{b'_{w,m} A_0})} \tag{30}$$

where

$$h_{o,w} = \frac{1}{\frac{C_{p,a}}{b'_{w,m} h_{c,o}} + \frac{y_w}{k_w}} \tag{31}$$

y_w in Equation (31) is the thickness of the water film. A constant of 0.005 inch was proposed by Myers (1967). In practice, (y_w/k_w) accounts for only 0.5–5% compared to ($C_{p,a}/b'_{w,m} h_{c,o}$), and has often been neglected by previous investigators. As a result, this term is not included in the final analysis.

$$b'_r = \frac{i_{s,p,i,m} - i_{r,m}}{T_{p,i,m} - T_{r,m}} \qquad \text{Slope of the air saturation curved at the mean coolant temperature and the inside wall temperature} \tag{32}$$

$$b'_p = \frac{i_{s,p,o,m} - i_{s,p,i,m}}{T_{p,o,m} - T_{p,i,m}} \qquad \text{Slope of a straight line between the outside and inside tube wall temperature} \tag{33}$$

$$b'_{w,p} = \frac{\Delta i_{s,w,p}}{\Delta T_{w,p}}$$
Slope of the air saturation curve at the water film temperature of the tube wall surface
(34)

$$b'_{w,m} = \frac{\Delta i_{s,w,m}}{\Delta T_{w,m}}$$
Slope of the air saturation curve at the water film temperature of the fin surface
(35)

Tube-side heat transfer coefficient, h_i is evaluated from the Gnielinski correlation (Gnielinski, 1976).

$$h_i = \frac{(f_i/8)(Re_{Di} - 1000)Pr}{1 + 12.7\sqrt{\frac{f_i}{8}}(Pr^{\frac{2}{3}} - 1)} \cdot \frac{k_i}{D_i}, 2300 < Re_{Di} < 10^4 \tag{36}$$

Where f_i is calculated using the correlation developed by Petukhov (1970), as shown below,

$$f_i = \frac{1}{(0.79 \ln Re_{Di} - 1.64)^2}, 3000 < Re_{Di} < 5 \times 10^6 \tag{37}$$

Note that the Reynolds number used in Equations (36) and (37) is based on the inside diameter of the tube.

To calculate the overall heat transfer coefficient, similarly, the wet fin efficiency must be evaluated through iteration. The wet fin efficiency, defined by Threlkeld (1970), is shown in Equation (38).

$$\eta_{f,wet} = \frac{i - i_{s,fm}}{i - i_{s,fb}} \tag{38}$$

where $i_{s,fm}$ is the saturated air enthalpy at the man temperature of fin and $i_{s,fb}$ is the saturated air enthalpy at the fin base temperature. The fin efficiency under wet condition is calculated using Equations (39) and (40).

$$\eta_{f,wet} = \frac{2r_i}{M_r(r_o^2 - r_i^2)}\left[\frac{K_1(M_T r_i)I_1(M_T r_o) - K_1(M_T r_o)I_1(M_T r_i)}{K_1(M_T r_o)I_o(M_T r_i) - K_o(M_T r_i)I_1(M_T r_o)}\right] \tag{39}$$

$$M_T = \sqrt{\frac{2h_{o,w}}{k_f t}} \tag{40}$$

The air side heat transfer coefficient under wet conditions was calculated using the following procedure (Wang et al., 1997):

1. Calculate total heat transfer coefficient $U_{o,w}$ using Equations (26) to (29)

2. Calculate fluid side heat transfer coefficient h_i using Equation (36)

3. Assume an arbitrary value for the condensate film temperature $T_{w,m}$, and calculate $b'_{w,m}$

4. Iteratively calculate air side overall heat transfer coefficient under wet condition $h_{o,w}$ using Equation (30). Fin efficiency is evaluated using Equations (39) and (40)

5. Calculate $i_{s,w,m}$ by using the following Equation,

$$i_{s,w,m} = i_{a,m} - \frac{C_{p,a}h_{o,w}\eta_{f,wet}}{b'_{w,m}h_{c,o}}\times(1-U_{o,w}A_0[\frac{b'_r}{h_i A_{p,i}} + \frac{b'_p \ln(\frac{D_c}{D_i})}{2\pi k_p L_p}])(i_{a,m}-i_{r,m}) \tag{41}$$

6. Calculate $T_{w,m}$ from $i_{s,w,m}$. If $T_{w,m}$ derived here is not equal that is assumed in step (3), then repeat step (3) ~ (6) until $T_{w,m}$ is constant

Obtain overall heat transfer coefficient and calculate sensible capacity transfer coefficient using Equation (31).

The next step is to calculate mass transfer coefficient $h_{d,o}$. Simultaneously heat and mass transfer process can be described by the process line equation from Threlkeld (1970):

$$\frac{di_a}{dW_a} = Le\frac{(i_a - i_{s,w})}{(W_a - W_{s,w})} + (i_g - 2501Le) \tag{42}$$

where R represent the ratio of sensible capacity transfer characteristics to the mass transfer performance,

$$Le = \frac{h_{c,o}}{h_{d,o}C_{p,a}} \tag{43}$$

However, for fin-and-tube heat exchanger, the saturated air enthalpy ($i_{s,w}$) at the mean temperature at the fin surface is different from that at the fin base, thus Equation (42) does not correctly describe the dehumidification process. A modification of the process line on the psychrometric chart corresponding to the fin-and-tube heat exchanger is described as follows:

From the energy balance of the dehumidification, one can get Equation (44).

$$\dot{m}_a di_a = \frac{h_{c,o}}{C_{p,a}} dA_{p,o}(i_{a,m} - i_{s,p,o,m}) + \frac{h_{c,o}}{C_{p,a}} dA_f(i_{a,m} - i_{s,w,m}) \tag{44}$$

From conservation of water condensate, one can get Equation (45).

$$\dot{m}_a dW_a = h_{c,o} dA_{p,o}(W_{a,m} - W_{s,p,o,m}) + h_{d,o} dA_f(W_{a,m} - W_{s,w,m}) \tag{45}$$

Dividing Equation (44) by Equation (45) yields

$$\frac{di_a}{dW_a} = \frac{Le \cdot (i_{a,m} - i_{s,p,o,m}) + Le \cdot (\varepsilon - 1) \cdot (i_{a,m} - i_{s,w,m})}{(W_{a,m} - W_{s,p,o,m}) + (\varepsilon - 1) \cdot (W_{a,m} - W_{s,w,m})} \tag{46}$$

where

$$\varepsilon = \frac{A_o}{A_{p,o}} \tag{47}$$

The mass transfer coefficient and $h_{d,o}$ is calculated following the procedures:

1. Calculate $W_{s,p,o,m}$ and $W_{s,w,m}$ from $i_{s,p,o,m}$ and $i_{s,w,m}$

2. Assume an arbitrary value for *Le*

3. Calculate the humidity ratio of the outlet air from experiment

4. Calculate the humidity ratio of the outlet air by Equation (45). If the humidity ratio calculated from step (4) equals that from step (3), then stop, else repeat step (2) to (4)

5. Determine $h_{d,o}$ from Equation (43)

Air-side heat and mass transfer coefficient and friction factor of fin-and-tube heat exchanger under wet condition are evaluated using Chilton-Colburn j, Chilton-Colburn j_m and f factor as follows:

$$j = \frac{h_a}{G_{max} C_{p,a}} \Pr^{2/3} \tag{48}$$

$$j_m = \frac{h_m}{G_{max}} Sc^{2/3} \tag{49}$$

$$f = \frac{\Delta P_a \rho_a D_h}{2 G_{max}^2 L_s} \Pr^{2/3} \tag{50}$$

2.2. CFD Simulation

2.2.1. Physics and governing equations

CFD simulation for all heat exchangers are conducted using ANSYS® Workbench™ 18.0. First, Solidworks® generates geometry file and exported it into Workbench™. Then, Meshing™, embedded meshing software in Workbench™ does the meshing; and finally, FLUENT® runs the simulation.

The governing equations of continuity, momentum (Navier-Stokes) and energy are listed as Equation (51) to (53).

$$\nabla \cdot (\rho \bar{u}) = 0 \qquad\qquad (51)$$

$$\nabla \cdot (\rho \bar{u} \bar{u}) = -\nabla p \nabla \cdot [\mu (\nabla \bar{u} + \nabla \bar{u}^T - \frac{2}{3} \nabla \cdot \bar{u})] \qquad\qquad (52)$$

$$\nabla \cdot [\rho \bar{u}(h + \frac{u^2}{2})] = \nabla \cdot (k \nabla T) \qquad\qquad (53)$$

For air side simulation, the assumptions are:

- Three-dimensional, single phase, steady state flow;
- Negligible gravitational effects;
- Ideal gas model for density calculation;
- Temperature dependent properties estimated with polynomial curve fitting other than density;
- Pressure work and kinetic energy are negligible.

In current study, eddies are expected at boundary layer detachment despite low Reynolds numbers. Since the transition between laminar and turbulent regimes is unknown and must be solved by the simulation, the two-equation k-ε realizable (RKE) model (Shih and Zhu, 1994) was used with enhanced wall functions enabled in every simulation. Another advantage of using turbulence model is that they can better solve a larger range of problems which is desired when simulating many samples using same CFD settings. Compared with standard k-ε model, RKE has improved performance for problems involving boundary layers under strong adverse pressure gradients or separation, rotation, recirculation and strong streamline curvature thus is suitable for problems in current study. And it has a higher rate of convergence when using RKE compared to

38

other models for many CFD simulations (Baceller, 2016). For corresponding bare tube simulation, same assumptions were applied.

Thermal properties for air, such as specific heat, thermal conductivity and viscosity are estimated with polynomial curve fitting as function of temperature (Baceller, 2016) and density is based on ideal-gas model.

For water side simulation, the assumptions are:

- Three-dimensional, single phase, steady state flow;

- Negligible gravitational effects;

- Temperature dependent properties estimated with polynomial curve fitting;

- Pressure work and kinetic energy are negligible.

The reason of choosing k-ε realizable (RKE) model with enhanced wall functions for waterside simulation is similar to that of airside.

Turbulent boundary conditions were set to default: 5% turbulence intensity and viscosity ratio of 10. The pressure-velocity coupling scheme used is the Coupled solver available in FLUENT®. A second order upwind space discretization is set to ensure better accuracy. Convergence criteria is defined as 1.0e-5 for continuity and velocities, 1.0e-6 for energy, and 1.0e-3 for turbulent kinetic energy (k) and eddy viscosity (ε). If the simulation does not meet the criteria, however it stabilizes into a solution, we assume that if the standard deviation of the last 100 iterations is less than 0.5% of the average, then it is converged.

2.2.2. Airside computational domain

BTHX computational domain:

The calculation domain for BTHX is shown in Figure 5 as well as the air flow direction. It is a two-dimensional cross section of two row staggered tubes of the heat exchanger. Boundary conditions are defined as:

- Constant and homogeneous velocity distribution at inlet

- Constant pressure at outlet (0.0 Pa gauge)

- Periodic flow at top and bottom of computational domain

- Tubes as walls, tube wall temperature is fixed at 350 K

- The air inlet temperature is fixed at 300 K

A triangular mesh element was set for the models and a refined boundary layer mesh at tube walls was modeled to capture the momentum and thermal boundary layer development with higher accuracy.
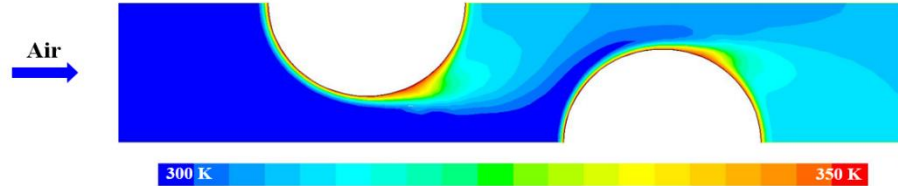
Figure 5 BTHX computational domain

bBTHX computational domain:

For airside simulation, there are different computational domain due to different simulation purpose. The main difference is tube bank number. For parametric study, only two tube banks are simulated while for metamodeling, tube bank numbers are from 1 to 15. The computational domain of bBTHX for parametric study is shown in Figure 6. It is a three-dimensional cross section of two rows of staggered tubes of the heat exchanger. End effects are neglected. Boundary conditions are defined as:

- Constant and homogeneous velocity distribution at inlet

- Constant pressure at outlet (0.0 Pa gauge)

- Periodic boundaries at left-right plane (xz-plane) and top-bottom plane (xy-plane) of computational domain

- Tubes as walls, tube wall temperature is fixed at 350 K

- The air inlet temperature is fixed at 300 K

Although hexahedron mesh is a robust meshing method with excellent stability and computational cost, it is time consuming in terms of generation. Time saved during computation sometimes cannot compensate the time consumed during generation, which is especially true for complicated geometries. Along with the increase of computing power, tetrahedral elements, which can be generated automatically even for complex shapes, have been paid more attention to. Moreover, it was observed that results obtained with quadratic tetrahedral elements and hexahedral elements were equivalent in terms of both accuracy and CPU time (Cifuentes and Kalbag, 1992; Wang et al., 2004), and the stability was found to be excellent even with irregular geometry such as human organs (Bourdin and Trosseille, 2007). Thus, for current design, quadratic tetrahedral mesh element was used. Thus, the choice of an unstructured mesh was justified by the greater easiness in controlling and adapting the mesh quality in an automatic way during optimization. And this has been proven to be accurate enough in tube bundle simulations (Ranut et al., 2014).
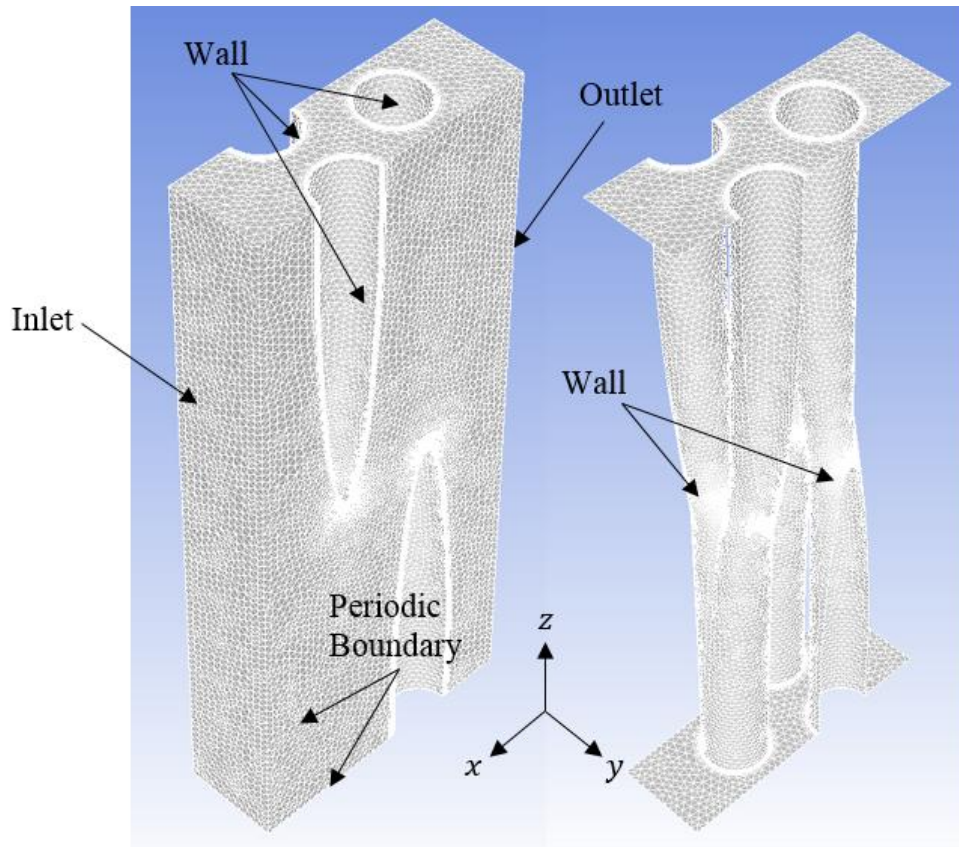
Figure 6 bBTHX computational domain

For metamodeling, tube bank ranges are from one to 15, the computational domain of 15 banks are shown in Figure 7.
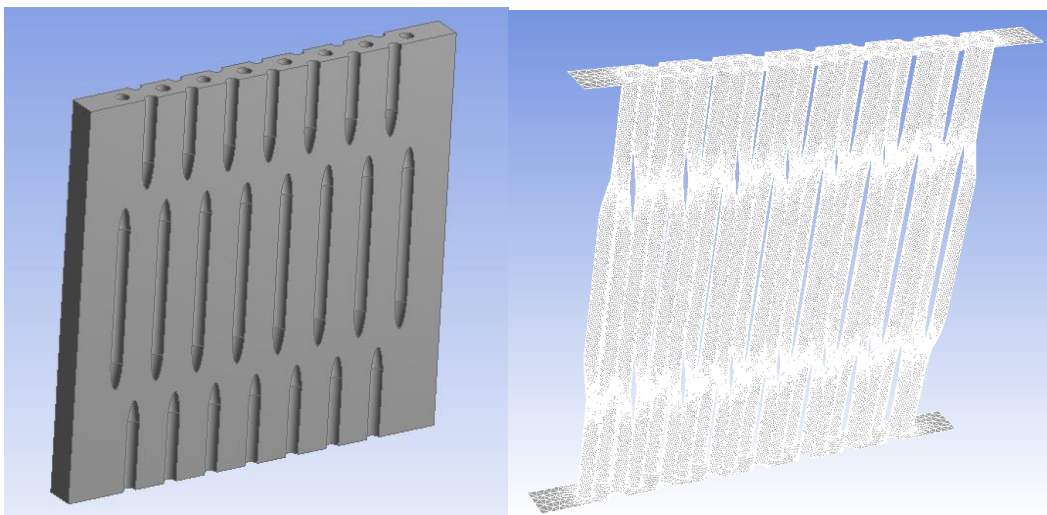
Figure 7 bBTHX computational domain – 15 banks

2.2.3. Waterside computational domain

BTHX computational domain:

The waterside computational domain is shown as Figure 8. A triangular mesh element is set for the models and a refined boundary layer mesh at tube walls is modeled to capture the momentum and thermal boundary layer development with higher accuracy. Here are the settings:

- Constant and homogeneous velocity distribution at inlet

- Constant pressure at outlet (0.0 Pa gauge)

- Tube wall temperature is fixed at 350 K

- The water inlet temperature is fixed at 360 K

Total tube length is 30 times diameter. The first half (15D) is there to ensure the second half is fully developed flow, as shown in Figure 9. Results of the second half are used to calculate heat transfer coefficient and pressure drop.
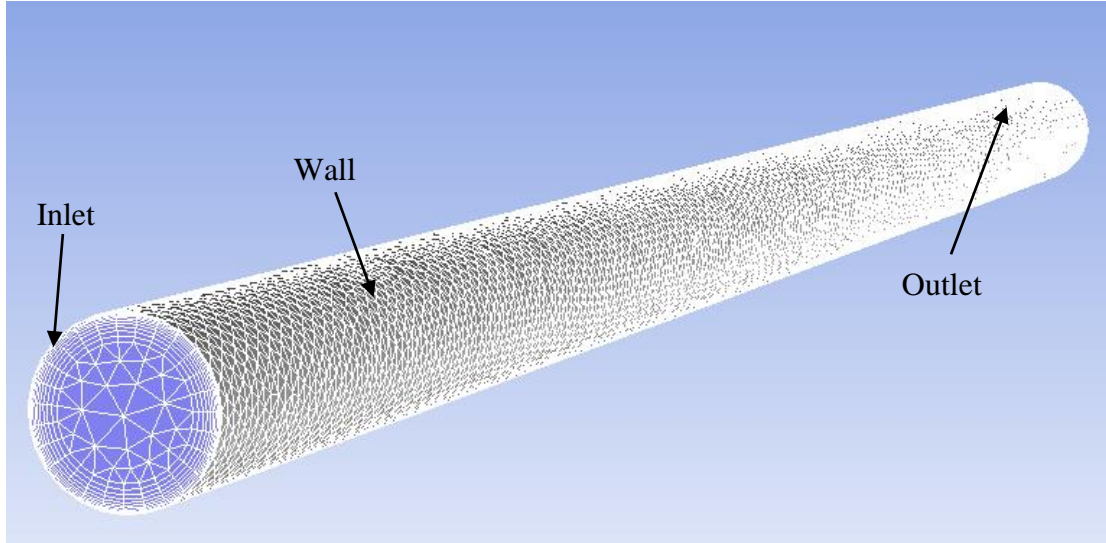
Figure 8 Waterside BTHX computational domain
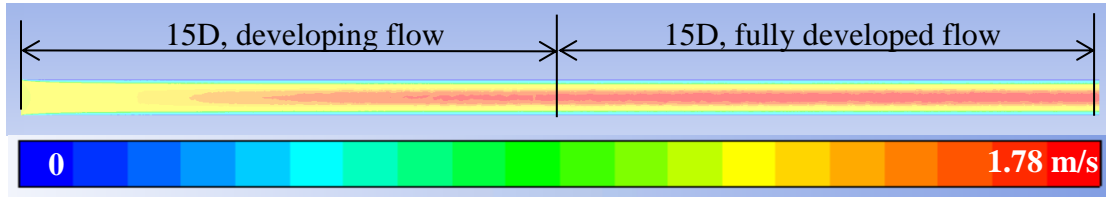
Figure 9 Velocity contour (d=0.6mm, V_w=1 m/s, laminar)

bBTHX computational domain:

The waterside computational domain is the same for parametric study and metamodeling. To give an accurate estimation of the tube side heat transfer and pressure drop, the entry length and the fully developed region need to be modeled separately. However, the entry length varies due to different geometries, thus the first task is to determine the entry length of each geometry. Since what really matters is the determination of computational domain for developing flow and fully developed flow instead of finding the entry length equation, we can only focus on heat exchanger with largest Reynolds number. Another parameter needs to be minimal is (l_1+l_2) (see chapter 4 for definition of l_1 and l_2) because in current design, the boundary layer reinitiates at each bifurcation, thus the flow pattern becomes stable after several bifurcations.

44

In the design domain, the one with largest Reynolds number and smallest (l_1+l_2) is the one with diameter equals 4 mm, bifurcation angle equals 60°, water velocity equals 1 m/s and length ratio equals 0.5.
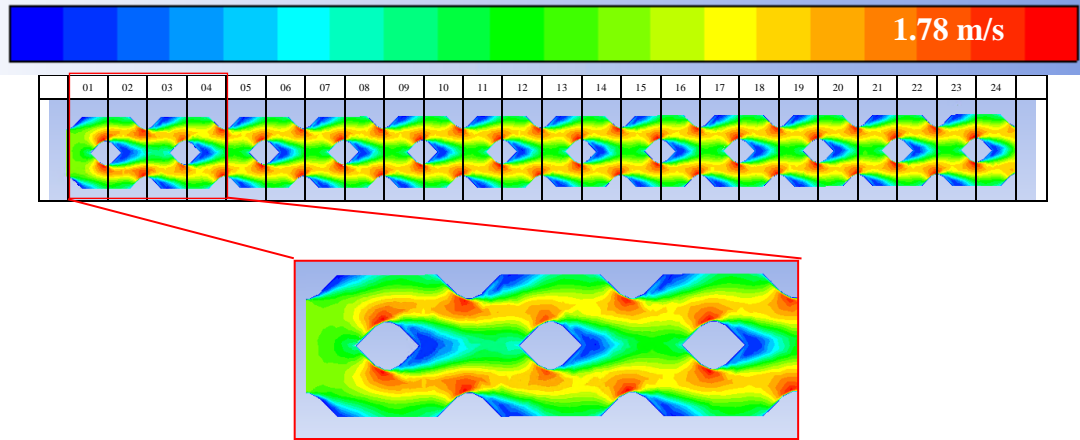
**Figure 10 Velocity contour at mid-plane, model A
(ID=4 mm, θ=60°, V$_w$=1 m/s, LR=0.5)**
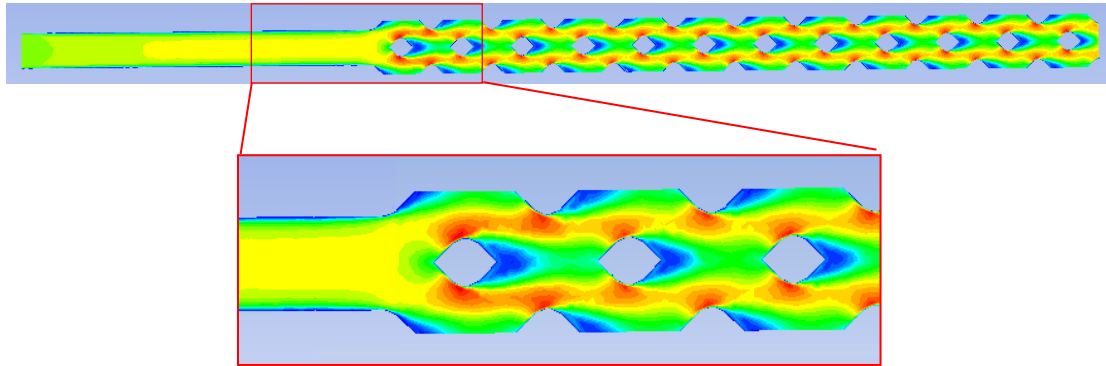
**Figure 11 Velocity contour at mid-plane, model B
(ID=4 mm, θ=60°, V$_w$=1 m/s, LR=0.5)**
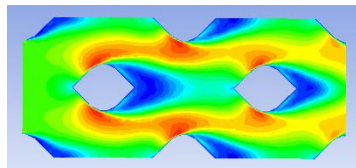
**Figure 12 Velocity contour at mid-plane, 4-segment model
(ID=4 mm, θ=60°, V$_w$=1 m/s, LR=0.5)**

Two models were built: Model A is with uniform velocity inlet and model B is with fully developed flow inlet. In reality, the tubes are connected with header, thus the inlet condition can

45

be assumed to be uniform water velocity. Figure 10 shows the velocity contour of the middle plane of model A. This computational domain is divided into 24 segments. To simulate the fully developed region, a straight tube is added to the inlet to ensure the inlet flow is fully developed when it comes to the bifurcation. The length of straight tube is 15 times the diameter. The velocity contour of model B is shown in Figure 11. Comparing the two enlarged figures, it is obvious that the major difference is in segment-01. The addition of bifurcation makes the velocity field almost identical after segment-02.
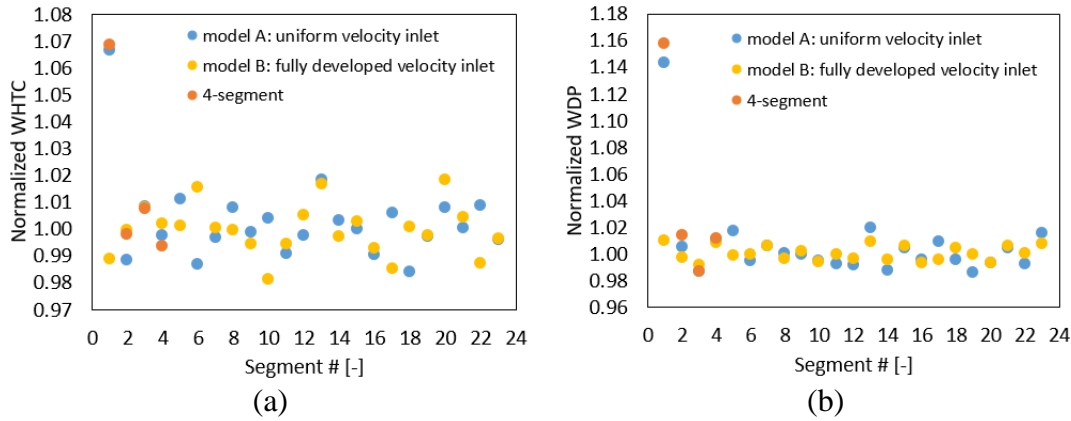
(a)   (b)
Figure 13 Normalized WHTC (a) and WDP (b) comparison

Waterside heat transfer coefficient (WHTC) and waterside pressure drop (WDP) are plotted in Figure 13 (a) and (b). From the two graphs, it should be seen that both WHTC and WDP of model A become stable around a certain value starting with segment 2. The maximum deviation is around ±2%. For model B, WDP and WHTC becomes stable starting with segment 1. It should be noted that all values are normalized based on the averaged values of model A starting with segment 2.

In current study, to simplify the calculation and save computational time, a 4-segment model is used. The velocity contour is shown in Figure 12. It looks almost identical to the first 4 segments in Figure 10. In Figure 13, results of 4-segment model are very close to the first 4

segments of model A. Thus 4-segment model's results can be used for developing flow and fully developed flow simultaneously. Results of segment 1~2 is used for developing flow, and averaged results of segment 3~4 is used for fully developed flow.

The selected point is the worst scenario, here is the verification using a random point. As shown in Figure 14, the results of 4-segment model match that with model A very well.
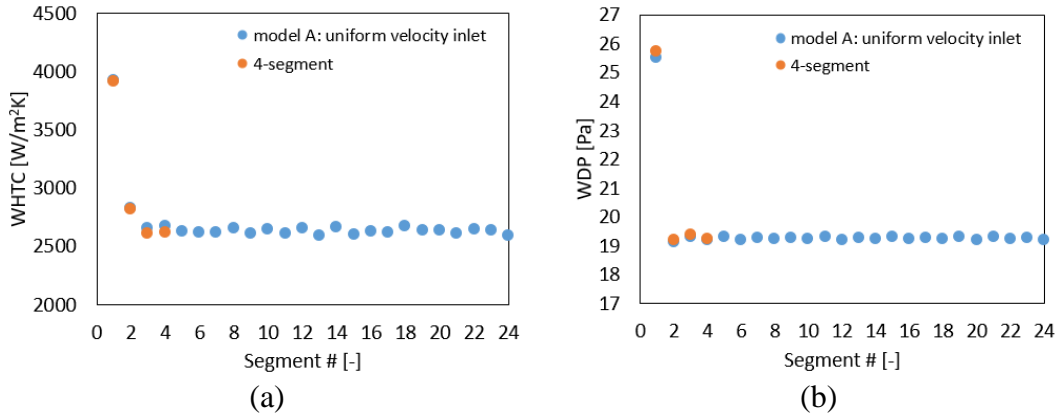
(a)   (b)
Figure 14 WHTC (a) and WDP (b) comparison
(ID=1 mm, θ=10°, V_w=0.1 m/s, LR=0.5)

Thus, the waterside computational domain is shown as Figure 15. A tetrahedral mesh element is set for the models and a refined boundary layer mesh at tube walls is modeled to capture the momentum and thermal boundary layer development with higher accuracy. Here are the settings:

- Constant and homogeneous velocity distribution at inlet

- Constant pressure at outlet (0.0 Pa gauge)

- Periodic boundaries at left-right plane (xz-plane) and top-bottom plane (xy-plane) of computational domain

- Tubes as walls, tube wall temperature is fixed at 350 K

- The water inlet temperature is fixed at 360 K

47
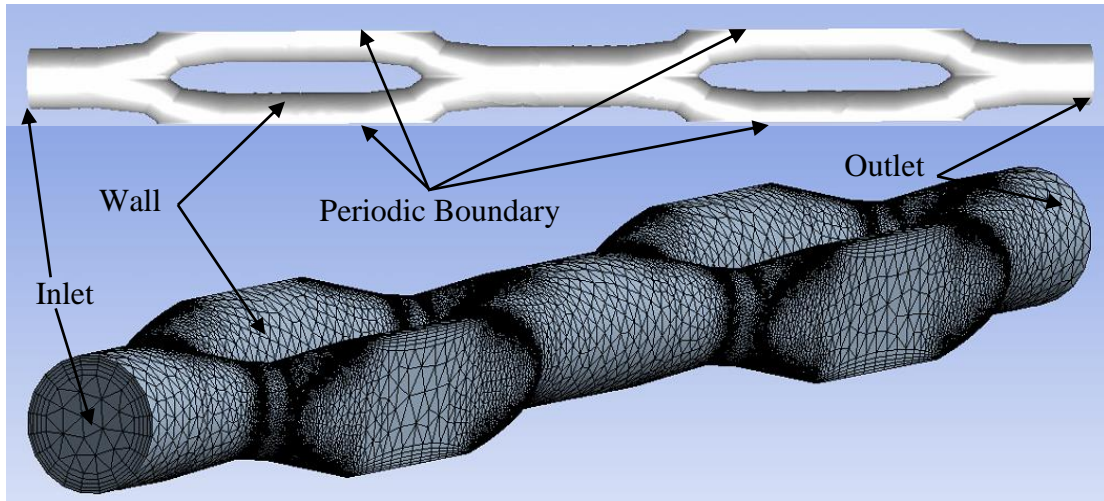
Figure 15 Waterside computational domain

2.2.4. CFD data reduction

UA-LMTD method was applied to calculate airside and waterside convention heat transfer coefficient, as shown in Equation (54) and (55).

$$\dot{Q} = \dot{m} \cdot c_p \left| T_o - T_i \right| = h \cdot A_o \cdot \Delta T_{ml} \tag{54}$$

$$h = \frac{\dot{m} \cdot c_p}{A_o} \cdot \frac{\left| T_o - T_i \right|}{\Delta T_{ml}} = \frac{\dot{m} \cdot c_p}{A_o} \cdot \frac{\left| T_o - T_i \right|}{\dfrac{\left[\left(T_w - T_i \right) - \left(T_w - T_o \right) \right]}{\ln \left[\left(T_w - T_i \right) / \left(T_w - T_o \right) \right]}} \tag{55}$$

For pressure drop, the dynamic pressure difference between inlet and outlet is negligible compared to static pressure difference. Thus, static pressure difference between inlet and outlet is regarded as the total pressure difference.

2.2.5. CFD Grid Uncertainty Analysis

The Grid Convergence Index (GCI) method (Roache, 1993; Roy and Oberkampf, 2011; ASME, 2009), which is based on Richardson extrapolation method (Richardson, 1910), is an acceptable and a recommended method to evaluate the grid convergence.

Here is the recommended procedure for GCI calculation (Procedure for Estimation and Reporting of Uncertainty Due to Discretization in CFD Applications, 2008):

Step 1: Define a representative cell, mesh, or grid size h as follows for two-dimensional and three dimensional computational domains.

$$h_{2D} = \left[\frac{\sum \Delta A_i}{N} \right]^{1/2} \tag{56}$$

$$h_{3D} = \left[\frac{\sum \Delta V_i}{N} \right]^{1/3} \tag{57}$$

where ΔV_i is the volume and ΔA_i is the area of the i th cell, and N is the total number of cells used for computation.

Step 2: Select three significantly different sets of grids where the element size ratio between subsequent grid resolutions is no less than 1.3. This value of 1.3 is based on experience and not on formal derivation. The refinement should be done systematically and the use of geometrically similar cells is preferable.

Step 3: Let $h_1 < h_2 < h_3$ and $r_{21} = h_2/h_1$, $r_{32} = h_3/h_2$, calculate the observed order of accuracy p^* using Equation (58) through (61). Note that $q(p) = 0$ for $r = const.$ and φ is a selected variable which is critical to the conclusions being reported. φ_k is the solution on the k_{th} grid.

$$\hat{p} = \left(\frac{1}{\ln r_{21}} \right) \left(\ln \left| \frac{\varepsilon_{32}}{\varepsilon_{21}} \right| + q(\hat{p}) \right) \tag{58}$$

$$q(\hat{p}) = \ln \left(\frac{r_{21}^{\hat{p}} - s}{r_{32}^{\hat{p}} - s} \right) \tag{59}$$

$$s = \mathrm{sgn}\ (\varepsilon_{21}/\varepsilon_{32}) \tag{60}$$

$$\varepsilon_{21} = \varphi_2 - \varphi_1 \tag{61}$$

Step 4: Calculate the extrapolated values as in Equation (62).

$$\varphi_{ext}^{21} = \frac{r_{21}^p \varphi_1 - \varphi_2}{\left| r_{21}^p - 1 \right|} \tag{62}$$

Step 5: Calculate and report the error estimates using Equation (63) and the grid convergence index (GCI) in Equation (64).

$$e_{ext}^{21} = \left| \frac{\varphi_{ext}^{21} - \varphi_1}{\varphi_{ext}^{21}} \right| \tag{63}$$

$$GCI_{fine}^{21} = \frac{F_s \cdot e_a^{21}}{r_{21}^p - 1} \tag{64}$$

where F_s is factor of safety. If solutions on three grids are available, then the following rules should be followed. It should be noticed that in Equation (62) and (64), order of accuracy p is different from the observed order of accuracy $\hat{p}$. When the observed order of accuracy $\hat{p}$ agrees with the formal order p_f within 10%, then the formal order of accuracy along with a safety factor of 1.25 is used in the GCI calculation. When the observed order of accuracy does not agree within 10%, then a factor of safety of 3.0 is used. And the order of accuracy is limited between 0.5 and the formal order. Setting the upper bound is because that allowing the order of accuracy to be much larger than the formal order causes the uncertainty estimates to be unreasonably small since the GCI goes to zero as p goes to infinity. Setting the lower bound is because that allowing the order of accuracy to go to zero causes the uncertainty estimate to approach infinity. These are summarized in Table 9 (Roy and Oberkampf, 2011). But if solutions on only two grids are available, $F_s = 3.0$ (Roache, 1993).

Table 9 Implementation of GCI

$\left|\dfrac{\hat{p} - p_f}{p_f}\right|$	F_s	p
≤ 0.1	1.25	p_f
> 0.1	3.0	min (max $(0.5, \hat{p})$, p_f)

The uncertainties of boundary points of the design space are fundamentally larger than that of other points because the combinations of lower and upper bounds yield the most skewed computational domains, thus having a higher potential for poorer mesh elements in terms of size and aspect ratios. Thus, the GCI method is employed for the 2^n samples represented by all variable combinations of 0's and 1's for an n-dimension design space plus one central sample. (Bacellar, 2016)

Airside GCI results: The numerical uncertainties of heat transfer coefficient and pressure drop are 2.2% and 4.0% for finer mesh, and 3.0% and 4.5% for coarse mesh, respectively, as shown in Figure 16. Mesh 2 (intermediate mesh) was selected as the final mesh.

Waterside GCI results: The numerical uncertainties of heat transfer coefficient and pressure drop are 4.0% and 3.6% for finer mesh, and 4.9% and 5.6% for coarse mesh, respectively, as shown in Figure 17. Mesh 2 (intermediate mesh) was selected as the final mesh.
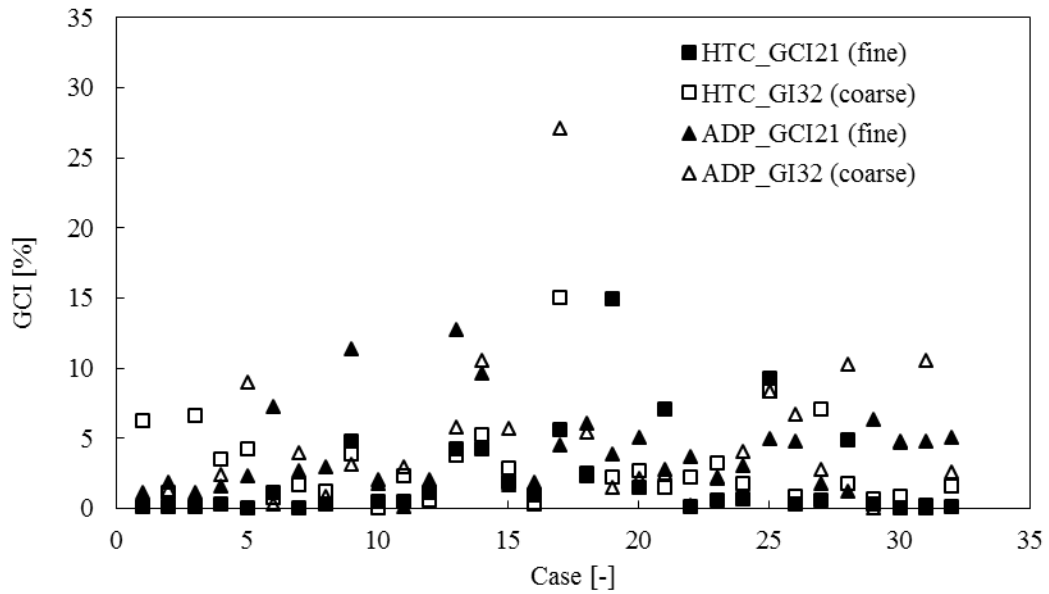
Figure 16 Airside GCI results
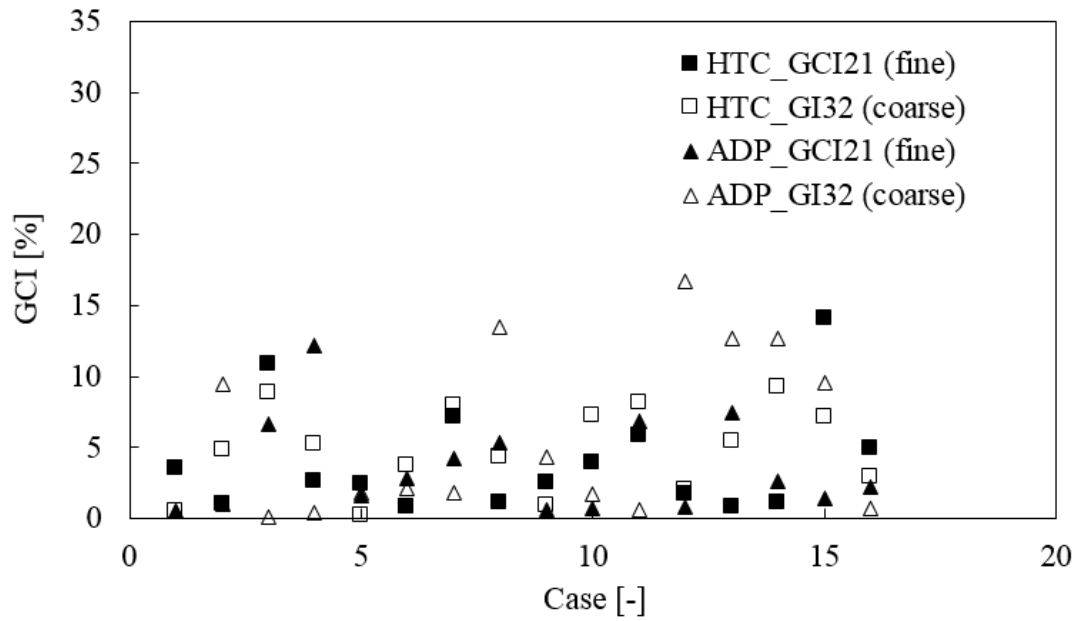
Figure 17 Waterside GCI results

53

2.2.6. New CFD automation approach

To do Approximation Assisted Optimization method, CFD automation is a necessity. In this dissertation, the CFD simulation was carried out using a parallel parameterized computational fluid dynamics (PPCFD) simulation, which was proposed by Abdelaziz (2009) and realized in ANSYS® Workbench™ 18.0 using two novel approaches proposed by the author. PPCFD automatically generates mesh and CFD journal files, runs the files and performs post processing to summarize and analyze the results. In Abdelaziz (2009)'s approach, Gambit was used for geometry and meshing and ANSYS® FLUENT® for simulations. Gambit, which was the only platform that allowed journaling and scripting therefore suitable for the automation method, is no longer available. Two novel approaches are proposed here to realize the PPCFD procedure in ANSYS® Workbench™.

The detailed steps of approach A are shown in Figure 18 (a) and as follows:

1) Generate design of experiment (DOE) table for parameters;

2) Use external code to generate a series of batch file, journal files for Workbench™, DesignModeler™, Meshing™ and FLUENT®;

3) Execute journal files for Workbench™, DesignModeler™, Meshing™ and FLUENT® using the journal files to generate geometry, generate mesh and run simulation in Workbench™;

4) Post process output data to obtain thermal-hydraulic performance.

The detailed steps of approach B are shown in Figure 18 (b) and as follows:

1) Build first case and set parametric table in ANSYS® Workbench™;

2) Generate design of experiment (DOE) table for parameters;

54

3) Import DOE table to parametric table in ANSYS® Workbench^{TM} and update the table to get output parameters;

4) Export parametric table and conduct post data process.

These two difference approaches both enable automatic calculation and allow for shape change. However, only approach A has the capability of topology change and allows for customized settings for geometry, meshing and CFD simulation. Approach A also has the advantage of fully parallel computation for every step: geometry generation, meshing and CFD simulation. Approach B only allows parallel computation for CFD simulation. And the parameter numbers of approach B cannot exceed the limit of 20, which is the largest number supported by parametric table in ANSYS® Workbench^{TM} 18.0. However, to use approach A, one needs to learn different programming languages including Python, JavaScript and Scheme. Considering Approach B is easy to learn and there is no topology change requirement for current study, Approach B was selected to be the PPCFD approach in current study.
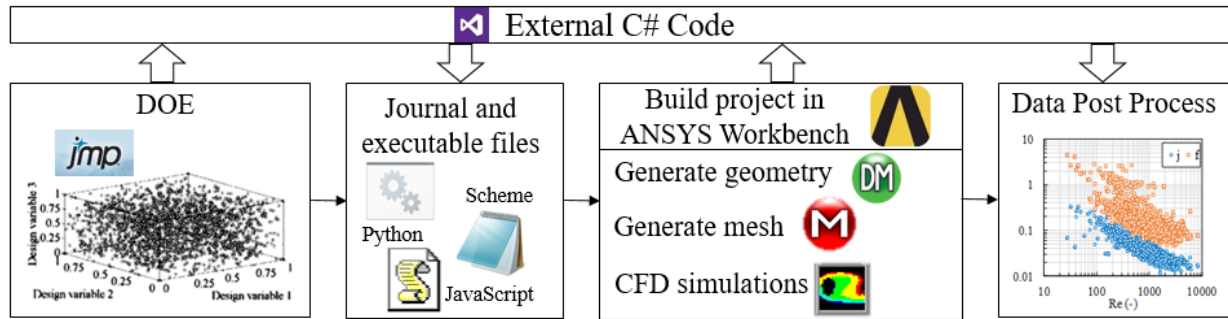
(a) Approach A
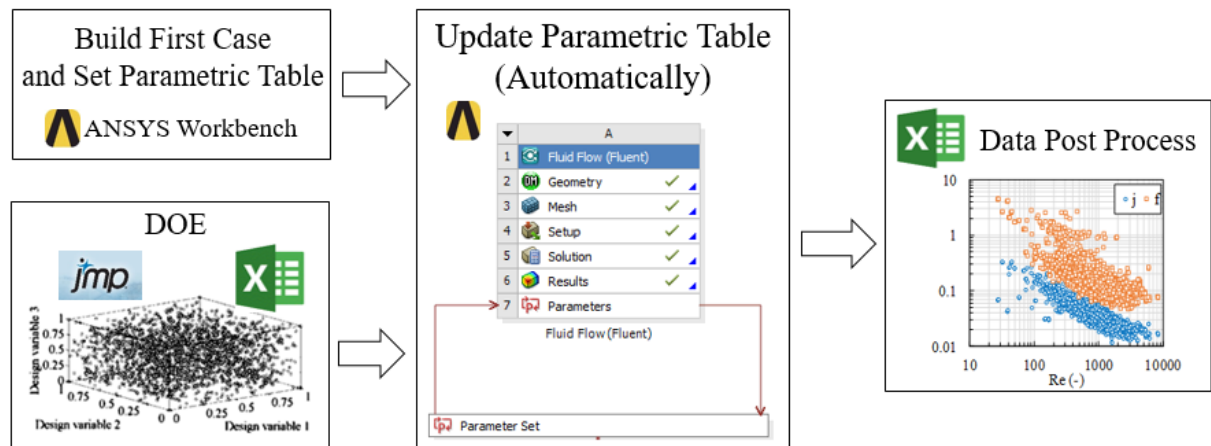
(b) Approach B

Figure 18 Two PPCFD approaches in ANSYS® Workbench™

2.3. Approximation Techniques and Optimization

2.3.1. Design of experiment

In many engineering problems, including current study, it is ideal to run simulations for each point in design domain to determine the relationship between input and output parameters. However, this is impossible because of the computational cost limitation. Hence, developing methods for efficiently selecting the experiments becomes important. Design of experiment (DOE) is a systematic approach to effectively sample the design space to achieve the optimal quality information of the relationship between input parameters and output responses. The quality of DOE plays a critical role in the accuracy of meta-model prediction. Different DOE generating methods are available in literature, such as random sampling, Latin hypercube sampling (LHS) (McKay et al., 2000), full-factorial designs (Box et al., 1986), maximum entropy sampling (MES) (Shewry and Wynn, 1987). In current study, Latin hypercube sampling (LHS) was used.

2.3.2. Kriging metamodeling

A meta-model or surrogate model, is a model of model. It is developed from the classical regression methodologies, which correlates data using least squares fitting methodologies. In current study, metamodeling was used to generate the airside and waterside heat transfer and friction correlations because it is hard to take into consideration of geometrical parameters using traditional regression methodologies. It is an approximation to system response constructed from sampling points, the design of experiments (DOE). Metamodeling is more applicable than classical regression methods for problems that the function form is not known a priori. Various metamodeling approaches are available, such as polynomial regression, spline regression, sparse grid, artificial neural network, kriging and hybrid model (Simpson et al., 2001), etc.

57

Kriging is an advanced interpolation technique that predicts the response of unknown design based on its linear distance from known design points and responses through a stochastic process, such as Gaussian process. Kriging technique provides superior performance for nonlinear problems and shows a higher degree of flexibility, and is recommended when design space has 50 or less variables (Wang et al., 2007). Kriging technique can fit higher order variations of the output parameters and auto refine the model by adding refinement points so that it can provide an improved response quality. Hence, in current study, Kriging method was used for metamodeling.

The accuracy of metamodel was evaluated using the Metamodel Acceptability Score (MAS) (Hamad, 2006). MAS was calculated using following equations.

$$e_i = \frac{\left| \hat{y}_i - y_i \right|}{y_i} \tag{65}$$

$$j_i = \begin{cases} 1, \text{ if } e_i < e_{max} \\ 0, \text{ if } e_i > e_{max} \end{cases} \tag{66}$$

$$MAS = \frac{\sum\limits_{i=1}^{N} j_i}{N} \times 100 \tag{67}$$

$$MAS \geq 1 - e_{max} \tag{68}$$

Where y_i is true value, $\hat{y}_i$ is predicted value by metamodel, e_i is error, e_{max} is maximum tolerance error user defined (usually 5% to 10%) and N is number of test samples. The metamodel is accurate is Equation (68) is satisfied.

2.3.3. Multi-scale HX optimization

2.3.3.1.   Modifications for current study

As computational power increases, it is possible to study enhanced surface performance improvement, flow arrangement, and circuitry using accurate segmented HX simulation tools, such as CoilDesigner® (Jiang et al., 2006). However, this requires the input of heat transfer and pressure drop of the new surface. This could be heat transfer and pressure drop correlations or data from CFD simulations or experiments. If the correlations or data come from CFD simulation of enhanced HX segment performance, then the method is regarded as multi-scale HX simulation.

Multi-scale simulation enables efficient integration of the enhanced HX segment performance prediction using CFD simulations with overall HX performance prediction using segmented ε-NTU method, which provides significant computational savings (Abdelaziz, 2009).

However, as far as the author knows, in all available applications of multi-scale HX simulations (Abdelaziz, 2009, Khaled et al. 2010, Bacellar et al. 2016), only airside was simulated using CFD while in-tube side was modeled using existing heat transfer and pressure drop correlations because the in-tube side geometry is round smooth tube, which has been comprehensively studied already. In current study, not only airside but also in-tube side geometries are new, thus the first improvement of current study is to apply multi-scale HX simulation on both air and in-tube side.

The second modification of current study is that it accounts for physical properties of working fluids so the metamodeling results could be used at any conditions. In previous studies, the airside CFD simulation was conducted at a specific working condition and later was used at different working conditions for optimization. This is acceptable due to the small variation of air

physical properties at different working conditions. In current study, working fluid at liquid side is water, of which the physical properties changes cannot be neglected. So, waterside's metamodel accounts for physical properties by using Reynolds number as an extra input in addition to geometry parameters.

2.3.3.2.   bBTHX solver

There are many mathematical models and simulations tools that have been developed for design and rating of heat exchangers. However, none of them are applicable to current heat exchanger design due to its unique geometry. So, a customized heat exchanger solver needs to be developed. The calculation segment is shown in Figure 19 and the flow chart is shown in Figure 20. The definition of tube per row (N_{tpr}), row number (N_r) and water segment number (N_{ws}) are shown in Figure 21.

$Water, \dot{m}_{i,k,in}, P_{i,k,in}, h_{i,k,in}$

$Air, \dot{m}_{i,k,out}, P_{i,k,out}, h_{i,k,out}$

$Air, \dot{m}_{i,k,in}, P_{i,k,in}, h_{i,k,in}$

$Water, \dot{m}_{i,k,out}, P_{i,k,out}, h_{i,k,out}$
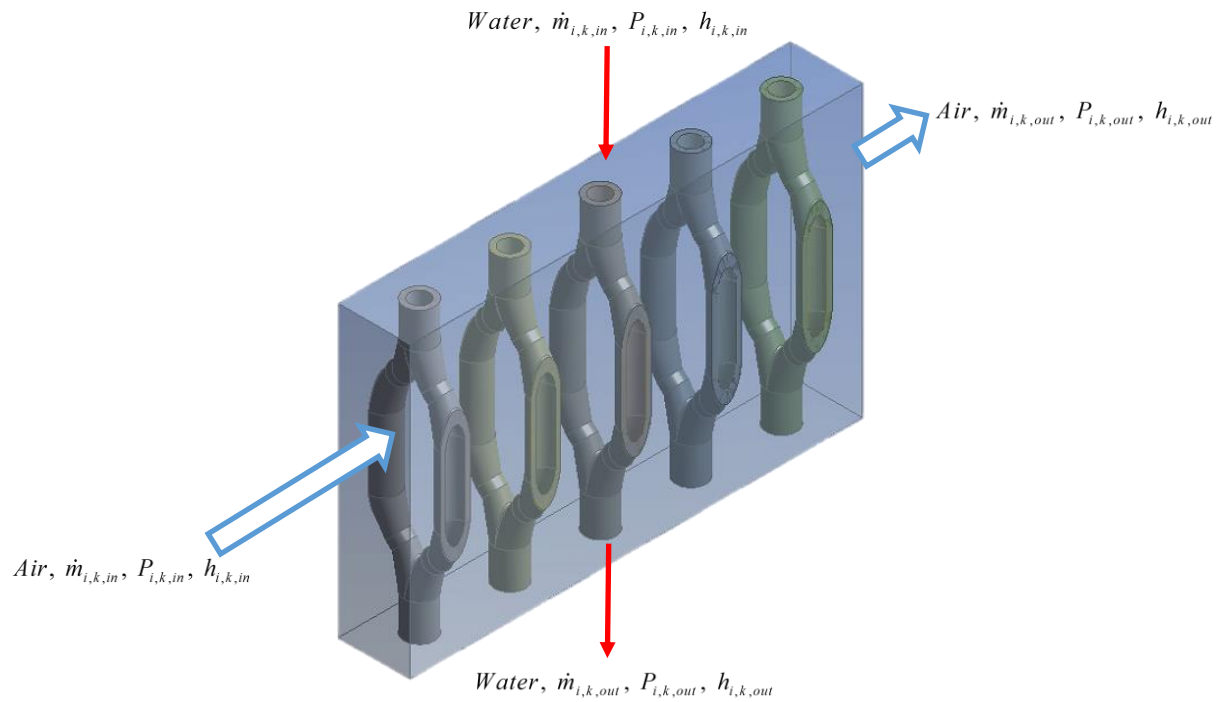
Figure 19 Segment of bBTHX solver
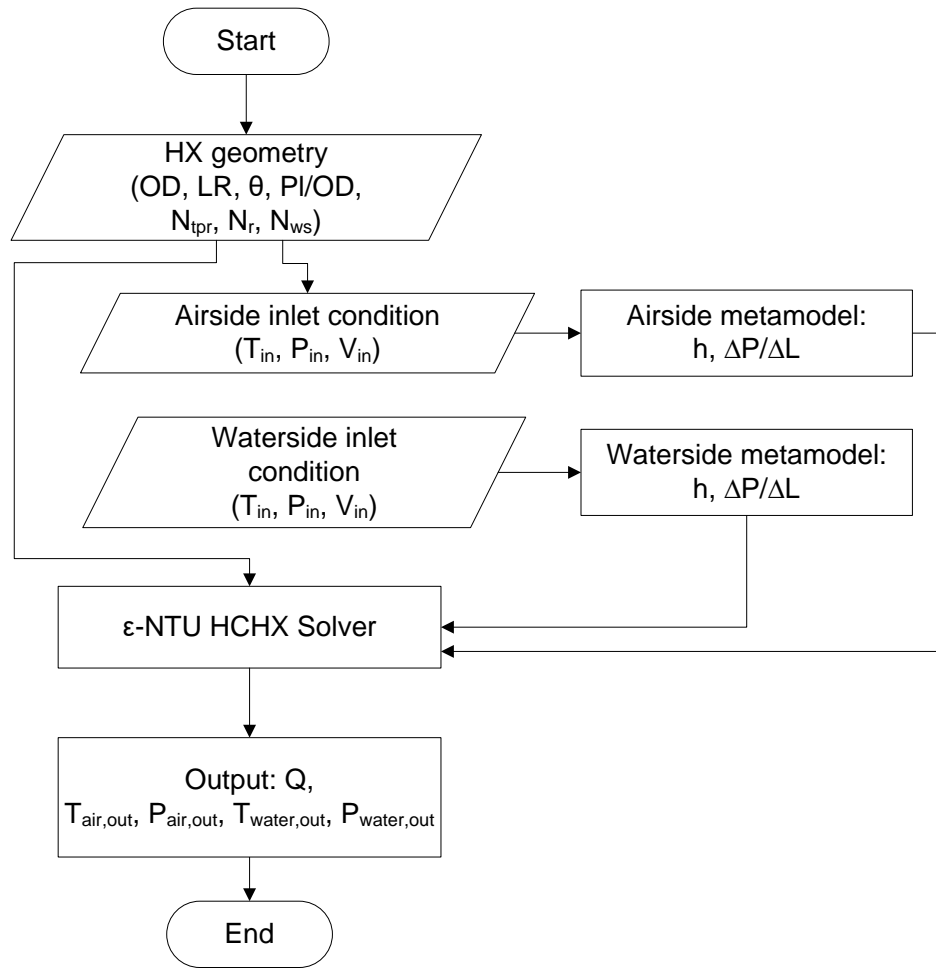
Figure 20 Flow chart of bBTHX solver

61
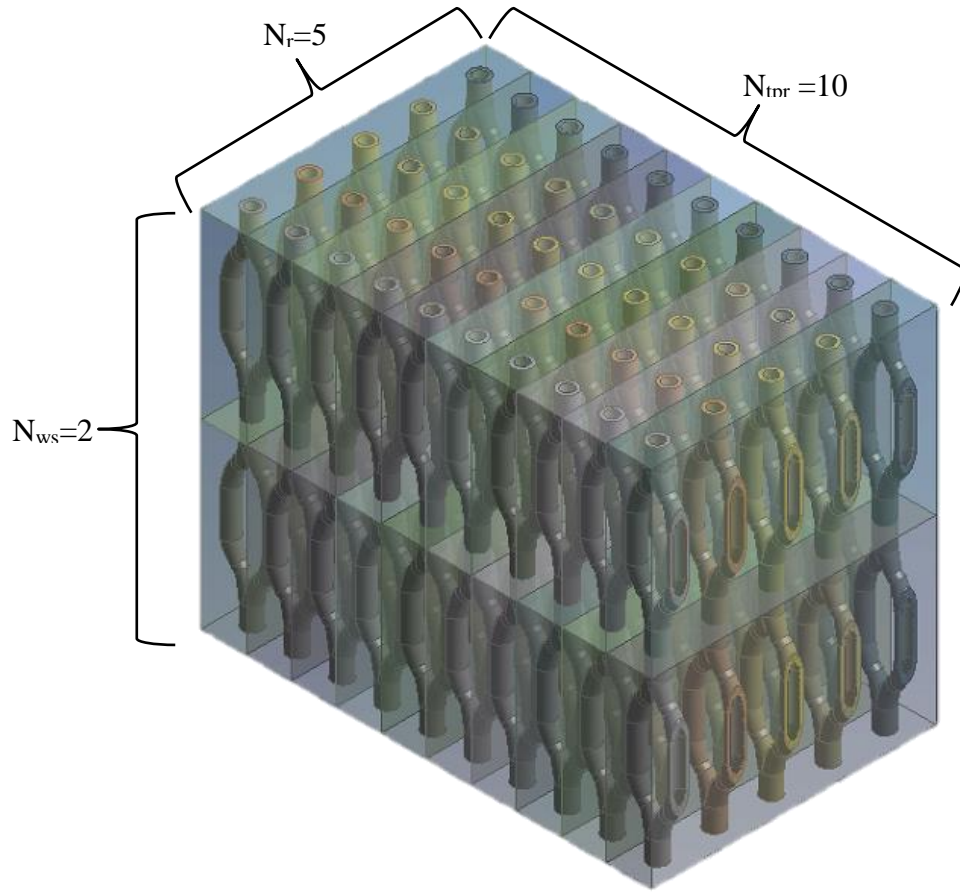
Figure 21 Definitions of N_{tpr}, N_r and N_{ws}

2.3.3.3.   Approximation assisted optimization

The key procedure of multi-scale HX optimization is Approximation Assisted Optimization (AAO). The detailed steps applied in AAO are as follows:

1) Airside Design of Experiments (DoE) and PPCFD;

2) Waterside Design of Experiments (DoE) and PPCFD;

3) Airside meta-model building and verification;

4) Waterside meta-model building and verification;

5) Segmented HX solver;

6) Multi-objective optimization.

The optimization framework is illustrated in Figure 22.

Multi-objective optimization (MOO) problem is an optimization problem that involves multiple objective functions, as formulated in Equation (69). The solution of multi-objective optimization is usually a set of tradeoff designs called Pareto front.

$$
\begin{aligned}
&\underset{\underset{\sim}{x}}{\text{minimize}} \quad f_i(\underset{\sim}{x}) \qquad\qquad i = 1,...,M \\
&\text{subject to: } g_j(\underset{\sim}{x}) \le 0 \qquad j = 1,...,J \\
&\qquad\qquad\;\; h_k(\underset{\sim}{x}) = 0 \qquad k = 1,...,K \\
&\qquad\qquad\;\; \underset{\sim}{x}_{lower} \le \underset{\sim}{x} \le \underset{\sim}{x}_{upper}
\end{aligned}
\tag{69}
$$

Equation (69) describes an objective optimization problem with design variable vector $\underset{\sim}{x}$ and objective f_i. There are M objectives in total and f_i refers to the ith objective. There are J inequality constraints and $g_j(\underset{\sim}{x})$ refers to the jth inequality constraint. There are also K equality

constraints and $h_k(\underset{\sim}{x})$ refers to the kth equality constraint. Lower bound of variable is $\underset{\sim}{x}_{lower}$ and upper bound is $\underset{\sim}{x}_{upper}$.

The problem above represented is solved using Multi-Objective Genetic Algorithms (MOGA) (Deb, 2001) in current study.
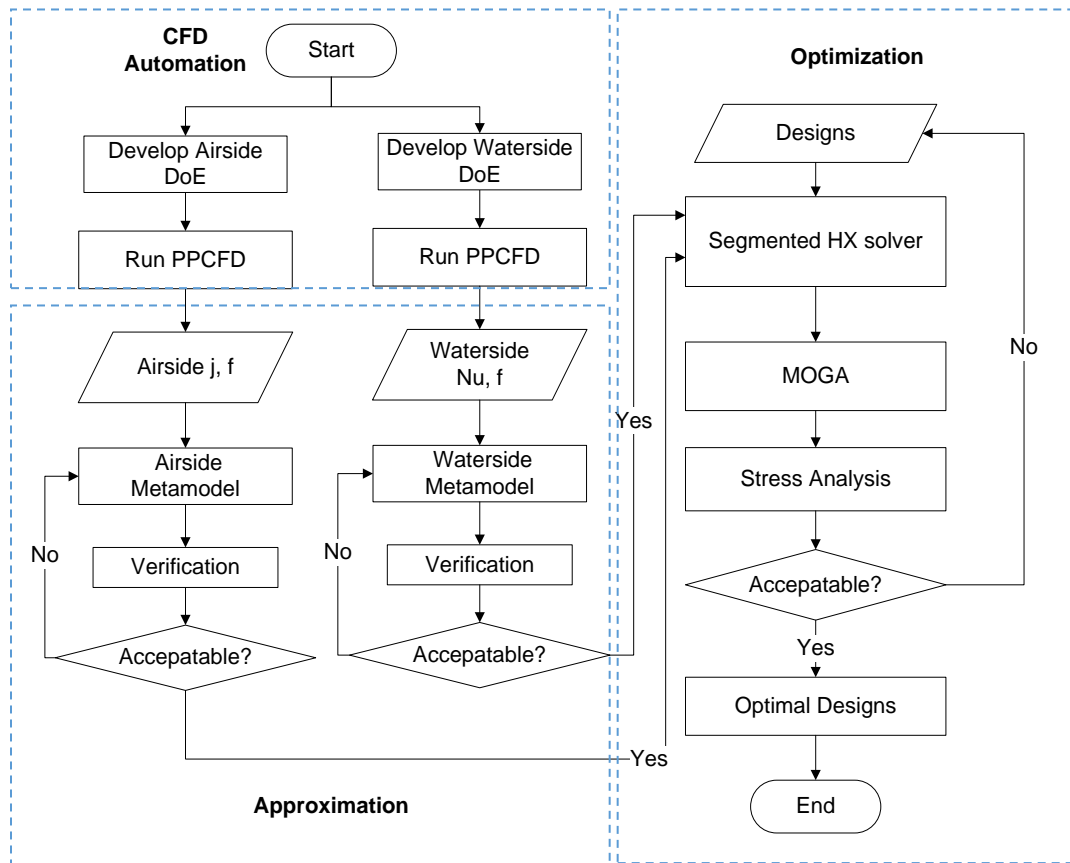
Figure 22 AAO flow chart

Chapter 3: Experimental Results and Discussions

3.1. *Dimensions of State-of-The-Art Heat Exchangers*

3.1.1. Round bare tube heat exchanger (BTHX)
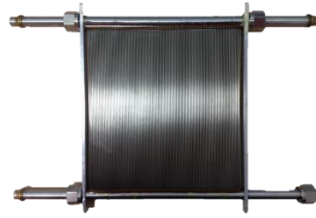
Figure 23 Picture of BTHX (OD=0.8 mm)

Round bare tube heat exchanger with small diameter had been proposed by Bacellar et al. (2014) and numerically investigated. However, no experimental work has been done for such heat exchangers. A prototype was manufactured using stainless steel bare tubes with outer diameter equals 0.8 mm, as shown in Figure 23. The dimension is $152\times150\times5$ mm.

3.1.2. sBTHX Shape optimized bare tube heat exchanger (sBTHX)

Shape optimized bare tube heat exchanger (sBTHX) with small diameter had been proposed by Bacellar et al. (2016) and numerically investigated. However, no experimental work has been done for such heat exchangers. A prototype was manufactured using 3D printing with air side hydraulic diameter equals 1.5 mm, as shown in Figure 24. The dimension is $100\times100\times18$ mm. And the material is titanium.
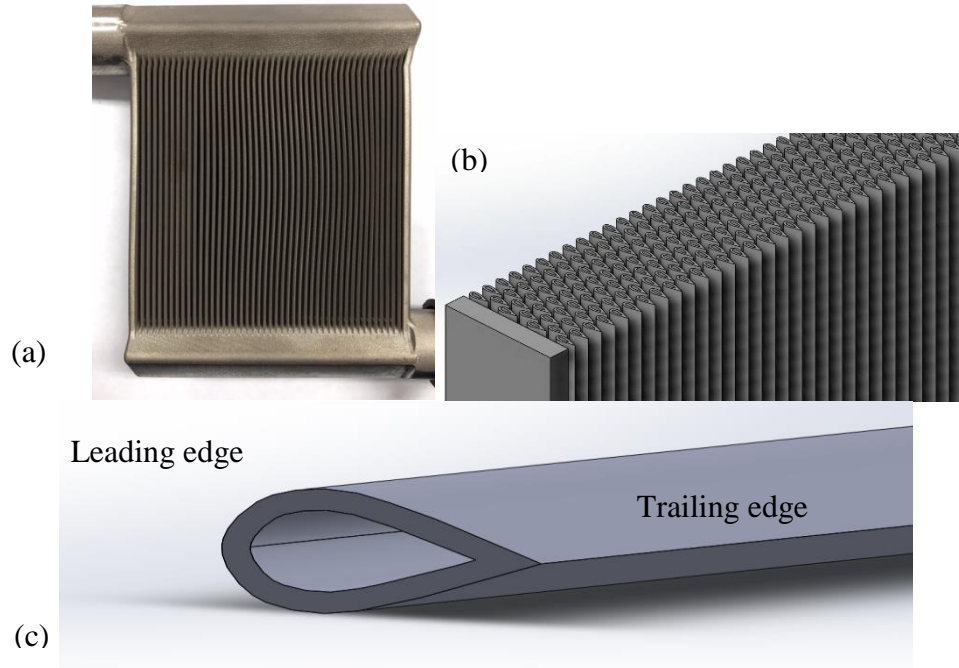
Figure 24 Pictures of sBTHX (D_h=1.5 mm) (a) overview, (b) tube pattern and (c) tube shape

3.1.3. Mini-channel heat exchanger (MCHX)

Figure 25 Picture of MCHX

A micro-channel heat exchanger was manufactured with dimension of 210×120×16 mm, as shown in Figure 25. It has the same air frontal area as the bare tube heat exchanger. Louvered fin pitch is 20. The material is aluminum.

Table 10 Dimensions of BTHX, sBTHX and MCHX

Type	Frontal area [m²]	Water cross section area [m²]	Air heat transfer area [m²]	Water heat transfer area [m²]	Envelop volume [m³]	Material volume [m³]	Material mass [kg]
BTHX	0.0228	0.0001	0.1826	0.1364	0.0001	0.000013	0.1269
sBTHX	0.0100	0.0002	0.2178	0.1100	0.0002	0.000020	0.1663
MCHX	0.0247	0.0002	0.5525	0.0735	0.0004	0.000060	0.1628
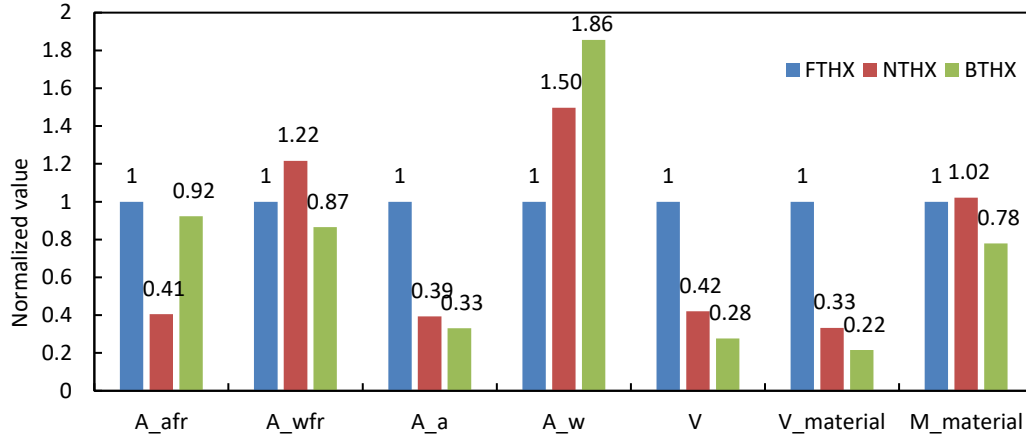
Figure 26 Comparison of dimensions of BTHX, sBTHX and MCHX

The dimensions of BTHX and sBTHX and MCHX are shown in Table 11 and normalized values are shown in Figure 26. The air frontal areas of BTHX and MCHX are similar. Due to the addition of fins, the air side heat transfer area of MCHX is about three times that of BTHC and sBTHX. BTHX and sBTHX have two thirds smaller volume and material volume than MCHX.

3.1.4. Slit fin-and-tube heat exchangers with tube diameter of 5 and 4 mm

Two slit fin-and-tube heat exchangers (Figure 27 and Figure 28) were manufactured by a company and the dimensions of these two heat exchangers are summarized in Table 11.
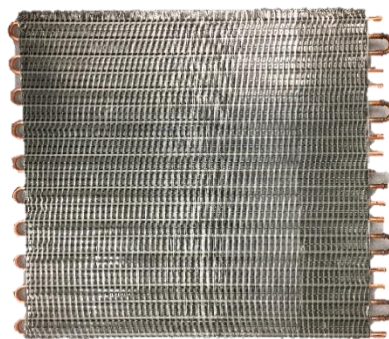
Figure 27 Picture of slit fin-and-tube heat exchanger (OD=5 mm)
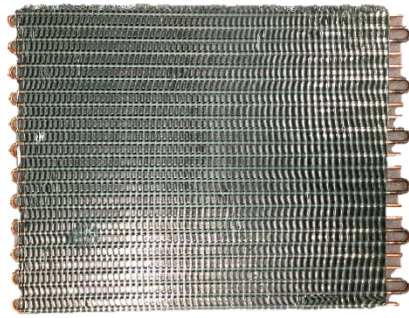
Figure 28 Picture of slit fin-and-tube heat exchanger (OD=4 mm)

Table 11 Dimensions of 5 and 4 mm slit fin-and-tube heat exchanger

	Primary Heat Transfer Area [m²]	Secondary Heat Transfer Area [m²]	Total Air Side Heat Transfer Area [m²]	Fin Material Volume [m³]	Tube Material Volume [m³]
5 mm	0.12	2.08	2.19	0.00011	0.000020
4 mm	0.12	1.83	1.94	0.00010	0.000020
	Tube Material Mass [kg]	Coil Length [m]	Coil Depth [m]	Coil Height [m]	Frontal Area [m²]
5 mm	0.21	0.39	0.011	0.38	0.148
4 mm	0.21	0.42	0.009	0.36	0.152

3.2. Experimental Test Using Air and Water Under Dry Condition

3.2.1. Test matrix for BTHX, sBTHX and MCHX

BTHX, sBTHX and MCHX are rated for about 1 kW, thus were tested using the same test matrix to make a fair comparison. Three different water flow rates and three different air flow rates were tested, as shown in Table 12. This test matrix was for comparing the performance of all three heat exchangers at dry condition.

Table 12 Test matrix for BTHX, sBTHX and MCHX

Test	Surface	Inlet Air Temperature [°C]	Inlet Air RH [%]	Inlet Water Temperature [°C]	Air Flow Rate [m³/s]	Water Flow Rate [g/s]
1	Dry	35	40	60	0.03	30
2	Dry	35	40	60	0.03	50
3	Dry	35	40	60	0.03	70
4	Dry	35	40	60	0.05	30
5	Dry	35	40	60	0.05	50
6	Dry	35	40	60	0.05	70
7	Dry	35	40	60	0.07	30
8	Dry	35	40	60	0.07	50
9	Dry	35	40	60	0.07	70

3.2.2. Test matrix for 4 and 5 mm slit fin-and-tube heat exchanger

Test matrix for 4 and 5 mm slit fin-and-tube heat exchanger is shown in Table 13.

Table 13 Test matrix for 4 and 5 mm slit fin-and-tube heat exchanger

Test	Surface	Inlet Air Temperature [°C]	Inlet Air RH [%]	Inlet Water Temperature [°C]	Air Velocity [m/s]	Air Flow Rate [m³/s]	Water Velocity [m/s]	Water Flow Rate [g/s]
1	Dry	35	40	60	1*	0.15	1.0	30
2	Dry	35	40	60	1	0.15	2.0	50
3	Dry	35	40	60	1	0.15	3.0	70
4	Dry	35	40	60	2.5	0.375	1.0	30
5	Dry	35	40	60	2.5	0.375	2.0	50
6	Dry	35	40	60	2.5	0.375	3.0	70
7	Dry	35	40	60	4*	0.6	1.0	30
8	Dry	35	40	60	4	0.6	2.0	50
9	Dry	35	40	60	4	0.6	3.0	70

3.2.3. Energy balance

The energy balance of all tests for each heat exchanger are all within $\pm 5\%$, as shown in Figure 29, Figure 30 and Figure 31.
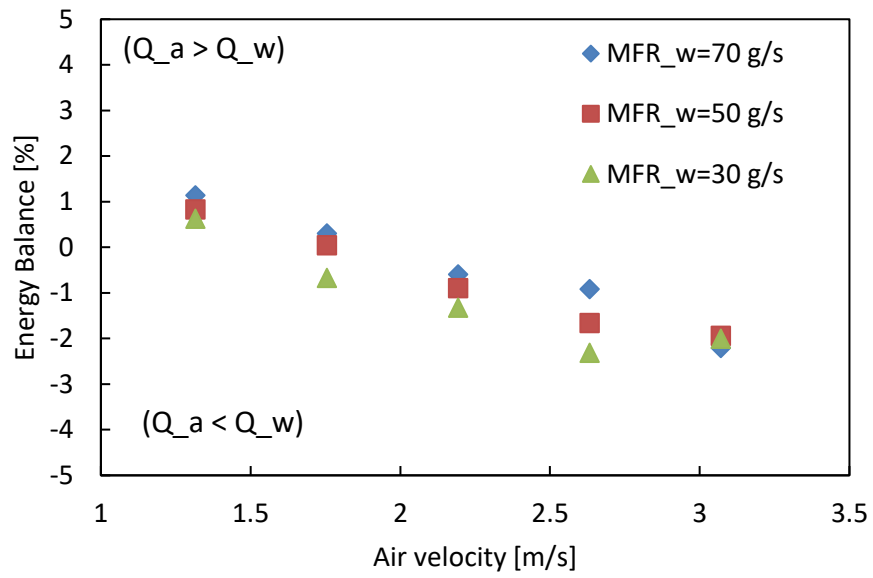
Figure 29 Energy balance of BTHX
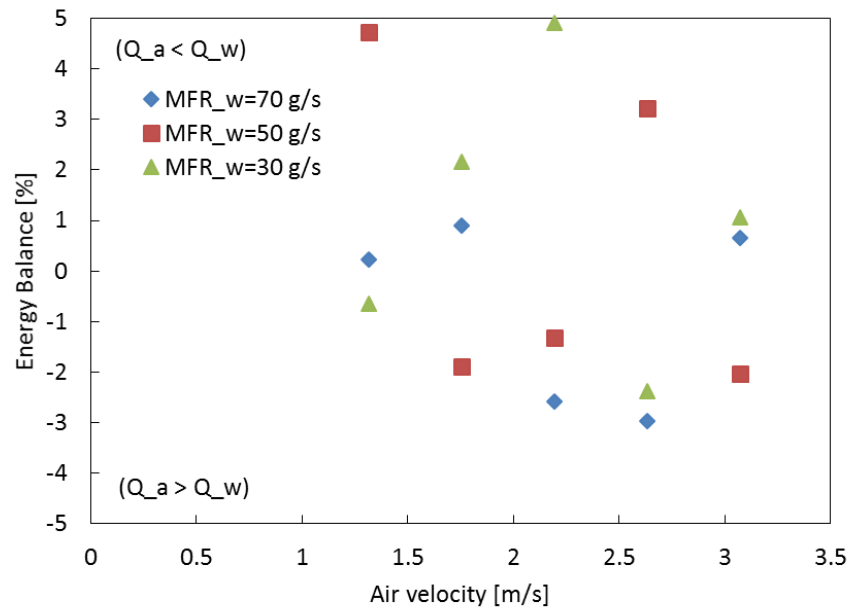
Figure 30 Energy balance of sBTHX
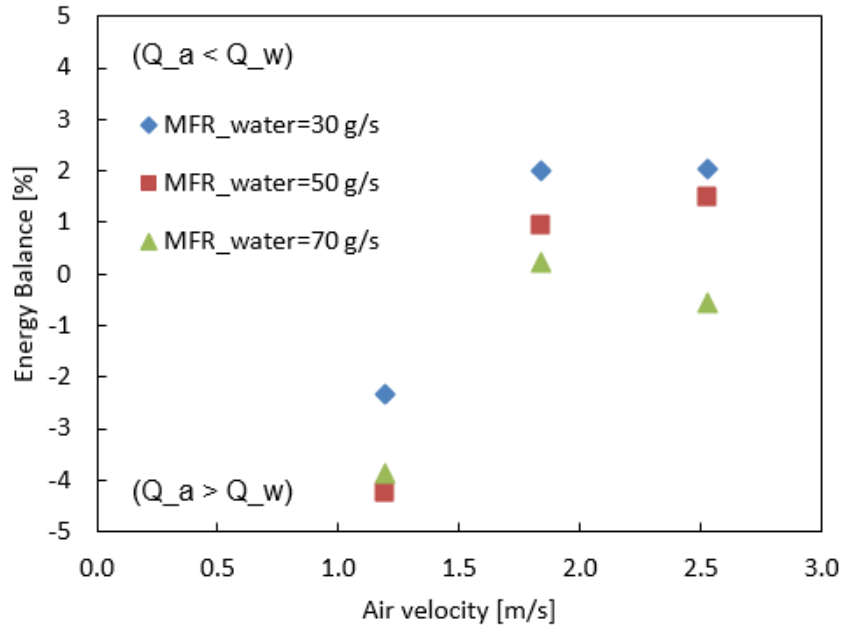
Figure 31 Energy balance of MCHX

3.2.4. Test results of BTHX

Figure 32 presents the heat exchanger capacity of BTHX, and airside pressure drop is shown in Figure 33. The airside heat transfer coefficient was calculated using Wilson plot method (Figure 34) and the results are shown in Figure 35. Chilton-Colburn j and f factor were calculated and plotted in Figure 36. The j and f factor correlations were developed using power law, as shown in Equation (70) and (71), as well as in Figure 37. A comparison of AHTC prediction of current correlation against existing correlations in literature further reveals the necessity of developing new correlations through experimental data, as shown in Figure 38.

$$j = 0.6499 \, \mathrm{Re}_{D_h}^{-0.496}, 175 \leq \mathrm{Re}_{D_h} \leq 400 \tag{70}$$

$$f = 1.0114 \, \mathrm{Re}_{D_h}^{-0.378}, 175 \leq \mathrm{Re}_{D_h} \leq 400 \tag{71}$$
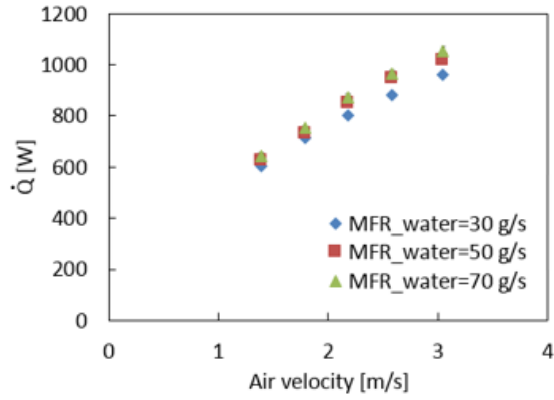
Figure 32 Heat exchanger capacity of BTHX
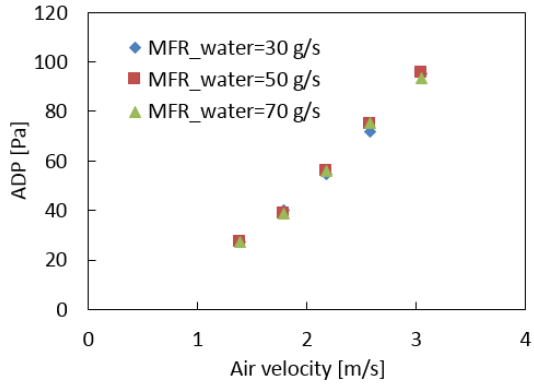
Figure 33 Airside pressure drop of BTHX
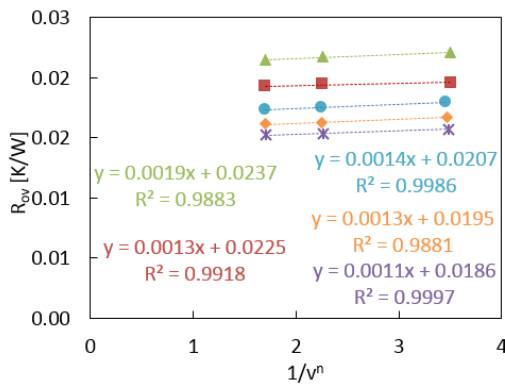
Figure 34 Airside Wilson plot of BTHX
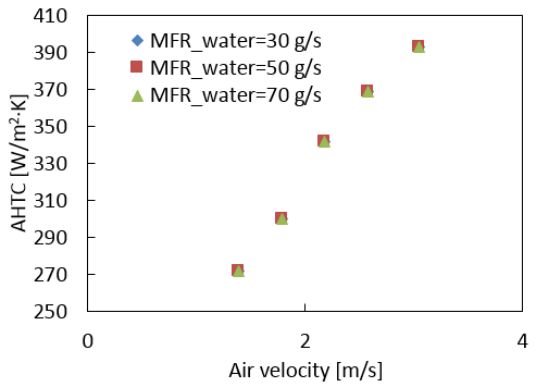
Figure 35 Airside heat transfer coefficient of BTHX
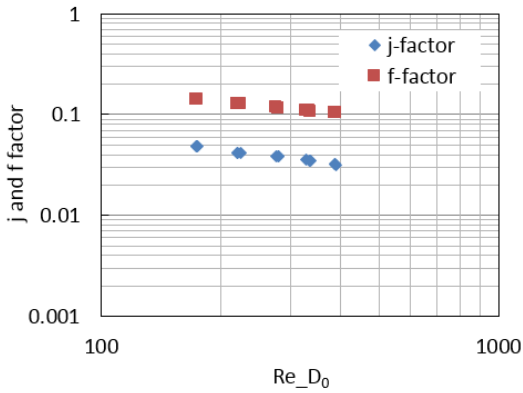
Figure 36 j and f factor of BTHX
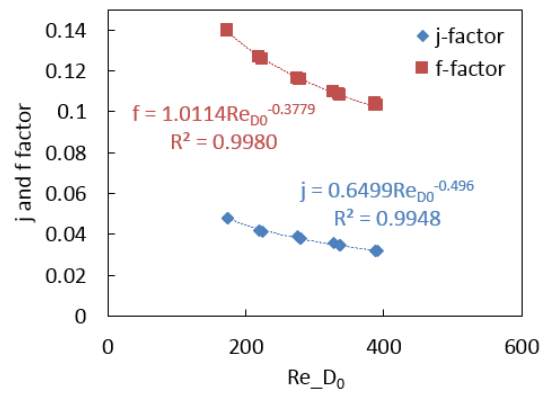
Figure 37 j and f factor power laws of BTHX
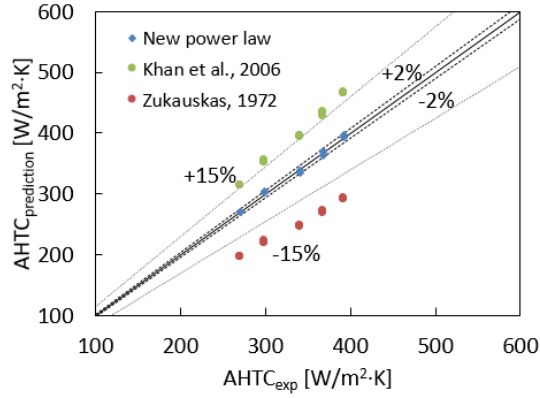
Figure 38 Comparison of correlations with experimental data for BTHX

3.2.5. Test results of sBTHX

Figure 39 presents the energy balance results, all of which were within ± 4.9%. Figure 40 presents the HX average capacity and airside pressure drop (ADP) is shown in Figure 41. Figure 42 presents the airside heat transfer coefficient using Wilson plot method (Wilson, 1915). AHTC is calculated for each airside velocity. Fitting equations for each velocity are shown on Figure 43, with y equals R_{ov} and x equals $1/V_w^n$. Chilton-Colburn j and f factor are shown in Figure 44. Note that the Reynolds number was calculated based on maximum velocity and airside hydraulic diameter due to the irregular tube shape. Hydraulic diameter is defined as:

$$D_h = \frac{4L_s A_{min}}{A_o} \tag{72}$$

where L_s is air flow pass depth and A_{min} is air free flow area.

There is no available correlation in literature for j and f factor for such geometry. Thus, new power law correlations of j and f factor against Reynolds number are developed, as shown in Figure 44. It should be noticed that Equations (73) and (74) could only be used for this certain heat exchanger geometry within the operation condition range as specified.

$$j = 1.1583 \cdot \mathrm{Re}_{D_h}^{-0.623} \, (562 \leq \mathrm{Re}_{D_h} \leq 1266, \mathrm{Pr} \approx 0.74, dry) \tag{73}$$

$$f = 1.3349 \cdot \mathrm{Re}_{D_h}^{-0.365} \, (562 \leq \mathrm{Re}_{D_h} \leq 1266, \mathrm{Pr} \approx 0.74, dry) \tag{74}$$

To examine the prediction of these new correlations and further explain the necessity of developing them, a comparison of new correlations against existing correlations for round bare tube bundle are presented in Figure 46 and Figure 47. When applying these equations, an equivalent diameter was used as outer diameter to ensure the minimum free flow area is the same. For AHTC prediction, discrepancy between experimental data and the new correlation prediction is within $\pm$ 2%. Zukauskas (1972) correlation gives a discrepancy of $\pm$ 15%. Predictions of Khan et al. (2006) correlation and Bacellar et al. (2016a) correlation fall beyond $\pm$ 15%. Even though Bacellar et al. (2016a) correlation is for bare tube bundle with small outer diameter of 0.5-2 mm (outer diameter of current design is 1.1 mm), the difference of tube shapes causes the inaccuracy of prediction. We can also conclude comparing with round tube, the new geometry has lower AHTC (though air side total heat transfer area is larger). It was already found that Zukauskas (1972) correlation over predicted ADP (Bacellar et al., 2016a) when using for small diameter tubes. So, for ADP prediction, only Bacellar et al. (2016a) correlation was used. The discrepancy between the prediction of new power law correlation and experimental data is within $\pm$ 2% while the maximum deviation of bare tube correlation prediction is about $\pm$ 25%. Thus, comparing with round tube, the new tube shape has lower ADP as well.
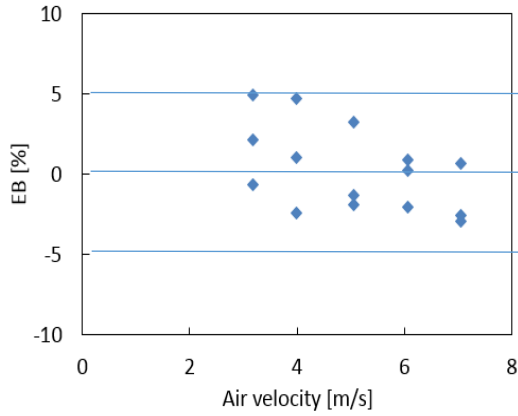
Figure 39 Energy balance of sBTHX
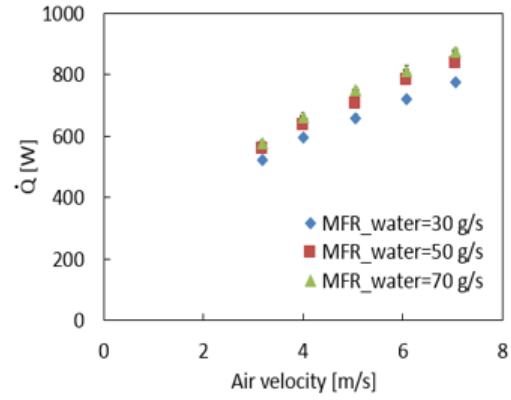
Figure 40 Heat exchanger average capacity of sBTHX
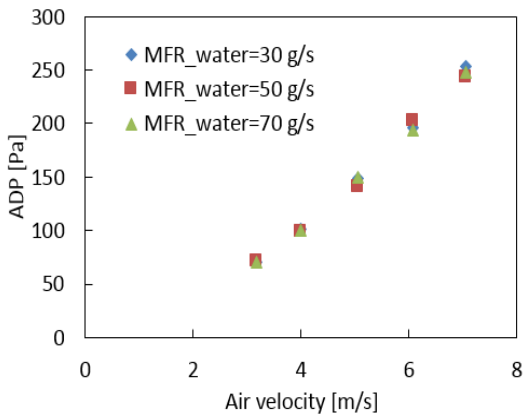
Figure 41 Air side pressure drop of sBTHX
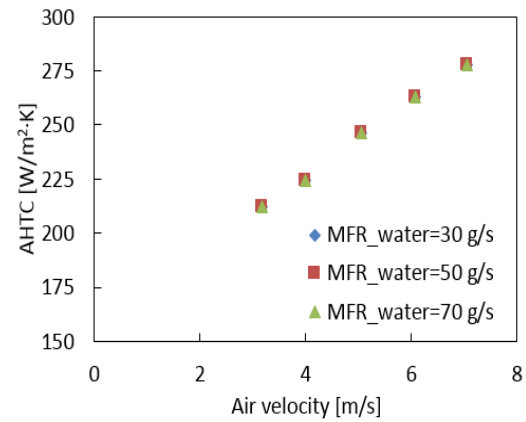
Figure 42 Air side heat transfer coefficient of sBTHX
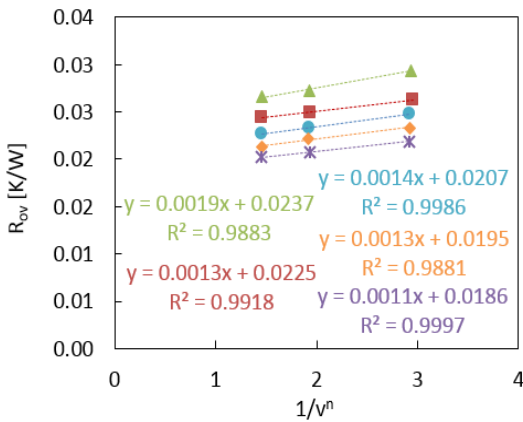
Figure 43 Wilson plot of sBTHX
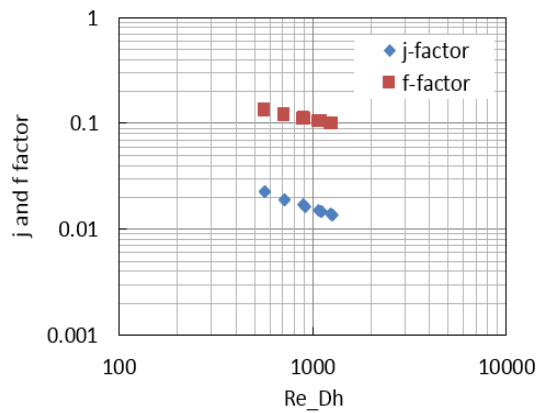
Figure 44 *j* and *f* factor of sBTHX
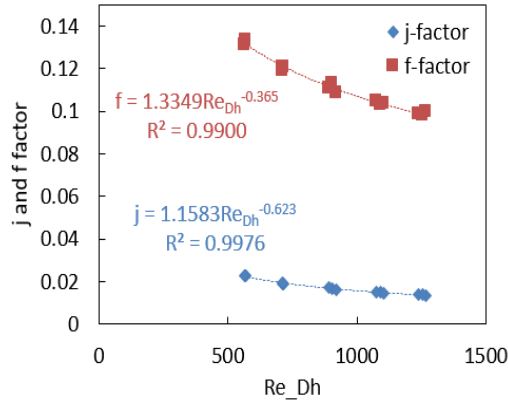
Figure 45 *j* and *f* factor correlation (sBTHX)
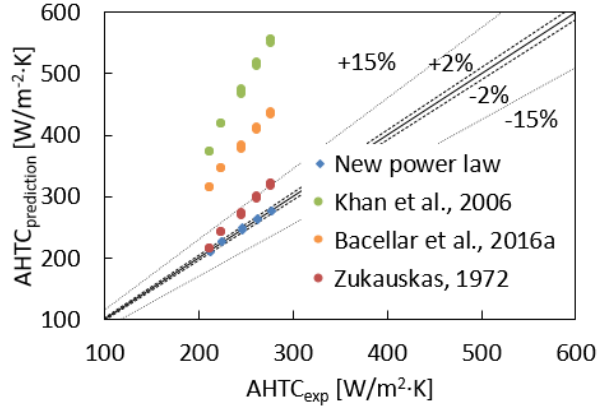
Figure 46 Comparison of AHTC prediction of new correlation against existing correlations (sBTHX)
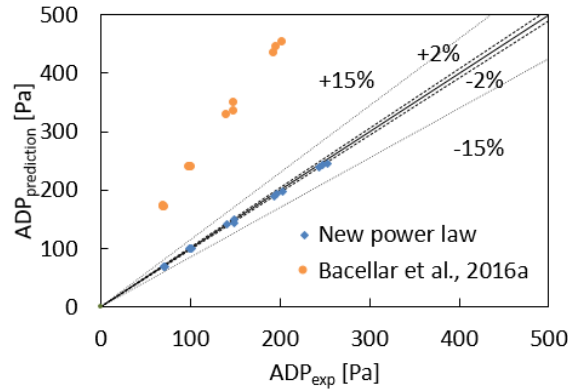
Figure 47 Comparison of ADP prediction of new correlation against existing correlations (sBTHX)

3.2.6. Test results of MCHX

HX average capacity is shown in Figure 48 and airside pressure drop (ADP) is shown in Figure 49. Test results are compared with simulation data from a software CoilDesigner® which is based on finite element heat exchanger model. The correlations used for airside are from Wang et al. (1999) while correlations used for waterside are from Dittus and Boelter (1930). Difference between simulated capacity and experimental data is within 6% (Figure 50) and maximum airside pressure drop discrepancy is 20% (Figure 51). Wilson plot graph is in Figure 52 and heat transfer

coefficient calculated using Wilson plot method is shown in Figure 53. The j and f factors are

plotted in Figure 54.
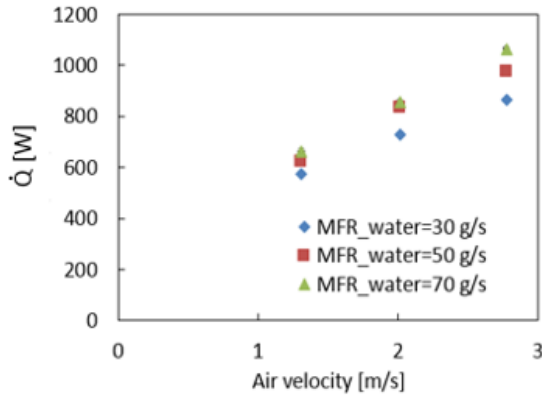
Figure 48 Heat exchanger capacity of MCHX
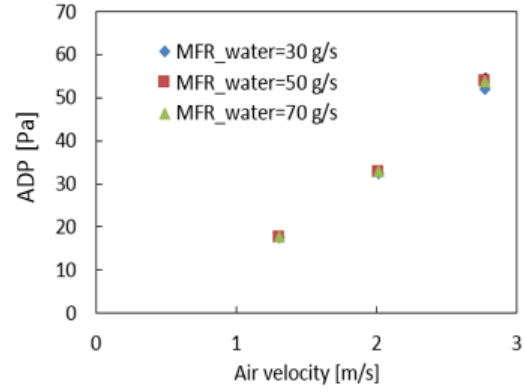
Figure 49 Airside pressure drop of MCHX
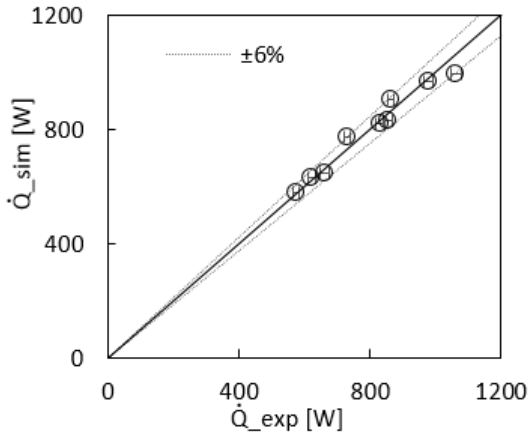
Figure 50 Simulation and experiments data comparison: heat exchanger capacity (MCHX)
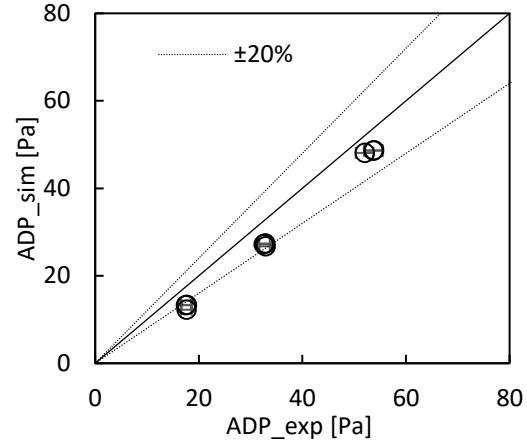
Figure 51 Simulation and experiments data comparison: airside pressure drop (MCHX)
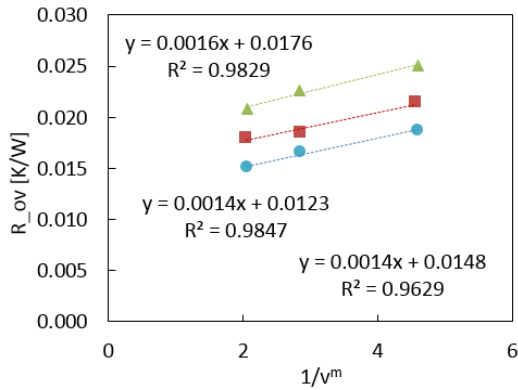
Figure 52 Wilson plot of MCHX
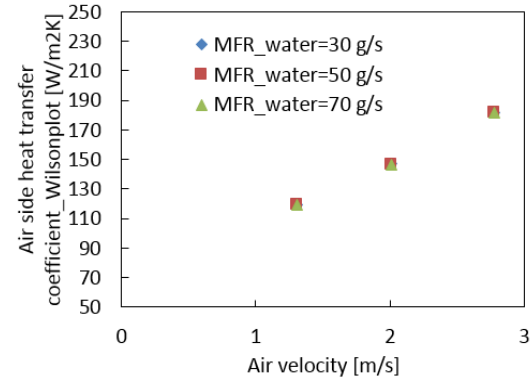
Figure 53 Airside heat transfer coefficient of MCHX
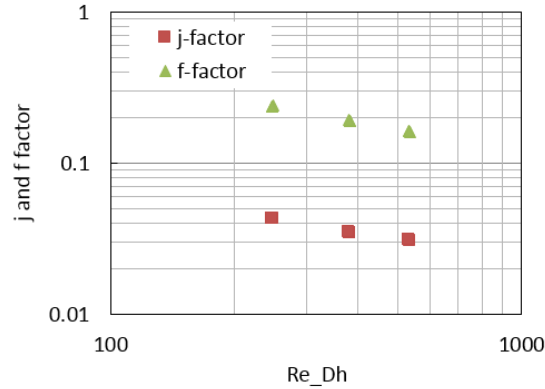
Figure 54 *j* and *f* factor of MCHX

3.2.7. Comparison of BTHX, sBTHX and MCHX

Capacity comparison: Heat exchanger capacities of three heat exchangers are shown in Figure 55, Figure 56 and Figure 57. The gradient of heat exchanger capacity over air velocity, which is the slope of the trend line, decreases as the air flow rate increases, and increases as water flow increases at a certain air velocity. This is because when the air flow rate increases or the water flow decreases, the portion of air side thermal resistance decreases, so the influence of air velocity on capacity diminishes, and vice versa. The gradient of heat exchanger capacity over water velocity, which could be seen by comparing the discrepancy of the trend lines, decreases as water flow rate increases, and increases as air flow rate increases. Similar reason could be used to explain this, which is that when water flow rate increases or air flow rate decreases, the portion of water side thermal resistance decreases, then the influence of water flow rate on capacity reduces. It should be noted that BTHX has the largest capacity among these three and it has larger benefit at lower water flow rate. This is meaningful at partial load condition.

Air side pressure drop comparison: The air side pressure drop is shown in Figure 58. The heat exchangers' air-side pressure drop increases non-linearly with the increase of air velocity and the slope increases as air velocity increases and this is because higher air velocity increases

frictional losses. The change in water flow rate causes the air density to change, resulting in a different air pressure drop, but the change is not significant. sBTHX has the largest air side pressure drop, followed by BTHX and MCHX. The reason is the face area of sBTHX is half of that of MCHX and BTHX and the air velocity at the same air side flow rate are higher. To make a fair comparison, the air side pressure drop is also plotted against air side velocity, as shown in Figure 60. By using the optimized tube shape design (sBTHX), the air pressure drop is lower than bare tube design (BTHX).

Water side pressure drop comparison: The water side pressure drop is summarized in Figure 59. The mini-channel heat exchanger has the largest water side pressure drop due to smallest water cross section area and largest water velocity.

Air side heat transfer coefficient: Figure 61 shows the air side heat transfer coefficient of three heat exchanges. It shows that BTHX has the largest heat transfer coefficient.
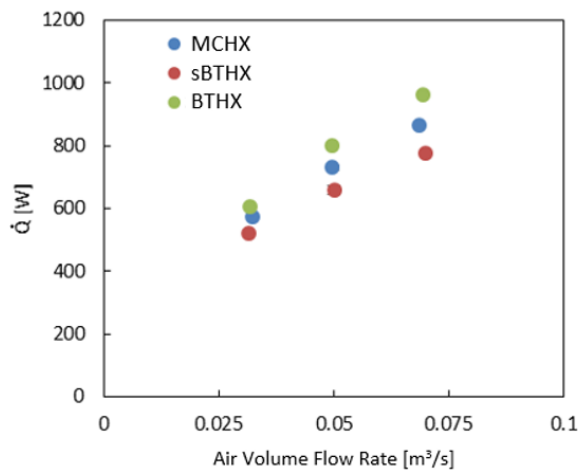
| **Figure 55 Capacity comparison of BTHX, sBTHX and MCHX at WFR=30 g/s** | **Figure 56 Capacity comparison of BTHX, sBTHX and MCHX at WFR=50 g/s** |
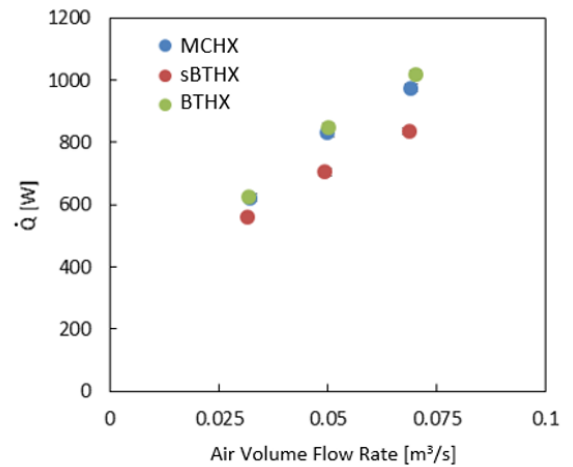
79
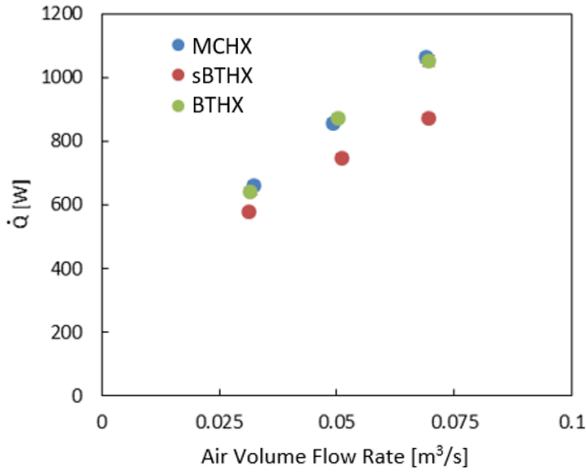
Figure 57 Capacity comparison of BTHX, sBTHX and MCHX at WFR=70 g/s
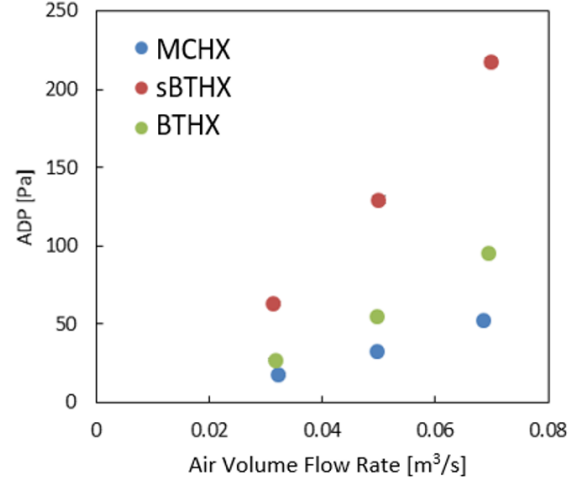
Figure 58 Air side pressure drop comparison of BTHX, sBTHX and MCHX
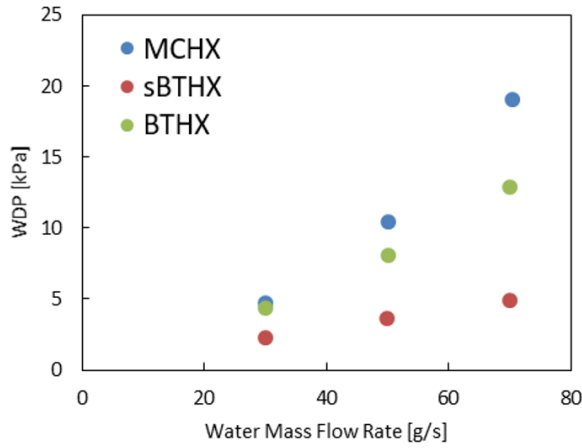
Figure 59 Water side pressure drop comparison of BTHX, sBTHX and MCHX
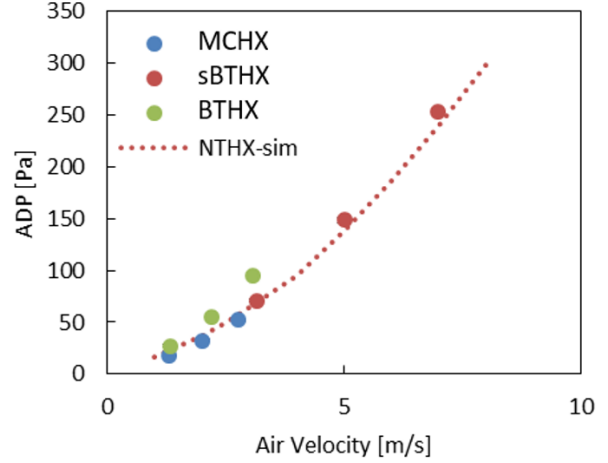
Figure 60 Air side pressure drop comparison of BTHX, sBTHX and MCHX
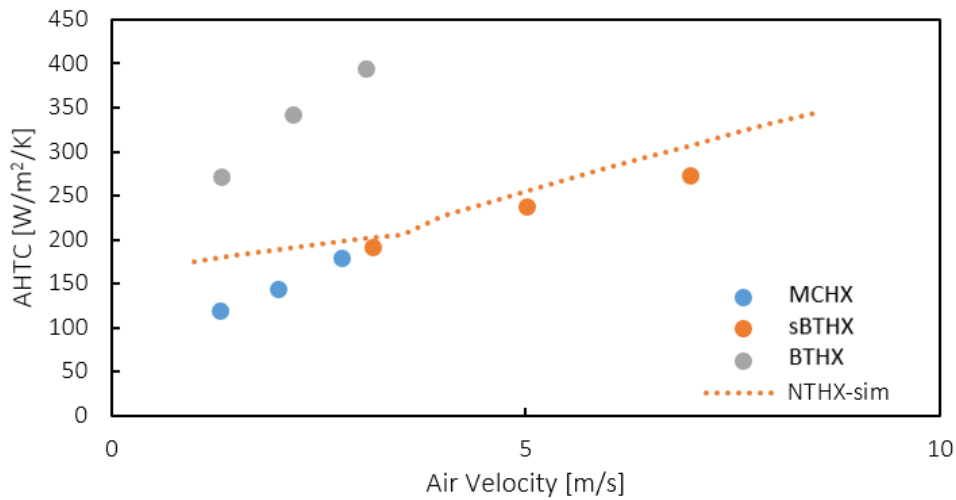
Figure 61 Air side heat transfer coefficient comparison of BTHX, sBTHX and MCHX

3.2.8. Test results of 5 and 4 mm slit fin-and-tube heat exchanger

Energy balances of 5 and 4 mm fin-and-tube heat exchanger test results are shown in Figure 62 and Figure 63. They are all within ±5%.
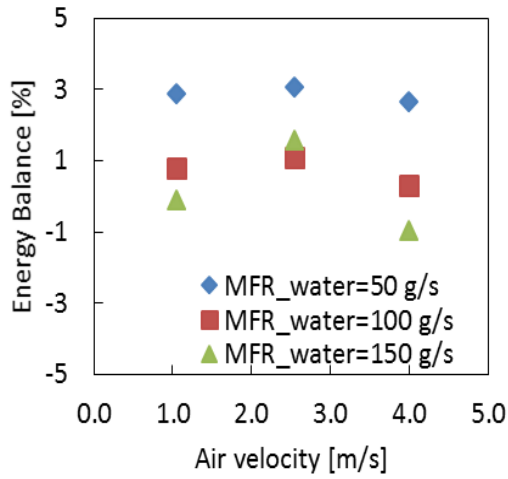
Figure 62 Energy balance of 5 mm coil
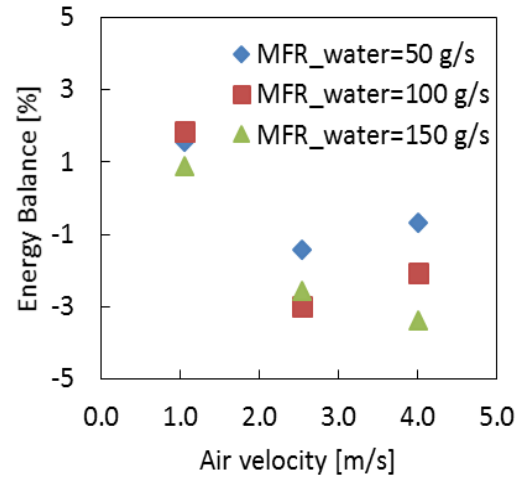
Figure 63 Energy balance of 4 mm coil
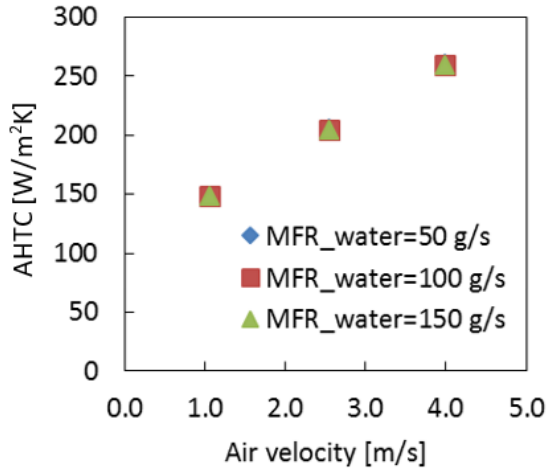
Figure 64 AHTC for 5 mm HX
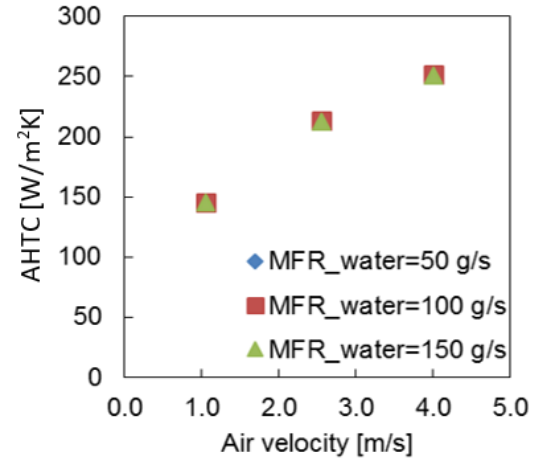
Figure 65 AHTC for 4 mm HX
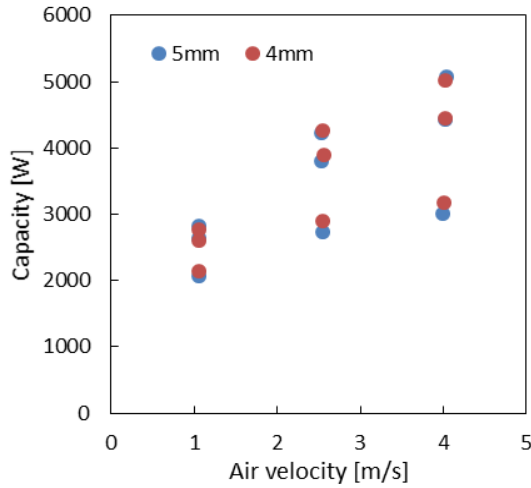
Figure 66 Capacity comparison of 5 and 4 mm HX
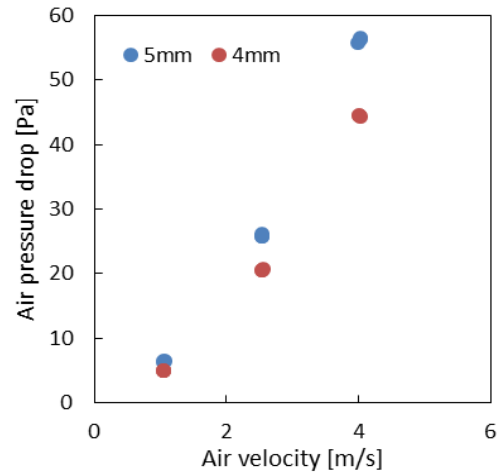
Figure 67 Air pressure drop comparison of 5 and 4 mm HX
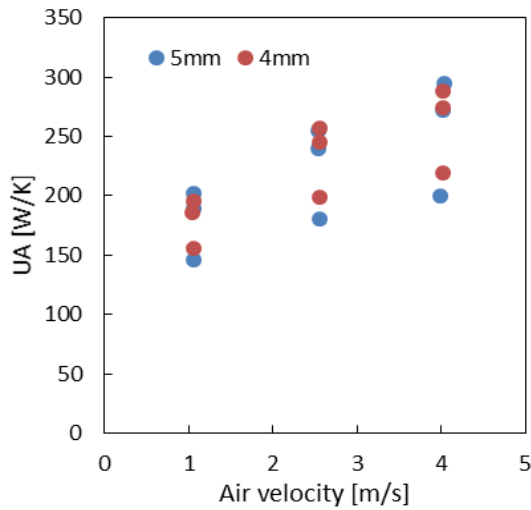
Figure 68 UA value comparison of 5 and 4 mm HX
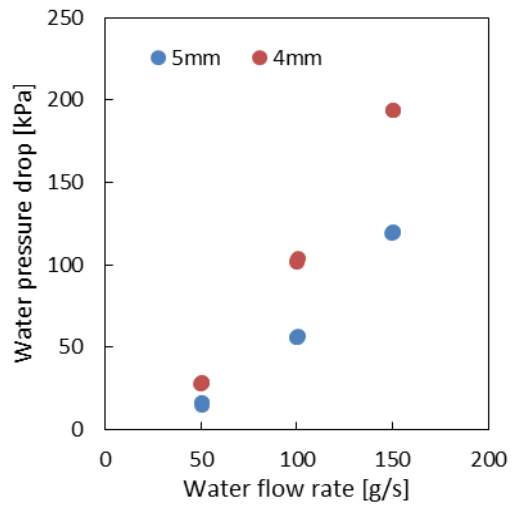
Figure 69 Water pressure drop comparison of 5 and 4 mm HX

Thermal performance: From heat transfer point of view, there is not much difference between 4 and 5 mm slit fin-and-tube heat exchangers. The capacities are shown in Figure 66. The heat transfer coefficients which were calculated based on Wilson plot are shown in Figure 64 and Figure 65, separately. The heat transfer areas for 4 and 5 mm heat exchanger are 19.4 and 2.19 m^2, respectively. Thus, the UA values of 4 and 5 mm heat exchanger are not much different, as shown in Figure 68.

82

Hydraulic performance: The air side pressure drops of 4 and 5 mm heat exchanger are shown in Figure 67. Water side pressure drops are shown in Figure 69. The reason that 4 mm heat exchanger has lower air pressure drop is due to smaller fin number. The higher water pressure drop for 4 mm heat exchanger is due to longer circuit length.

The 4 and 5 mm coils' j and f factors are compared with test data from literature (Wang et al., 2001) for traditional slit fin-and-tube heat exchangers with larger diameter (7.6 mm). As shown in Figure 70 and Figure 71, j and f factors for both 4 and 5 mm coil are larger than 7.6 mm diameter heat exchanger. The j and f factors calculated using correlation from Wang et al. (2001) are also shown in these two graphs.
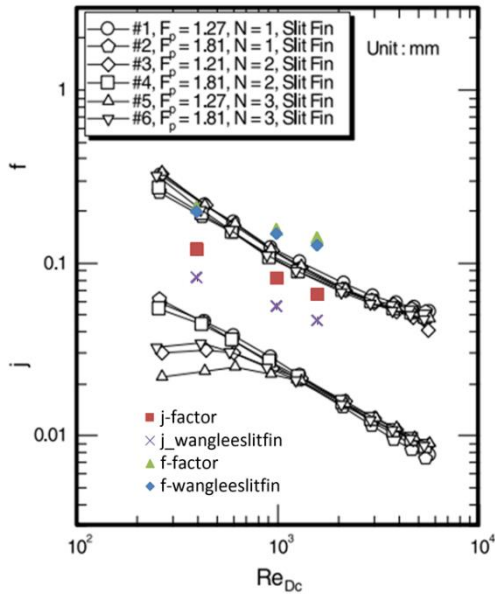
Figure 70 Comparison of j and f factor of 4 mm heat exchanger with literature data (7.6 mm, Wang et al., 2001)
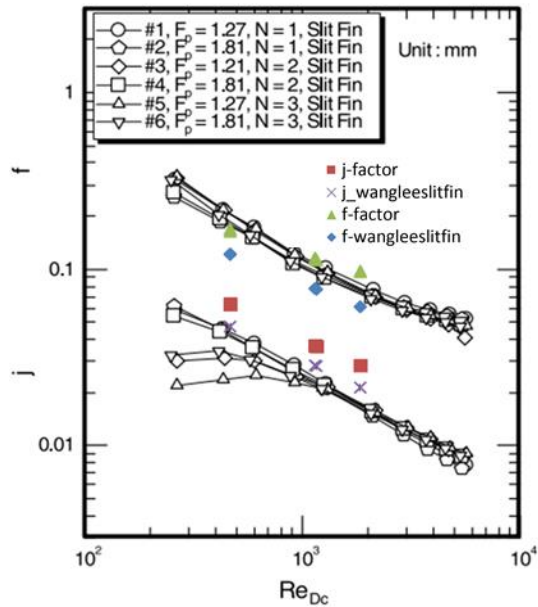
Figure 71 Comparison of j and f factor of 5 mm heat exchanger with literature data (7.6 mm, Wang et al., 2001)

3.3. _Experimental Test Using Air and Water Under Dehumidifying Condition_

3.3.1. Test matrix for BTHX

Among three 1 kW heat exchangers, BTHX was tested under wet condition for both vertical (Figure 72) and horizontal tube orientation (Figure 73), and the test matrix is shown in Table 14. Three different air flow rates, three different water flow rates and three different inlet air relative humidity were tested.

Table 14 Wet condition test matrix for BTHX

Test	Inlet Air Temperature [°C]	Inlet Air RH [%]	Inlet Water Temperature [°C]	Air Flow Rate [m³/s]	Water Flow Rate [g/s]
1	26.7	35	7.2	0.03	20
2	26.7	35	7.2	0.03	35
3	26.7	35	7.2	0.03	50
4	26.7	35	7.2	0.06	20
5	26.7	35	7.2	0.06	35
6	26.7	35	7.2	0.06	50
7	26.7	35	7.2	0.09	20
8	26.7	35	7.2	0.09	35
9	26.7	35	7.2	0.09	50
10	26.7	50	7.2	0.03	20
11	26.7	50	7.2	0.03	35
12	26.7	50	7.2	0.03	50
13	26.7	50	7.2	0.06	20
14	26.7	50	7.2	0.06	35
15	26.7	50	7.2	0.06	50
16	26.7	50	7.2	0.09	20
17	26.7	50	7.2	0.09	35
18	26.7	50	7.2	0.09	50
19	26.7	70	7.2	0.03	20
20	26.7	70	7.2	0.03	35
21	26.7	70	7.2	0.03	50
22	26.7	70	7.2	0.06	20
23	26.7	70	7.2	0.06	35
24	26.7	70	7.2	0.06	50
25	26.7	70	7.2	0.09	20
26	26.7	70	7.2	0.09	35
27	26.7	70	7.2	0.09	50

Figure 72 Vertical tube orientation of BTHX under wet condition
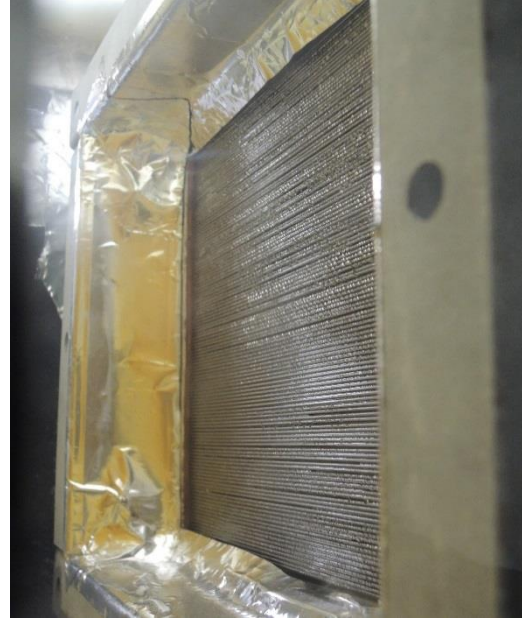
Figure 73 Horizontal tube orientation of BTHX under wet condition

3.3.2. Test matrix of sBTHX

The test matrix of sBTHX under wet condition is summarized in Table 15.

Table 15 Test matrix for sBTHX

Test	Inlet Air Temperature	Inlet Air RH	Inlet Water Temperature	Air Velocity	Water Mass Flow Rate
	[°C]	[%]	[°C]	[m/s]	[g/s]
1	26.7	50	12.0	0.03	20
2	26.7	50	12.0	0.03	35
3	26.7	50	12.0	0.03	50
4	26.7	50	12.0	0.06	20
5	26.7	50	12.0	0.06	35
6	26.7	50	12.0	0.06	50
7	26.7	50	12.0	0.09	20
8	26.7	50	12.0	0.09	35
9	26.7	50	12.0	0.09	50
10	26.7	70	12.0	0.03	20
11	26.7	70	12.0	0.03	35
12	26.7	70	12.0	0.03	50
13	26.7	70	12.0	0.06	20
14	26.7	70	12.0	0.06	35
15	26.7	70	12.0	0.06	50
16	26.7	70	12.0	0.09	20
17	26.7	70	12.0	0.09	35
18	26.7	70	12.0	0.09	50

3.3.3. Test matrix of 4 and 5 mm slit fin-and-tube heat exchanger

Both 4 and 5 mm slit fin-and-tube heat exchangers are tested under wet condition. The test matrix is shown in Table 16.

Table 16 Test matrix for 5 and 4 mm slit fin-and-tube heat exchanger

Test	Inlet Air Temperature [°C]	Inlet Air RH [%]	Inlet Water Temperature [°C]	Air Velocity [m/s]	Water Velocity [m/s]
1	26.7	50	7.2	1	1.0
2	26.7	50	7.2	1	2.0
3	26.7	50	7.2	1	3.0
4	26.7	50	7.2	2.5	1.0
5	26.7	50	7.2	2.5	2.0
6	26.7	50	7.2	2.5	3.0
7	26.7	50	7.2	4	1.0
8	26.7	50	7.2	4	2.0
9	26.7	50	7.2	4	3.0

3.3.4. Test results for BTHX

This heat exchanger prototype was tested under both vertical and horizonal orientations, as summarized in Table 1. The inlet air conditions were fixed dry bulb temperature of 26.7°C with various relative humidity of 35%, 50% and 70%. The inlet air frontal velocity varied at 3, 6 and 9 m/s. The inlet water temperature was 12°C and the water mass flow rates were 20, 35 and 50 g/s, respectively. For the horizontal orientation test, only conditions of the smallest and largest air velocity were tested.

The results from the wet test conditions are summarized in Figure 74 through Figure 83, where vertical orientation is on the left and horizontal orientation is on the right. Energy balance (EB) for all data points are within ±5%, as shown in Figure 74 and Figure 75. Here the effects of inlet air humidity, air flow rate and water flow rate and orientation on heat exchanger capacity, sensible capacity, latent capacity and airside pressure drop (ADP) are discussed.

3.3.4.1. Effect of inlet air relative humidity (RH)

When inlet air relative humidity (RH) is 35%, the heat exchanger is at dry condition, meaning there is only sensible cooling. As inlet air relative humidity increases from 35% to 70%, overall heat transfer capacity increases (Figure 76) for the vertical tube orientation tests. However, when air RH changes from 35% to 50%, heat exchanger capacity decreases slightly at horizontal orientation (Figure 77). Increased RH also leads to lower sensible capacity (SC), as shown in Figure 78 and Figure 79. This is because higher inlet air humidity leads to additional condensing water accumulation on the heat exchanger surface, which reduces dry surface area and restrains sensible capacity transfer. Accordingly, latent capacity increases (Figure 80 and Figure 81) as inlet RH increases. In terms of airside pressure drop, larger inlet air humidity results in larger airside pressure drop due to the bridging effect formed by retained condensate water between the tubes (Figure 82 and Figure 83).

3.3.4.2. Effect of inlet air flow rate (AFR)

As air flow rate (AFR) increases, total capacity (Figure 76 and Figure 77), sensible capacity (Figure 78 and Figure 79) and airside pressure drop (Figure 82 and Figure 83) all increase while latent capacity either increases or decreases (Figure 80 and Figure 81). The change of latent capacity is also affected by other factors such as inlet air humidity, water flow rate, condensate removal, heat exchanger orientation and heat exchanger geometry. For this HX, the latent capacity either decreases or increases depending on test condition (Figure 80 and Figure 81). Generally, as air flow rate increases, total capacity increases, causing water outlet temperature to increase, resulting in higher average wall temperature. The latent capacity transfer is expected to decrease due to increased wall surface temperature. However, larger air flow rate also means more moisture in the air stream, which produces more condensation. Besides, there are also other factors need to

be considered such as the ease of condensate water removal. Thus, whether latent capacity increases or decreases depends on which factor is dominant. Here explains the effect of AFR under vertical orientation. The most crucial factor under vertical orientation is the inlet air RH. When inlet air RH is low, the surface is partially wet and sensible capacity transfer is the dominant factor, leading to latent capacity decrease. This phenomenon was observed in the experiment, as shown in Figure 84 (a) and (b). Compare the results at AFR=0.06 and 0.09 m^3/s, it can be noticed that as air flow rate increases, wet surface area becomes smaller and dry surface area becomes larger, especially on the top of the heat exchanger. When inlet air RH is high, the surface is fully wet, the extra moisture in the air becomes the dominant factor, causing latent capacity to increase. Figure 84 (c) and (d) show that both surfaces are fully wet. Next, the effect of AFR under horizontal orientation will be explained. Here, the most crucial factor is removal of condensate water. At horizontal orientation, it is hard to remove the condensate water at low flow rate due to the orientation, as shown in Figure 85 (a). Instead of flowing along the tubes as in the cases of vertical orientation, condensate water just accumulates in between the tubes and forms a water bridge if the air flow is not strong enough. At higher velocity as shown in Figure 85 (b), the condensate water is blown out by the incoming air flow. Water splashes in the downstream of air flow, leaving water marks on the wind tunnel duct wall. For pressure drop, higher air flow rate results in higher ADP, which is expected (Figure 82 and Figure 83). One interesting phenomenon is under vertical orientation, airside pressure drop for RH=35% and 70% is not much affected by waterside flow rate, but airside pressure drop for RH=50% increases as water flow rate increases. This is because for each heat exchanger geometry, there is a certain maximum amount of water retention corresponding to a specific condition. When RH is 50%, the amount of retained water has not reached its maximum yet, thus the increase of waterside flow rate will cause latent capacity

increase, enhancing the bridging effect. When RH is 70%, the amount of retained water has reached maximum, and consequently the extra condensing water flows down the tubes.

3.3.4.3.   Effect of inlet water flow rate (WFR)

As water flow rate increases, total capacity (Figure 76 and Figure 77), sensible capacity (Figure 78 and Figure 79) and latent capacity (Figure 80 and Figure 81) all increase. Water flow rate increase has a negligible effect on airside pressure drop when inlet air RH=35% and 70% but it leads to airside pressure drop increase when RH=50%. This has been discussed previously.

3.3.4.4.   Effect of heat exchanger tube orientation

When there is no water condensate, there is no difference regarding total capacity, sensible capacity, latent capacity and airside pressure drop between heat exchanger operating under either orientation. Under the wet conditions, compared with heat exchanger under vertical tube orientation, the horizontal tube orientation tests show smaller total capacity (Figure 76 and Figure 77), sensible capacity (Figure 78 and Figure 79) and latent capacity (Figure 80 and Figure 81). However, the airside pressure drops (Figure 82 and Figure 83) under horizontal tube orientation are larger than those under vertical tube orientation due to bridging effect. Thus, it is recommended to operate this heat exchanger under vertical orientation if there is condensation.
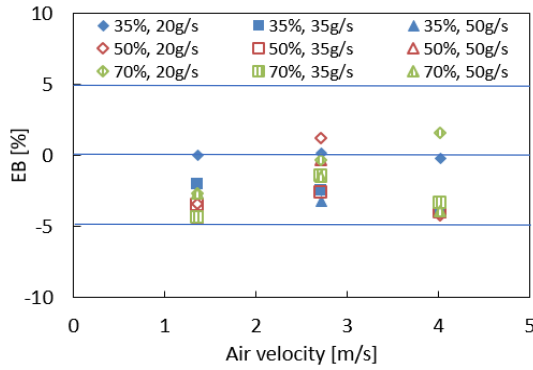
Figure 74 Energy balance (BTHX, vertical)
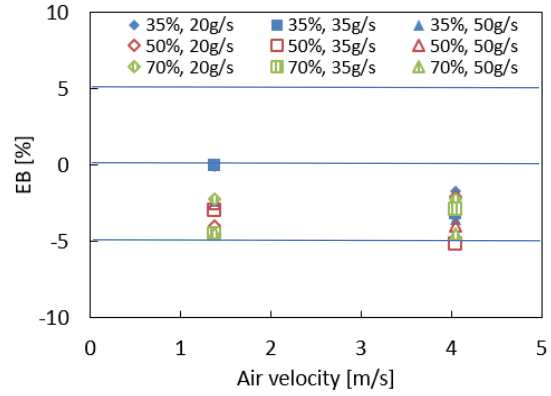
Figure 75 Energy balance (BTHX, horizontal)
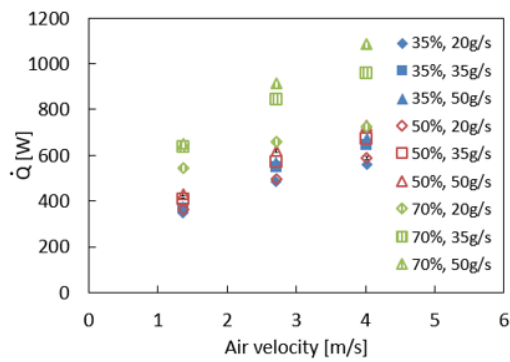
Figure 76 Heat exchanger capacity (BTHX, vertical)
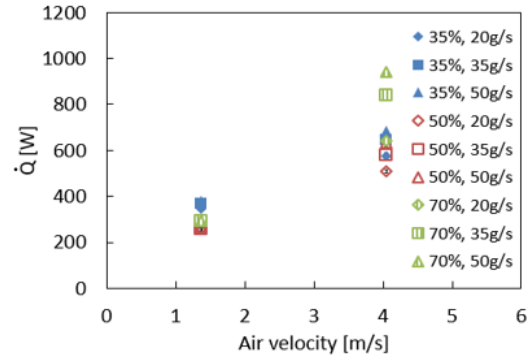
Figure 77 Heat exchanger capacity (BTHX, horizontal)
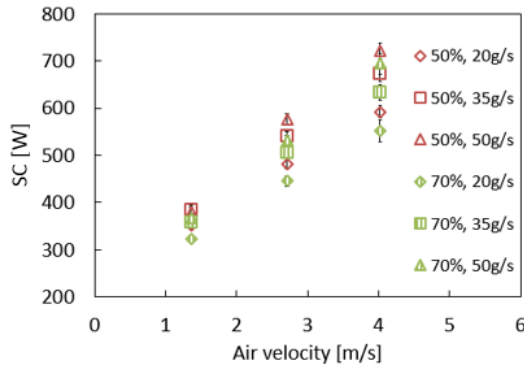
Figure 78 Sensible capacity (BTHX, vertical)
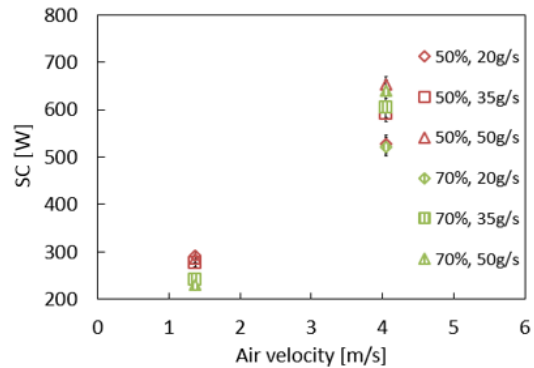
Figure 79 Sensible capacity (BTHX, horizontal)

90
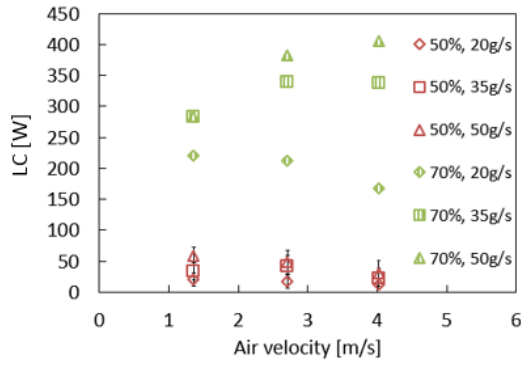
Figure 80 Latent capacity (BTHX, vertical)
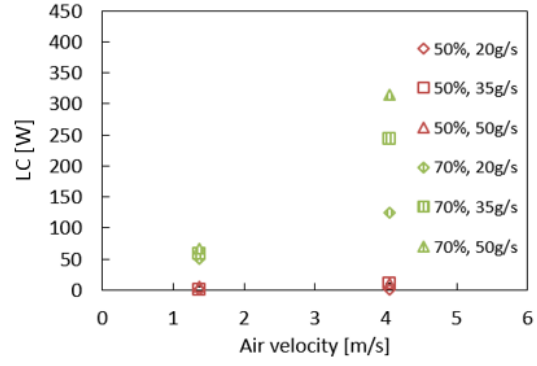
Figure 81 Latent capacity (BTHX, horizontal)
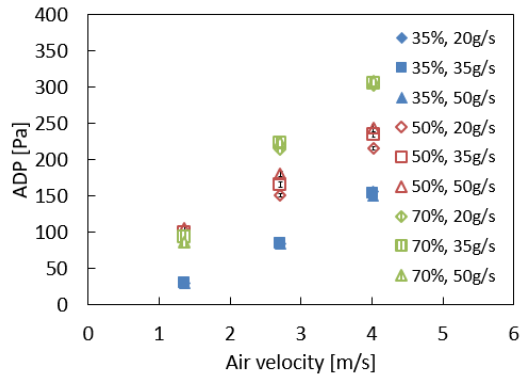
Figure 82 Airside pressure drop (BTHX, vertical)
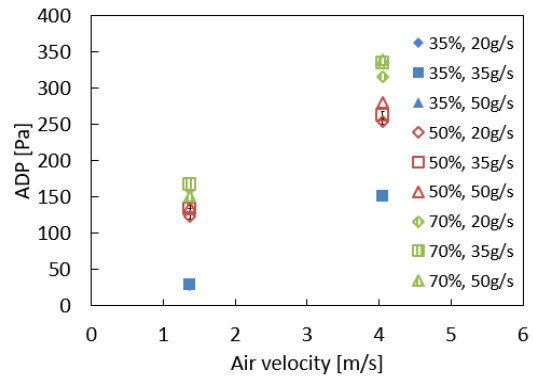
Figure 83 Airside pressure drop (BTHX, horizontal)

(a)
RH=50%, WRF=50 g/s AFR=0.06 m^3/s

(b)
RH=50%, WRF=50 g/s AFR=0.09 m^3/s

(c)
RH=70%, WRF=50 g/s AFR=0.06 m^3/s

(d)
RH=70%, WRF=50 g/s AFR=0.09 m^3/s
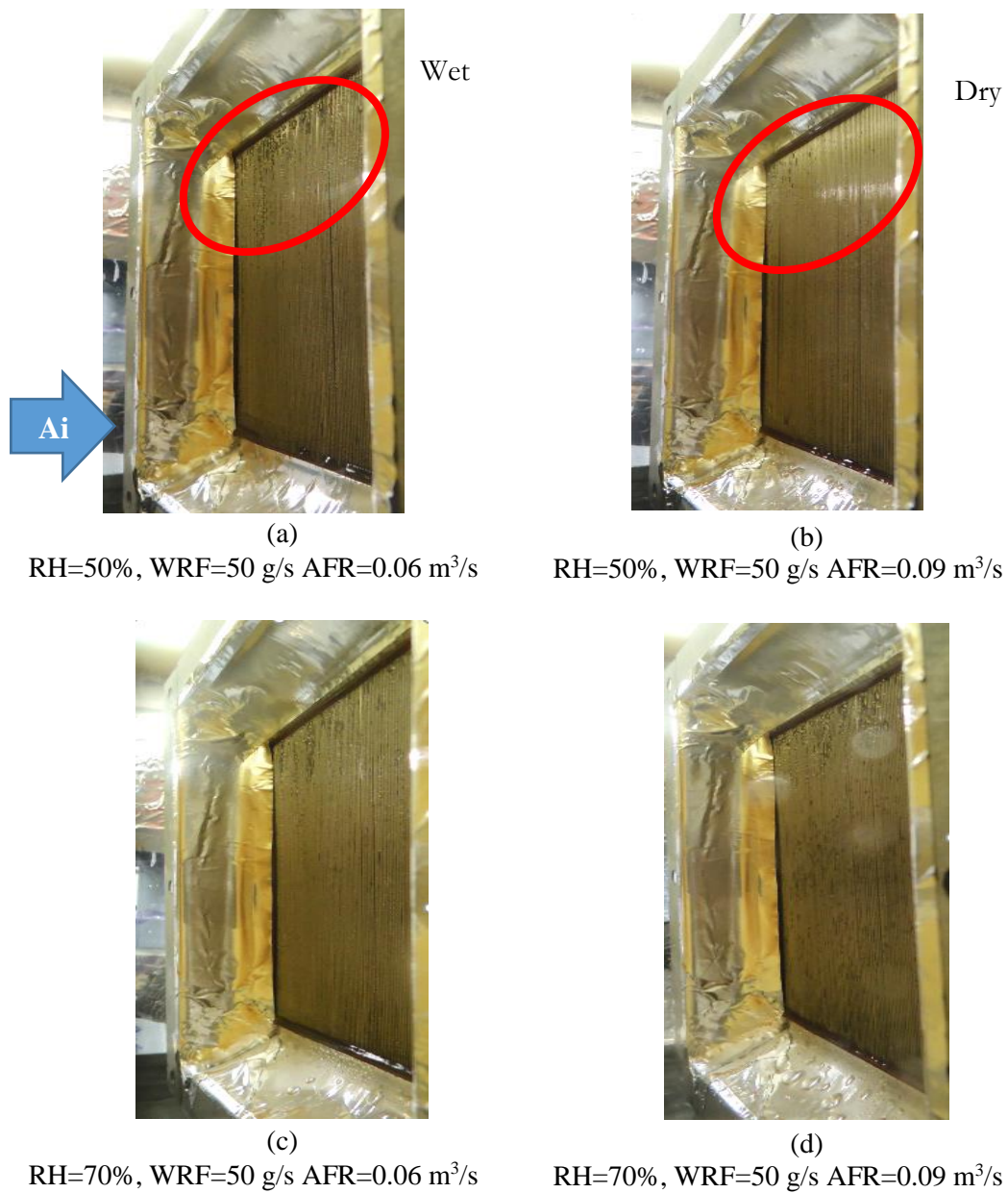
Figure 84 Effect of air flow rate on condensation at RH=50% (a)(b) and RH=70% (c)(d) under vertical orientation (BTHX)

| No blow out effect | Water marks due to blow out effect |

(a)
RH=70%, AFR=0.03 m³/s,
WRF=35 g/s

(b)
RH=70%, AFR=0.09 m³/s,
WRF=35 g/s
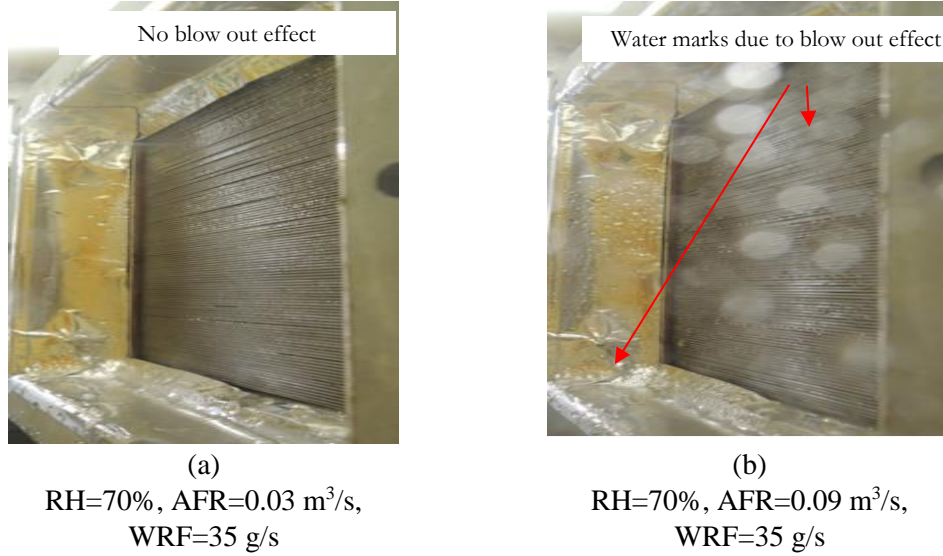
Figure 85 Effect of air flow rate on condensation at RH=70% under horizontal orientation (BTHX)

3.3.4.5.   j, j_m and f factors

Here the j, j_m and f factor results are discussed only under the preferred vertical tube orientation. As it was already demonstrated, existing j and f factor correlations for bare tube bundles under dry condition in literature are not applicable for such small diameter tubes (Bacellar et al., 2016a) and there are no available wet condition correlations, so that new correlations are developed.

Figure 86 presents the variation of f factor on the effect of inlet air RH and Reynolds number. Friction increases as inlet air RH increases from 35% to 70% due to the bridging effect of condensate water. Correlations of f factor were developed as power law based on Reynolds number, as shown in Equation (75), (76) and (77). Maximum deviation for f factor is within $\pm 2\%$ under dry condition and $\pm 15\%$ under wet condition (Figure 87).

$$f = 1.705 \cdot \text{Re}_{D_o}^{-0.45} (200 \leq \text{Re}_{D_o} \leq 600, \text{Pr} \approx 0.74, dry) \tag{75}$$

$$f = 209.33 \cdot \text{Re}_{D_o}^{-1.157} (200 \leq \text{Re}_{D_o} \leq 600, \text{Pr} \approx 0.74, RH = 50\%) \tag{76}$$

93

$$f = 38.67 \cdot \text{Re}_{D_o}^{-0.837} (200 \leq \text{Re}_{D_o} \leq 600, \text{Pr} \approx 0.74, RH = 70\%) \tag{77}$$

Figure 88 and Figure 90 present the variation of j and j_m factor by the effect of inlet air RH and Reynolds number. The variation of j and j_m factor by the relative humidity effect of inflow air is not sensitive. This is consistent with observations by Wang et al. (2000) and Phan et al. (2011). Correlations of j and j_m factor are developed as power law based on Reynolds number, as shown in Equations (78) and (79). Maximum deviations for j and j_m factor are within $\pm 10\%$ (Figure 89 and Figure 91).

$$j = 1.004 \cdot \text{Re}_{D_o}^{-0.559} (200 \leq \text{Re}_{D_o} \leq 600, \text{Pr} \approx 0.74) \tag{78}$$

$$j_m = 0.6978 \cdot \text{Re}_{D_o}^{-0.487} (200 \leq \text{Re}_{D_o} \leq 600, \text{Pr} \approx 0.74, wet) \tag{79}$$
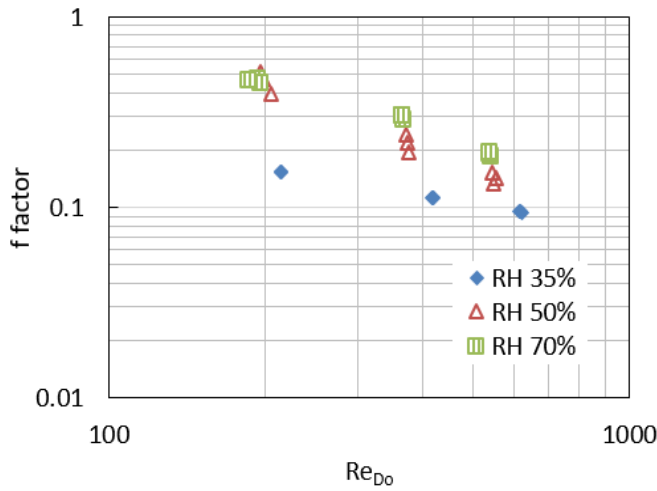
Figure 86 *f* factor (BTHX, wet, vertical)
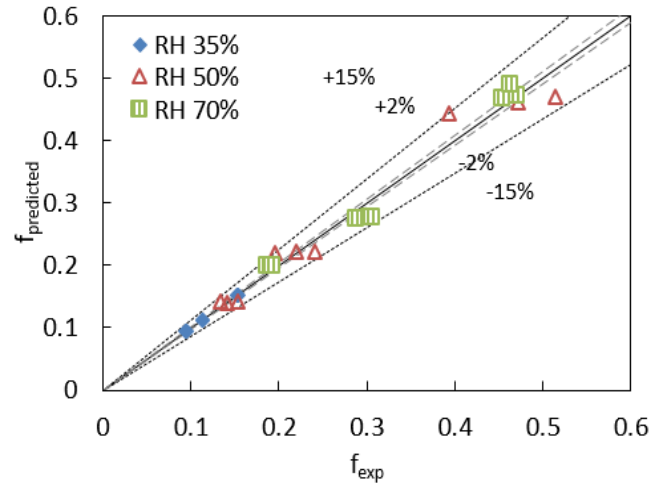
Figure 87 Prediction of *f* factor correlation (BTHX, wet, vertical)

94
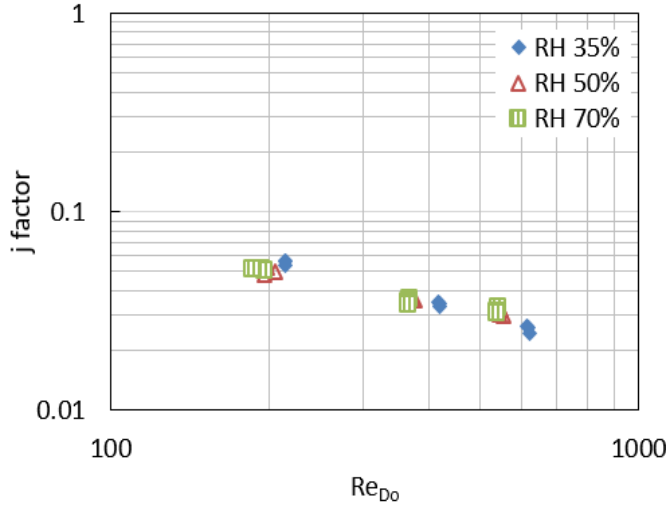
Figure 88 *j* factor (BTHX, wet, vertical)
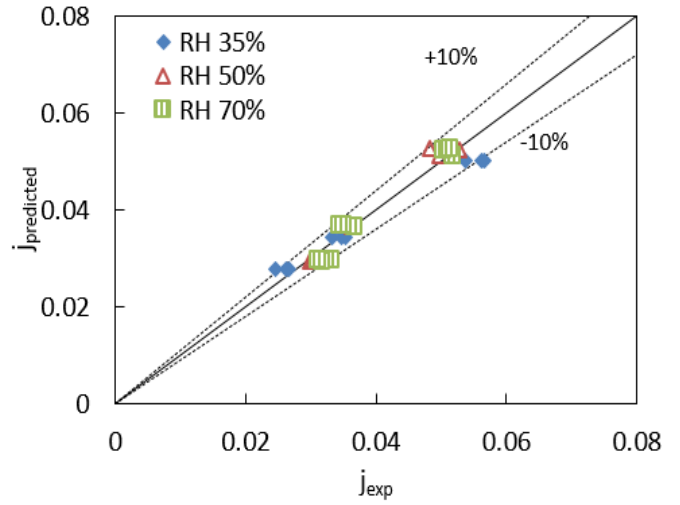
Figure 89 Prediction of *j* factor correlation (BTHX, wet, vertical)
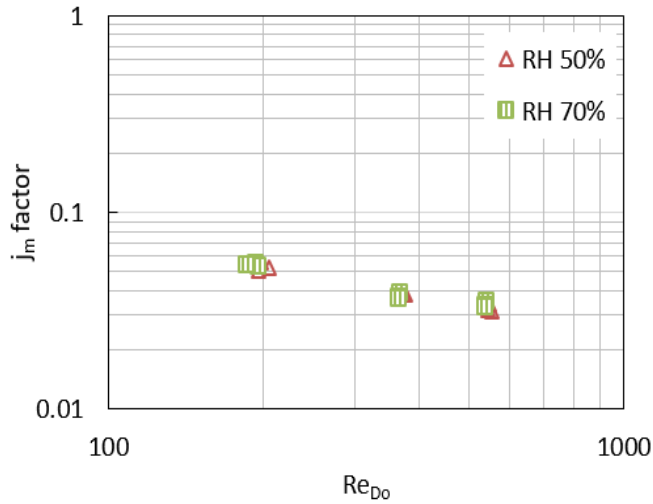
Figure 90 *jₘ* factor (BTHX, wet, vertical)
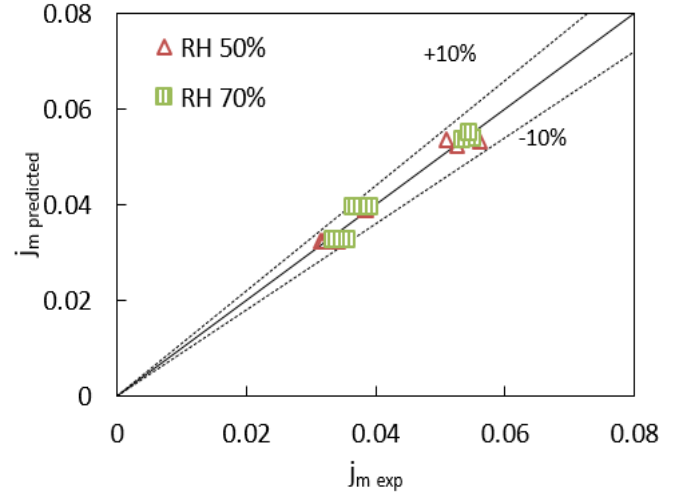
Figure 91 Prediction of *jₘ* factor correlation (BTHX, wet, vertical)

3.3.5. Test results for sBTHX

Wet condition test results are summarized in Figure 92 through Figure 96, with results for low inlet air relative humidity (RH=50%) on the left and high inlet air relative humidity (RH=70%) on the right. Figure 92 shows the energy balance of all wet condition tests are within ±4.3%. Here the effects of inlet air humidity, air flow rate and water flow rate on heat exchanger capacity, sensible capacity, latent capacity, airside pressure drop are discussed respectively. Chilton-Colburn j, Chilton-Colburn jₘ and f factor are shown in Figure 97.

95
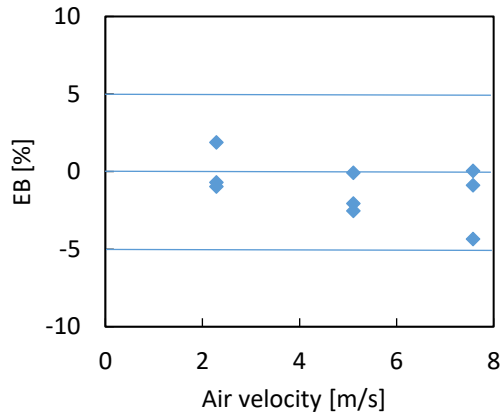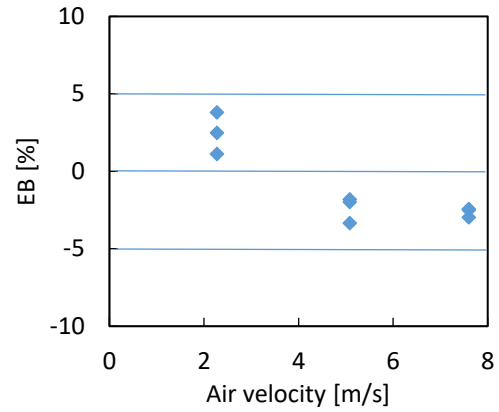
(a)　　　　　　　　　　　　　　**(b)**

Figure 92 Energy balance for (a) RH=50% and (b) RH=70% (sBTHX, wet)
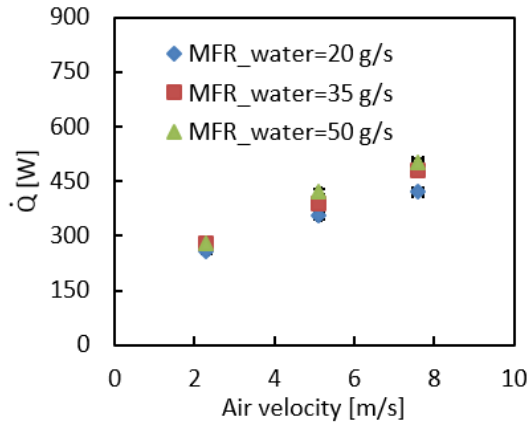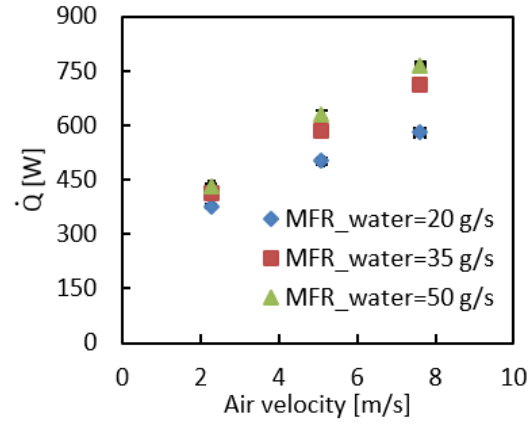
(a)　　　　　　　　　　　　　　**(b)**

Figure 93 Heat exchanger average capacity for (a) RH=50% and (b) RH=70% (sBTHX, wet)
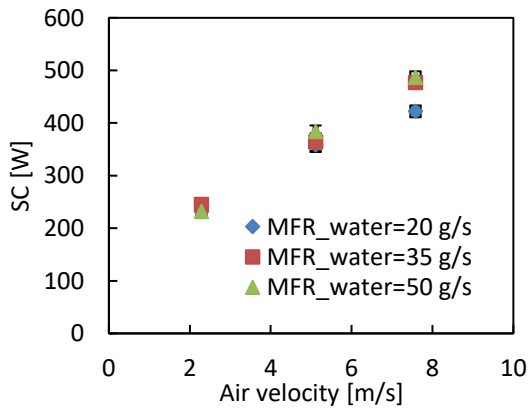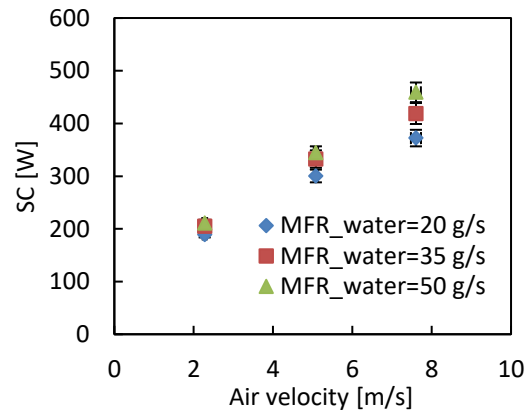
(a)　　　　　　　　　　　　　　**(b)**

Figure 94 Sensible capacity for (a) RH=50% and (b) RH=70% (sBTHX, wet)
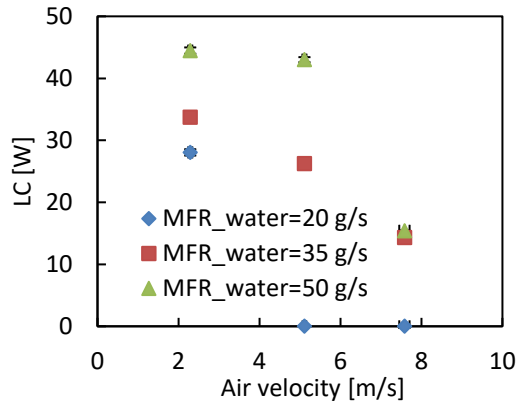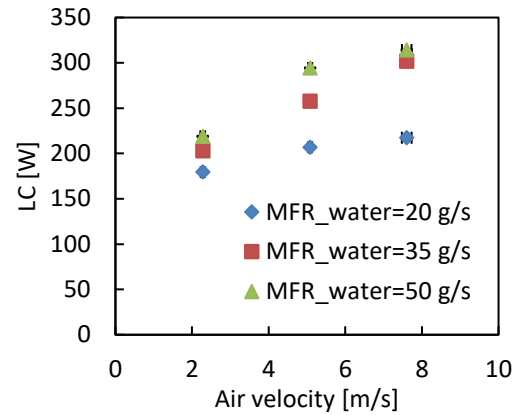
Figure 95. Latent capacity for (a) RH=50% and (b) RH=70% (sBTHX, wet)
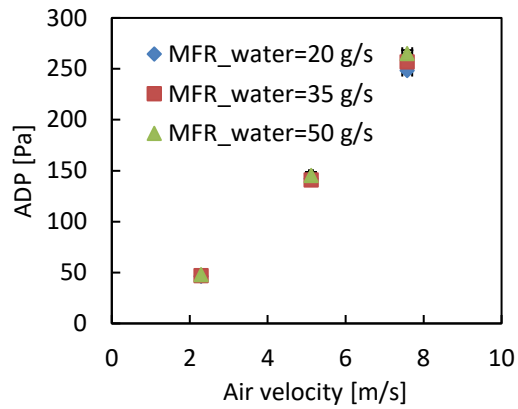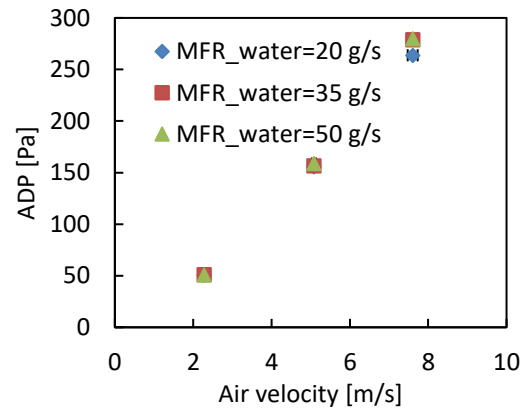
Figure 96. Air side pressure drop for (a) RH=50% and (b) RH=70% (sBTHX, wet)
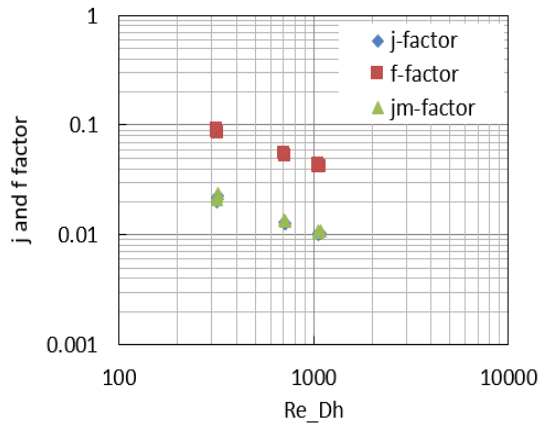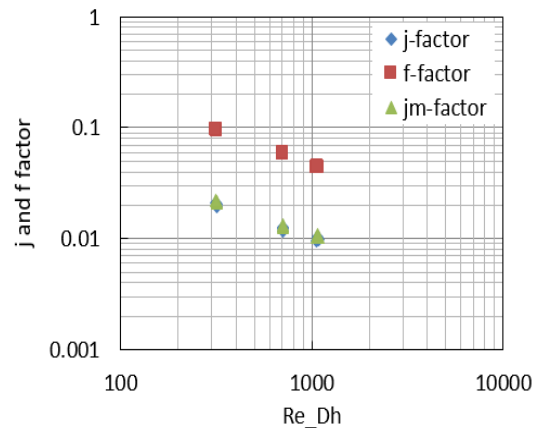
Figure 97. j and f factor for (a) RH=50% and (b) RH=70% (sBTHX, wet)

3.3.5.1.   Effect of inlet air relative humidity (RH)

From heat transfer point of view, larger inlet air humidity leads to larger latent capacity (LC, comparing Figure 94 (a) and (b)), lower sensible capacity (SC, comparing Figure 95 (a) and (b)) and larger overall heat exchanger capacity ($\dot{Q}$, comparing Figure 93 (a) and (b)). This is because higher inlet air humidity leads to additional condensing water accumulation on the heat exchanger surface, which reduces dry surface area and restrains sensible capacity transfer. From airside pressure drop point of view, larger inlet air humidity results in larger airside pressure drop (comparing Figure 96 (a) and (b)). This difference is within 11%, which is not a significant penalty for the trade-off in latent capacity improvement. Comparison with dry condition pressure drop is discussed later.

3.3.5.2.   Effect of inlet air flow rate (AFR)

As air flow rate increases, total capacity (Figure 93), sensible capacity (Figure 94) and airside pressure drop (Figure 96) increase. However, latent capacity either increases (Figure 95 (b)) or decreases (Figure 95 (a)). It is also affected by other factors like inlet air humidity and heat exchanger geometry. For this HX, latent capacity decreases (Figure 95 (a)) for the 50% RH test condition and increases for the 70% RH (Figure 95 (b)) test condition. Typically, as air flow rate increases, total capacity increases, causing waterside outlet temperature increase, resulting in higher average wall temperature. Therefore, the latent capacity transfer is expected to decrease due to increased wall surface temperature. However, larger air flow rate also means more moisture in the airstream, which will produce more condensation. This conflict indicates that whether latent capacity increases or decreases depends on which factor is dominant. When inlet air RH is low, the surface is partially wet, thus sensible capacity transfer dominates. So, the surface temperature increase is the dominant factor compared with airstream moisture increase, leading to latent

capacity decrease. This phenomenon is observed in the experiment, as shown in Figure 98. Dark area on the surface is wet surface and light area is dry surface. Comparing AFR=0.03, 0.06 and 0.09 m^3/s, as air flow rate increases, wet surface area is smaller and dry surface area becomes larger. When inlet air humidity ratio is high, the surface is fully wet, the extra moisture in the air becomes the dominant factor, causing latent capacity to increase.

For pressure drop, higher air flow rate results in higher ADP, as expected (Figure 96).

(a)
RH=50%, WFR=35 g/s
AFR=0.03 m^3/s

(b)
RH=50%, WFR=35
g/s AFR=0.06 m^3/s

(c)
RH=50%, WFR=35
g/s AFR=0.09 m^3/s
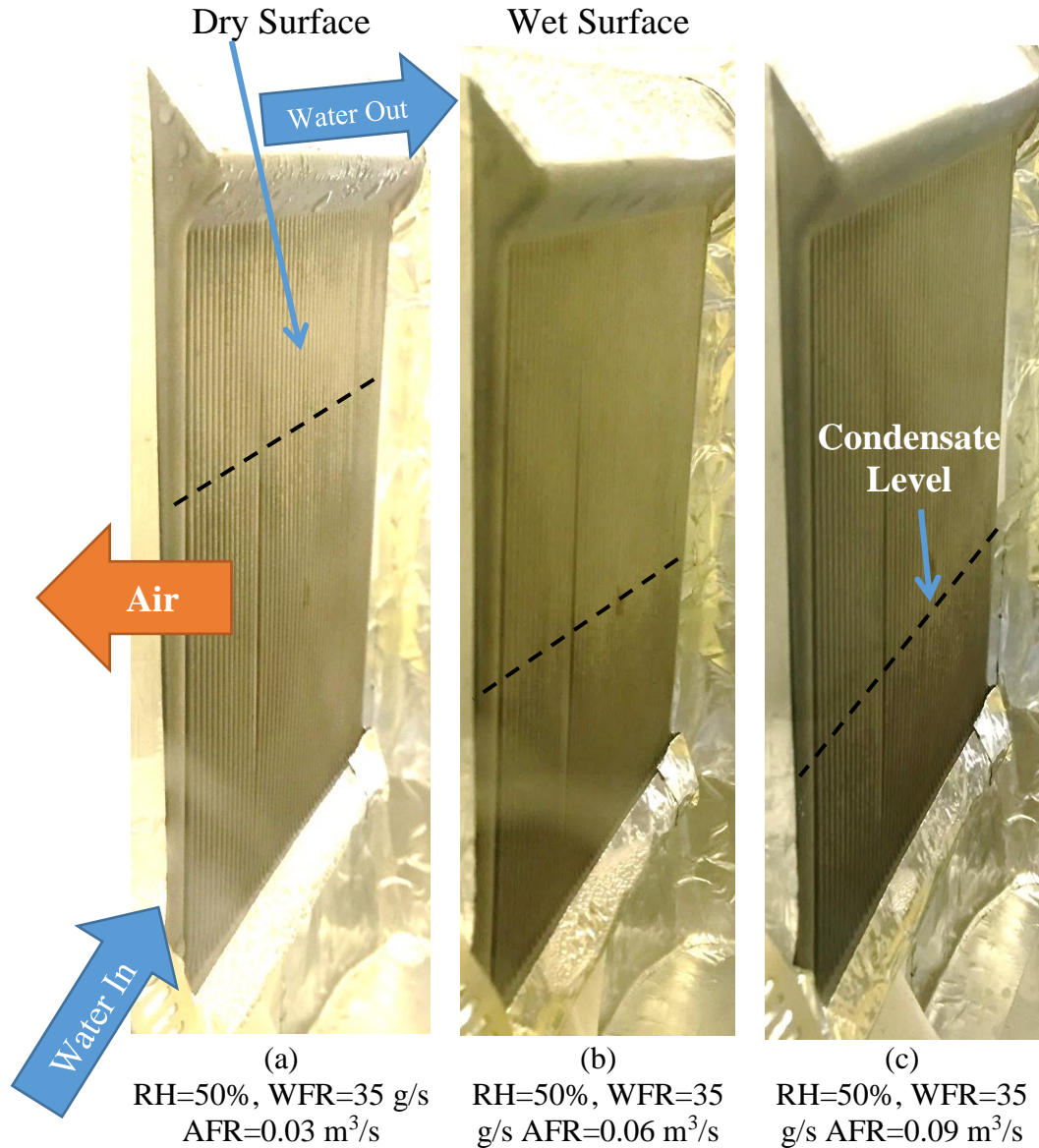
Figure 98 Effect of air flow rate on condensation at RH=50% (sBTHX, wet)

3.3.5.3.   Effect of inlet water flow rate (WFR)

As waterside flow rate increases, sensible capacity (Figure 94), latent capacity (Figure 95) and total capacity (Figure 93) all increase. The effect of water flow rate on airside pressure drop is negligible (Figure 96). Figure 99 presents the condensate level of three different water flow rates at inlet RH=50%. Only RH=50% pictures are selected because it is hard to recognize the difference on fully wet surface at inlet RH=70%.

(a)	(b)	(c)
RH=50%, AFR=0.03 m³/s,	RH=50%, AFR=0.06 m³/s,	RH=50%, AFR=0.09 m³/s,
WFR=20 g/s	WFR=30 g/s	WFR=50 g/s
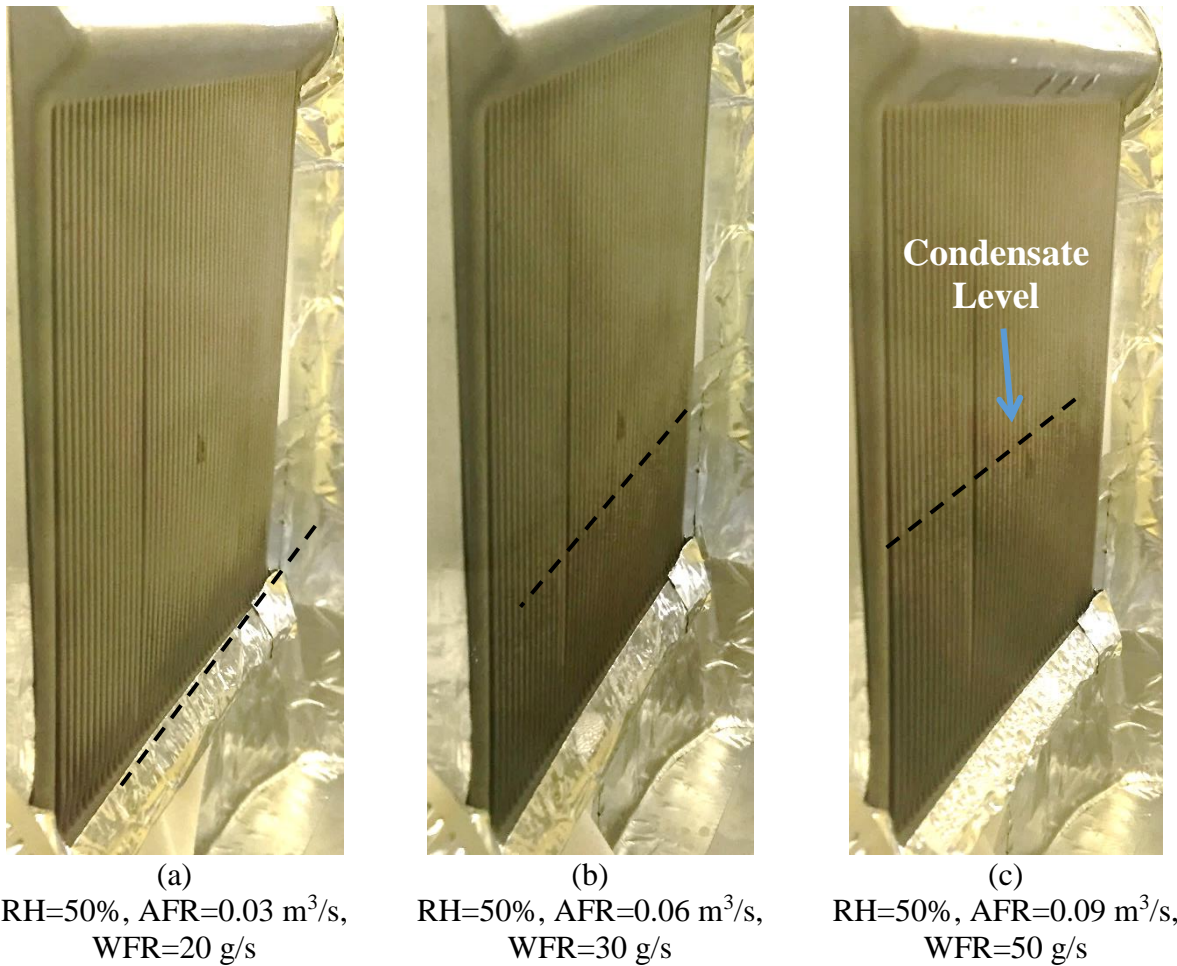
Figure 99 Effect of water flow rate on condensation (sBTHX, wet)

3.3.5.4.   Comparison of dry and wet condition

Comparison of dry and wet condition airside heat transfer coefficient, airside pressure drop, and j and f factors are summarized in Figure 100, Figure 101 and Figure 102, respectively. AHTC is sensible capacity transfer coefficient. Dry condition's sensible capacity transfer coefficient is higher than that of wet condition at the same air side velocity. Figure 101 shows the pressure drop variation due to different inlet air humidity levels. Airside pressure drop under RH=70% is 0~11% larger than that of RH=50%, and is 0~15% larger compared with that of dry condition. And the pressure drop penalty is more obvious at low air velocity (< 5 m/s). The most important reason of

low airside pressure drop penalty is the header shape. As shown in Figure 24, the header of heat exchanger is diamond shape so that condensate water flows away easily along the header instead of accumulates at the bottom of the heat exchanger. This reduces the water bridging effect between tubes, which was observed in most fin-and-tube heat exchangers. Another reason why there is almost no pressure drop penalty at high air velocity (> 5 m/s) is the blow out effect. Figure 104 shows water was blew out by air from backside of the heat exchanger. Two arcs formed by water were marked on the graph.

Figure 102 shows j and f factors on the effect of inlet relative humidity for dry and wet conditions. As Reynolds number increases, j and f factors decrease. Addition of latent capacity decreases j factor. As inlet relative humidity increases from 50% to 70%, j factor decreases and f factor increases slightly. However, the variation of j and f factors on the relative humidity effect of inflow air is not sensitive. The present results are similar to that of Fu et al. (1995), Wang et al. (2000) and Phan et al. (2011).

Figure 103 presents the variation of j_m factor on the effect of inlet relative humidity. As inlet relative humidity increases from 50% to 70%, j_m factor slightly decreases. The slight degradation of mass transfer performance may due to the condensate retention phenomenon between tubes. This is consistent with observations by Phan et al. (2011).

Correlations for j, j_m and f factor were developed for wet condition test shown in Figure 105 as power law based on Reynolds number in Equation (80), (81) and (82). Maximum deviations are within $\pm$7% of j_m and f factor prediction and are within $\pm$10% of j factor.

$$j = 0.6678 \cdot \mathrm{Re}_{D_h}^{-0.604} \, (315 \leq \mathrm{Re}_{D_h} \leq 1080, \mathrm{Pr} \approx 0.74, wet) \tag{80}$$

$$j_m = 0.6853 \cdot \mathrm{Re}_{D_h}^{-0.599} \, (315 \le \mathrm{Re}_{D_h} \le 1080, \mathrm{Pr} \approx 0.74, wet) \tag{81}$$

$$f = 6.2974 \cdot \mathrm{Re}_{D_h}^{-0.615} \, (315 \le \mathrm{Re}_{D_h} \le 1080, \mathrm{Pr} \approx 0.74, wet) \tag{82}$$
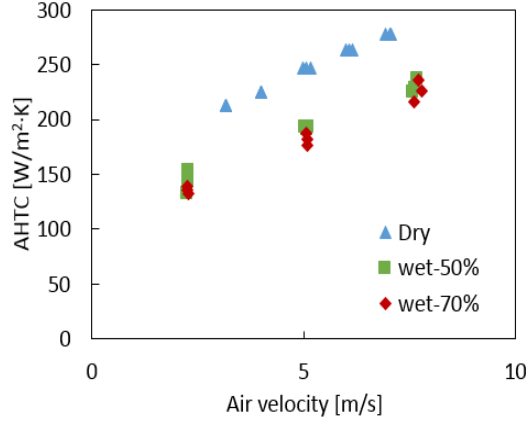
Figure 100 Comparison of AHTC under dry and wet condition (sBTHX)
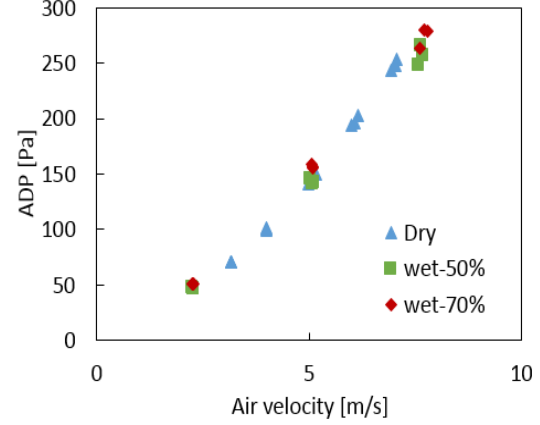
Figure 101 Comparison of ADP under dry and wet condition (sBTHX)
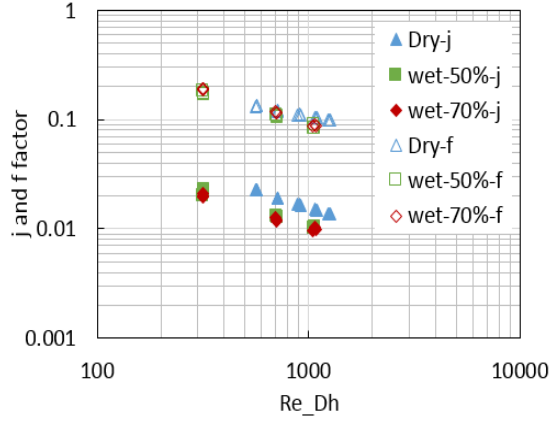
Figure 102 Comparison of j and f factor under dry and wet condition (sBTHX)
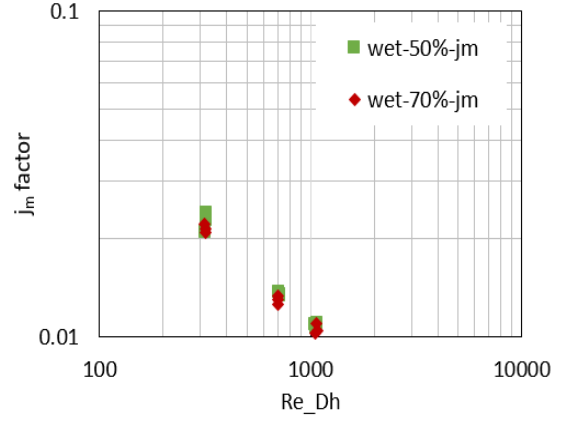
Figure 103 Comparison of j_m factor at different RH level (sBTHX)

**Figure 104 Water blow out effect for sBTHX
(RH=70%, AFR=0.09 m³/s, WFR=50g/s)**
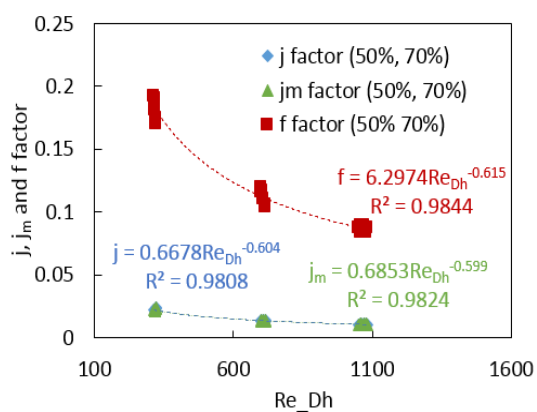
**Figure 105 Wet condition j, j_m and f factor
correlation (sBTHX)**
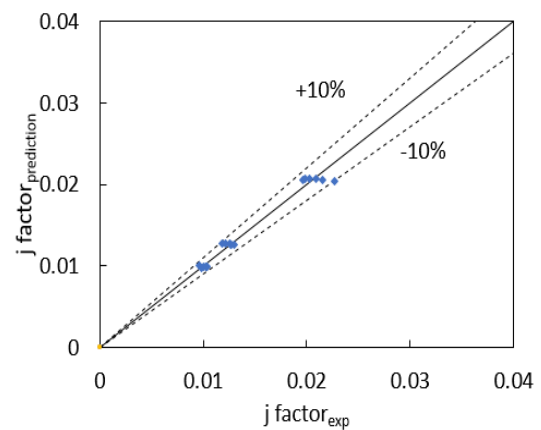
**Figure 106 Prediction of wet condition j
factor correlation (sBTHX)**
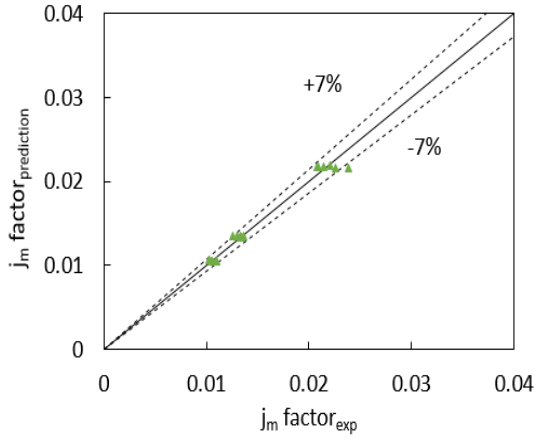
Figure 107 Comparison of wet condition j_m factor correlation with experimental data (sBTHX)
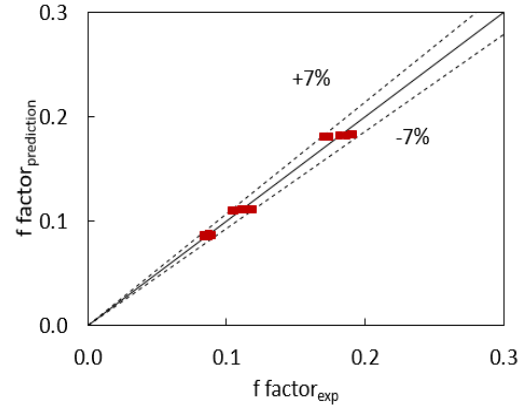
Figure 108 Comparison of wet condition f factor correlation with experimental data (sBTHX)

3.3.6. Test results of 5 and 4 mm slit fin-and-tube heat exchanger

Energy balance for both heat exchangers is within ±5%, as shown in Figure 109 and Figure 110 separately. The total capacities of both heat exchanger are shown in Figure 111 and Figure 112. The total capacities of 4 mm heat exchanger are slightly higher than that of 5 mm coil. The air side pressure drops are shown in Figure 113 and Figure 114. The air side pressure increases both as air and water flow rate increases. This is due to the blockage caused by condensation water. The air side pressure drop is slightly lower than that of 5 mm coil. Sensible capacities are shown in Figure 115 and Figure 116 and latent capacities are shown in Figure 117 and Figure 118. The sensible capacities of both heat exchanger are similar, but latent capacities for 4 mm coil are higher than those of 5 mmm coil. j, j_m and f factors are shown in Figure 119 and Figure 120, respectively.
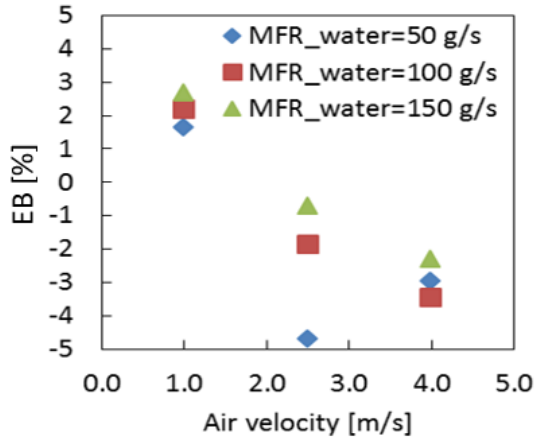
Figure 109 Energy balance for 5 mm coil under wet condition
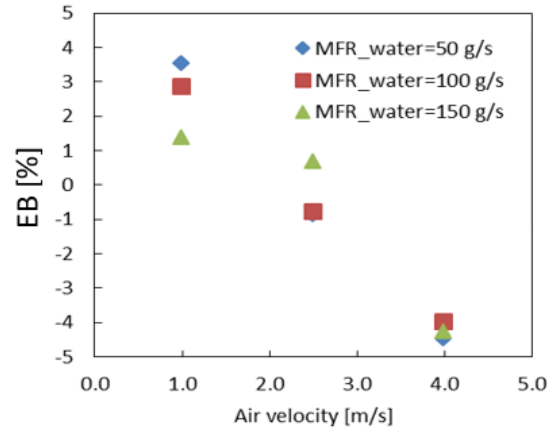
Figure 110 Energy balance for 4 mm coil under wet condition
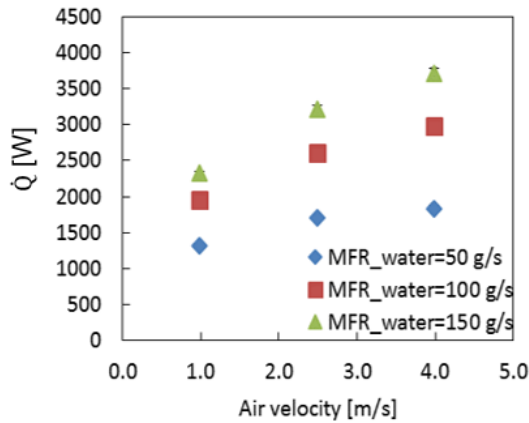
Figure 111 Capacity for 5 mm coil under wet condition
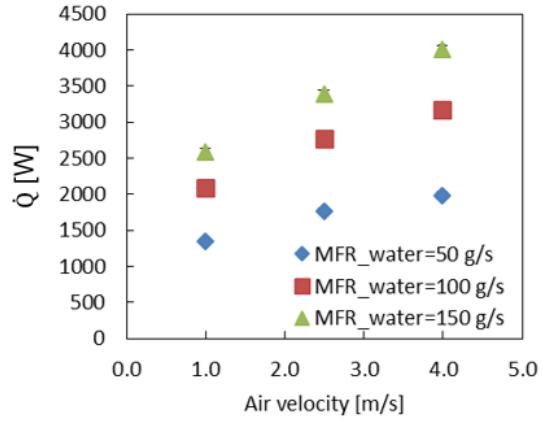
Figure 112 Capacity for 4 mm coil under wet condition
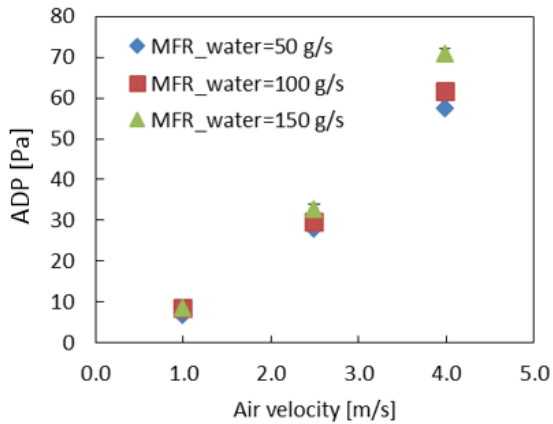
Figure 113 Air side pressure drop for 5 mm coil under wet condition
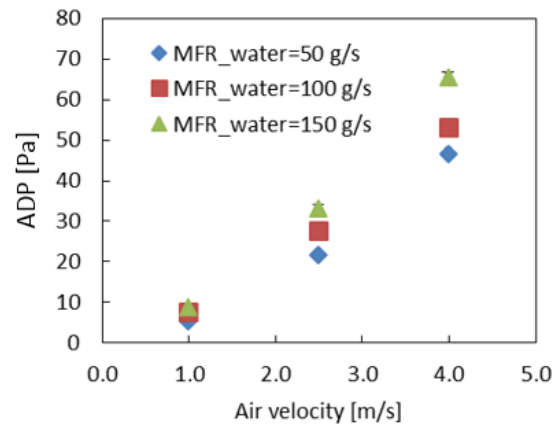
Figure 114 Air side pressure drop for 4 mm coil under wet condition
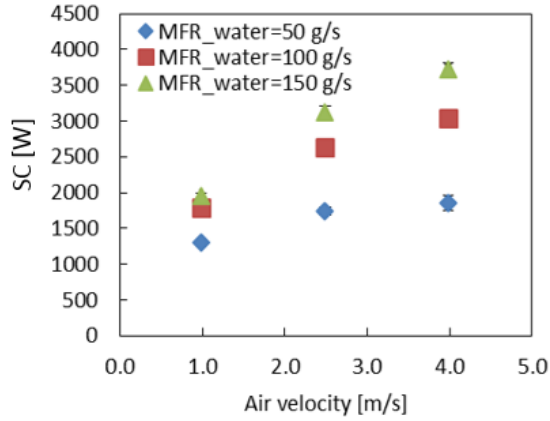
Figure 115 Sensible capacity for 5 mm coil under wet condition
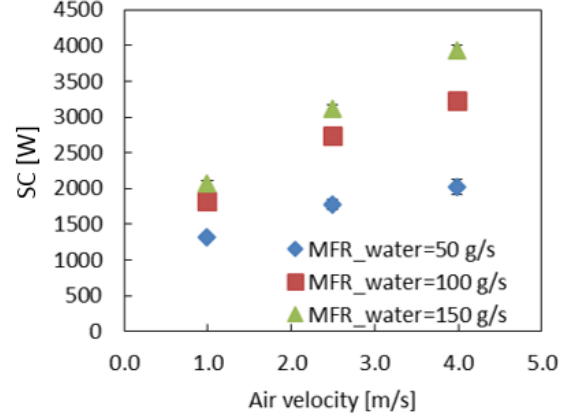
Figure 116 Sensible capacity for 4 mm coil under wet condition
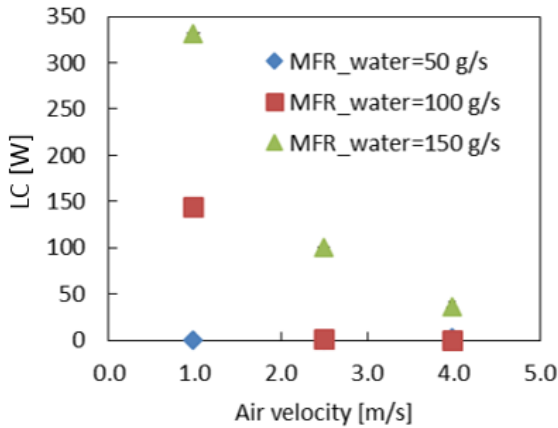
Figure 117 Latent capacity for 5 mm coil under wet condition
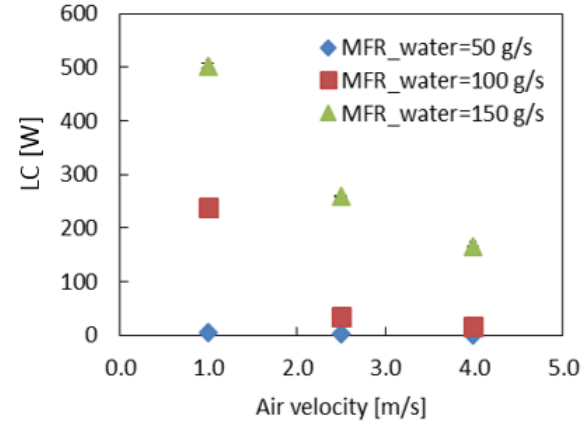
Figure 118 Latent capacity for 4 mm coil under wet condition
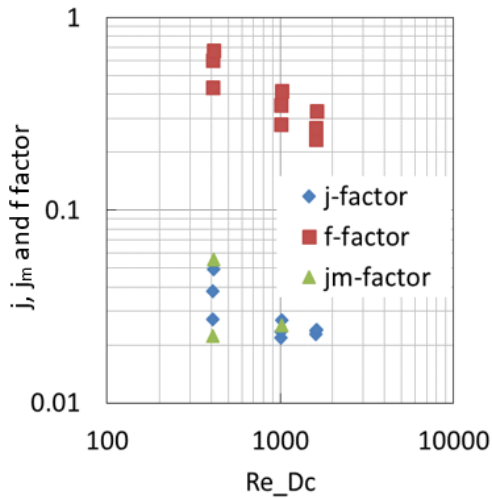
Figure 119 j, j_m and f factor for 5 mm coil under wet condition
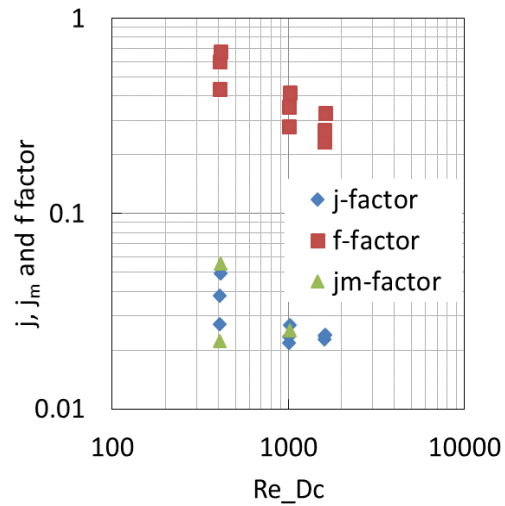
Figure 120 j, j_m and f factor for 4 mm coil under wet condition

3.3.7. Comparison of all heat exchangers

AHTC and ADP/Depth for all baseline heat exchangers are plotted in Figure 121. BTHX has the largest AHTC as well as ADP/Depth. There are three reasons for this:

The first is for different heat exchangers, the mass flux based on free flow area is different. As shown in Figure 122, the mass flux for BTHX is the highest. However, in Figure 123, even if we plot the AHTC and ADP/Depth over mass flux, values of BTHX are still on the top.

The second reason is boundary layer interruption and redevelopment. From heat transfer point of view, the highest Nusselt number appears at the beginning of boundary layer. For different types of fins, their design principle is also boundary layer interruption and redevelopment, as shown in Figure 124. In bare tube designs, for each tube, the boundary layer redevelops, as shown in Figure 125. However, for fins, especially louvered fins and slit fins, the louver and slit size are also small, this cannot sufficiently explain the phenomenon.

The third reason is about the shape. Round tube has intrinsic advantage over flat plate regarding heat transfer. Flat plate and round tube were simulated using the same condition. Inlet air velocity is 2 m/s and temperature is 300 K and the wall temperature is 350 K. The temperature contours are as shown in Figure 126 and Figure 127. From Figure 128 and Figure 129, flat plate has better hydraulic performance while round tube has better heat transfer performance.
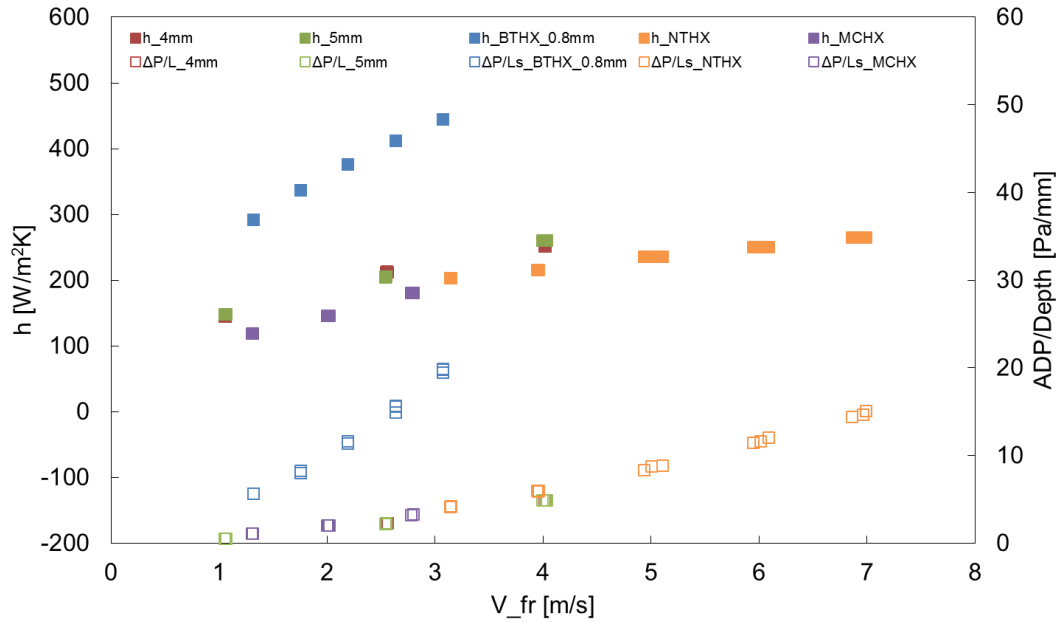
Figure 121 Air side heat transfer coefficient and pressure drop per depth for baseline heat exchangers
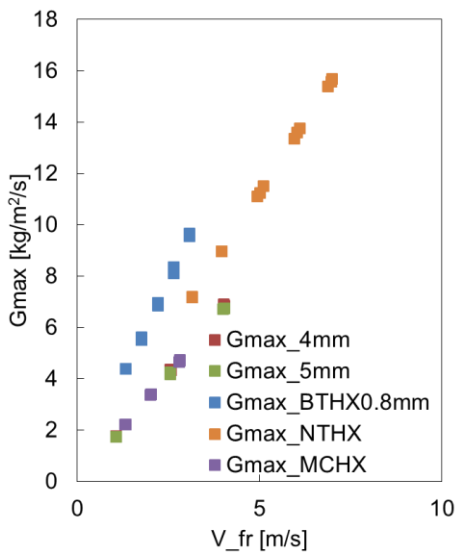
Figure 122 G_max for all baseline heat exchangers
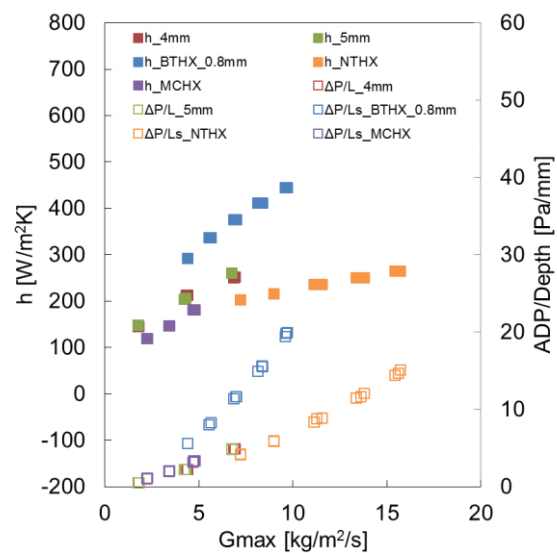
Figure 123 Air side heat transfer coefficient and pressure drop per depth over G_max for baseline heat exchangers.
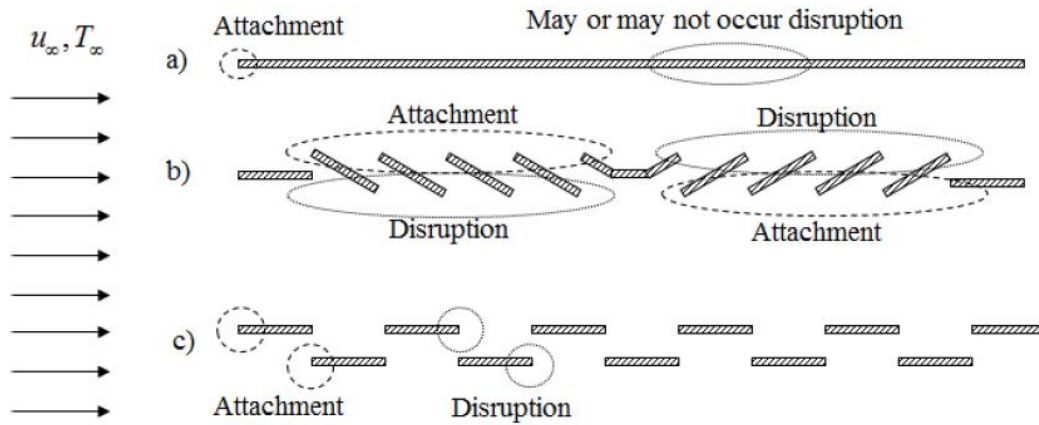
Figure 124 Boundary layer disruption and attachment regions on different fin types: a) Plain, b) Louver and c) Slit. (Bacellar, 2016)
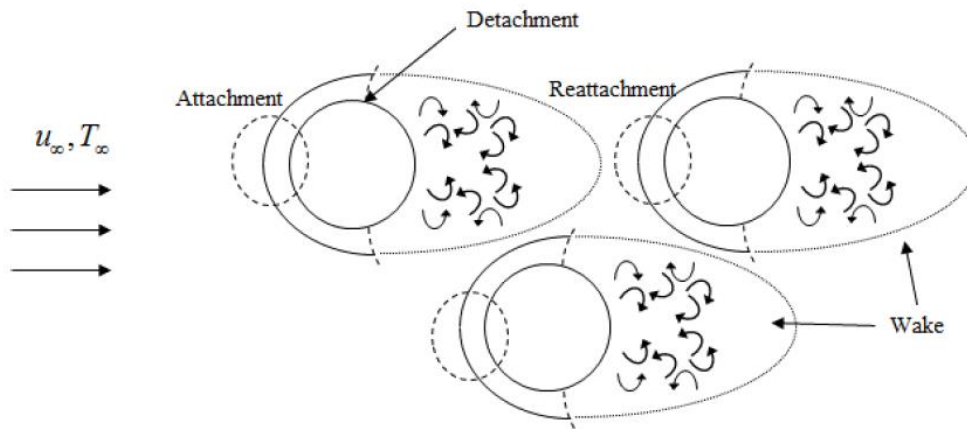
Figure 125 Boundary layer disruption and attachment regions on a round tube bundle (Bacellar, 2016)
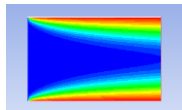
Figure 126 Flat plate temperature contour plot (CFD results)
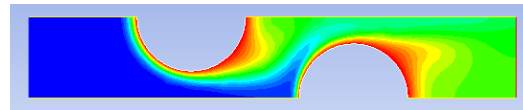
Figure 127 Round tube temperature contour plot (CFD results)
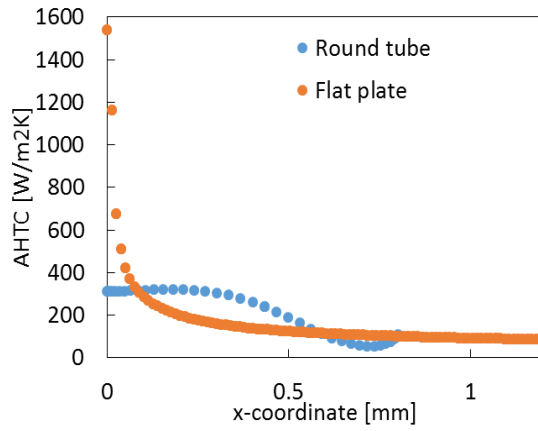
Figure 128 AHTC of flat plate and round tube (CFD results)
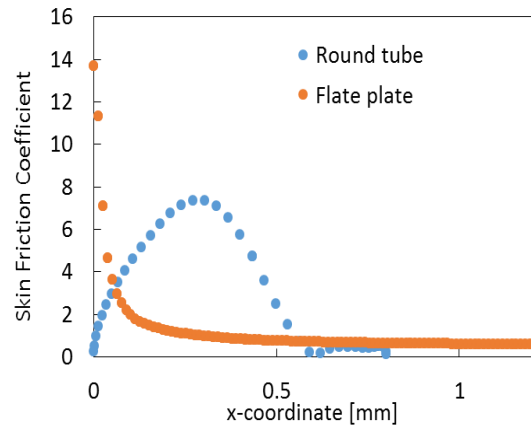
Figure 129 Skin friction coefficient of flat plate and round tube (CFD results)

Chapter 4: Bifurcated Bare Tube Heat Exchanger (bBTHX) Design

4.1. *Design Concept*

The innovative design is inspired by human lung and blood vein structure. If directly copying the nature, the design would be hierarchical bifurcated tubes, such as fractal channels for electronic cooling. However, the biggest disadvantage of using multi-level hierarchical bifurcated structure is the low utility of space. So, for fractal channels, the round disc shape (Pence, 2002) or sandwich structure (Chen and Cheng, 2002) are common designs to better utilize space. However, in the application, such designs would dramatically increase the difficulty of header design due to irregular header shape and increase the difficulty of manufacturing due to the small branch tube diameter so that it might not be able to be 3D printed. It may also increase the difficulty of heat pump/air conditioner system geometry design if the new heat exchanger is used as evaporator or condenser because of the irregular geometry. Thus, in current study, instead of using multi-level hierarchical bifurcated tubes, only two levels of tubes are used.

This novel heat exchanger consists of two levels of tubes, the main tubes and the branch tubes. Main tubes are all vertical tubes as shown in Figure 130 of which outer diameters are symbolled as D_1 while branch tubes are labeled as D_2. Longitudinal tube pitch (P_l) is defined as the center distance of two adjacent main tubes. The transversal tube pitch (P_t) is then defined as the central distance of two adjacent rows, as shown in Figure 131. Bifurcation angle (θ) is the angle between branch tube and the center line. Centerlines of all tubes generate a honeycomb structure consisting of multiple hexagons in this example, indicated by dotted line. Figure 132 shows the heat exchanger shape with header and the flow directions of two fluids on both sides. Tubes can be either staggered or in-line in the air flow direction. For staggered configuration, two

112

different patterns are studied in current research, as shown in Figure 133 (a) and (b). Darker tubes are first row and lighter tubes are second row. The difference between these two configurations is that the bypass flow, which flows through the honeycomb area formed by first row tube, hits the main tube of second row in pattern 1 while it hits the part of main tube and bifurcated tubes of second row in pattern 2. Computational domain is shown in the red box.
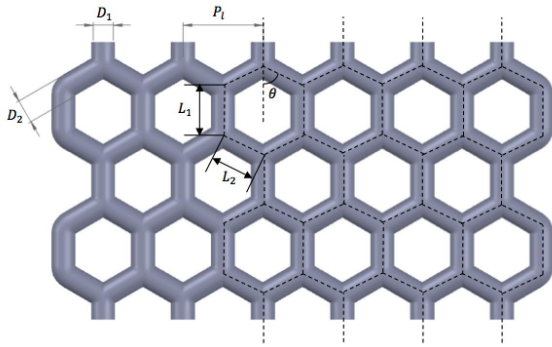
Figure 130 bBTHX-tube structure
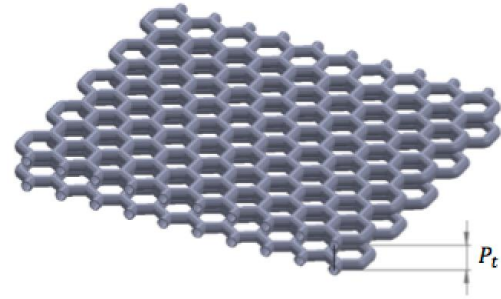
Figure 131 Two rows of bBTHX in staggered pattern
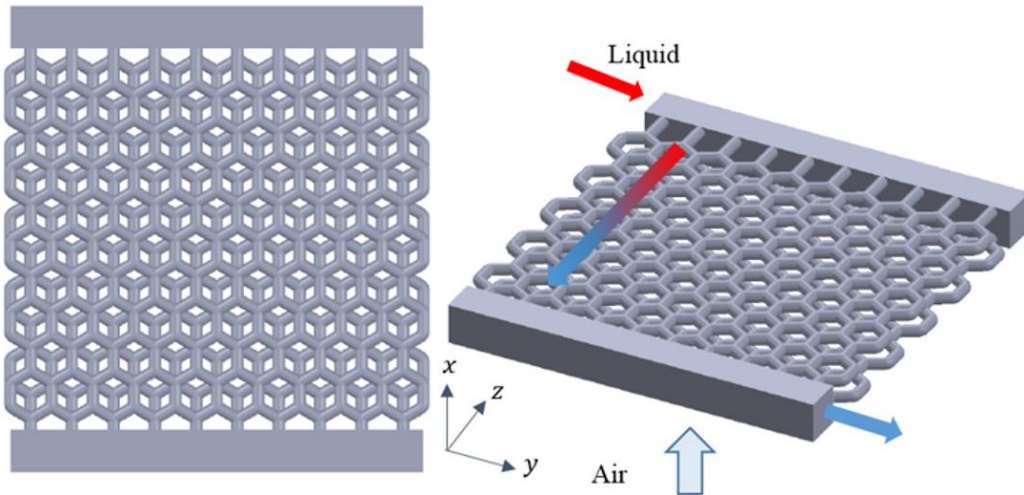
Figure 132 bBTHX schematic (staggered) and simulation domain

113

(a)   (b)
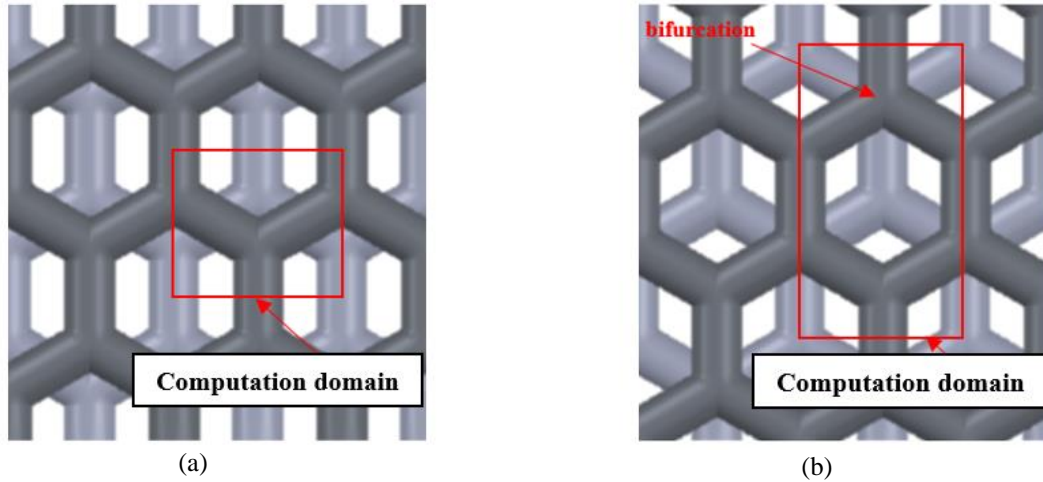
Figure 133 Two staggered patterns of bBTHX: pattern 1 (a) and pattern 2 (b)

4.2. *Airside First Order Analysis*

Airside heat transfer area is one of the key parameters to enhance airside heat transfer. Before further investigation of the new heat exchanger, first order analysis was conducted to evaluate airside heat transfer area by comparing the compactness and material utilization of current design and baseline heat exchangers. Compactness is defined as airside total heat transfer area over heat exchanger envelope volume and material utilization is defined as airside total heat transfer area over heat exchanger material volume.

The assumptions for first order analysis include: (1) same liquid side cross section area; (2) same tube pitch ratio; (3) same tube bank number; (4) same tube thickness ratio; (4) constant inlet air velocity, and (5) FPI of finned heat exchangers are all 30. Figure 134 and Figure 135 show the results of compactness and material utilization, respectively. It can be seen that at large diameter range (>1 mm), mini-channel heat exchanger and plain fin-and-tube heat exchanger have larger compactness and material utilizations due to additional secondary surface area. However, as diameter becomes smaller, the advantage of secondary surface area diminishes. Compactness and

114

material utilization of round bare tube heat exchanger with diameter less than 1 mm are similar to that of finned heat exchangers. bBTHX even has larger compactness and material utilization than finned heat exchangers. Thus, current study focuses on small diameter bifurcated bare tube HX.

Another advantage of small diameter is the reduced internal volume, which means less refrigerant charge if applied in air conditioner and heat pump systems, leading to reduced system weight and less environmental impact.
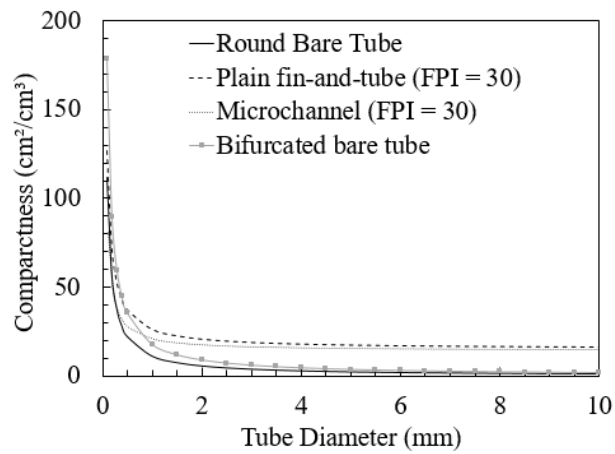
Figure 134 First order analysis: compactness
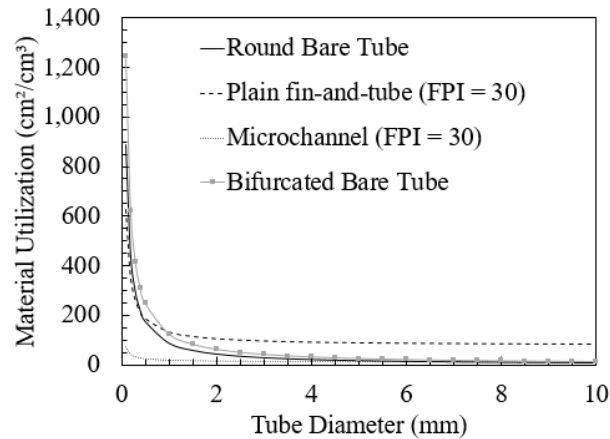
Figure 135 First order analysis: material utilization

4.3. *Parametric Study*

The airside parameters studied are summarized in Table 17 and the waterside parameters studied are summarized in Table 18. Diameter ratio (DR) is defined as the ratio of D_1 over D_2 and

length ratio (LR) is defined as the ratio of length of main tube (L_1) over length of branch tube (L_2). DR was fixed to be 0.7 to maintain the mass flux constant inside tubes in current study. To compare the heat exchanger's performance, the main tube's diameter (D_1) was kept the same as the diameter of bare tube heat exchanger (D) in comparison.

Table 17 Airside Parametric Study Parameters for BTHX and bBTHX

Types	Parameters	Units	BTHX	bBTHX
Constants	P_l	[mm]	1.5D	1.5D_1
	P_t	[mm]	1.5D	1.5D_1
	DR	-	-	0.7
Variables	D or D_1	[mm]	0.8, 2, 3, 4	0.8, 2, 3, 4
	V_a	[m/s]	0.5, 2, 3.5, 5	0.5, 2, 3.5, 5
	θ	[deg]	-	10, 35, 60
	LR	-	-	0.5, 1.5, 2.5
	Pattern	-	-	1, 2

Table 18 Waterside Parametric Study Parameters for BTHX and bBTHX

Types	Parameters	Units	BTHX	bBTHX
Constants	P_l	[mm]	-	1.5D_1
	DR	-	-	0.7
Variables	D or D_1	[mm]	0.8, 2, 3, 4	0.8, 2, 3, 4
	V_w	[m/s]	0.1,0.3,0.6,1	0.1,0.3,0.6,1
	θ	[deg]	-	10, 35, 60
	LR	-	-	0.5, 1.5, 2.5

4.4. *Experimental Validation of Airside Hydraulic Performance*

The airside CFD model was validated against experimental data measured from a four-bank HX with 0.8 mm diameter, 1.19 mm longitudinal pitch and 1.24 mm transverse pitch. Working fluids are air and water. The test facility and measurements followed the ASHRAE standards (ASHRAE, 1987, 2000). The average uncertainty in the capacity measurements was 2.71%, whereas the pressure drop was 2.91%. Deviations for heat transfer coefficient between experimental data and simulation data range from 1% (at higher air side velocity) to 15% (at lower

116

air side velocity). Over-prediction of pressure drop was observed, and addition of a correction factor of 0.61 brought the maximum deviation down to 7%. Details could be found in Baceller et al., 2016.

One bBTHX sample was 3D printed by Connex 3 Systems Objet500 using VeroWhite filament, as shown in Figure 136. There are 13 tubes per row and 7 rows in total. Diameter for first layer tube is 2 mm, diameter ratio is 0.7, longitudinal pitch is 3 mm, transverse pitch is 3 mm and length ratio is 1.732. Due to leakage issue, this sample was only tested to validate the air side pressure drop for now and a new leak tight prototype is on the way to validate heat transfer. Similar to bare tube heat exchanger, consistent over-prediction of pressure drop is also observed. Experimental validation shows a good agreement of less than 3% after applying a correction factor of 0.51, as shown in Figure 137. The potential reasons for deviation include but are not limited to experimental uncertainties, model uncertainties and manufacturing uncertainties. Note that in the following session, data shown are all simulation data, without correction since, the observed pressure drop is related to lots of factors including material type, surface roughness, manufacturing method, etc.

(a) (b) (c)
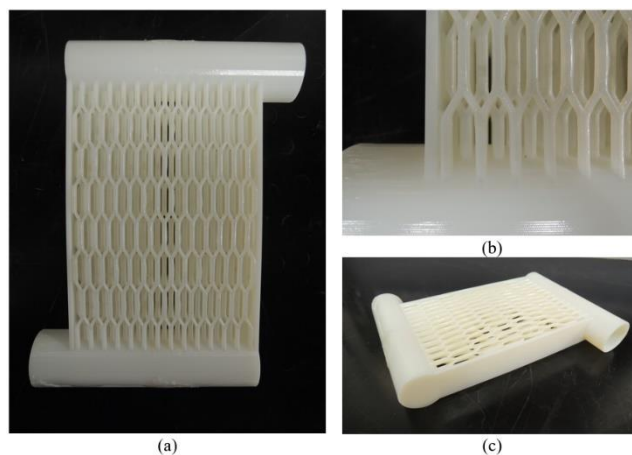
Figure 136 bBTHX sample
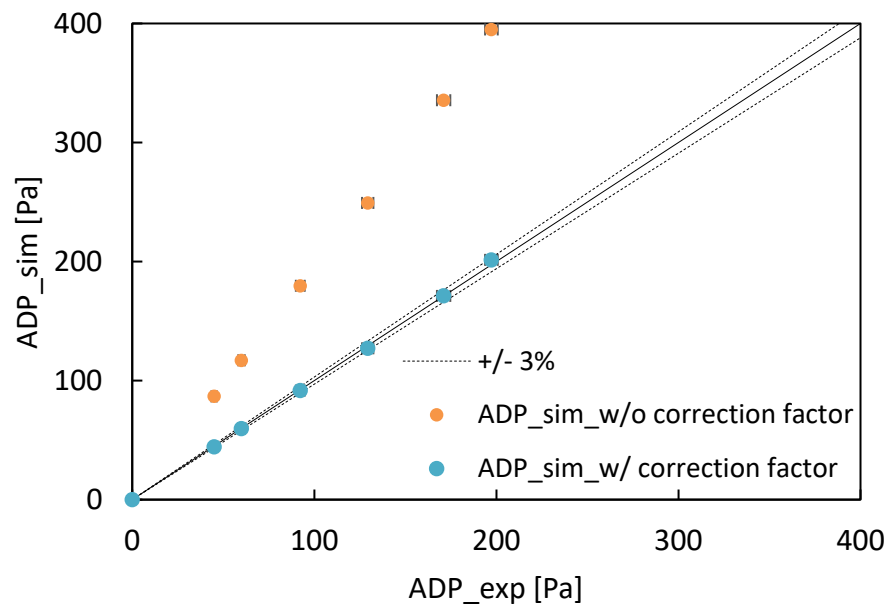
Figure 137 Experimental validation for bBTHX air side pressure drop

4.5. *Airside Simulation Results and Discussion*

4.5.1. Heat transfer area

The comparison of all bBTHX configurations studied is summarized in Figure 138. As the bifurcation angle increases or the length ratio decreases, the bifurcation number will have to increase for a certain heat exchanger length, resulting in a larger heat transfer area improvement. Diameter has no effect on heat transfer area improvement as long as the diameter ratio is fixed. The difference between pattern 1 and pattern 2 is more obvious at larger bifurcation angle. It can be noticed that for geometry with $\theta=10°$, there is nearly no heat transfer area improvement, and even degradation. Theoretically, tubes with bifurcations should have larger total area than bare tubes with same diameter because the area of two branch tubes with small diameter are larger than tube with larger diameter. However, when the bifurcation angle is very small (for example, $10°$), the merging area of secondary tube balances out the extra area that created by secondary tubes, resulting in similar or even smaller heat transfer area than baseline, as illustrated in Figure 139.
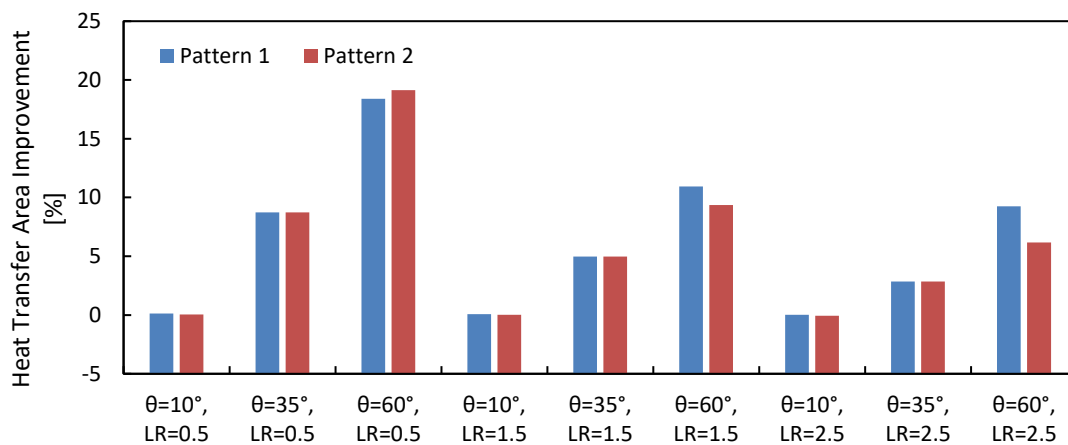
Figure 138 Air-side heat transfer area improvement compared with BTHX
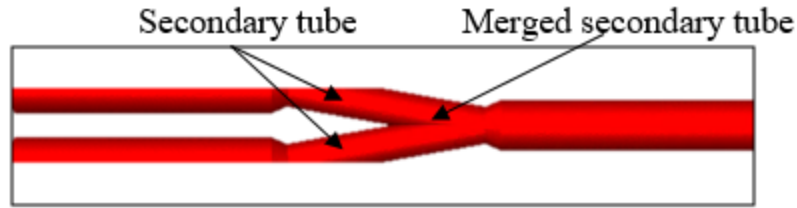
Figure 139 bBTHX tube configuration with θ=10°, LR=2.5, pattern 1

4.5.2. Free flow area

The decrease in free flow area results in stronger flow acceleration, leading to larger mass flux, thus larger heat transfer coefficient. So, this factor needs to be considered separately in order to make a fair comparison of heat transfer coefficient later. The free flow area percentage reduction is plotted in Figure 140. It shows the same trend as that of heat transfer area improvement. Free flow area decreases as bifurcation angle increases or length ratio decreases.
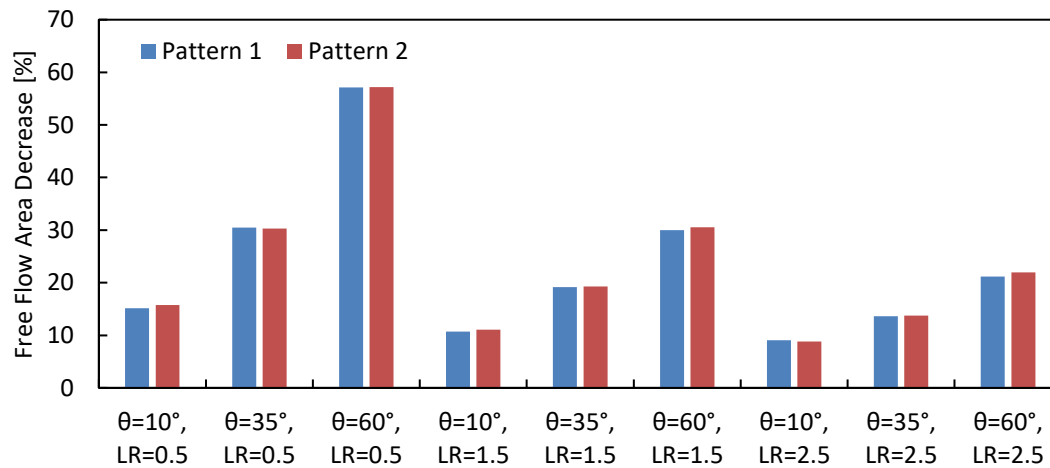
Figure 140 Air-side free flow area decrease compared with BTHX

4.5.3. Air-side heat transfer coefficient (AHTC)

Since it will be overwhelming to plot all data in a single plot, representative points are selected to illustrate the influence of each parameter. The results are summarized in Figure 141 through Figure 144. AHTC of bBTHX is higher than that of BTHX at higher air velocity (2, 3.5 and 5 m/s) and might be lower when air velocity is low (0.5 m/s).

120

Effect of air velocity: The effect of air velocity on AHTC is shown in Figure 141. As air velocity increases, the AHTC increases non-linearly for all cases.
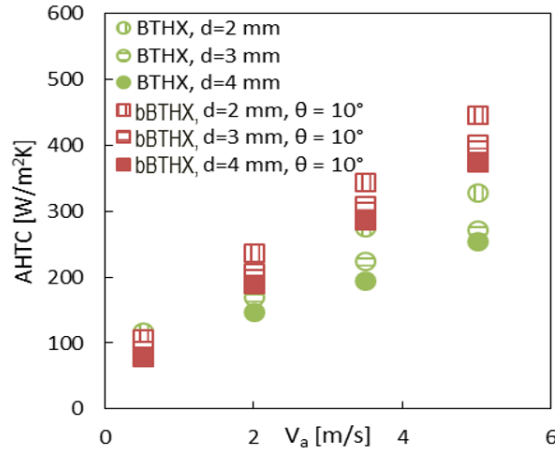
Figure 141 Effect of velocity and diameter on AHTC
(θ=10°, LR=0.5, Pattern 1)

Effect of diameter: The effect of diameter on AHTC is also shown in Figure 141. AHTC increases as diameter decreases. This can be explained by using definition of AHTC and Nusselt number. The relationship between AHTC and diameter as shown in Equation (86) can be derived by using the definition of Nusselt number and Reynolds number as shown in Equation (83), (84) and (85).

$$Nu = \frac{hD}{k} \tag{83}$$

$$Nu = C_0 \, \mathrm{Re}^m \, \mathrm{Pr}^n \, (m, n \in [0,1]) \tag{84}$$

$$\mathrm{Re} = \frac{UD}{v} \tag{85}$$

$$h = \frac{U^m}{v^m} C_0 k \, \mathrm{Pr}^n \frac{1}{D^{1-m}} \tag{86}$$

Effect of bifurcation angle: AHTCs of bBTHX with different bifurcation angles are shown in Figure 142. AHTC increases as bifurcation angle increases. The main reason is that the increase of bifurcation angle leads to smaller free flow area, as shown in Figure 140, thus better flow mixing.
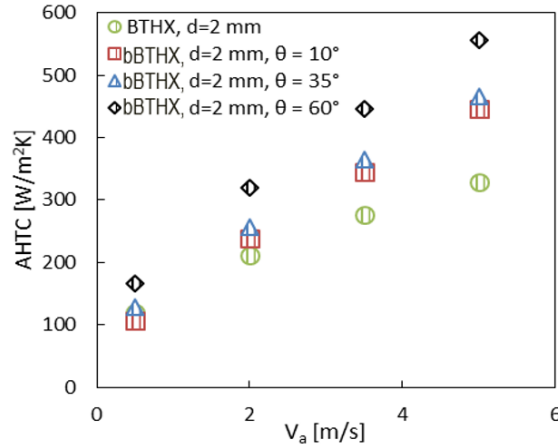
Figure 142 Effect of bifurcation angle on AHTC
(d=2 mm, LR=0.5, Pattern 1)

Effect of length ratio: AHTCs of different bBTHX with different LR are shown in Figure 143. It can be found that AHTC increases as length ratio decreases. This can also be explained using the free flow area percentage decrease (Figure 140) described before. Designs with smaller LR have smaller free flow area. Another reason is with smaller length ratio, there are more bifurcation structures in unit volume, which enhance 3D flow mixing and result in higher AHTC.
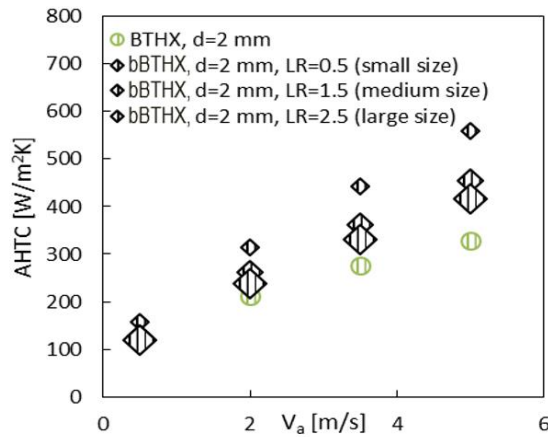
Figure 143 Effect of LR on AHTC
(d=2 mm, θ=60°, Pattern 2)

Effect of pattern: Two different patterns have been studied and the difference is shown in Figure 144. Pattern 2 has higher AHTC than pattern 1. The free flow area and heat transfer area for pattern 1 and 2 per unit envelope volume are similar thus the difference in AHTC must come from the pattern itself.

122
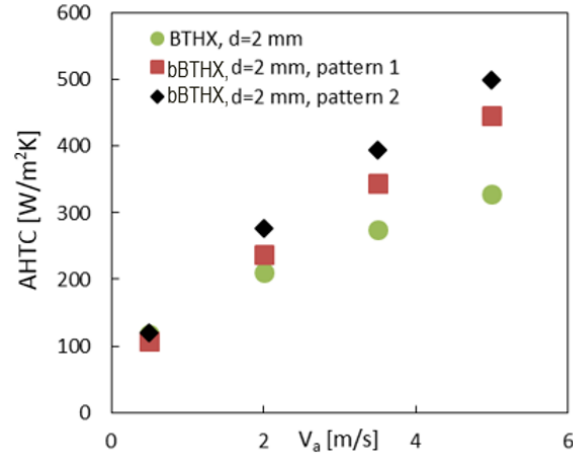
Figure 144 Effect of pattern on AHTC
(d=2 mm, θ=10°, LR=0.5)

Take the configuration in Figure 144 (d=2 mm, θ=10°, LR=0.5) as an example, I plotted

the contours of surface heat transfer coefficient at 5 m/s to see the difference between two patterns,

as shown in Figure 145. In the computational domain, two rows of tubes are calculated and the

results are plotted separately. The difference mainly comes from the second-row tube. For pattern

1, there is certain area on each of secondary tube surface where the heat transfer coefficient is

nearly zero due to the blockage of first row tube. For pattern 2, the effect of blockage is reduced

by staggering the second-row tube to let the bifurcation area of second row tube be in the middle

of the bypass area formed by first row tube, thus the average AHTC on secondary tube is higher

than that of pattern 1. Therefore, pattern 2 geometry has higher heat transfer coefficient.
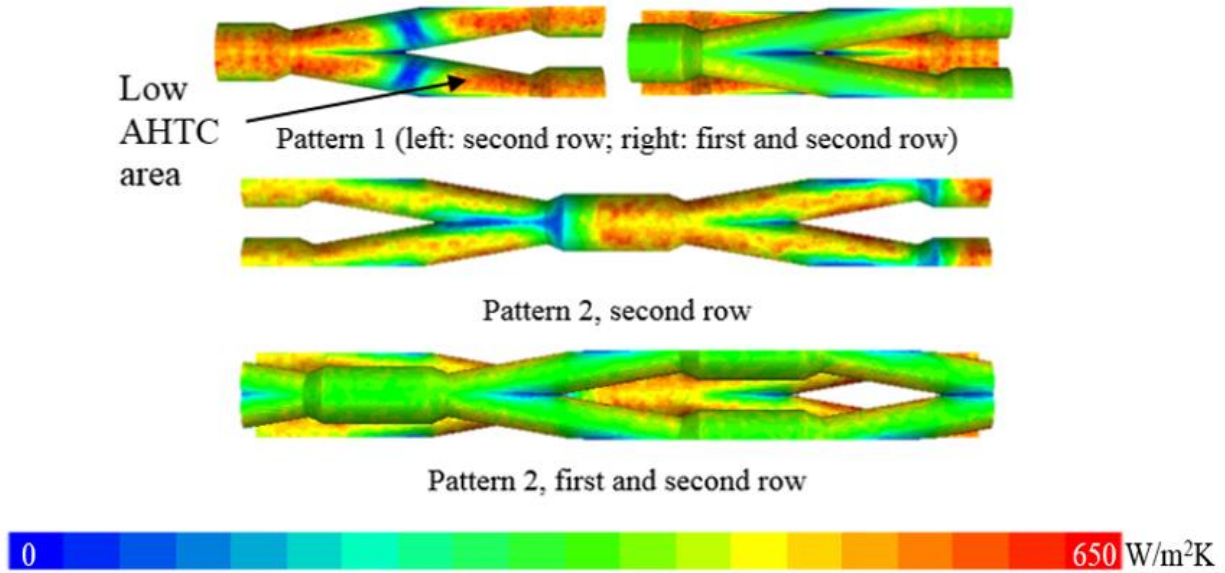
**Figure 145 Surface heat transfer coefficient of pattern 1 and 2
(d=2 mm, θ=10°, LR=0.5, Va=5 m/s)**

4.5.4. Overall conductance (hA)

To find out which geometry is better for heat exchanger design, the comparison of overall conductance (represented using hA value) per envelope volume, which is the product of heat transfer coefficient and heat transfer area, is necessary. The influence of air velocity, diameter, bifurcation angle, length ratio (LR) and different pattern on overall conductance are the same as that on AHTC. Thus, here this part is not repeated.
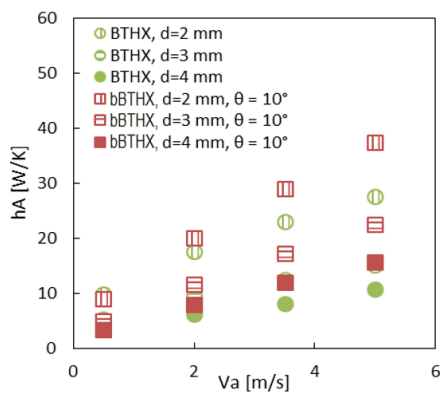
**Figure 146 Effect of diameter on airside hA
(θ=10°, LR=0.5, Pattern 1)**
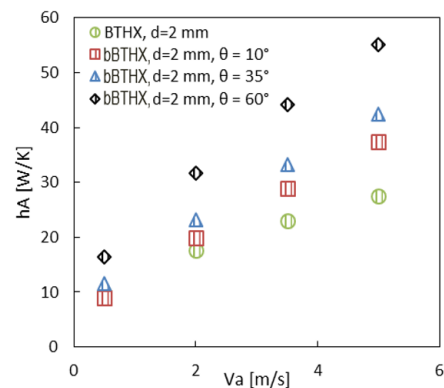
**Figure 147 Effect of bifurcation angle on airside hA
(d=2 mm, LR=0.5, Pattern 1)**
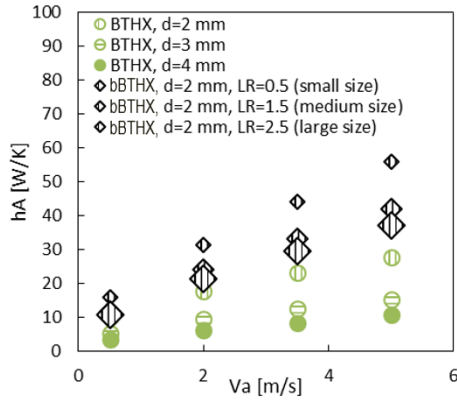
**Figure 148 Effect of LR on airside hA
(d=2 mm, θ=60°, Pattern 2)**
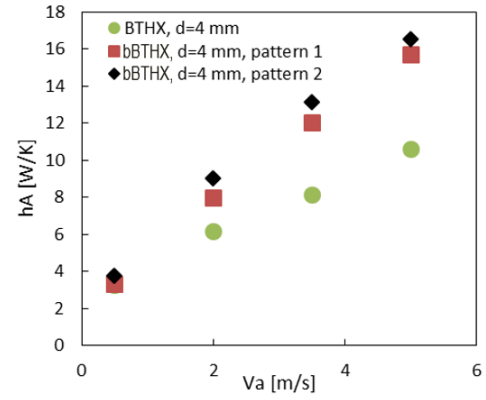
**Figure 149 Effect of pattern on airside hA
(d=2 mm, θ=10°, LR=0.5)**

4.5.5. Air-side pressure drop (ADP) per depth

First, the influence of air velocity, diameter, bifurcation angle, length ratio (LR) and different pattern on air side pressure drop (ADP) per depth are discussed. Again, representative data are summarized in Figure 150 through Figure 154.

Effect of air velocity: The effect of air velocity on ADP/Depth is shown in Figure 150. As air velocity increases, ADP/Depth increases non-linearly.

Effect of diameter: The effect of diameter on ADP/Depth is also shown in Figure 150. It is easy to understand that ADP/Depth increases as diameter decreases.
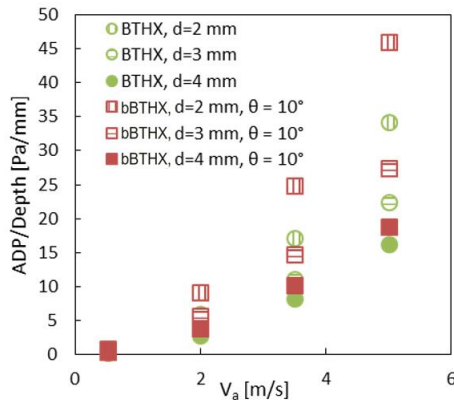
Figure 150 Effect of diameter on ADP/Depth (θ=10°, LR=0.5, Pattern 1)

125

Effect of bifurcation angle: ADP/Depth values of bBTHX with different bifurcation angles are shown in Figure 151. Increase of bifurcation angle is related to decrease of free flow area, larger mass flux, thus larger ADP/Depth.
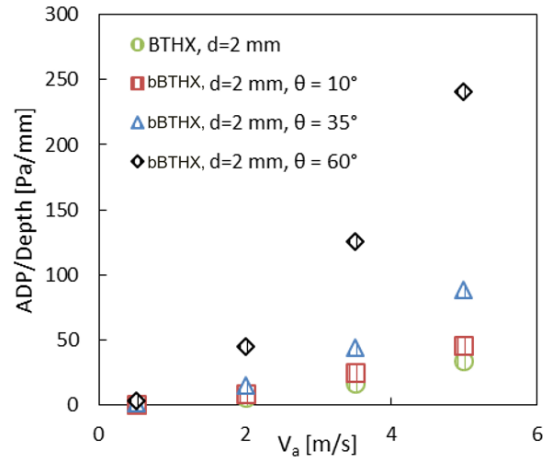
Figure 151 Effect of bifurcation angle on ADP/Depth (d=2 mm, LR=0.5, Pattern 1)

Effect of pattern: This was discussed in detail in AHTC comparison. It is easy to tell from Figure 153 that pattern 2 has more flow bypass area as compared to pattern 1 thus ADP is smaller for pattern 2.
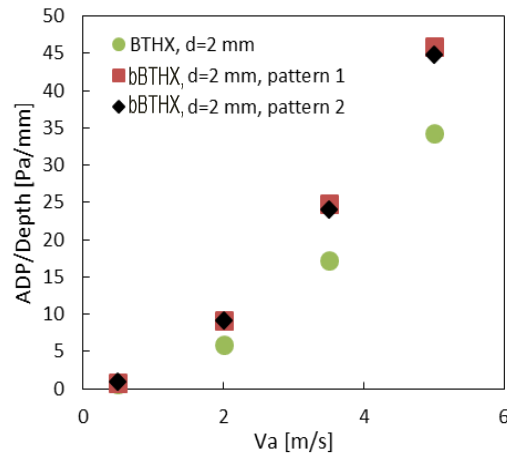
Figure 152 Effect of pattern on ADP/Depth

126

Pattern 1

Pattern 2

Flow bypass area
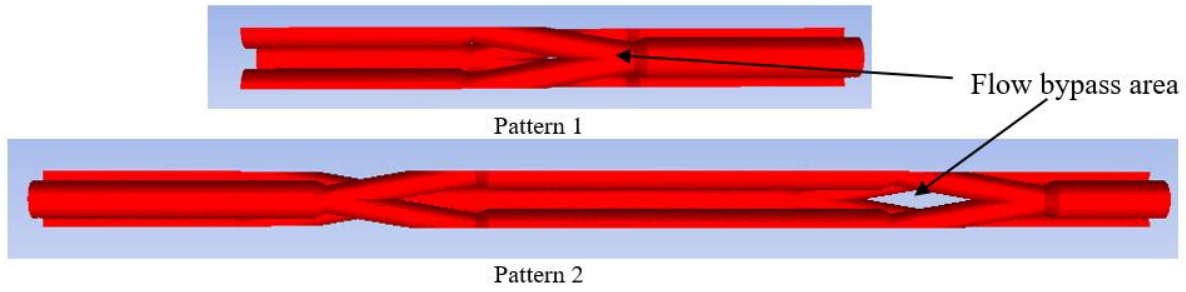
Figure 153 Geometry of bBTHX at θ=10°, LR=2.5, Pattern 2

Effect of length ratio: ADP/Depth of different bBTHX with different LR are shown in Figure 154 and Figure 155. The difference between the two graphs is the bifurcation angle. Bifurcation angle is 60° in Figure 154 and 10° in Figure 155. As length ratio increases, ADP/Depth decreases. This is expected considering that as length ratio increases, free flow area increases, thus ADP/Depth decreases. However, it should be noticed that in Figure 155, as length ratio increases, the ADP/Depth of bBTHX is smaller than BTHX.
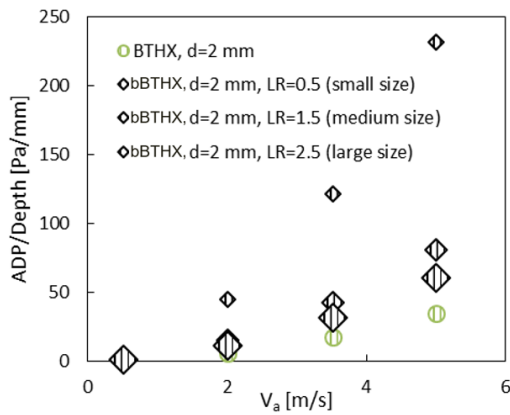
Figure 154 Effect of LR on ADP/Depth (d=2 mm, θ=60°, Pattern 2)
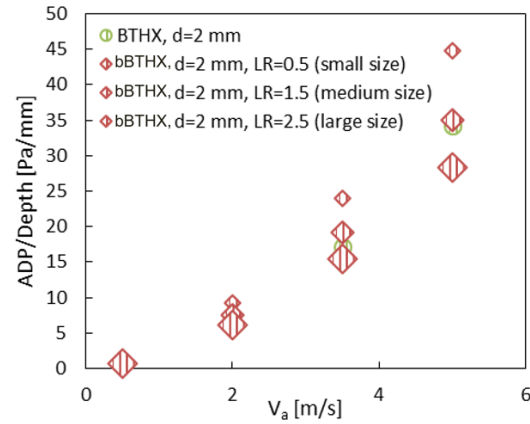
Figure 155 Effect of LR on ADP/Depth (d=2 mm, θ=10°, Pattern 2)

4.5.6. Summary of airside simulation results

Based on previous discussion we conclude that the bBTHX geometry has larger heat transfer area, AHTC and overall conductance than BTHX thus it has immense potential to be applied in air-cooled heat exchanger field. Table 19 summarizes the influence of air velocity,

diameter, bifurcation angle, length ratio (LR) and different pattern on AHTC, ADP and overall

conductance.

Table 19 Summary of airside parametric study

	Air velocity	Tube diameter	Bifurcation angle	Length ratio	Pattern
AHTC ↑	↑	↓	↑	↓	2
ADP ↓	↓	↑	↓	↑	2
hA ↑	↑	↓	↑	↓	2

Note: ↑: increase; ↓: decrease

4.6. *Waterside Simulation Results and Discussion*

4.6.1. Heat transfer area

Since the bBTHX is a bare tube heat exchanger, the waterside heat transfer area is close to airside heat transfer area, thus the analysis of heat transfer area is the same as in Chapter 4.5.1.

4.6.2. Heat transfer coefficient

This section discusses about the effect of different parameters on heat transfer coefficient.

Effect of water velocity: The effect of water velocity on WHTC is shown in Figure 156. As the water velocity increases, the waterside heat transfer coefficient (WHTC) increases for all cases. And for all cases, the bBTHX has a larger WHTC than BTHX. The advantage of WHTC improvement is more obvious at the laminar flow cases for BTHX. This is because for bBTHX, even when Reynolds number is low, the addition of bifurcation will cause boundary layer re-initiation, secondary flow and flow mixing, which all contribute to a higher local heat transfer coefficient.

Effect of diameter: The effect of diameter on WHTC is also shown in Figure 156. The WHTC increases as diameter decreases. This can be explained by using the definitions of WHTC and Nusselt number. This analysis is the same as that of airside, shown in Equation (83) through (86).
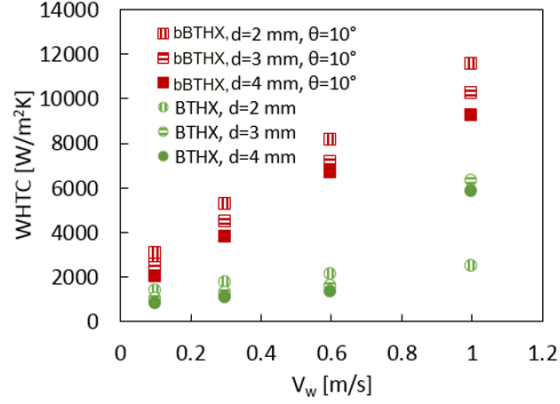
Figure 156 Effect of velocity and diameter on WHTC (θ=10°, LR=0.5)

Effect of bifurcation angle: The WHTCs of bBTHX with different bifurcation angles are shown in Figure 157. WHTC increases as bifurcation angle increases. As bifurcation angle increase, the velocity vector change of original flow is larger, causing more flow mixing. This is consistent with findings in fractal channels by Wang et al. (2007).
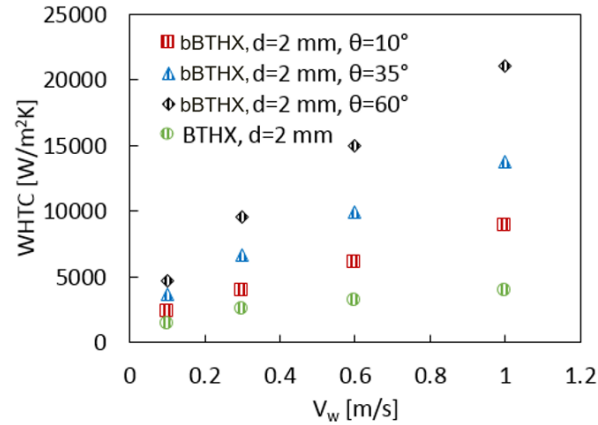
Figure 157 Effect of bifurcation angle on WHTC (d=2 mm, LR=1.5)

Effect of length ratio: the WHTCs of different bBTHX with different LR are shown in Figure 158. It can be found that the WHTC increases as LR decreases. This is because the WHTC is area-averaged HTC, designs with smaller LR have more bifurcations in unit length, resulting in larger overall WHTC.
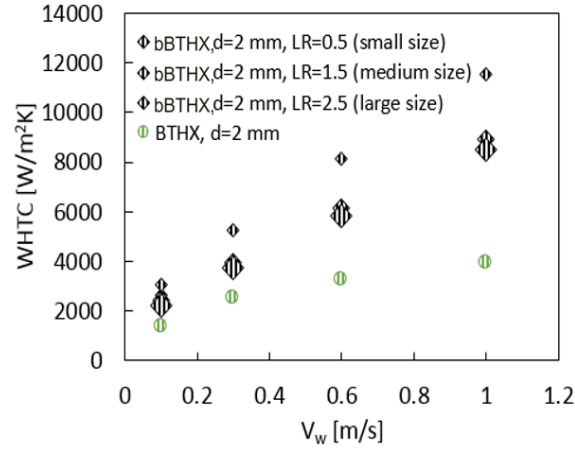
Figure 158 Effect of LR on WHTC (d=2 mm, θ=10°)

4.6.3. Overall conductance

To find out which geometry is better for heat exchanger design, the comparison of overall conductance per envelope volume, which is the product of heat transfer coefficient and heat transfer area, is necessary. Here the area A is calculated based on unit length. The influences of velocity, diameter, bifurcation angle, and length ratio (LR) on overall conductance are the same as that on AHTC. Thus, here we do not repeat it.
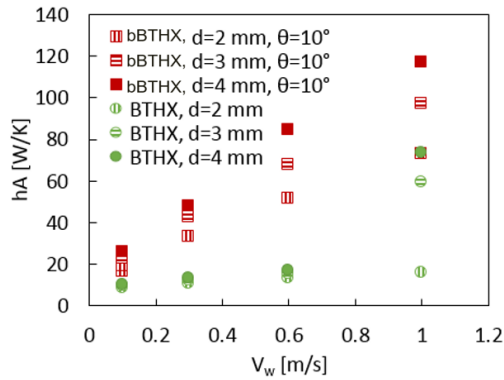
Figure 159 Effect of velocity and diameter on hA (d=2 mm, θ=10°)
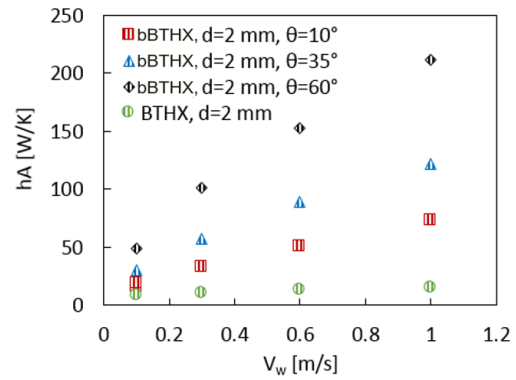
Figure 160 Effect of bifurcation angle on hA (d=2 mm, LR=1.5)
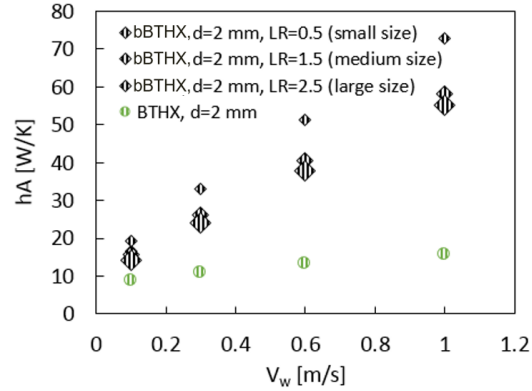
Figure 161 Effect of LR on hA
(d=2 mm, θ=10°)

4.6.4. Water-side pressure drop (WDP) per length

This section first discusses about the influences of water velocity, diameter, bifurcation angle and length ratio (LR) on water side pressure drop (WDP) per length. The definition of length is shown in Figure 162.
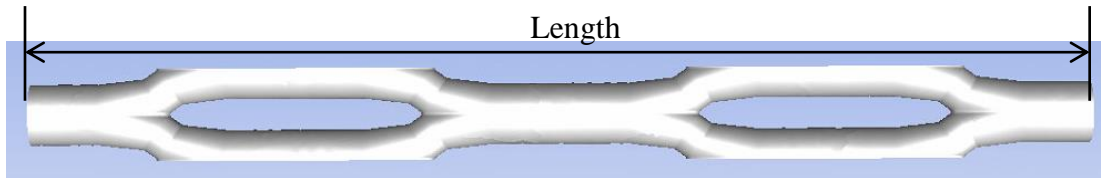
Figure 162 bBTHX computational domain

Effect of water velocity: The effect of water velocity on WDP/Depth is shown in Figure 163. As water velocity increases, WDP/Depth increases non-linearly.

Effect of diameter: The effect of diameter on WDP/Depth is also shown in Figure 163. It is easy to understand that WDP/Depth increases as diameter decreases.

132
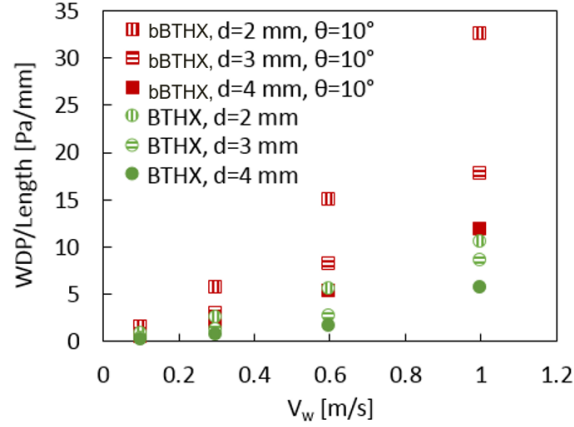
Figure 163 Effect of velocity and diameter on WDP/Length (θ=10°, LR=0.5)

Effect of bifurcation angle: WDP/Depth of bBTHX with different bifurcation angles are shown in Figure 164. Increase of bifurcation angle is related to better flow mixing and more secondary flow motions, leading to larger ADP/Depth. This is explained in detail later.
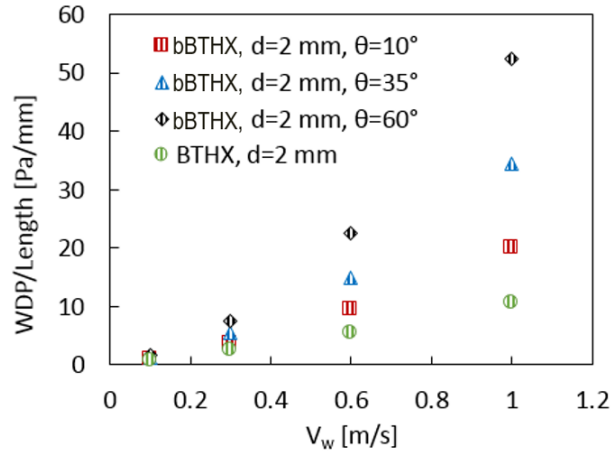
Figure 164 Effect of bifurcation angle on WDP/Length (d=2 mm, LR=1.5)

Effect of length ratio: WDP/Depth of bBTHX with different length ratios are shown in Figure 165. Designs with smaller LR have more bifurcations in unit length, resulting in larger pressure drop per depth.
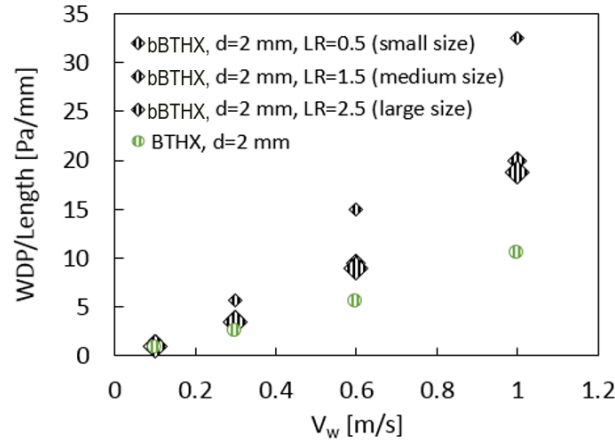
Figure 165 Effect of length ratio on WDP/Length (d=2 mm, θ=10°)

4.6.5. j and f factors

j and f factors are calculated using Equation (23) and Equation (24), respectively. Here, f factor refers to Fanning friction factor. Figure 166 summarizes the results of j factors. From this graph, it can be found that j factor increases as Reynolds number decreases for both BTHX and bBTHX. And j factor of bBTHX increases as LR decreases or bifurcation angle increases. This is consistent with the findings in Chapter 4.5.2. The two points highlighted inside the red circle are in turbulence regime.
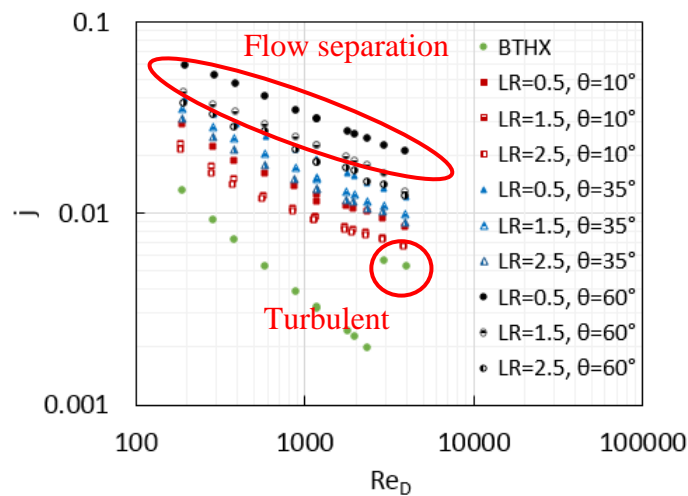
Figure 166 *j* factor of waterside parametric study results for bBTHX

Figure 167 summarizes the results of f factors. From this graph, we can find that f factor increases as Reynolds number decreases for both BTHX and bBTHX. And f factor of bBTHX increases as LR decreases or bifurcation angle increases. This is consistent with the findings in Chapter 4.5.4.
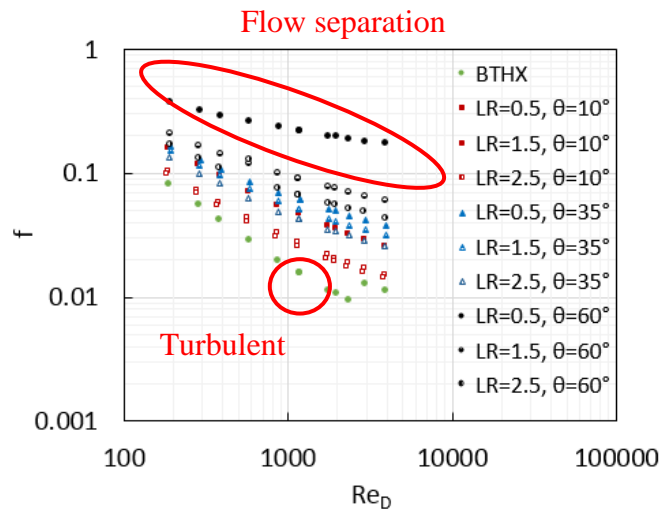
Figure 167 *f* factor of waterside parametric study results for bBTHX

Figure 168 summarizes the results of j/f value. From this graph, it can be found that for cases that bifurcation angle is 35°, j/f values are similar when LR equals 0.5, 1.5 and 2.5. For cases that bifurcation angle is 10° and 60°, j/f values increase as LR increases. The j/f value of most cases of bBTHX are higher than those of BTHX. For cases that LR=0.5 and θ=60°, j/f value is lower than that of BTHX. One reason is flow separation, which generates large form drag. This is explained in detail in Chapter 4.8. Again, j/f value of BTHX in turbulent regime is much higher than that in laminar regime. However, for such heat exchangers, the operating conditions are mostly in laminar regime.

135
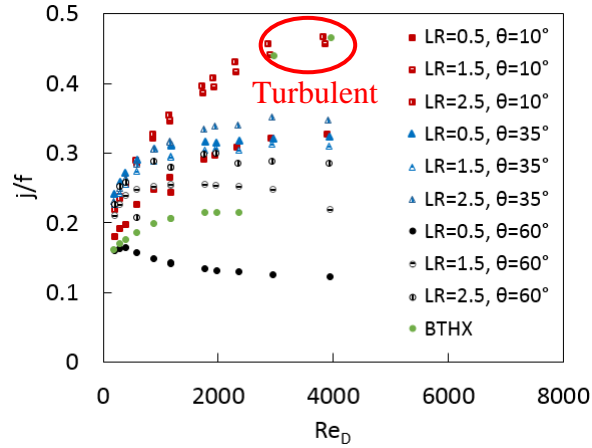
Figure 168 *j/f* value of waterside parametric study results for bBTHX

Another lesson learned here is that j and f factor can be described as the functions of Reynolds number and geometry parameters. And this is the theoretical foundation of building metamodel. In metamodeling, Nusselt number and f factor are used. Nusselt number is expressed as the function of Reynolds number, Prandtl number and geometry parameters while f factor is expressed as the function of Reynolds number and geometry parameters.

4.6.6. Summary of waterside simulation results

Based on previous discussion it is found that the bBTHX geometry has larger heat transfer area, WHTC and overall conductance than BTHX thus it has immense potential to be applied in air-cooled heat exchanger field. Table 19 summarized the influence of water velocity, diameter, bifurcation angle and length ratio (LR) on WHTC, WDP/Length and overall conductance.

Table 20 Summary of waterside parametric study

	Water velocity	Tube diameter	Bifurcation angle	Length ratio
WHTC ↑	↑	↓	↑	↓
WDP/Length ↓	↓	↑	↓	↑
hA ↑	↑	↓	↑	↓

Note: ↑: increase; ↓: decrease

136

In real heat exchanger design, what engineers care most is the heat transfer capacity per power input. Here the overall conductance and WDP/Length of bBTHX and BTHX are compared. From Figure 169, bBTHX has higher overall conductance. But BTHX can have considerably high overall conductance when it transients to turbulent flow.
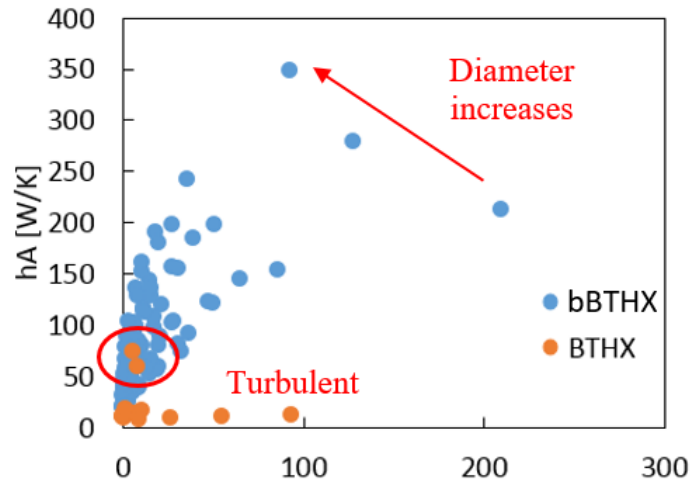
Figure 169 Overall conductance and WDP/Length comparison

4.7. Airside Thermal and Hydraulic Mechanisms

4.7.1. Heat Transfer Mechanism

There are three main reasons for AHTC improvement. To illustrate this, I use the data for 0.8 mm since it was validated experimentally.

Reason 1: bBTHX has larger mass flux based on free flow area (Figure 170). And it can also be noticed that even with the same mass flux, bBTHX still has a higher AHTC (Figure 171). This is due to reasons 2 and 3.

137
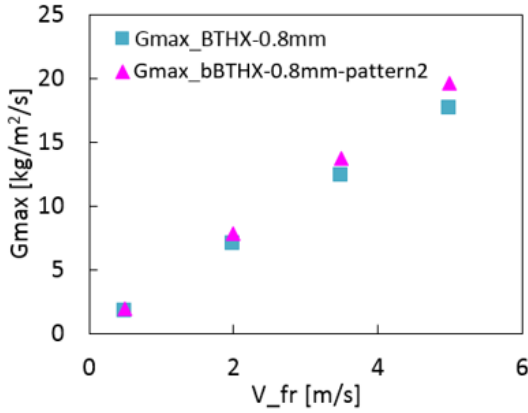
Figure 170 Mass flux of bBTHX and BTHX (d=0.8 mm, θ=10°, LR=2.5, Pattern 2)
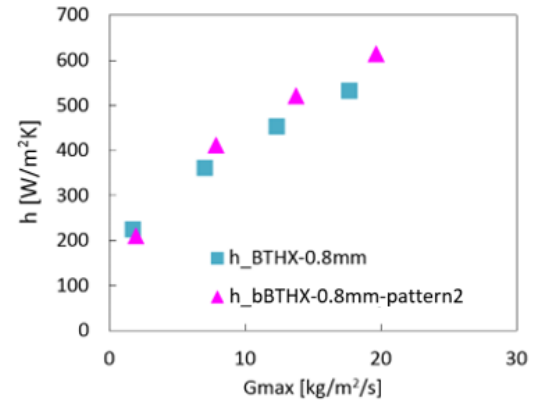
Figure 171 AHTC of bBTHX and BTHX with same mass flux (d=0.8 mm, θ=10°, LR=2.5, Pattern 2)

Reason 2: Branch tube of bBTHX has smaller diameter, and it can be seen from Figure 172 that smaller diameter bare tube with same pitch value has larger AHTC.
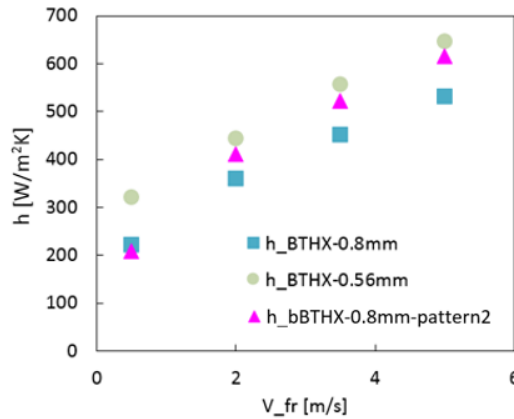
Figure 172 AHTC of BTHX with different diameter

Reason 3: 3D boundary layer development. This will be explained in detail in the following hydraulic performance discussion. Briefly, 3D boundary layer formed around bifurcation enhances flow mixing, resulting in higher heat transfer coefficient. This phenomenon could not be observed in BTHX due to 2D flow assumption. Thus factors, for example, smaller length ratio, that can lead to more bifurcation structures in a certain control volume have positive impact on heat transfer coefficient improvement.

138

4.7.2. Flow friction mechanism

Here explains the reason why bBTHX could have lower pressure drop for some designs. Still, the results of 0.8 mm BTHX and bBTHX are used here to explain the reasons because they were validated experimentally. Figure 173 shows ADP/Depth of bBTHX is about 4~12% lower than that of BTHX at air velocity of 3.5 and 5 m/s.
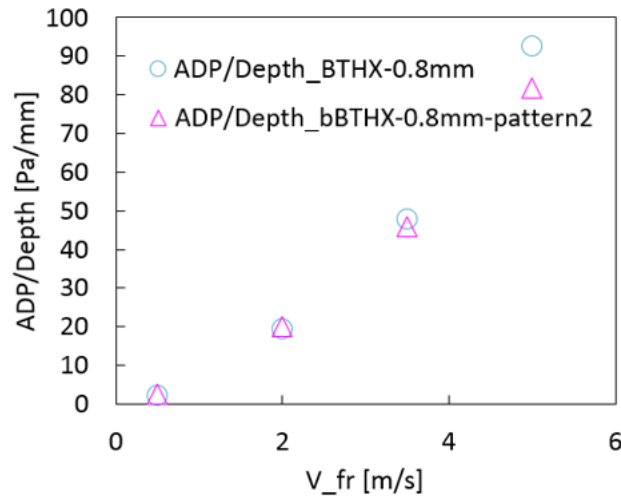
Figure 173 ADP/Depth of bBTHX and BTHX
(d=0.8 mm, θ=10°, LR=2.5, Pattern 2)

Reason 1: For designs with bifurcation equals 10° and LR equals 2.5, the increase of heat transfer area and decrease of free flow area are the smallest among all configurations.

Reason 2: There is flow bypass in bBTHX designs (as shown in Figure 174) and at larger length ratio, the effect of bypass is more obvious. From Figure 174, it can be noticed that there is a sharp decrease of pressure drop for bBTHX where there is flow bypass at the bifurcation.
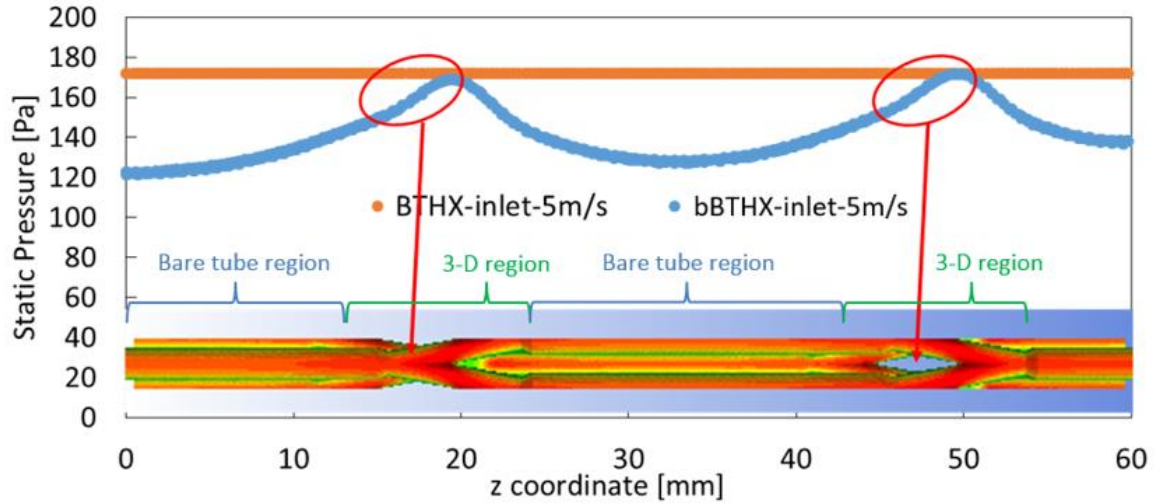
Figure 174 Flow bypass at bifurcation (d=0.8 mm, θ=10°, LR=2.5, Pattern 2)

Reason 3: Lower flow rate at bare tube region. For bBTHX, it can be divided into two regions, one is bare tube region which consists of staggered vertical tubes, and this configuration is the same as BTHX. The other region is 3D flow region, where the bifurcations is. This is shown in Figure 174. bBTHX has smaller velocity magnitude in that region, as shown in Figure 175, the cross section selected are shown in Figure 176. Note that the computational domain for BTHX is 2D, here a 3D graph is used to make it easier for readers to understand.
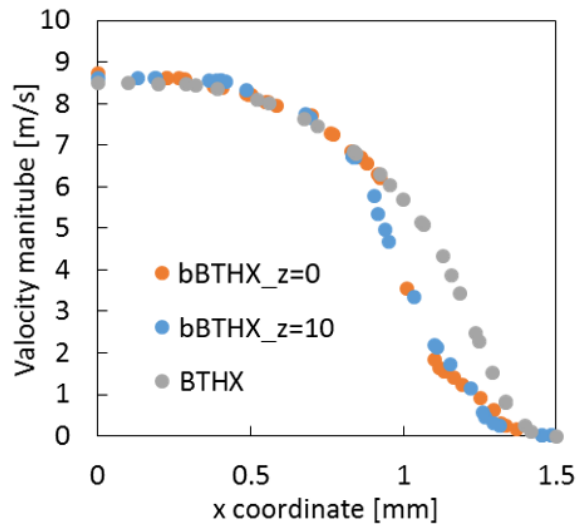
Figure 175 Radial velocity magnitude of BTHX and bBTHX

140

z=0 mm z=10 mm

BTHX

(a)   (b)
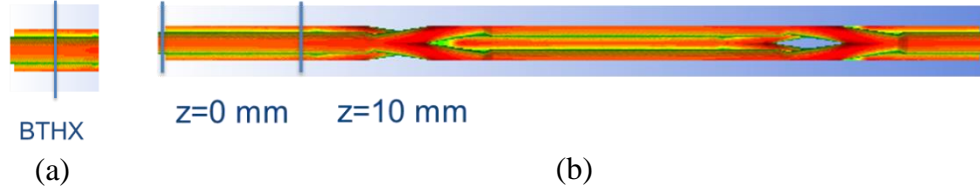
Figure 176 Cross section of BTHX (a) and bBTHX (b)
(z=0 mm and z=10 mm)

Reason 4: 3D flow at bifurcation. In 3D region of bBTHX, there is z direction velocity, as shown in Figure 177. This 3D flow phenomenon occurs at the bifurcation only and is the key mechanism causing the improvement of AHTC and decrease of ADP/Depth for bBTHX simultaneously.
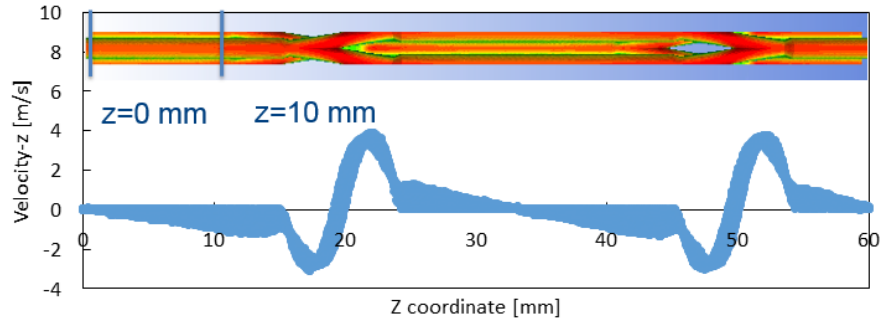
Figure 177 Airside velocity in z direction for bBTHX

To understand the influence of z direction velocity, the drag coefficient of sphere and cylinder are shown in Figure 178. Solid line is for sphere and dotted line is for cylinder. At low Reynolds number, the cylinder has lower drag coefficient but at larger Reynolds number, the sphere has lower pressure drop. In this study, the Reynolds number range is from 23 to 233. Plotting the Nusselt number for cylinder and sphere, it can be found the sphere's Nusselt number is always larger than cylinder, as shown in Figure 179. In current design, the bifurcation enables 3D flow just like the sphere does.

141
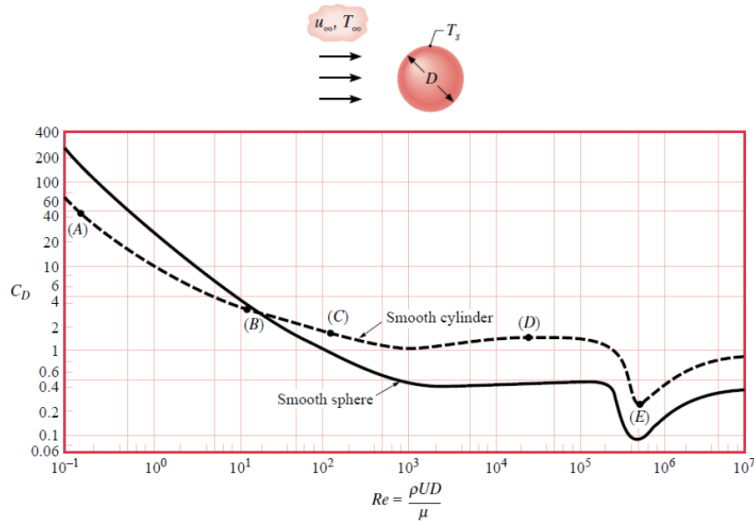
Figure 178 Drag coefficient for cylinder and sphere in free flow
(Incropera, 2007)
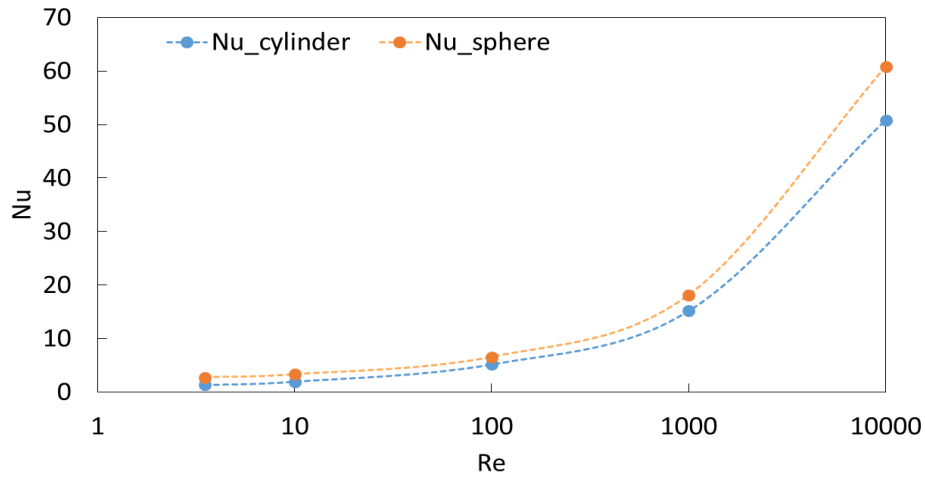
Figure 179 Nusselt number of cylinder and sphere in free flow
(Correlations from Incropera, 2007)

4.7.3. Summary of airside mechanisms

Novel bifurcated bare tube heat exchanger had 15% higher air-side heat transfer coefficient and 4~12% lower air-side pressure drop than baseline bare tube heat exchanger with same diameter (0.8 mm), frontal area, volume at a certain air velocity range (3.5~5 m/s). All the mechanism and their influences on AHTC and ADP/Depth are summarized in Table 21. The key mechanism that enables some designs in the parametric study to have higher heat transfer coefficient and smaller pressure drop is 3D flow enabled by bifurcation in bBTHX design.

142

Table 21 Summary of all airside mechanisms

	AHTC	ADP/Depth
Larger mass flux	+	+
Branch tube (smaller OD)	+	+
Flow bypass	-	-
Lower flow rate at bare tube region	-	-
3D flow	+	-

4.8. Waterside thermal and hydraulic mechanisms

In this section, the thermal and hydraulic mechanisms of waterside are discussed. Figure 180 shows the velocity contour of BTHX and bBTHX, the color map scales are the same and only fully developed regions are presented. It can be found that due to the addition of bifurcation, the flow in bBTHX is quite different from that of BTHX.

4.8.1. Smaller branch tubes

The diameter of branch tubes is 0.7 of the main tube diameter. As discussed before, $h \propto \dfrac{1}{D^{1-m}}$, where $0 \leq m \leq 1$, thus smaller tubes will result in higher heat transfer coefficient. Similarly, the relationship between pressure drop and diameter can be derived. Equation (87), (88) and (89) show smaller diameter tubes results in larger pressure drop.

$$\Delta P = f \frac{l}{D} \frac{\rho V^2}{2} \tag{87}$$

$$f \propto \frac{1}{\mathrm{Re}^m}, \ 0 < m \leq 1 \tag{88}$$

$$\Delta P / l \propto \frac{1}{\mathrm{Re}^m} \frac{l}{D} \frac{\rho V^2}{2} \propto \frac{1}{\left(\dfrac{VD}{v}\right)^m} \frac{l}{D} \frac{\rho V^2}{2} \propto \frac{1}{D^{m+1}}, \ 0 < m \leq 1 \tag{89}$$

In current design, addition of small diameter tube improves local heat transfer coefficient and leads to higher pressure drop. This is illustrated in the following section.

4.8.2. Boundary layer interruption and redevelopment

Figure 180 presents the velocity contour of middle plane in BTHX and bBTHX. The definition of middle plane is also shown. Figure 180 shows at the bifurcation, flow is interrupted and boundary layer redevelops at the bifurcation. Figure 181 shows the velocity vector. Flow is brought to rest at the forward stagnation point, with an accompanying rise in pressure. The kinetic pressure converts to static pressure. The boundary layer redevelopment boosts local heat transfer, but contributes to larger pressure drop as well.

Pressure along the flow direction of bBTHX is plotted in Figure 182. Pressure of BTHX is also plotted as a comparison. bBTHX has a higher pressure drop compared with BTHX with the same inlet diameter. Static pressure is related to kinetic pressure; thus, velocity contour is also plotted in Figure 182. Static pressure of bBTHX spikes at the bifurcation. But right after it, there is a sudden drop due to velocity increase which is related to the surface shape change. Another reason that bBTHX has larger pressure drop is smaller branch tubes, as discussed before. Figure 182 shows the static pressure drops faster in branch tube region, and slower in main tube region, and the slope of main tube region is similar to bare tube with same diameter. But the slope of branch tube region is slightly higher than that of bare tube with same diameter due to the local loss of bifurcation and boundary layer redevelopment.

Local heat transfer coefficient also spikes at the bifurcation where the stagnation point is, which can be seen from Figure 183. After the short entry length, surface heat transfer of BTHX becomes very stable, which is expected because it is laminar flow and the Nusselt number is constant theoretically. Smaller diameter bare tube has a larger local heat transfer coefficient. So, for bBTHX, the heat transfer coefficient is higher in branch tube region. At large diameter tube region, the heat transfer coefficient of bBTHX is quite similar to that of BTHX.

144
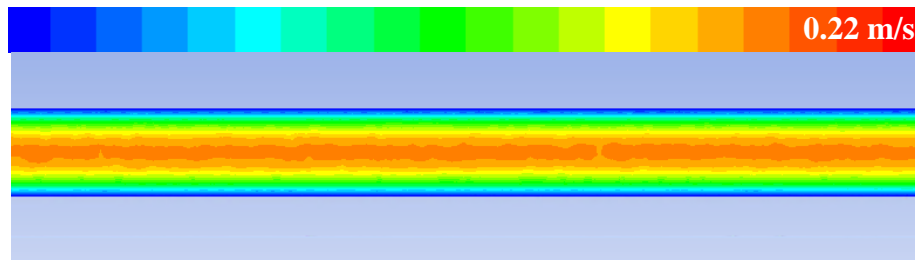
(a)
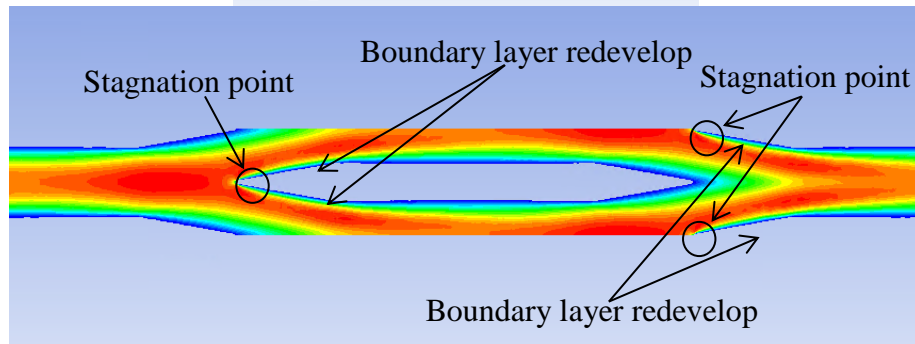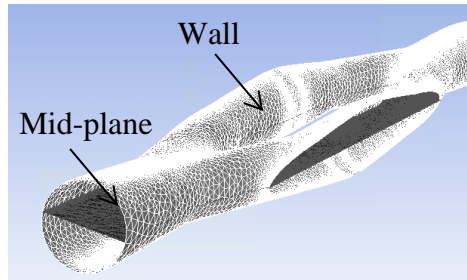
(b)

Figure 180 Velocity contour of fully developed region of BTHX at mid-plane (a) (d=2 mm, V_w=0.1 m/s) and bBTHX (b) (d=2mm, θ=10°, LR=0.5, V_w=0.1 m/s)
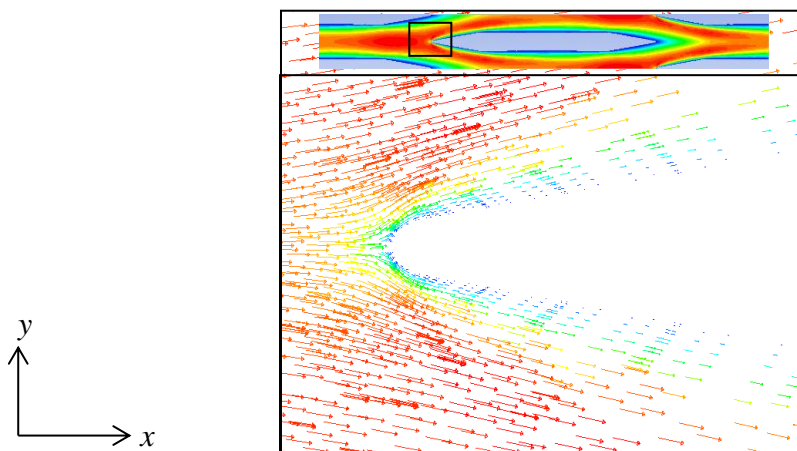
Figure 181 Velocity vector at bifurcation at mid-plane (color is velocity magnitude) (d=2mm, θ=10°, LR=0.5, V_w=0.1 m/s)
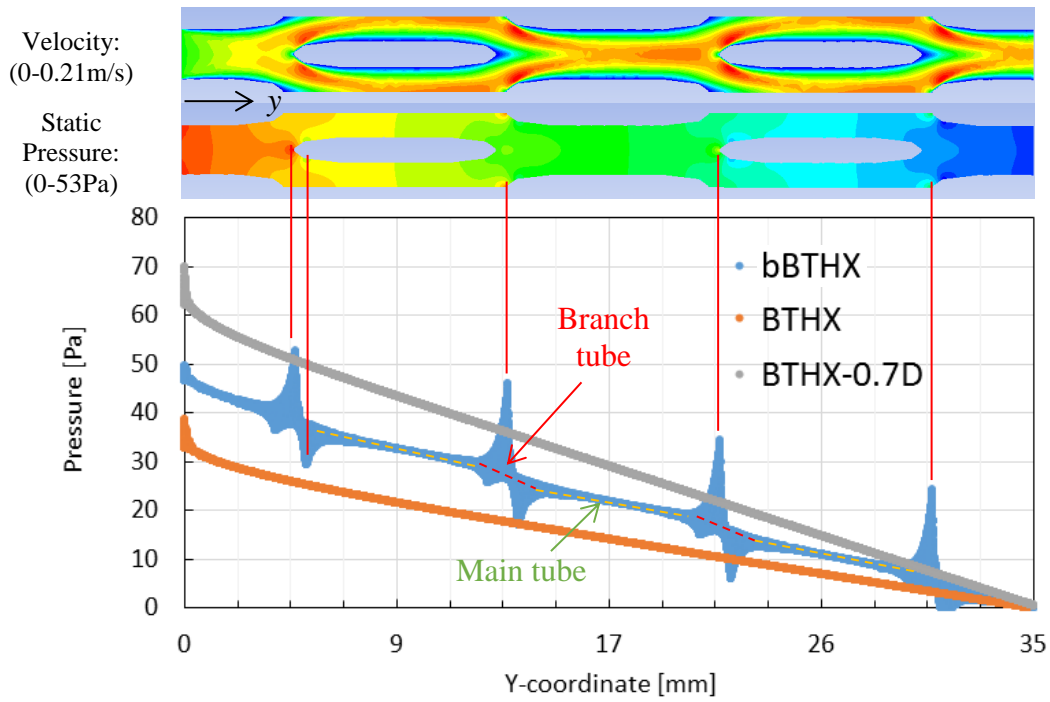
Figure 182 Static pressure of BTHX (d=2 mm, V_w=0.1 m/s), BTHX-0.7D (d=1.4 mm, V_w=0.1 m/s) and bBTHX (d=2mm, θ=35°, LR=2.5, V_w=0.1 m/s) at mid-plane
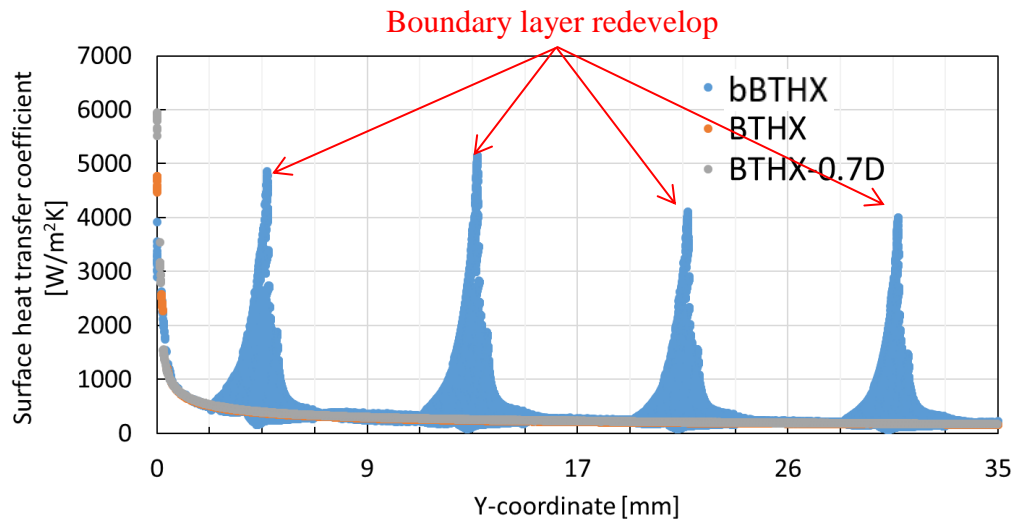
Figure 183 Surface heat transfer coefficient of BTHX (d=2 mm, V_w=0.1 m/s), BTHX-0.7D (d=1.4 mm, V_w=0.1 m/s) and bBTHX (d=2mm, θ=35°, LR=2.5, V_w=0.1 m/s)

4.8.3. Flow separation

Flow separation is not found in all cases, but in those with large bifurcation angle. As discussed before, boundary layer redevelops at the bifurcation. But as the boundary layer develops, there is a chance that the pressure gradient becomes adverse, causing flow deceleration and separation. Figure 184 shows the boundary layer detaches from the surface and a stable pair of wake is formed in the downstream region. The flow is separated but steady and the formation of the wake generates high form drag, in addition to friction drag caused by surface shear.
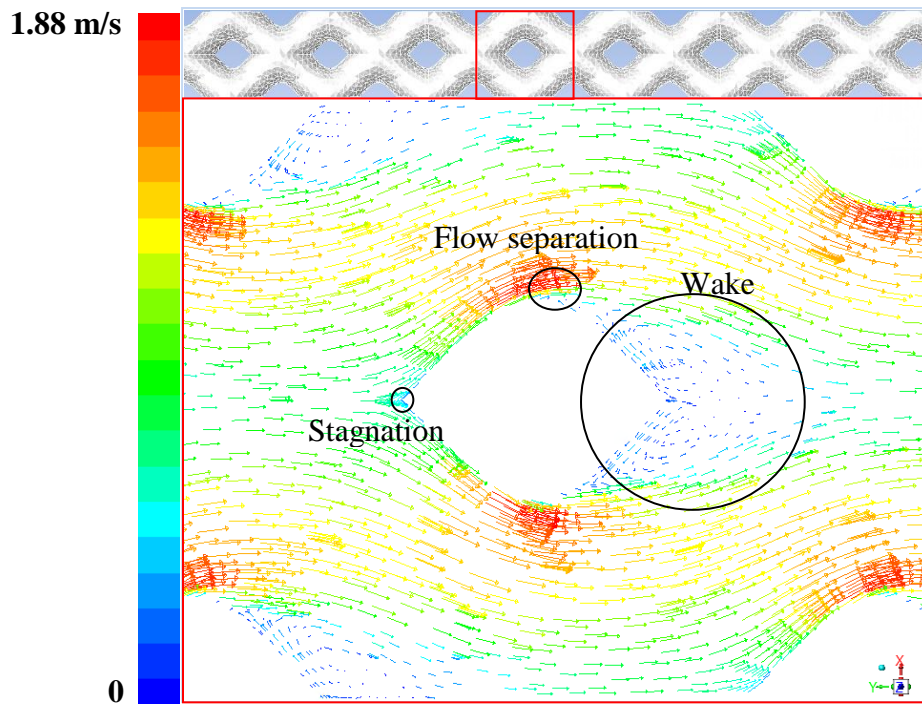
Figure 184 Velocity field of bBTHX (d= 4 mm, LR=0.5, θ=60°, V_w=1 m/s, Re=3943) at mid-plane

Then here explains why cases with bifurcation angle equals 60° has considerably larger f factor than others. The most important reason is flow separation. As length ratio increases, the f factor decreases. This is not only because larger length ratio results in less bifurcation per length, but also due to the smoother transition of angle, as shown in Figure 185. Comparing (a) (b) and (c), as LR increases, the geometry becomes more streamline, thus the flow separation point is further in the downstream, and the wake area generated is smaller. The difference between (b) and

147

(c) is smaller than that between (a) and (b). This explains why in Figure 167, f factor of cases with bifurcation angle 60° and LR 0.5 is much larger than others.

| (a) LR=0.5 | (b) LR=1.5 | (c) LR=2.5 |
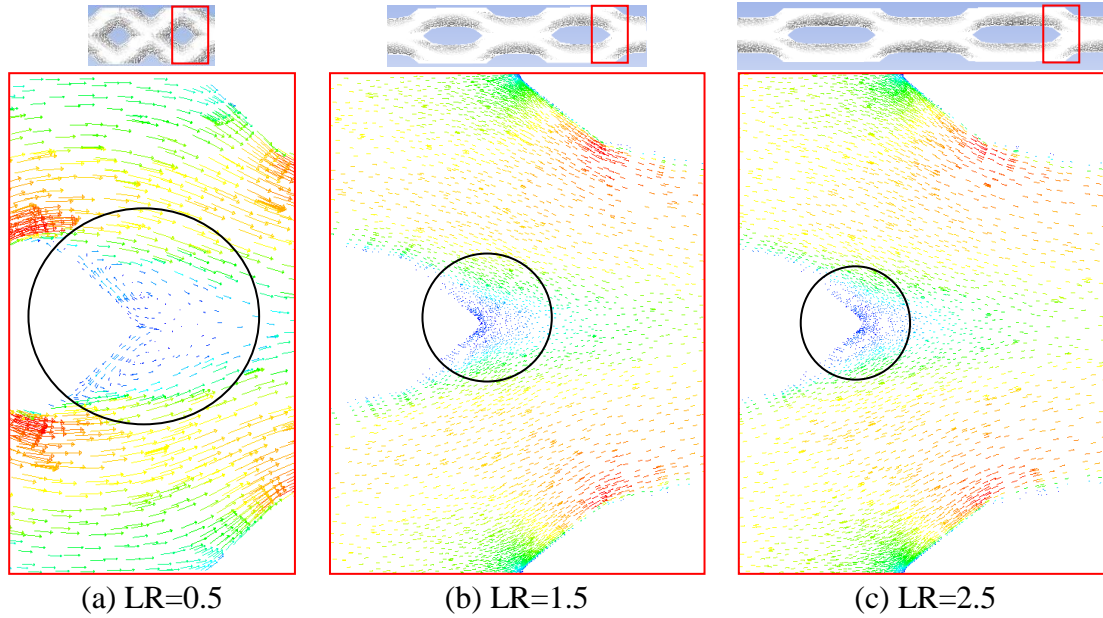
Figure 185 Effect of LR on flow separation
(d= 4 mm, θ=60°, V$_w$=1 m/s)

4.8.4. Secondary flow

Secondary flow is also not found in all cases, but in those with large bifurcation angle. Figure 186 shows that there is secondary flow due to the shape change of the tube. In this example, bifurcation angle is large, so there is a separated region of flow near the inside of the tube bend. The swirling secondary flow occurs because of the imbalance of centripetal forces because of the curvature of the tube centerline (Munson et al., 2006). Secondary flow acts to replace the slow-moving fluid near the walls with faster-moving fluid, therefore generating large viscous friction at the wall. Secondary flow also enhances thermal mixing by bringing colder flow from inside to the wall, thus larger local Nusselt number (Senn and Poulikakos, 2004). Another influence on heat transfer is that secondary flow changes the location of the highest temperature, as shown in Figure 187.
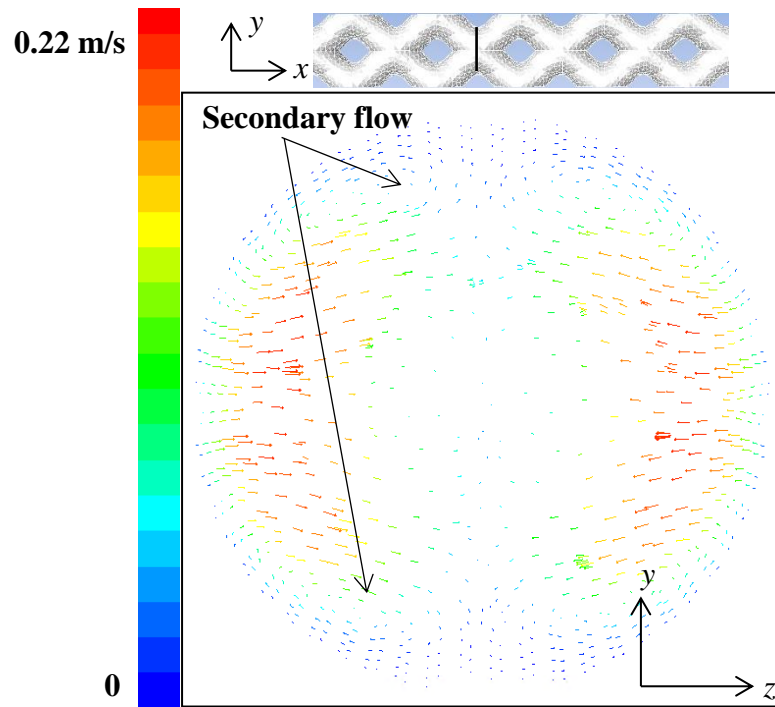
Figure 186 Velocity field of Secondary flow (d= 2 mm, LR=0.5, θ=60°, V$_w$=0.1 m/s)

(a) No secondary flow

(d= 2 mm, LR=0.5, θ=10°, V_w=0.1 m/s)

(b) With secondary flow

(d= 2 mm, LR=0.5, θ=60°, V_w=0.1 m/s)
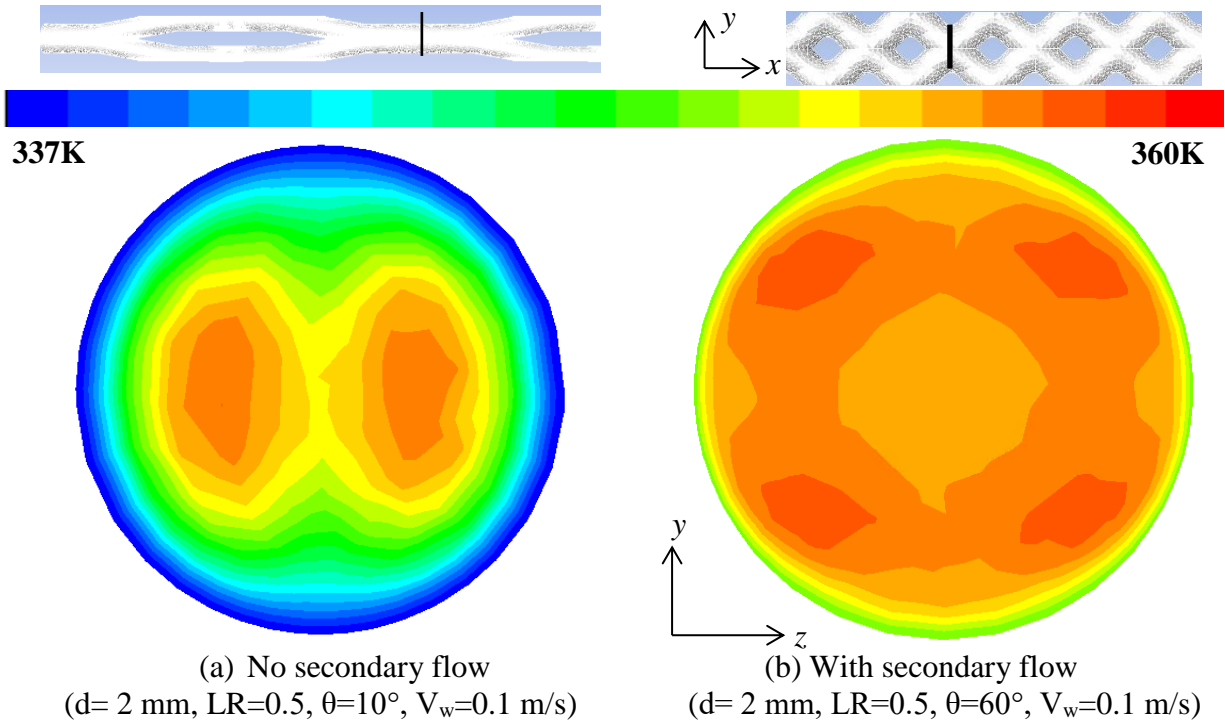
Figure 187 Temperature contour of geometry without (a) and with (b) secondary flow

4.8.5. Summary of waterside mechanisms

The heat transfer and pressure drop characteristics of bBTHX have several unique features due to addition of bifurcations.

- The branch tube with smaller diameter increases heat transfer coefficient as well as pressure drop.

- At bifurcation, flow splits into two streams and boundary layer interrupts and redevelops along the wall. This enhances heat transfer and increases pressure drop. Pressure drop and heat transfer coefficient spike at stagnation point.

- The shape of bifurcation along the waterflow direction is usually close to oval shape, causing flow separations when the angle is large. This results in heat transfer coefficient increase but accompanying with form drag.

- Secondary flow, found in geometries with large bifurcation angle, enhances flow mixing with accompanying larger pressure loss. Secondary flow also changes the location of the highest temperature flow.

Table 22 Summary of all waterside mechanisms

	WHTC	WDP/Depth
Branch tube (smaller ID)	+	+
Boundary layer redevelop	+	+
Flow separation	+	+
Secondary flow	+	+

Chapter 5: bBTHX Optimization

5.1. *Airside Meta-Model*

The input and output parameters of bBTHX airside meta-model is summarized in Table 23. Chilton - Colburn j and f factors are selected as the output parameters. As stated before, the accuracy of metamodel is evaluated using the Metamodel Acceptability Score (MAS) (Hamad, 2006). 100% of j and f factor predicted are within 15% deviation from CFD values, as shown in Figure 188.

Table 23 Summary of airside meta-model

Input parameters (normalized)	N_r	D_1	P_l/D_1	P_t/D_1	LR	θ	V_a
Output parameters	j				f		
Meta-model points	783						
Random points for verification	50						
Metamodel Acceptability Score	j				f		
	100% within 15%				100% within 15%		

(a)   (b)
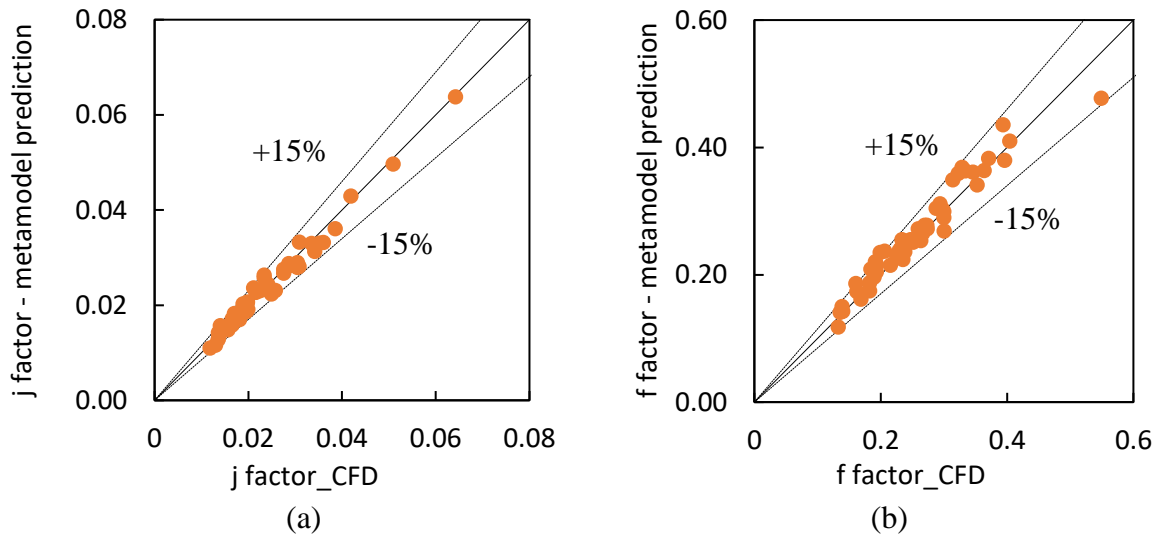
Figure 188 Airside metamodel prediction of j factor (a) and f factor (b)

5.2. *Waterside Meta-Model*

The input and output parameters of bBTHX waterside meta-model are summarized in Table 24. Nusselt number and WDP/segment are selected as the output parameters and the definition of one segment is shown in Figure 189. It is the minimum segment during bBTHX modeling. As stated before, the accuracy of metamodel is evaluated using the Metamodel Acceptability Score (MAS) (Hamad, 2006). 100% of Nusselt number predicted are within 8% deviation from CFD Nusselt values. 96% of WDP/segment predicted by meta-model are within 10% deviation from CFD results, as shown in Figure 190.

Table 24 Summary of waterside meta-model

Input parameters (normalized)	D_1	P_l/D_1	LR	θ	V_w
Output parameters	Nu		WDP/segment		
Meta-model points	258				
Random points for verification	25				
Metamodel Acceptability Score	Nu		WDP/segment		
	100% within 8%		96% within 10%		

Figure 189 Definition of one segment on waterside

(a)	(b)
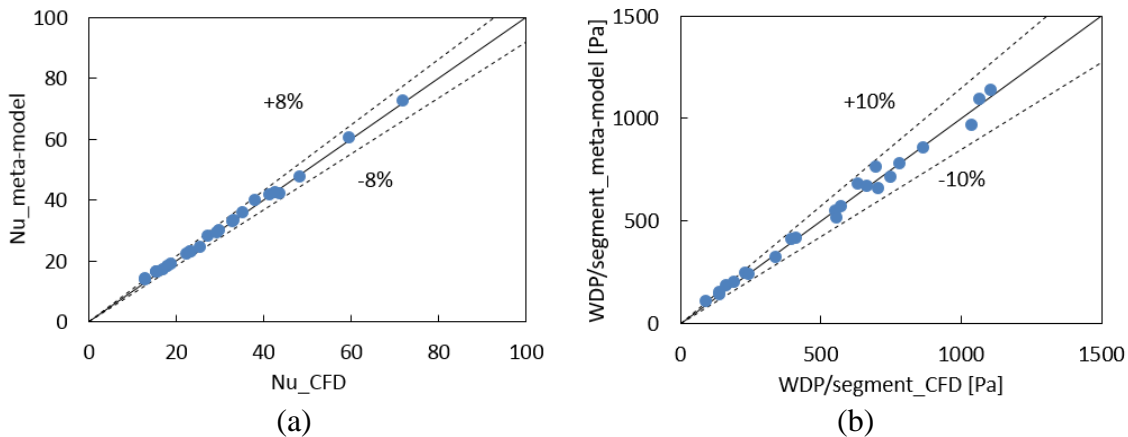
Figure 190 Waterside metamodel prediction of Nusselt number (a) and ADP/segment (b)

153

5.3. *bBTHX Solver and Validation*

5.3.1. bBTHX area correction

The heat transfer area calculated using geometry parameters approximates the area of bBTHX geometry model built in ANSYS® software. bBTHX heat transfer area of one segment calculated using geometry parameters is shown in Equation (90) and (91).

$$A_{air} = 2\pi D_{1,o} L_1 + 4\pi D_{2,o} L_2 \tag{90}$$

$$A_{water} = 2\pi D_{1,i} L_1 + 4\pi D_{2,i} L_2 \tag{91}$$

Where $D_{1,o}$ and $D_{2,o}$ are outer diameter of main tube and branch tube and $D_{1,i}$ and $D_{2,i}$ are inner diameter of main tube and branch tube. The other parameters are shown in Figure 191. From this graph, the heat transfer area calculated using the above two equations are heat transfer area of several cylinders built around the centerline of bBTHX which is different from the real geometry. Thus, correction is needed.
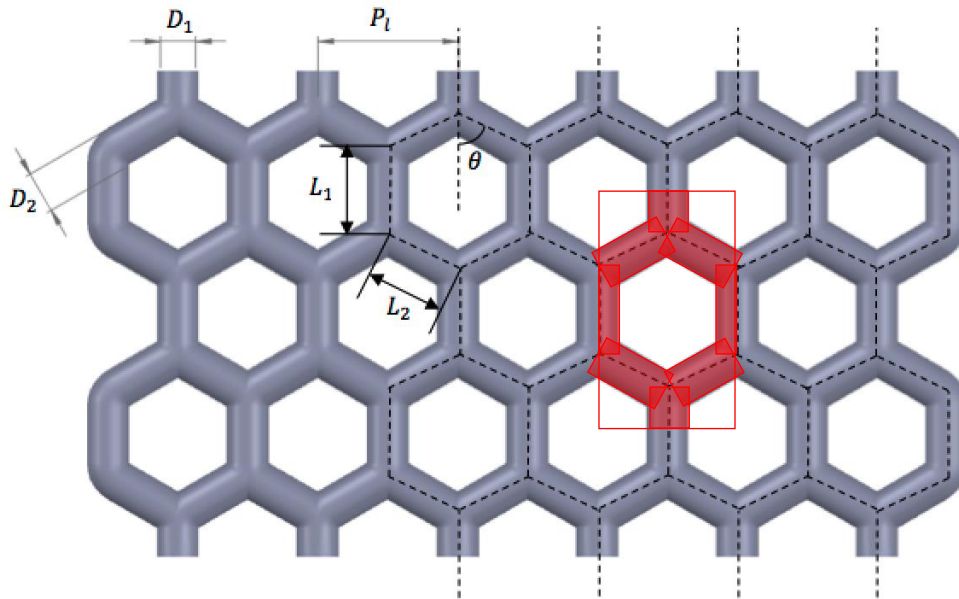
Figure 191 Heat transfer area calculation for bBTHX
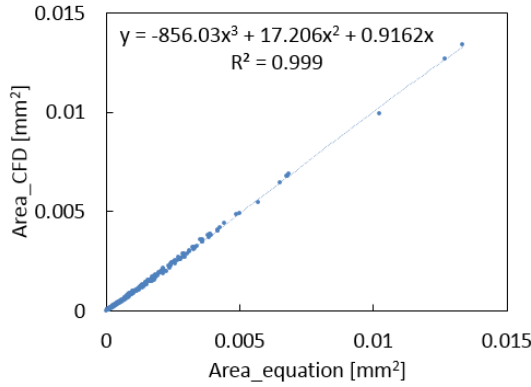
Figure 192 Heat transfer area correction equation for bBTHX
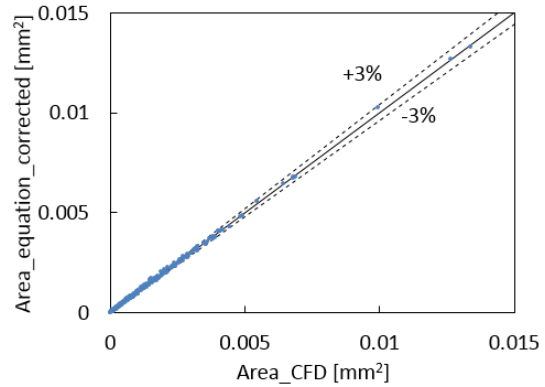
Figure 193 Heat transfer area verification against CFD results for bBTHX

Using heat transfer area output from CFD software FLUENT® as the real value, a correction correlation was developed, as shown in Figure 192 and Equation (92). And the maximum deviation of the predicted values is within ±3%, as shown in Figure 193.

$$A_{CFD} = -856.03A_{equ}^3 + 17.206A_{equ}^2 + 0.9162A_{equ} \tag{92}$$

5.3.2. CFD Verification

The bBTHX solver is verified against simulation results. This simulation is done using air and water simultaneously. The tube wall is set to be aluminum with thickness of 0.3 mm.

The input parameters are:

Table 25 Inlet conditions of bBTHX solver verification case

	T_{in} [K]	P_{in} [kPa]	V_{in} [m/s]	h [W/m²K]	ΔP [Pa]
Air	300	101.325	4.9	280.1	25.3
Water	360	101.325	0.1	4858	245.6

Table 26 Geometry parameters of bBTHX solver verification case

OD [mm]	Thickness [mm]	ID [mm]	P_l/OD [-]	θ [deg]	LR [-]	Tube per row [-]	Tube segment # [-]	Row # [-]
1.7	0.3	1.1	2.38	47.58	2.3	10	2	1

The simulation domain is shown in Figure 194.
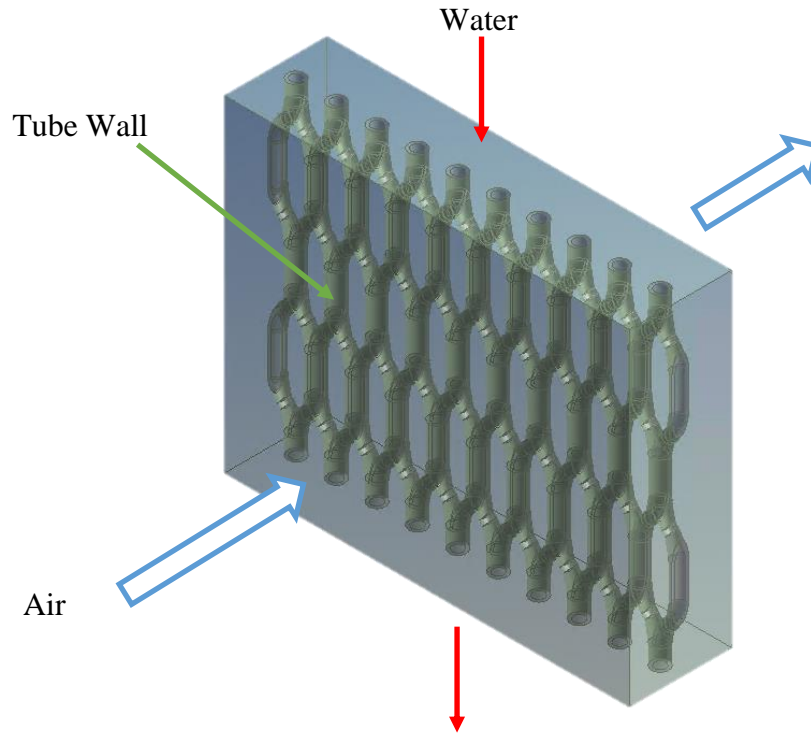
Figure 194 Single segment computational domain for bBTHX

Results of CFD and bBTHX solver are shown in Table 27. The percentage difference between heat exchanger capacities is 0.44%. Thus, the solver is verified.

Table 27 Comparison of simulation results from CFD and solver for bBTHX

	$T_{air,\ out}$ [K]	$T_{water,\ out}$ [K]	ΔP_{air} [Pa]	ΔP_{water} [Pa]	Q [W]	Q_{diff} [-]
CFD	303.73	352.66	24.8	245.28	28.28	0.44%
Solver	303.40	352.60	25.2	245.60	28.40	

5.4. *Design Problem (DP)*

The application of the methodology is to design a single-phase air-to-water heat exchanger which can deliver the same capacity as baseline but with smaller envelope volume, smaller material volume and lower total pumping power. Since the material volume is usually directly related to envelope volume so that the two optimization objectives are total power and heat exchanger envelope volume. Two baseline heat exchangers are selected, a conventional louvered fin mini-channel heat exchanger (MCHX) and a bare tube heat exchanger (BTHX) with outer

diameter of 0.8 mm. These two heat exchangers are plotted in Figure 195. However, these two heat exchangers are not optimized heat exchangers.
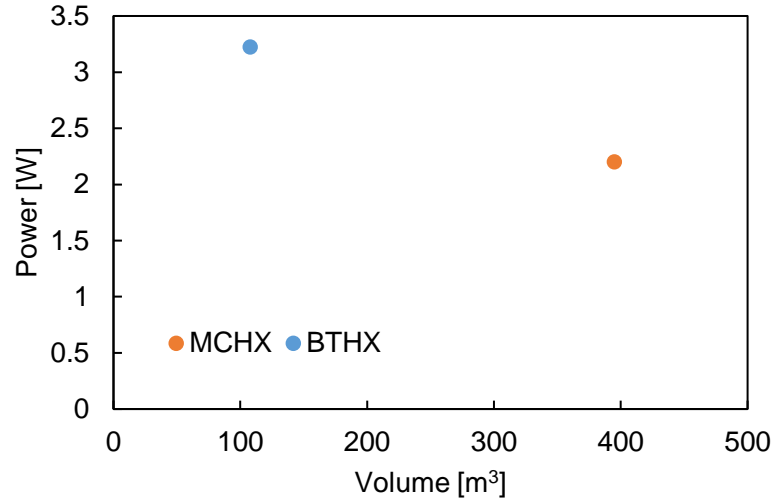
Figure 195 Two baseline heat exchangers for optimization

5.4.1. DP I: Single-Phase Heat Exchanger

5.4.1.1.   Baseline heat exchanger

The first application of the methodology is a single-phase air-to-water heat exchanger. A louvered mini channel radiator, as shown in Figure 25, was chosen to be baseline for comparison. This new heat exchanger is designed to deliver the same capacity (835W) for such application. This MCHX is a one slab heat exchanger with 11 tubes and 2 ports per tube. The airside hydraulic diameter is 1.94 mm. Other parameters are summarized in Table 28. The aspect ratio is 1.8, but in current optimization, its reciprocal 0.56 is used. This MCHX has been tested under dry condition using air and water and design condition used here is one of the testing conditions. The MCHX's data can be found in appendix and the experimental data has been compared to predictions using correlations from literature (Wang et al., 1999). The maximum deviation for capacity and pressure drop are ±6 and $\pm20\%$ respectively (Figure 196).

Table 28 Baseline MCHX

Metric	Unit	Value
Air flow rate	m³/s	0.05
Air inlet temperature	K	308.15
Water flow rate	g/s	50
Water inlet temperature	K	333.15
Heat load	W	835
Air pressure drop	Pa	32.8
Water pressure drop	kPa	11.0
Air heat transfer coefficient	W/m²·K	158
Airside heat transfer area	m^2	0.5525
Water heat transfer coefficient	W/m²·K	2007.4
Waterside heat transfer area	m^2	0.0735
Total pumping power (air+water)	W	2.2
Volume	cm³	395
Material volume	cm³	59.5
Length	m	0.23
Height	m	0.1175
Depth	m	0.016
Airside frontal area	m^2	0.0247
Aspect ratio (length/height or height/length)	-	1.8 or 0.56
Number of banks	-	1
Tube per bank	-	11
Fin per Inch (FPI)	-	20
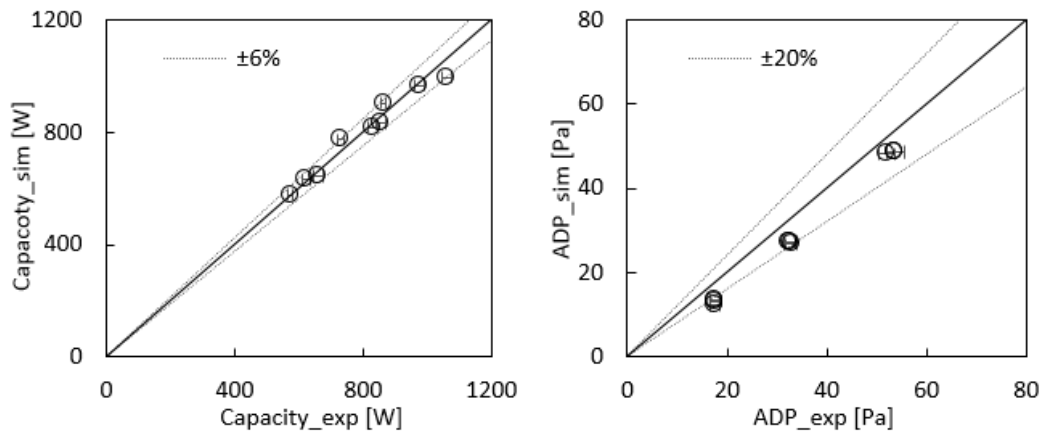
Figure 196 Deviation of capacity and airside pressure drop against experimental data for MCHX

5.4.1.2.　Optimization problem

The design problem here is described as below. Two objectives are total power and heat exchanger volume. The constraints include (1) total heat exchanger capacity should be similar or larger than baseline; (2) total power is 30% less than baseline; (3) total heat exchanger volume is 30% less than baseline; and (4) aspect ratio (AR) is similar to baseline. The last three constraints are dismissed for the real calculation because these will cause the calculation time to be much longer. The 30% better points were selected manually after the Pareto curve is produced.

$$
\begin{aligned}
&\text{Optimization I:}\\
&\quad \min Power\\
&\quad \min V_{HX}\\
&s.t.\\
&\quad \dot{Q}_{baseline} \leq \dot{Q} \leq 1.1 \cdot \dot{Q}_{baseline}\\
&\quad 0.9 \cdot AR_{baseline} \leq AR \leq 1.1 \cdot AR_{baseline}\\
&\quad \boxed{\begin{aligned}
&Power \leq 0.7 \cdot Power_{baseline}\\
&V_{HX} \leq 0.7 \cdot V_{HX\_baseline}\\
&A_{fr} \leq A_{fr\_baseline}
\end{aligned}}
\end{aligned}
$$

5.4.1.3.　Optimization results and discussion

Optimization results data can be found in the appendix. The Pareto front is plotted in Figure 197. Pareto front points are those have 30% lower total power and 30% smaller volume than baseline MCHX with smaller frontal area. Pareto front with no constrains are plotted on the graph as well. The following paragraphs discuss the difference between the Pareto front points.

Along the Pareto front line, the volume increases while power decreases. The outer diameter of the tube increase (Figure 198) is the main reason of volume increase. Transverse pitch (Pt/OD) reaches the minimum limit (1.5) and does not change while longitudinal pitch (Pl/OD) stays constant at smaller volume and experiences a sudden increase. This change is accompanied

by the diameter and length ratio sudden changes (Figure 198). Pl/OD has a relationship with LR, as shown in Figure 199. As Pl/OD increases, LR tends to decrease. This is because larger Pl/OD results in lower airside heat transfer coefficient, thus LR needs to be smaller to increase the heat transfer coefficient, and vice versa.

Designs with larger volumes also have larger airside frontal area (Figure 197), airside heat transfer area (Figure 201), larger waterside heat transfer area (Figure 202) and larger material volume (Figure 205). Larger airside frontal area will cause the air velocity to decrease, thus airside heat transfer coefficient (Figure 201) and airside pumping power (Figure 203) decreases as the design volume increases.

As design diameter increases, the waterside velocity decreases, resulting in lower waterside heat transfer coefficient (Figure 202) and lower waterside pumping power (Figure 203). Airside total power percentage decreases as volume increases, as shown in Figure 204. Figure 205 presents the aspect ratio and material volume. The aspect ratio is controlled within the range of 0.49~0.62 to maintain a similar value as baseline (0.56). Material volume increases as heat exchanger envelope volume increases.
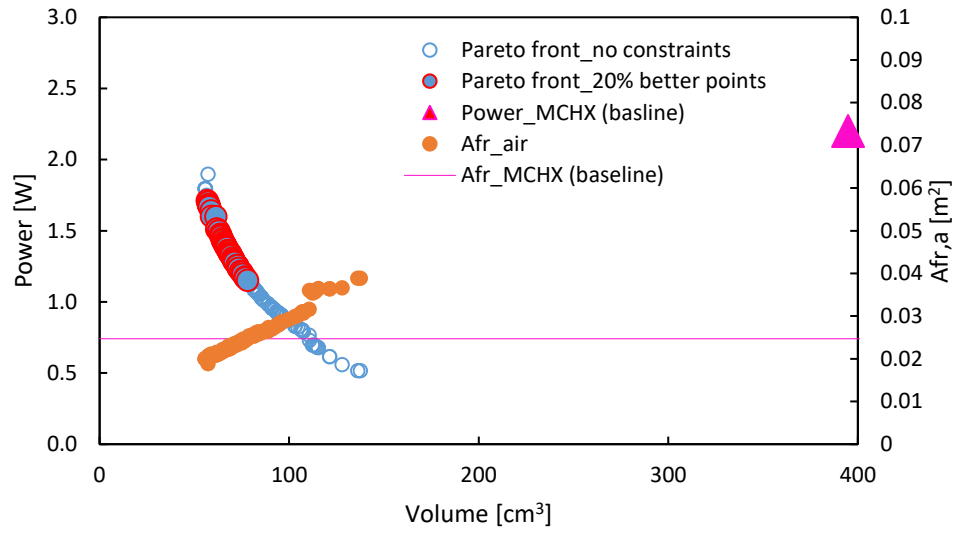
Figure 197 Pareto front (DP I)
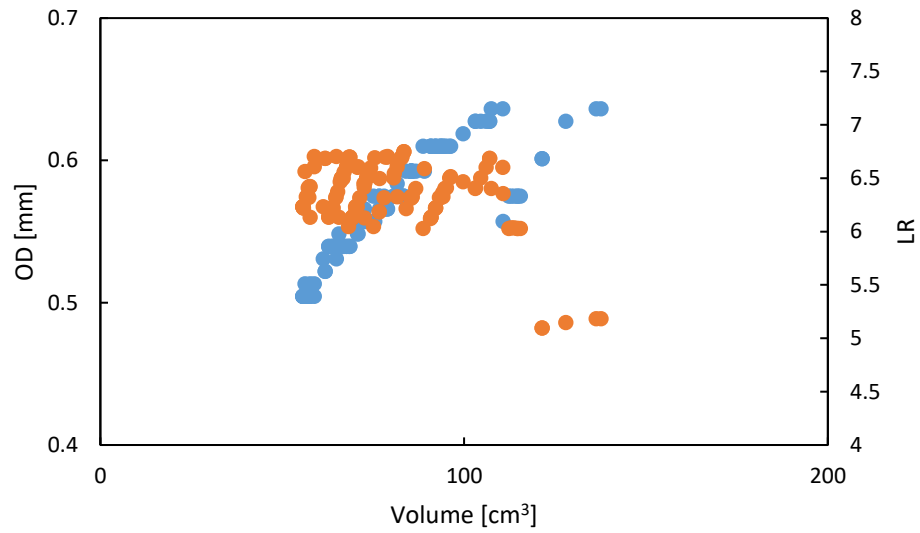
Figure 198 OD and LR of Pareto front points w/o constraints (DP I)

161
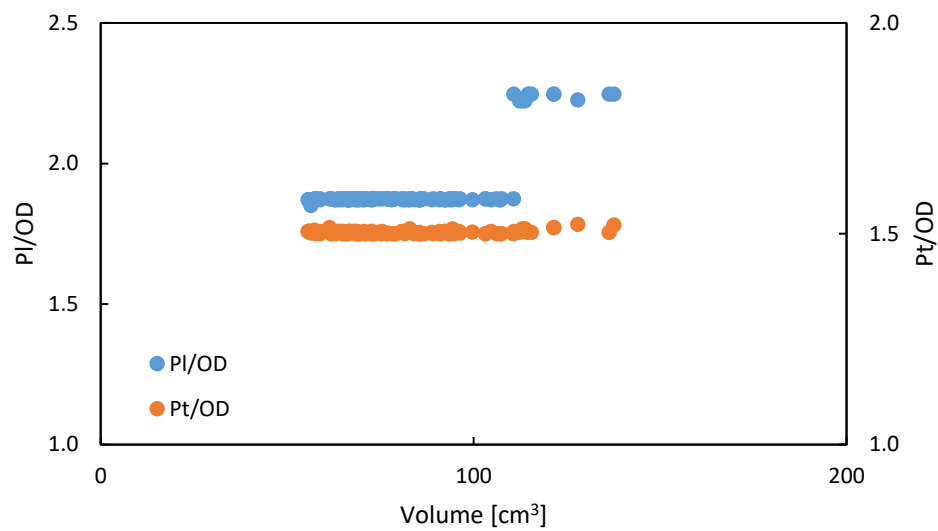
Figure 199 Pl and Pt of Pareto front points w/o constraints (DP I)
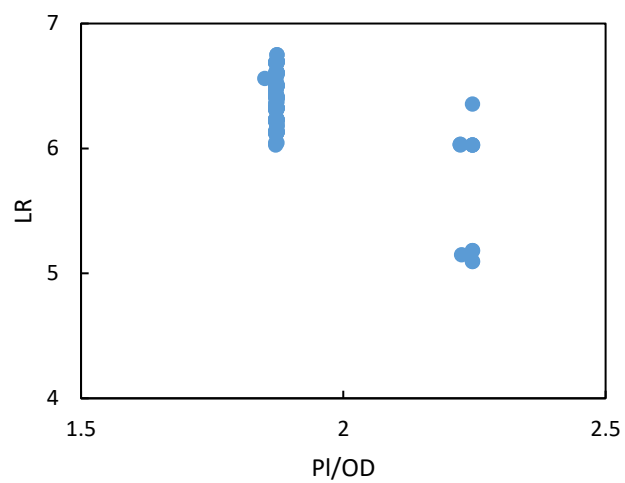
Figure 200 LR and Pl/OD of Pareto front points w/o constraints (DP I)

162
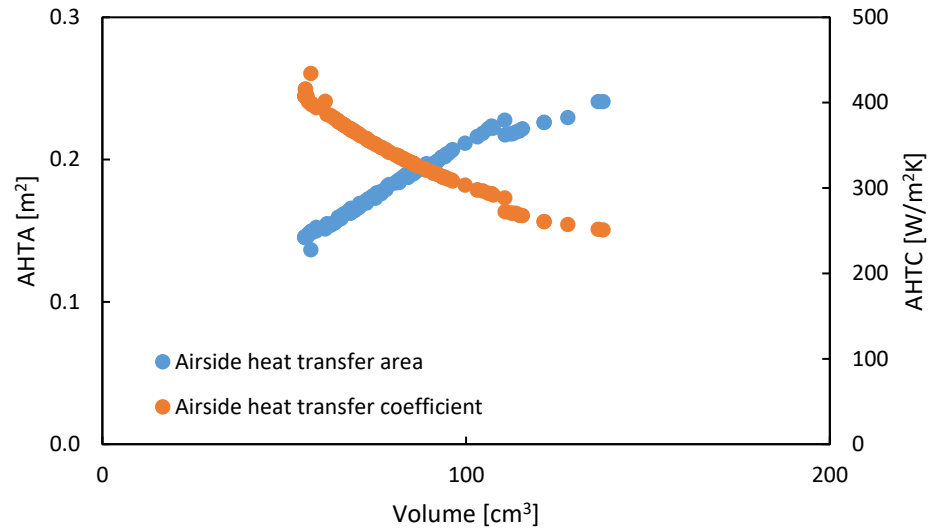
Figure 201 AHTA and AHTC of Pareto front points w/o constraints (DP I)
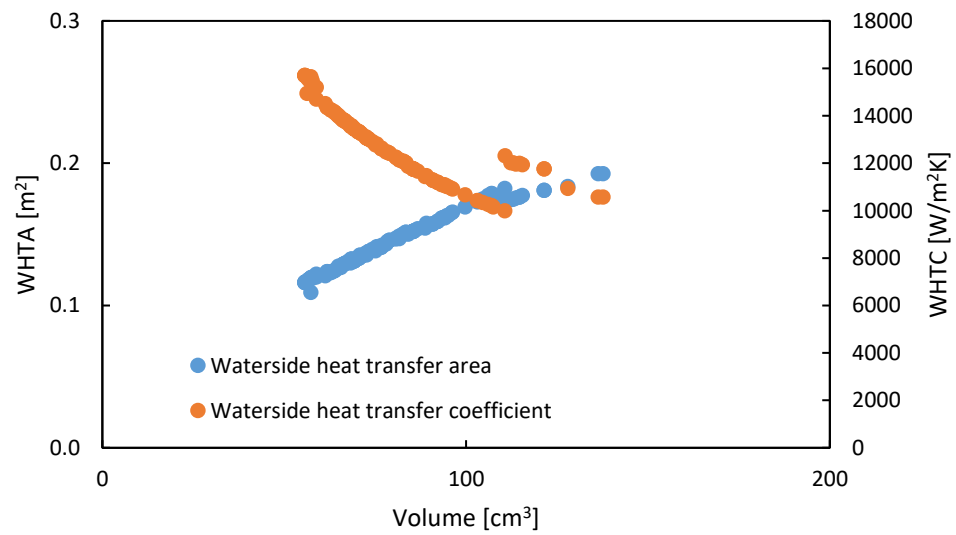
Figure 202 WHTA and WHTC of Pareto front points w/o constraints (DP I)

163
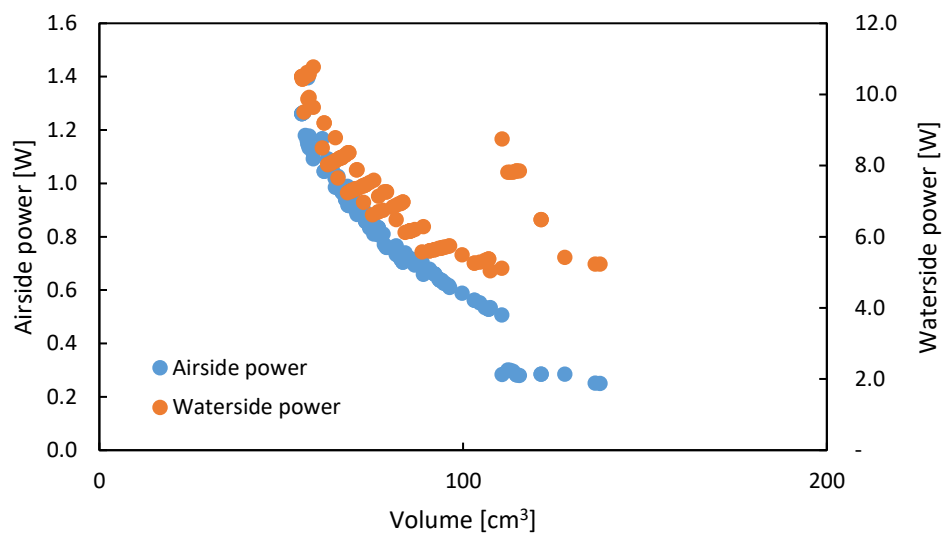
Figure 203 Airside and waterside pumping power of Pareto front points w/o constraints (DP I)
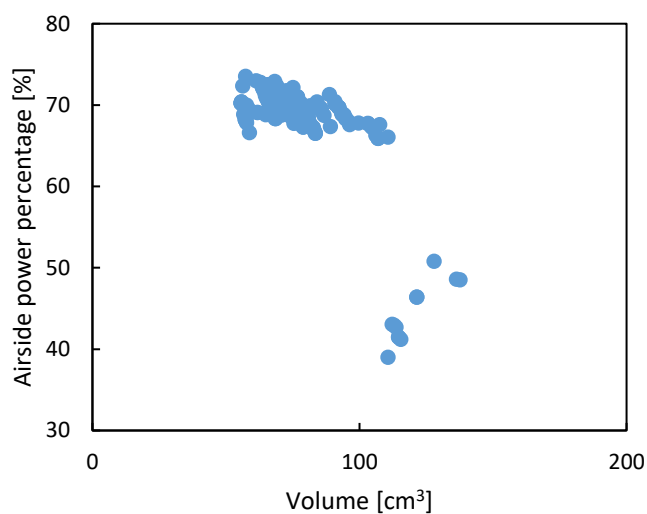
Figure 204 Airside power percentage of Pareto front points w/o constraints (DP I)

164
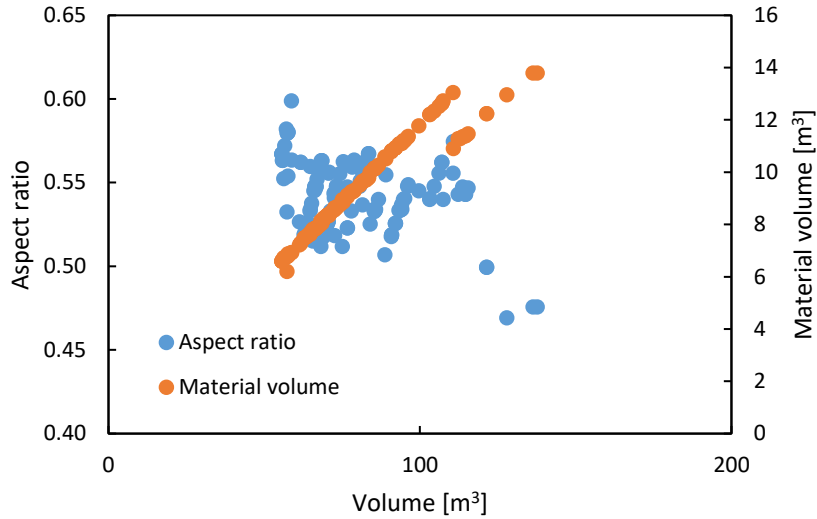
Figure 205 Aspect ratio and material volume of Pareto front points w/o constraints (DP I)

5.4.1.4. Results verification

The optimization results were verified against CFD simulation results. Three points from Pareto front were selected and CFD runs were conducted. Table 29 shows the comparison of the airside heat transfer coefficient (AHTC), airside pressure drop (ADP), waterside heat transfer coefficient (WHTC) and waterside pressure drop (WDP). Note WDP means waterside pressure drop per simulation domain. The maximum percentage deviation of AHTC, ADP, WHTC and ADP is 6.4%, which is acceptable. Thus, the Pareto front is verified.

Table 29 Optimization results verification against CFD simulation (DP I)

Optimization results				CFD results				Percentage deviation			
AHTC [W/m²K]	ADP [Pa]	WHTC [W/m2K]	WDP [Pa]	AHTC [W/m²K]	ADP [Pa]	WHTC [W/m²K]	WDP [Pa]	AHTC [%]	ADP [%]	WHTC [%]	WDP [%]
386.38	20.91	14346.31	649.91	401.19	22.04	13538.14	622.92	3.8%	5.4%	-5.6%	-4.2%
370.00	18.79	13665.71	586.06	384.30	19.99	13740.29	618.43	3.9%	6.4%	0.5%	5.5%
351.90	17.46	12772.66	467.64	361.44	17.81	13028.65	467.81	2.7%	2.0%	2.0%	0.04%

5.4.1.5. Selected optimal design and baseline comparison:

One of the verified optimal designs is compared with baseline heat exchanger. Table 30 summarized all parameter values and percentage differences. This optimal design has 38% lower

total pumping power, 83% smaller volume and 87% smaller material volume. In following paragraphs, each parameter will be examined separately.

Higher airside heat transfer coefficient: bBTHX has 134% higher airside heat transfer coefficient than baseline. Mechanisms of enhancing heat transfer were discussed in previous chapters, including larger mass flux, branch tube with smaller diameter and 3D flow caused by the addition of bifurcation. Another reason is the air frontal velocity of bBTHX (2.2 m/s) is slightly higher than that of MCHX (2.02 m/s).

Lower airside pressure drop: Despites the reasons discussed that can reduce the airside pressure drop, the most important reason for a lower pressure drop is the reduction in depth. bBTHX's depth is 75% smaller than that of MCHX. The ADP/Depth value of bBTHX is higher than MCHX.

Higher waterside heat transfer coefficient: bBTHX has five times higher waterside heat transfer coefficient than baseline. The reasons were discussed in Chapter 4.8, i.e. smaller OD branch tube, boundary layer redevelopment and flow separation.

Lower waterside pressure drop: Waterside pressure drop of bBTHX is 25% lower than baseline. The reason is that it has smaller water flow path. Tube length of bBTHX is 11.24 mm while that of MCHX is 23 mm. bBTHX has larger WDP/Length value.

Lower total pumping power: bBTHX has 38% lower total pumping power, which is mainly due to the reduction on airside pressure drop.

Smaller volume and material volume: bBTHX has about 83% smaller volume and 87% smaller material volume than baseline.

Table 30 Comparison of selected optimal design and baseline MCHX (DP I)

Metric	Unit	MCHX (experimental data)	bBTHX (simulation data)	%diff
Air flow rate	m³/s	0.05	0.05	
Air inlet temperature	K	308.15	308.15	
Water flow rate	g/s	50	50	
Water inlet temperature	K	333.15	333.15	
Heat load	W	835	845.9	1.3%
Air pressure drop	Pa	32.8	18.8	-42.7%
Water pressure drop	kPa	11.0	8.3	-24.5%
Air heat transfer coefficient	W/m²·K	158	370	134.2%
Airside heat transfer area	m²	0.5525	0.1639	-70.3%
Water heat transfer coefficient	W/m²·K	2007.4	13665	580.7%
Waterside heat transfer area	m²	0.0735	0.13115	78.4%
Total pumping power (air+water)	W	2.2	1.36	-38.2%
Volume	cm³	395	67.71	-82.9%
Material volume	cm³	59.5	7.96	-86.6%
Length	M	0.23	0.2022	-12.1%
Height	M	0.1175	0.1124	-4.3%
Depth	M	0.016	0.004	-75.0%
Airside frontal area	m²	0.0247	0.022744	-7.9%
Aspect ratio (length/height or height/length)	-	1.8 or 0.56		
Number of banks	-	1	4	
Tube per bank	-	11	200	
Fin per Inch (FPI)	-	20	-	
Pl/OD	-	-	1.8739	
Pt/OD	-	-	1.506	
LR	-	-	6.609	
θ	°	-	62.79	
effectiveness		0.565	0.572	

5.4.2. DP II: Single-Phase Heat Exchanger of diameter 0.8 mm

5.4.2.1.   Baseline heat exchanger

The second application of the methodology is also a single-phase air-to-water heat exchanger. And the bare tube heat exchanger (BTHX) with diameter of 0.8 mm is used as baseline for comparison. To make a fair comparison, this bifurcated bare tube heat exchanger's diameter is controlled to be 0.8 mm and the tube bank number is controlled to be four, which are the same as those of bare tube heat exchanger. The experimental data of BTHX can be found in the appendix and the key parameters are summarized in Table 31.

Table 31 Baseline BTHX

Metric	Unit	BTHX
Air flow rate	m³/s	0.05
Air inlet temperature	K	308.15
Water flow rate	g/s	50
Water inlet temperature	K	333.15
Heat load	W	849
Air pressure drop	Pa	55.9
Water pressure drop	kPa	6.8
Air heat transfer coefficient	W/m²·K	343
Airside heat transfer area	m^2	0.183
Water heat transfer coefficient	W/m²·K	9196
Waterside heat transfer area	m^2	0.137
Total pumping power (air+water)	W	3.145
Volume	cm³	109
Material volume	cm³	12.81
Length	m	0.152
Height	m	0.1498
Depth	m	0.0048
Airside frontal area	m^2	0.0228
Aspect ratio (length/height)	-	1.0
Number of banks	-	4
Tube per bank	-	121

5.4.2.2. Optimization problem

The design optimization problem here is described as below. Two objectives are total power and heat exchanger volume. The constraints include (1) total heat exchanger capacity should be similar or larger than baseline; (2) total power is 10% less than baseline; (3) total heat exchanger volume is 10% less than baseline; (4) aspect ratio (AR) is similar to baseline; (5) outside diameter of first level tube is the same as baseline; and (6) tube bank number is the same as baseline. The last three constraints are dismissed for the real calculation because these will cause the calculation time to be much longer. The 10% better points were selected manually after the Pareto curve is produced.

Optimization II:
$$\min Power$$
$$\min V_{HX}$$
$$s.t.$$
$$\dot{Q}_{baseline} \leq \dot{Q} \leq 1.1 \cdot \dot{Q}_{baseline}$$
$$0.9 \cdot AR_{baseline} \leq AR \leq 1.1 \cdot AR_{baseline}$$
$$OD = OD_{baseline}$$
$$N_{tubebank} = N_{tubebank,baseline}$$
$$\boxed{\begin{array}{l} Power \leq 0.9 \cdot Power_{baseline} \\ V_{HX} \leq 0.9 \cdot V_{HX\_baseline} \\ A_{fr} \leq A_{fr\_baseline} \end{array}}$$

5.4.2.3. Optimization results and discussion

Optimization results data can be found in the appendix. The Pareto front is plotted in Figure 206. Pareto front points are those have 10% lower total power and 10% smaller volume than baseline BTHX. They also have smaller frontal area than baseline. Pareto front with no constrains are plotted on the graph as well.

169

As shown in Figure 207, the transverse pitch reaches the minimum limit (1.5) and does not change while longitudinal pitch increases, resulting in larger airside frontal area (Figure 206), airside heat transfer area (Figure 208), larger volume and larger material volume (Figure 213). Larger airside frontal area will cause the air velocity to decrease, thus airside heat transfer coefficient decreases. Figure 210 shows bifurcation angle θ and length ratio are related to each other. This is because larger length ratio and smaller bifurcation both leads to smaller airside heat transfer coefficient, so to maintain similar heat transfer capacity, larger length ratio is always accompanied by a larger bifurcation angle. Again, larger volume designs have larger airside frontal area, thus lower frontal velocity and smaller airside pressure drop. So, the airside pumping power decreases as the design volume increases (Figure 211).

The waterside heat transfer area also increases as heat exchanger volume increases while waterside heat transfer coefficient does not change much, as shown in Figure 209. Since the airside thermal resistance is dominant thus the change in waterside thermal resistance has very limited effect on the overall heat transfer capacity.

As for power consumption, the airside fan power decreases as heat exchanger volume increases. But larger airside frontal area also means longer water flow path, so waterside pumping power increases (Figure 211). Airside total power percentage decreases as volume increases, as shown in Figure 212. Figure 213 presents the aspect ratio and material volume. The aspect ratio is controlled within the range of 0.9~1.1 to maintain a similar value as baseline (1.0). Material volume increases as heat exchanger envelope volume increases.
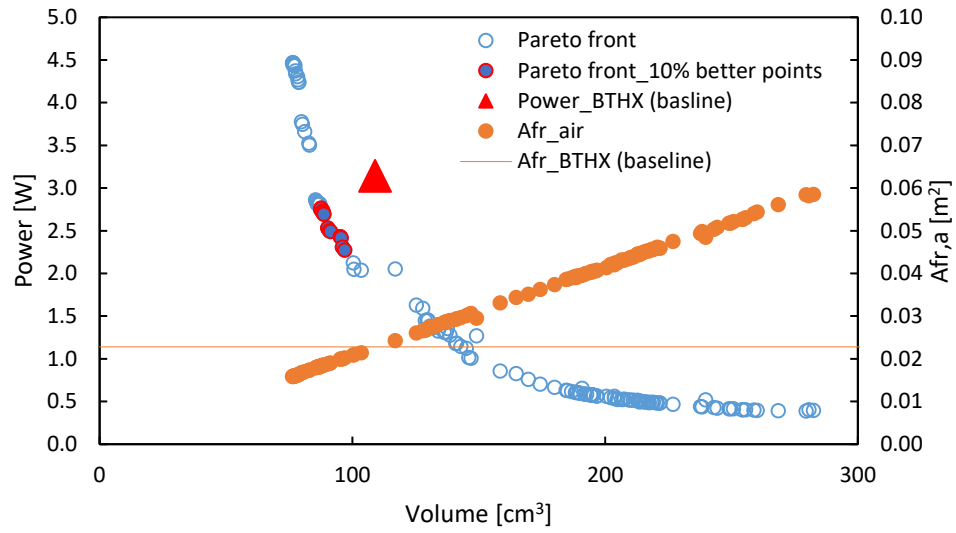
Figure 206 Pareto front (DP II)

Figure 207 Pl and Pt of Pareto front points w/o constraints (DP II)

171
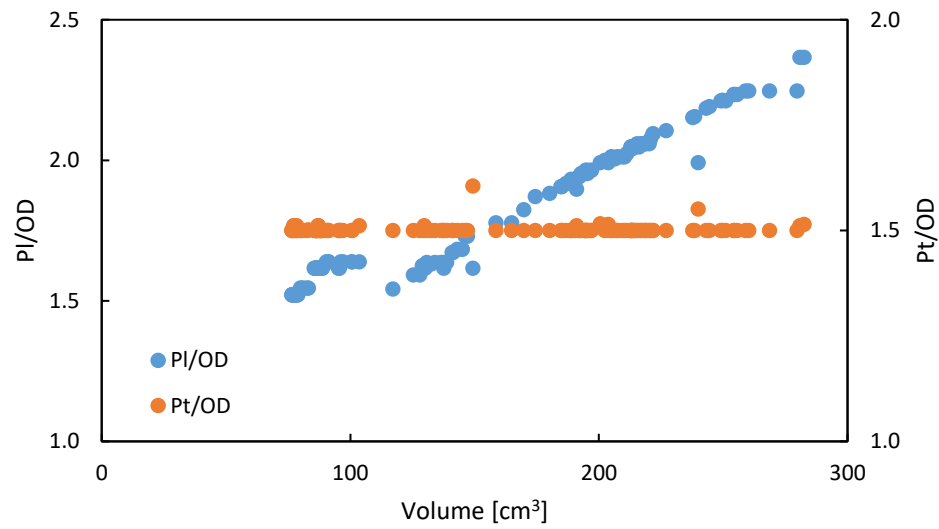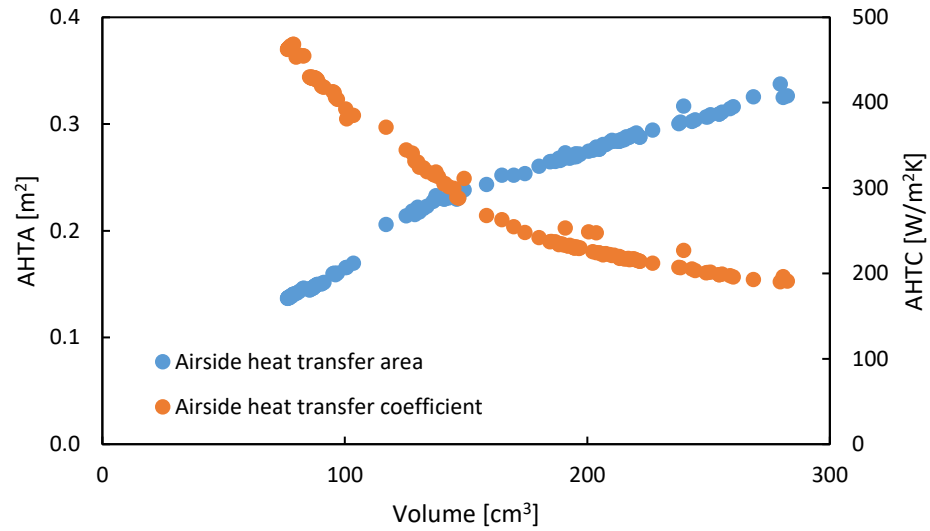
Figure 208 AHTA and AHTC of Pareto front points w/o constraints (DP II)
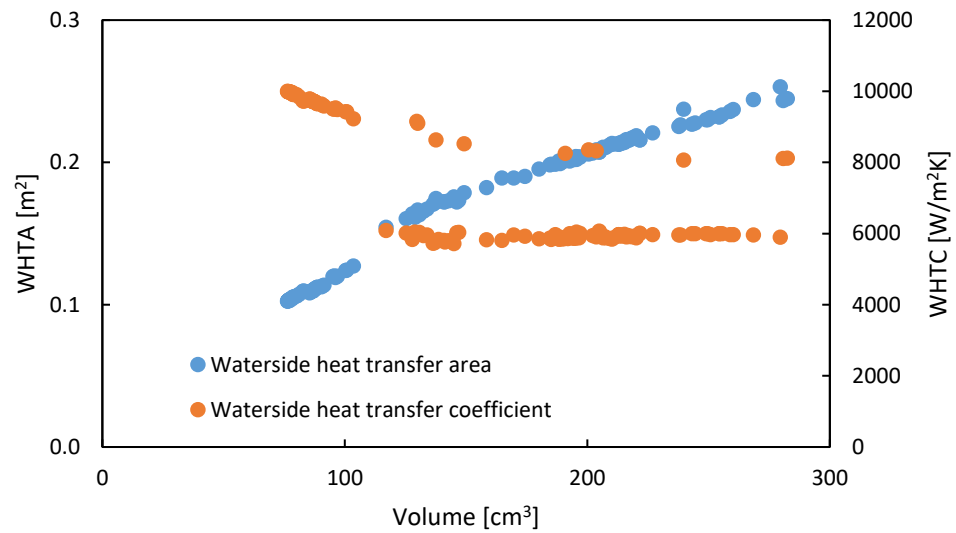
Figure 209 WHTA and WHTC of Pareto front points w/o constraints (DP II)

172
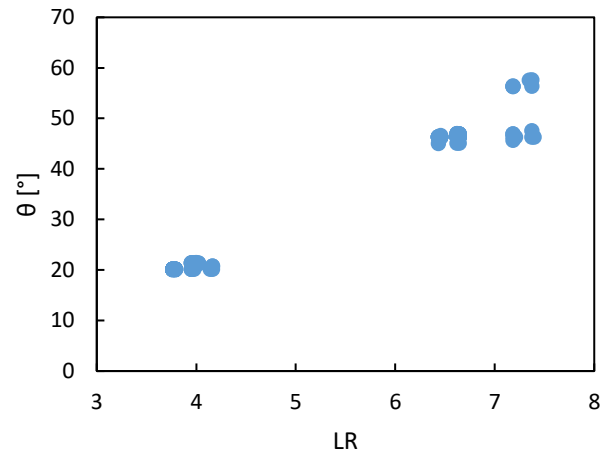
Figure 210 Bifurcation angle and length ratio of Pareto front points w/o constraints (DP II)
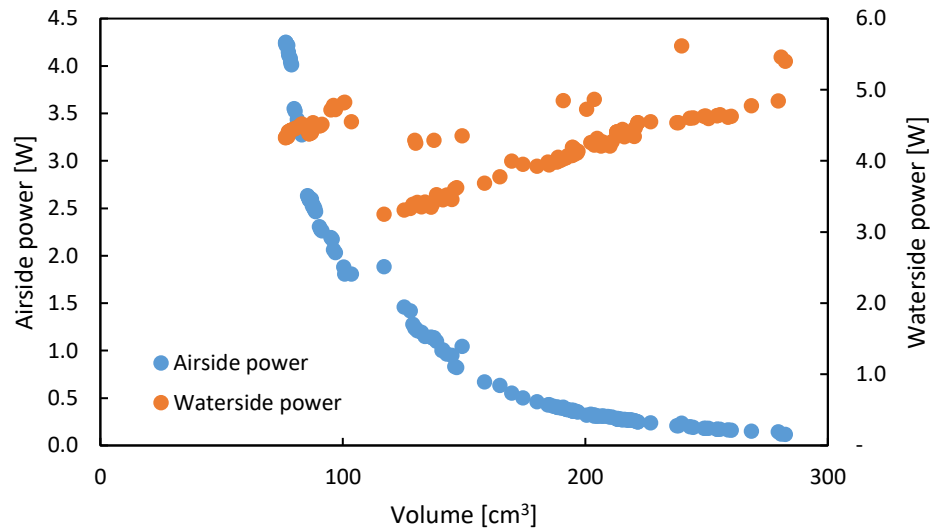
Figure 211 Airside and waterside pumping power of Pareto front points w/o constraints (DP II)
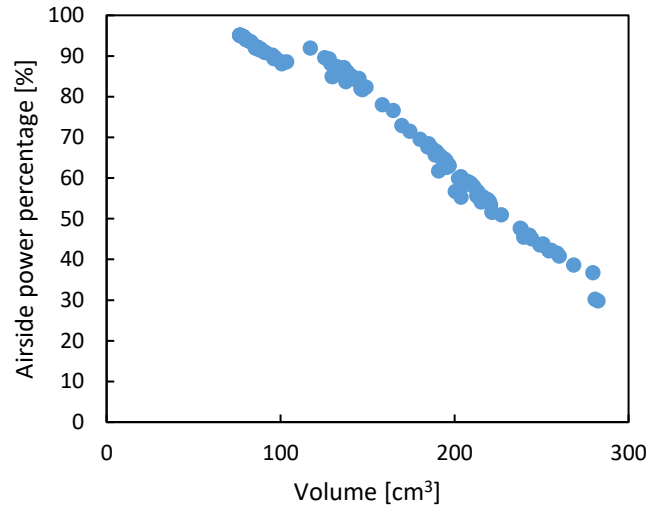
Figure 212 Airside power percentage of Pareto front points w/o constraints (DP II)
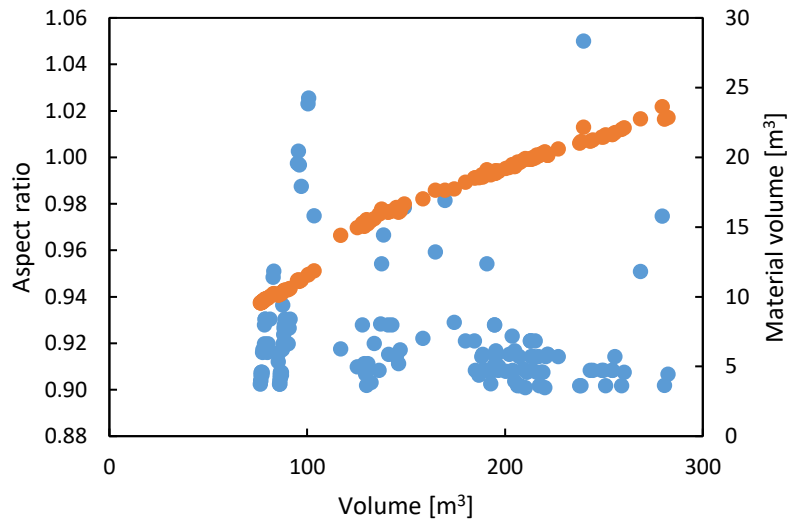
Figure 213 Aspect ratio and material volume of Pareto front points w/o constraints (DP II)

5.4.2.4.   Results verification

The optimization results were verified against CFD simulation results. Three points from Pareto front were selected and CFD runs were conducted. Table 32 compares airside heat transfer coefficient (AHTC), airside pressure drop (ADP), waterside heat transfer coefficient (WHTC) and

waterside pressure drop (WDP). The maximum percentage deviation of AHTC, ADP, WHTC and ADP is 5.3%, which is acceptable. Thus, the Pareto front is verified.

Table 32 Optimization results verification against CFD simulation (DP II)

Optimization results				CFD results				Percentage deviation			
AHTC [W/m^{2}K]	ADP [Pa]	WHTC [W/m2K]	WDP [Pa]	AHTC [W/m^{2}K]	ADP [Pa]	WHTC [W/m^{2}K]	WDP [Pa]	AHTC [%]	ADP [%]	WHTC [%]	WDP [%]
403.88	40.60	9486.7	464.68	407.80	41.96	9100.7	439.87	1.0%	3.3%	-4.1%	-5.3%
454.94	65.23	9722.4	444.73	226.93	6.07	5780.6	456.41	2.3%	-1.8%	-1.7%	-0.7%
221.76	6.19	5878.3	459.51	461.64	67.15	10128.9	430.99	1.5%	2.9%	4.2%	-3.1%

5.4.2.5.   Selected optimal design and baseline comparison

Here we select one of the verified optimal design and compare it with baseline heat exchanger.

Table 33 summarized all parameter values and percentage differences. This optimal design has 28% lower total pumping power, 11% smaller volume and 10% smaller material volume. Discussions of each parameter are as follows.

Higher airside heat transfer coefficient: bBTHX has 12% higher airside heat transfer coefficient than baseline. bBTHX has less tube number per bank and smaller frontal area, thus inlet air velocity is higher for bBTHX, which will lead to higher airside heat transfer coefficient. The addition of bifurcation increases flow mixing and enhance heat transfer. Branch tube with smaller diameter is also beneficial for heat transfer enhancement.

Lower airside pressure drop: bBTHX has 27% lower airside pressure drop. As discussed in Chapter 4.7, flow bypass, smaller flow rate at bare tube region and 3D flow are the main mechanisms that contributes to lower airside pressure drop. And 3D flow is the only mechanism that contributes to both heat transfer enhancing and pressure drop reduction. In current case, the Reynolds number is 113. From Figure 178, the drag coefficient is about one for smooth sphere and is about two for smooth cylinder, meaning the drag force per length of smooth sphere is 50% lower

than smooth cylinder with the same diameter. From Figure 179, Nusselt number is about 5.5 for cylinder and 6.9 for sphere, meaning that heat transfer coefficient of sphere is 25% higher than that of cylinder of the same diameter. Another reason is the bBTHX has a larger longitudinal pitch (1.64) than baseline (1.5) and a large length ratio (7.18) which are both beneficial for lower pressure drop. This indicates that though addition of bifurcation usually increases airside pressure drop, the introduction of 3D flow will result in lower airside pressure drop than bare tube bundles with proper design.

Higher waterside heat transfer coefficient: bBTHX has 84% higher waterside heat transfer coefficient than baseline. Besides the three reasons as discussed in Chapter 4.8, i.e. smaller OD branch tube, boundary layer redevelopment and flow separation, the most important reason is in current case, it is turbulent flow due to the existence of bifurcation. But for baseline, it is laminar flow and the heat transfer coefficient is calculated using laminar flow heat transfer coefficient correlation.

Lower/Higher waterside pressure drop: As for waterside pressure drop, note that the experimental waterside pressure drop is 6.8 kPa. However, in experiment, the pressure drop in the heat exchanger header is also measured as well as all connection fittings and tubes in between the different pressure transducer. If using laminar f factor equation (f=64/Re), then the waterside pressure drop of baseline drops to 2.4 kPa. And bBTHX has two times the waterside pressure drop which is consistent with the simulation results. The total power of baseline drops to 2.915 W if theoretical waterside pressure drop is used. However, since airside pressure drop dominates, the bBTHX still has 65% lower total pumping power than baseline.

Lower total pumping power: bBTHX has 28% lower total pumping power. This is mainly due to the reduction on airside pressure drop.

176

Smaller volume and material volume: bBTHX has about 10% smaller volume and material

volume than baseline.

Table 33 Comparison of selected optimal design and baseline BTHX (DP II)

Metric	Unit	BTHX (experimental data)	bBTHX (simulation data)	% diff
Air flow rate	m³/s	0.05	0.05	-
Air inlet temperature	K	308.15	308.15	-
Water flow rate	g/s	50	50	-
Water inlet temperature	K	333.15	333.15	-
Heat load	W	849	865.7	2%
Air pressure drop	Pa	55.9	40.6	-27%
Water pressure drop	kPa	6.8 (2.4kPa, laminar)	4.7	-45%
Air heat transfer coefficient	W/m²·K	359	403.4	**12%**
Airside heat transfer area	m²	0.183	0.16	**-13%**
Water heat transfer coefficient	W/m²·K	4825	8892	**84%**
Waterside heat transfer area	m²	0.137	0.128	**-7%**
Total pumping power (air+water)	W	3.15	2.27	**-28%**
Volume	cm³	109	96.8	**-11%**
Material volume	cm³	12.81	11.54	**-10%**
Length	m	0.152	0.141	-7%
Height	m	0.1498	0.143	-5%
Depth	m	0.0048	0.0048	-
Airside frontal area	m²	0.0228	0.0202	-11%
Number of banks	-	4	4	-
Tube per bank	-	121	109	-10%
Pl/OD	-	1.5	1.64	9.3%
Pt/OD	-	1.49	1.5	0.7%
LR	-	-	7.18	-
θ	°	-	46.92	-
effectiveness		0.574	0.585	

Chapter 6: bBTHX Application

In this chapter, two applications of the new heat exchanger are discussed. The first one is car radiator, and the second is indoor coil for hybrid variable refrigerant flow (VRF) system. The advantages of utilizing it as car radiator and indoor coil for hybrid variable VRF system include smaller volume, less material volume and inner volume and lower pumping power.

6.1. *Car Radiator*

6.1.1. Baseline heat exchanger

Current design can be applied as car radiator due to the advantages of smaller volume, less material volume and, inner volume and lower pumping power when delivering the same capacity. A louvered fin radiator is used as baseline for comparison. This car radiator has been tested under dry condition using air and water and here the design condition is one of the testing condition. The experimental data can be found in appendix and the experimental data has been compared to predictions using correlations from literature (Wang et al., 1999), as shown in Figure 215. Other parameters are summarized in Table 34.

Figure 214 Louvered fin car radiator
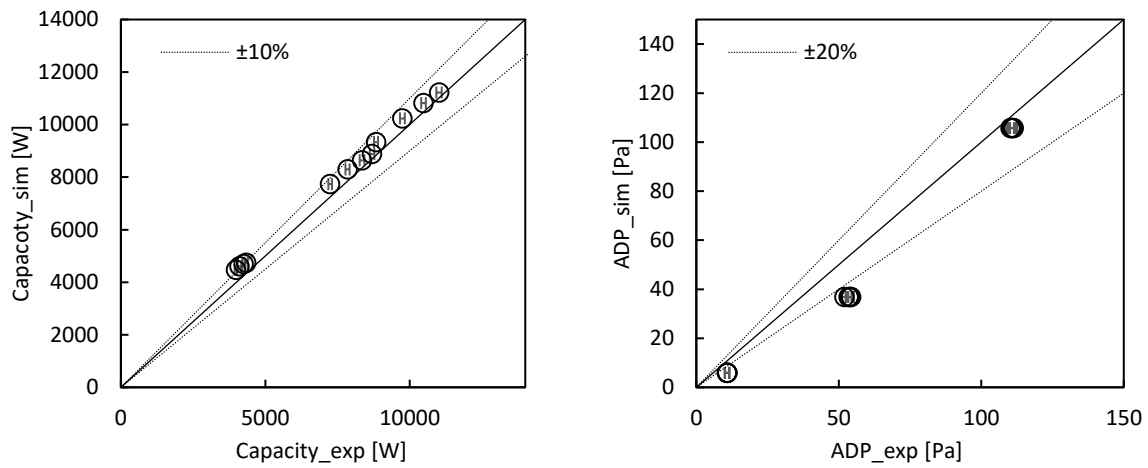
Figure 215 Louvered fin car radiator experimental data and correlation comparison

Table 34 Baseline car radiator

Metric	Unit	Value
Air flow rate	m³/s	0.772
Air inlet temperature	K	308.15
Water flow rate	g/s	279.2
Water inlet temperature	K	333.15
Heat load	W	10477.2
Air pressure drop	Pa	111
Water pressure drop	kPa	10.6
Air heat transfer coefficient	W/m²·K	148
Airside heat transfer area	m²	9.3469
Water heat transfer coefficient	W/m²·K	1666
Waterside heat transfer area	m²	1.1463

179

Total pumping power (air+water)	W	88.74
Volume	cm³	6716.25
Material volume	cm³	1220
Internal volume	cm³	753
Length	m	0.457
Height	m	0.4211
Depth	m	0.0349
Airside frontal area	m²	0.1925
Aspect ratio (length/height or height/length)	-	1.09
Number of banks	-	2
Tube per bank	-	42
Fin per Inch (FPI)	-	15.3

6.1.2. Design optimization

Two objectives are minimizing total power and heat exchanger volume. The constraints include (1) total heat exchanger capacity should be similar or larger than baseline; (2) total power is 30% less than baseline; (3) total heat exchanger volume is 30% less than baseline; (4) aspect ratio (AR) is similar to baseline and (5) frontal area is similar to baseline.

Optimization:

$$\min Power$$

$$\min V_{HX}$$

$s.t.$

$$0.9 \cdot \dot{Q}_{baseline} \le \dot{Q} \le 1.1 \cdot \dot{Q}_{baseline}$$

$$Power \le 0.7 \cdot Power_{baseline}$$

$$V_{HX} \le 0.7 \cdot V_{HX\_baseline}$$

$$0.9 \cdot AR_{baseline} \le AR \le 1.1 \cdot AR_{baseline}$$

$$0.9 \cdot A_{fr,baseline} \le A_{fr} \le 1.1 \cdot A_{fr,baseline}$$

6.1.3. Optimization results and discussion

The optimization results in shown in Figure 216. One of the designs was selected to be the final design and the comparison results are summarized in Table 35. The bBTHX car radiator has 30% less total pumping power, 68.1% less heat exchanger envelope volume and 87.1% less

material volume, which meet the design goal. Another advantage of bBTHX is that the water mass

of the heat exchanger is 66.7% less than baseline because it has 66.7% less internal volume. For a

car radiator, reduction in total mass of heat exchanger can contribute to car overall efficiency. The

CFD verification results is shown in Table 36.
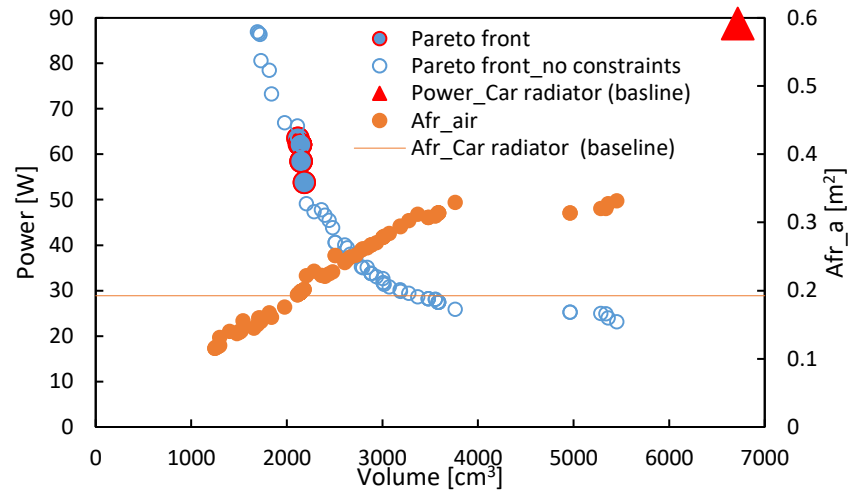
Figure 216 Optimization results of car radiator design

Table 35 Comparison of bBTHX car radiator design and baseline

Metric	Unit	Baseline (experimental data)	bBTHX (simulation data)	%diff
Air flow rate	m³/s	0.772	0.772	-
Air inlet temperature	K	308.15	308.15	-
Water flow rate	g/s	279.2	279.2	-
Water inlet temperature	K	333.15	333.15	-
Heat load	W	10477.2	10428.7	-0.5%
Air pressure drop	Pa	111	71.1	**-35.9%**
Water pressure drop	kPa	10.6	15.4	**45.3%**
Air heat transfer coefficient	W/m²·K	148	388.5	**162.5%**
Airside heat transfer area	m²	9.3469	2.0819	**-77.7%**
Water heat transfer coefficient	W/m²·K	1666	8816	**429.2%**
Waterside heat transfer area	m²	1.1463	1.5612	**36.2%**
Total pumping power (air+water)	W	88.74	62.13	**-30.0%**
Volume	cm³	6716.25	2140.6	**-68.1%**
Material volume	cm³	1220	157.58	**-87.1%**
Internal volume	cm³	753	250.56	**-66.7%**
Length	m	0.457	0.4412	-3.5%
Height	m	0.4211	0.4457	5.8%
Depth	m	0.0349	0.012	-65.6%
Airside frontal area	m²	0.1925	0.196	1.8%
Aspect ratio (length/height or height/length)	-	1.09	1.01	-7.3%
Number of banks	-	2	9	
Tube per bank	-	42	186	
Fin per Inch (FPI)	-	15.3	-	

Table 36 Design point verification against CFD simulation for car radiator design

Optimization results				CFD results				Percentage deviation			
AHTC [W/m²K]	ADP [Pa]	WHTC [W/m2K]	WDP [Pa]	AHTC [W/m²K]	ADP [Pa]	WHTC [W/m²K]	WDP [Pa]	AHTC [%]	ADP [%]	WHTC [%]	WDP [%]
388.50	71.11	8816.0	901.06	370.53	73.09	8684.3	887.63	-4.63%	2.78%	-1.49%	-1.49%

6.2. *Indoor Coil of Hybrid Variable Refrigerant Flow (HVRF) System*

Besides being applied as car radiator, the bBTHX can also be applied as indoor coil in hybrid VRF (HVRF) system. VRF system is multiple-unit split-type system. Compared with traditional central air conditioning unit, VRF system can achieve higher efficiency by modulating

the flow of refrigerant according to individual area cooling and heating load. Heat recovery VRF system can also save compressor work by internal heat recovery.

Traditional VRF system is shown in Figure 217 and hybrid VRF system is shown in Figure 218. Instead of using refrigerant inside home, hybrid VRF system utilizes water (or other coolant) coils as indoor unit. Compared with traditional VRF system, there is less concern of flammability of refrigerant, giving a wider selection of refrigerants. Fin-and-tube heat exchangers are usually used as indoor coils to exchange heat between coolant and indoor air. Current bifurcated bare tube heat exchanger design can be produced using 3D printing technology, thus there is a possibility of applying bBTHX as indoor unit for hybrid VRF system. Offsite and onsite 3D printing manufacturing could be both possible in the future.
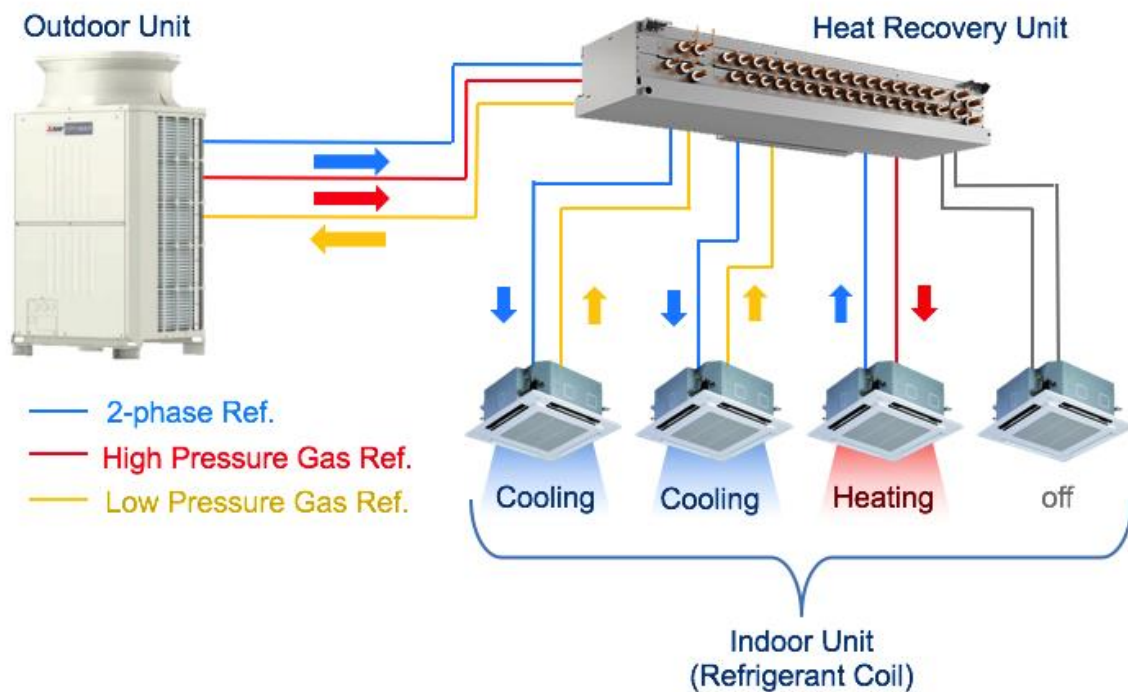
Figure 217 Traditional VRF System (with Heat Recovery)
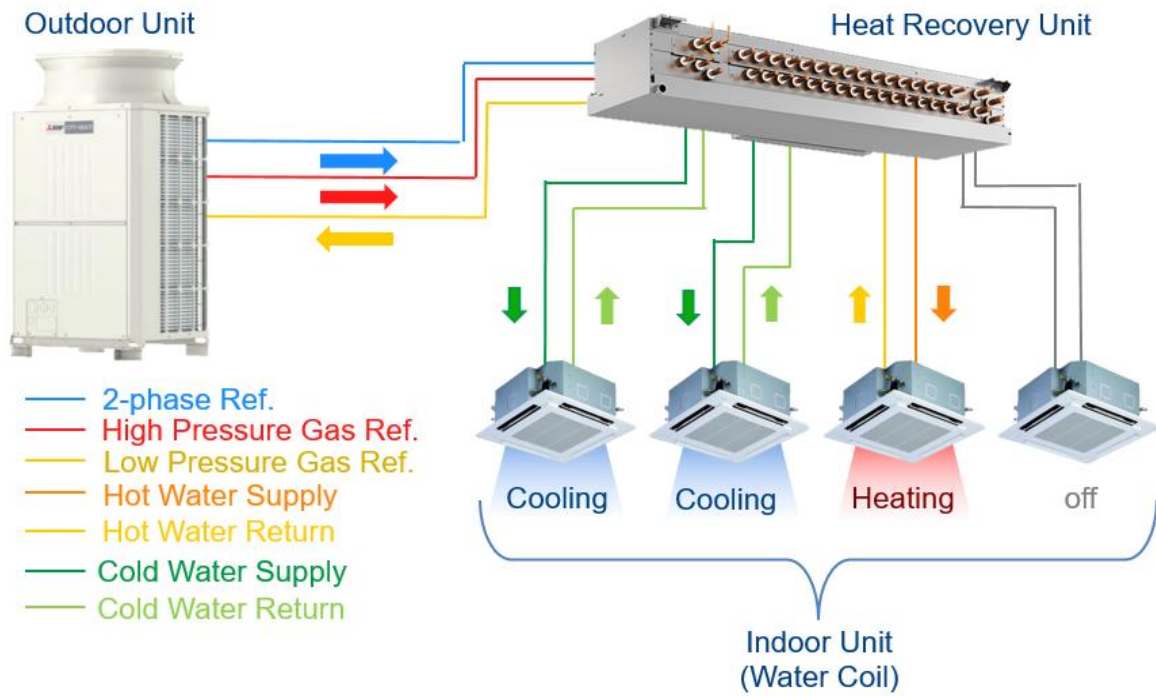
Figure 218 Hybrid VRF System

In this chapter, system performance of HVRF is numerically simulated using VapCyc®
(Winkler et al., 2008) software. For comparison, traditional VRF system is chosen as baseline. The
refrigerant investigated are R410A, R290 (Propane) and R600a (Isobutane). R410A is a widely
used refrigerant in market while R290 and R600a are flammable refrigerants which are not
applicable in traditional refrigerant system.

6.2.1. Traditional R410A VRF system design (baseline)

Traditional VRF system is evaluated using R410A as refrigerant. The piping design
restrictions shown in Figure 219 are used. It is from Mitsubishi HVRF system data book
(Mitsubishi, 2012). The schematic of traditional VRF system is shown in Figure 220. Due to AHRI
VRF testing standard (AHRI, 2010), the minimum indoor unit quantity is two, thus in current
study, two indoor units are designed. Length is 110 m (360 feet) for refrigerant pipe A and 60 m
(196 feet) for pipe B. Diameter of pipe A is 9.5 mm (0.375 inches) and diameter of pipe B is 16
mm (0.625 inches). Both indoor and outdoor units are traditional fin-and-tube heat exchangers.
The simulation condition is dry test condition for air condition mode from AHRI standard (AHRI,
2008). Ambient dry/wet bulb temperature is 35/23.9°C and indoor air dry/wet bulb temperature is
26.7/19.4° C. The vapor compression cycle is simulated using steady state vapor compression
simulation tool VapCyc® (Winkler et al., 2008).
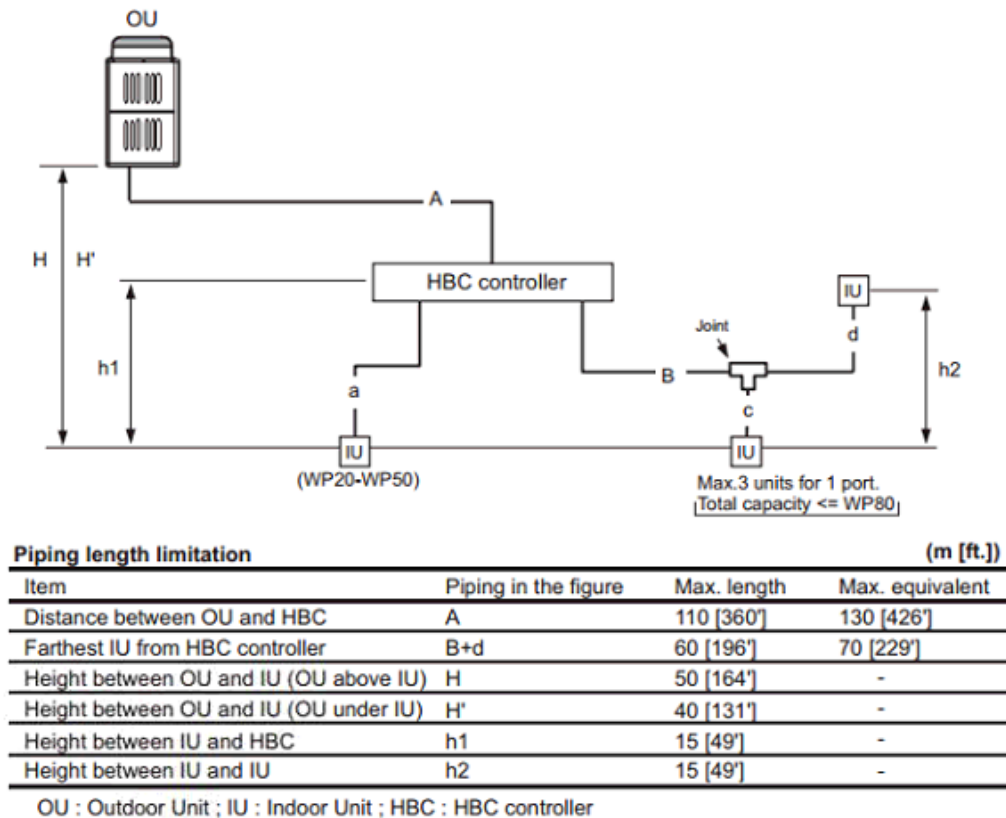
**Figure 219 VRF piping design restrictions
(from Mitsubishi data book)**

Piping length limitation (m [ft.])

Item	Piping in the figure	Max. length	Max. equivalent
Distance between OU and HBC	A	110 [360']	130 [426']
Farthest IU from HBC controller	B+d	60 [196']	70 [229']
Height between OU and IU (OU above IU)	H	50 [164']	-
Height between OU and IU (OU under IU)	H'	40 [131']	-
Height between IU and HBC	h1	15 [49']	-
Height between IU and IU	h2	15 [49']	-

OU : Outdoor Unit ; IU : Indoor Unit ; HBC : HBC controller

Figure 220 Schematic of traditional VRF system

Convergence criteria for high pressure side is subcooling temperature equals 5.5 K and convergence criteria for low pressure side is suction super heat temperature equals 5 K. Power input to the fan motors are 36 W and 18 W for 1 m^3/s airflow rate for evaporator and condenser, respectively. The air flow rate for evaporator is 0.283 m^3/s each, and the air flow rate for condenser is 0.693 m^3/s total. Figure 221 shows the baseline traditional R410A VRF system schematic in

VapCyc® and the corresponding properties of each state point are summarized in Table 37. The system evaluation results are shown in Table 38. COP is defined as the ratio of capacity over total power.
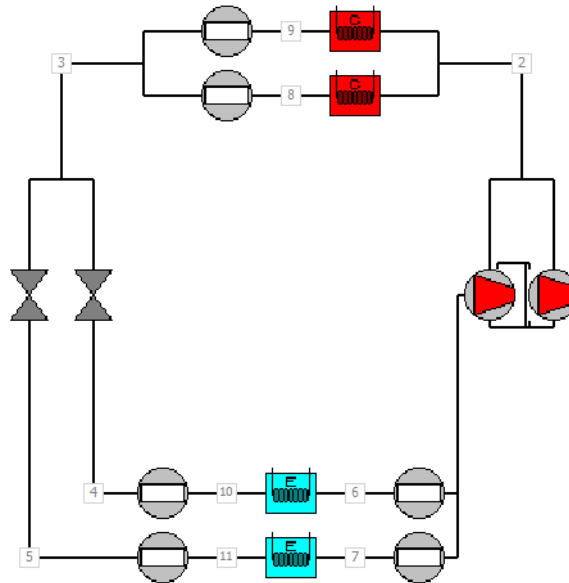
Figure 221 Baseline traditional R410A VRF system schematic

Table 37 Simulation results for baseline R410A VRF system

Junction	T [K]	P [kPa]	x	H [kJ/kg]	Delta T$_{sat}$ [K]
1	279.9	843.8	1.1	428.6	5.0
2	356.9	2775.3	1.1	480.5	38.0
3	311.0	2630.8	-1.0	263.3	-5.5
4	279.3	969.7	0.2	263.3	0.0
5	279.3	969.7	0.2	263.3	0.0
6	282.5	945.3	1.1	428.6	4.0
7	282.5	945.3	1.1	428.6	4.0
8	311.1	2700.3	-1.0	263.3	-6.6
9	311.1	2700.3	-1.0	263.3	-6.6
10	279.3	969.7	0.2	263.3	0.0
11	279.3	969.7	0.2	263.3	0.0

Table 38 Baseline R410A VRF system performance

COP	Capacity	P_comp	P_eva,fan	P_con,fan	P_total	Refrigerant charge
[-]	[W]	[W]	[W]	[W]	[W]	[kg]
3.14	6869.04	2153.71	20.38	12.48	2186.57	17.83

6.2.2. Hybrid R410A VRF system design

6.2.2.1.   Refrigerant loop design

The piping design restriction of HVRF system is also from Figure 219. The schematic of traditional VRF system is shown in Figure 222. Two indoor units are designed with the height of 15 m (49 feet). Pipe A is refrigerant loop and the length is 110 m (360 feet). Pipe B is water pipe and the length is 60 m (196 feet) and the heights of two indoor units are both 15 m (49 feet). The diameter of pipe B is 22 mm (0.875 inches) (Mitsubishi, 2012). Outdoor unit is the same traditional fin-and-tube heat exchanger as what was used for baseline. Indoor unit is bBTHX. The design of bBTHX is discussed later. Outdoor unit and indoor unit exchange heat through a plate heat exchanger. The simulation condition is dry test condition for air condition mode from AHRI standard (AHRI, 2008). Ambient dry/wet bulb temperature is 35/23.9°C and indoor air dry/wet bulb temperature is 26.7/19.4° C. The vapor compression cycle is simulated using steady state vapor compression simulation tool VapCyc® (Winkler et al., 2008).
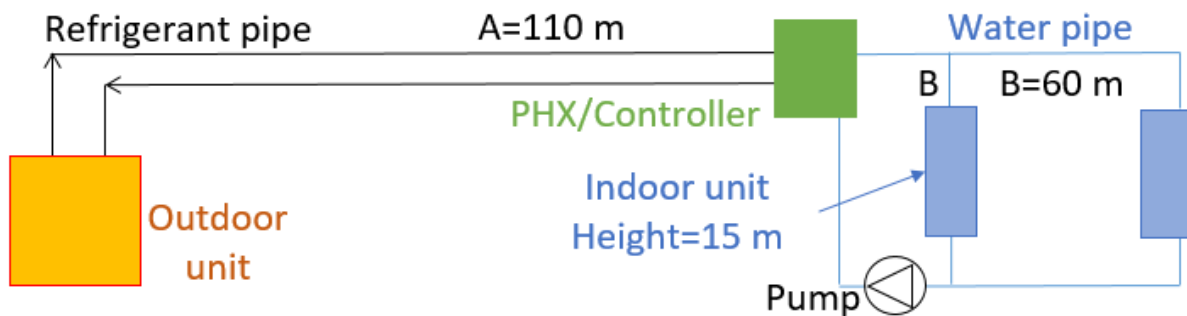
Figure 222 Schematic of HVRF system

Convergence criteria for high pressure side is subcooling temperature equals 5.5 K and convergence criteria for low pressure side is suction super heat temperature equals 5 K. Power input to the fan motor is 18 W for 1 m³/s airflow rate for condenser. Figure 221 shows the R410A

HVRF system schematic in VapCyc® and the corresponding properties of each state point are summarized in Table 39 and Table 40.
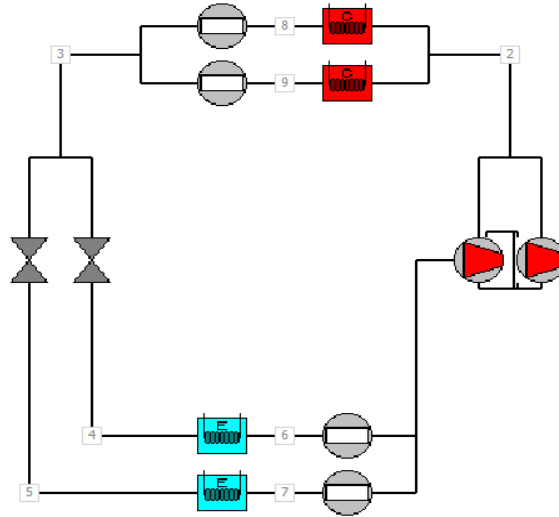
Figure 223 R410A HVRF system schematic

Table 39 Simulation results for R410A HVRF system

Junction	T [K]	P [kPa]	x	h [kJ/kg]	Delta T_{sat} [K]
1	278.2	798.3	1.1	428.1	5.0
2	358.6	2775.0	1.1	482.5	39.7
3	311.4	2652.1	-1.0	263.9	-5.5
4	275.8	870.8	0.3	263.9	0.0
5	275.8	870.8	0.3	263.9	0.0
6	280.1	870.8	1.1	428.1	4.2
7	280.1	870.8	1.1	428.1	4.2
8	311.4	2698.3	-1.0	263.9	-6.2
9	311.4	2698.3	-1.0	263.9	-6.2

Table 40 R410A HVRF system performance

Capacity [W]	P_comp [W]	P_con,fan [W]	Refrigerant charge [kg]
6862.17	2277.11	12.48	10.51

6.2.2.2.   Indoor unit coil design

Indoor unit of HVRF system is a fan coil unit which consists of air-to-water heat exchanger, fan and motor, drain pan and drainage pump. Different indoor units can be used for HVRF system,

such as ducted or ceiling fan coil unit, floor mounted fan coil unit and cassettes fan coil unit. Among these three types, ducted or ceiling fan coil unit is the most compact design thus was selected as the indoor unit type for current study. The picture of such kind of indoor coil unit is shown in Figure 224 and the flow direction is shown in Figure 225. The model number is PEFY-WP32VMA-E. The specifications are summarized in Table 41 and Figure 226.

Figure 224 Indoor coil unit
(Mitsubishi, 2012)
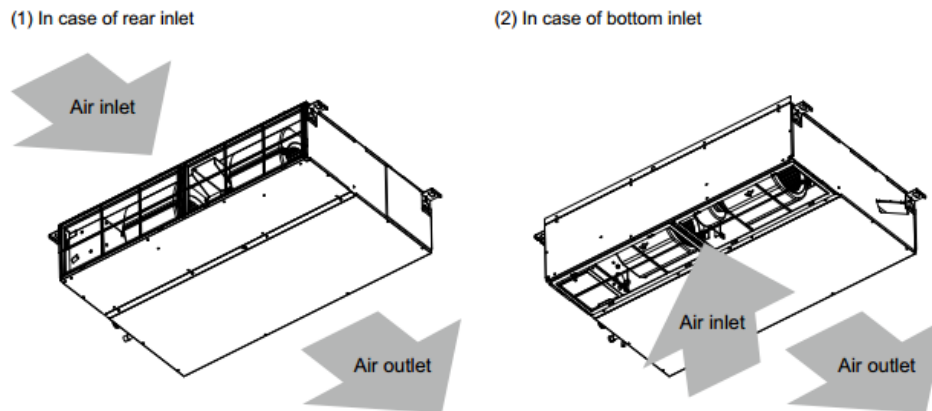
Figure 225 Airflow direction of indoor coil unit
(Mitsubishi, 2012)

Table 41 Specifications of indoor unit (Mitsubishi, 2012)

Model		PEFY-WP32VMA-E
Power source	—	1-phase 220-230-240V 50/60 Hz
Capacity	kW	3.6
External finish	—	Galvanized steel plate
External dimension H × W × D	mm	250 x 900 x 732
Net Weight	kg	26
Heat exchanger	—	Aluminum cross fin and copper tube
Water volume	L	1.0
Fan Air flow rate	m³/s	0.20-0.242-0.283
Motor output	W	85
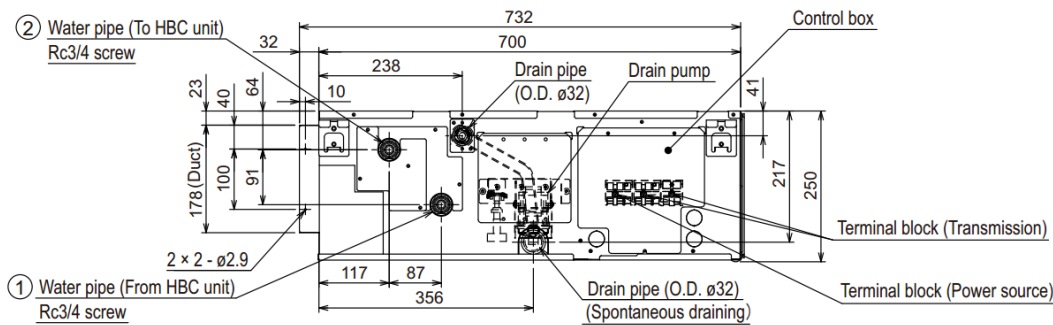
Model	A	B	C	D	E	F	G	①Water pipe (From HBC unit)	②Water pipe (To HBC unit)
PEFY-WP20VMA-E	700	754	800	660	7	600	658		
PEFY-WP25, 32VMA-E	900	954	1000	860	9	800	858	Rc3/4 screw	
PEFY-WP40, 50VMA-E	1100	1154	1200	1060	11	1000	1058		

Figure 226 Dimensions of indoor coil unit (Mitsubishi, 2012)

The fin-and-tube heat exchanger is placed diagonally inside the indoor coil unit. The frontal area (H x W) limit for the heat exchanger is approximately 250 x 900 mm. Here we design two heat exchangers, one is a 5 mm slit fin-and-tube heat exchanger with enhanced micro fin tube on waterside and the other is bBTHX. Here are the assumptions and design conditions:

- Inlet air and water temperatures are 26.7 and 7 °C.

- Inlet air flow rate is 0.283 m³/s and inlet water flow rate is 0.163 kg/s.

- Design capacity is 3413 W.

191

- Dimension limitation is 250 x 900 x 100 mm.

Indoor unit A (Baseline): 5 mm slit fin-and-tube heat exchanger

This heat exchanger is designed based the 5 mm slit fin-and-tube heat exchanger that has been tested and the correlations used are experimentally validated. Data and validation can be found in appendix. The tube internal surface is micro fin, but the specification data cannot be shown due to confidentiality. The heat exchanger specifications are shown in Table 42. Note fan power is the product of ADP and air volume flow rate over efficiency.

Table 42 Design of indoor unit A - 5 mm slit fin-and-tube HX (simulation data)

Tube per bank	-	42	Capacity	W	3464
Tube bank #	-	1	T_water_out	K	285.2
Circuit #	-	7	T_air_out	K	289.3
Tube length	m	0.25	ADP	Pa	11.79
Tube OD	mm	5	WDP	kPa	25.75
Tube ID	mm	4.6	AHTA	m^2	4.14
Tube spacing	mm	21	WHTA	m^2	0.15
FPI	-	22	fin effectiveness		0.796
$H \times W \times D$	mm	250 x 882 x 11.4	AHTC	W/m^2K	121
A_fr	m^2	0.221	WHTC	W/m^2K	10521
Water volume	L	0.174	Tube material volume	cm^3	31
Volume	cm^3	2513.7	Total material volume	cm^3	249
Fin material volume	cm^3	218	Total power (100% efficiency)	W	7.53
			Fan efficiency	-	0.6
			Fan Power	W	5.5

Indoor unit B: bBTHX

The second indoor unit is bBTHX. An optimization problem is defined to find the proper design.

bBTHX Optimization:

The design optimization problem here is described as below. Two objectives are total power and heat exchanger volume. The constraints include (1) total heat exchanger capacity should be similar or larger than baseline; (2) total power is 30% less than baseline; (3) total heat exchanger volume is 30% less than baseline; (4) aspect ratio (AR) is similar to baseline; and (5) frontal area is similar to baseline. Note here the power means the sum of product of pressure drop and volume flow rate of water and air and the efficiency is assumed to be one.

Optimization:
$$\min Power$$
$$\min V_{HX}$$
$$s.t.$$
$$0.9 \cdot \dot{Q}_{baseline} \leq \dot{Q} \leq 1.1 \cdot \dot{Q}_{baseline}$$
$$Power \leq 0.7 \cdot Power_{baseline}$$
$$V_{HX} \leq 0.7 \cdot V_{HX\_baseline}$$
$$0.9 \cdot AR_{baseline} \leq AR \leq 1.1 \cdot AR_{baseline}$$
$$0.9 \cdot A_{fr,baseline} \leq A_{fr} \leq 1.1 \cdot A_{fr,baseline}$$

Optimization results and discussion:

The optimization results are shown in Figure 227. One of the designs was selected to be the final design and the results are summarized in Table 43. Comparing the two distinctive designs, the advantages of applying bBTHX as an indoor coil for VRF system are clear. It has 75.4% less total material volume and 65.1% less envelope volume than baseline 5 mm fin-and-tube heat exchanger. bBTHX also has 37.9% less water volume, meaning that the fan coil unit has less water

193

mass during operation. The waterside heat transfer coefficient of bBTHX is 17.2% lower than that of 5 mm coil but it has much larger waterside heat transfer area and 62.7% waterside pressure drop. This means comparing to the method of using micro fins to enhance waterside heat transfer, using bifurcation would result in much lower pressure drop and slightly lower heat transfer. The CFD verification of the design point is summarized in Table 44.
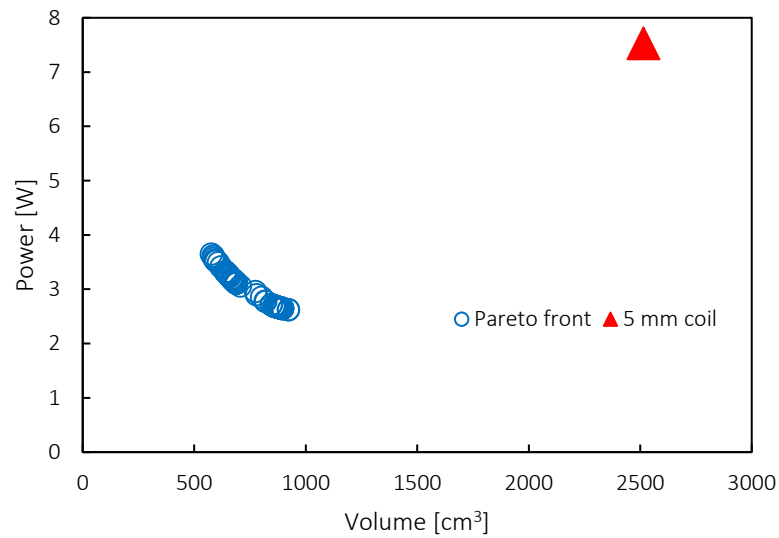
Figure 227 Optimization results of bBTHX indoor unit coil

Table 43 Design of indoor unit B – bBTHX (simulation data)

Tube per bank	-	548	Capacity	W	3449	-0.4%
Tube bank #	-	5	T_water_out	K	285.2	0.0%
Tube length	m	0.25	T_air_out	K	289.6	0.1%
Tube OD	mm	0.56	ADP	Pa	4.62	**-60.8%**
Tube ID	mm	0.50	WDP	kPa	9.6	**-62.7%**
Pl/OD	-	2.95	AHTA	m^2	1.22	**-70.5%**
Pt/OD	-	1.51	WHTA	m^2	0.98	**553.3%**
LR		5.48	AHTC	W/m^{2}K	262.6	**117.0%**
θ		19.7	WHTC	W/m^{2}K	8714.6	**-17.2%**
H × W × D	mm	250 x 900 x 3.9	Total material volume	cm^3	61.2	**-75.4%**
A_fr	m^2	0.225	Water volume	L	0.108	**-37.9%**
			Volume	cm^3	877.5	**-65.1%**
			Total power (100% efficiency)	W	2.66	**-64.7%**
			Fan efficiency	-	0.6	
			Fan Power	W	2.18	**-60.4%**

Table 44 Design point verification against CFD simulation for HVRF indoor coil

Optimization results				CFD results				Percentage deviation			
AHTC [W/m^{2}K]	ADP [Pa]	WHTC [W/m2K]	WDP [Pa]	AHTC [W/m^{2}K]	ADP [Pa]	WHTC [W/m^{2}K]	WDP [Pa]	AHTC [%]	ADP [%]	WHTC [%]	WDP [%]
262.55	4.62	8714.6	1180.08	270.31	4.75	8284.8	1121.63	2.95%	2.86%	-4.9%	-5.0%

6.2.2.3.   Water loop pressure drop calculation

The water loop friction needs to be evaluated to get the total power consumption for HVRF system. Total water loop pressure drop includes (1) pressure drop of plate heat exchanger, (2) pressure drop of water loop piping and (3) pressure drop of indoor unit. Pressure drop of plate heat exchanger is calculated using PHEsim^{TM}, a steady state plate heat exchanger simulation tool. The results are summarized in Table 45.

Table 45 Pressure drop of plate heat exchanger (waterside)

T_water_in	T_water_out	Mass flow rate	Pressure drop
[K]	[K]	[kg/s]	[Pa]
285.15	280.2	0.326	1419.07

Pressure drop of water loop piping is calculated using Equation (37), which is developed by Petukhov (1970). There are two identical indoor unit with inner diameter of 20 mm, length of 392 feet and height of 49 feet. The tube is assumed to be smooth PVC pipe. The pressure drop of water loop is shown in Table 46.

Table 46 Pressure drop of water loop piping

ID	Length	DP_fric	DP_height	DP_total
[mm]	[m]	[kPa]	[kPa]	[kPa]
20	119.5	23.95	149.4	173.7

Pressure drop of indoor unit is calculated previously. Pressure drop is 25.75 kPa for indoor coil A and 9.6 kPa for indoor coil B. Pumping power of water loop with two different indoor units are summarized in Note that pumping power is defined as the product of water volume flow rate and waterside pressure drop (WDP) over efficiency.

Table 47 Pumping power of water loop

Indoor unit	Amount	Water flow rate	DP_PHX	DP_Piping	DP_Indoor unit	Efficiency	Pumping power
		[kg/s]	[kPa]	[kPa]	[kPa]		[W]
A	2	0.163	1.419	173.7	25.75	0.5	65.48
B	2	0.163	1.419	173.7	9.6	0.5	60.22

6.2.2.4.   Summary

The R410A HVRF system's performances with different indoor coil units are summarized in Table 48. For each system, there are two indoor units.

Table 48 R410A HVRF system performance with two different indoor units

Indoor unit	COP	Capacity	P_comp	P_con,fan	P_waterloop	P_eva,fan	P_total	Refrigerant charge
[-]	[W]	[W]	[W]	[W]	[W]	[W]	[kg]
A	2.90	6862.17	2277.11	12.48	65.48	11	2366.07	10.51
B	2.91	6862.17	2277.11	12.48	60.22	4.36	2354.17	10.51

6.2.3. Hybrid R290 and R600a VRF system

The biggest advantage of Hybrid VRF system is the possibility of utilizing flammable refrigerants. Two HVRF system are evaluated using R290 and R600a. The assumptions are the same as R410A HVRF system. The simulation results for R290 are summarized in Table 49 and Table 50.
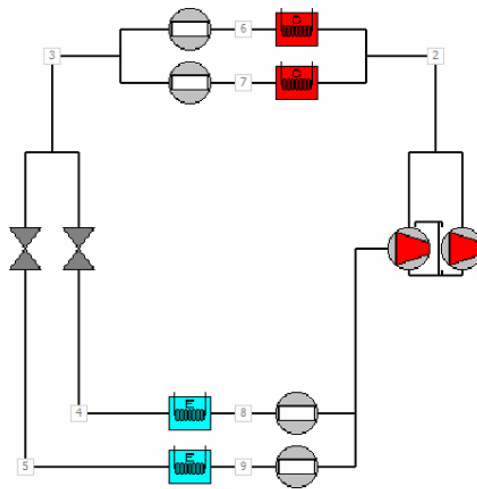
Figure 228 R290 HVRF system schematic

Table 49 Simulation results for R290 HVRF system

Junction	T [K]	P [kPa]	x	h [kJ/kg]	Delta T_{sat} [K]
1	279.6	495.9	1.1	585.2	5.0
2	342.9	1601.0	1.1	671.9	22.8
3	311.8	1503.7	-1.0	303.0	-5.5
4	276.1	518.7	0.3	303.0	0.0
5	276.1	518.7	0.3	303.0	0.0
6	311.8	1528.8	-1.0	303.0	-6.2
7	311.8	1528.8	-1.0	303.0	-6.2
8	280.1	518.7	1.1	585.2	4.0
9	280.1	518.7	1.1	585.2	4.0

Table 50 R290 HVRF system performance

Capacity [W]	P_comp [W]	P_con,fan [W]	Refrigerant charge [kg]
6869.13	2111.14	12.48	5.66

The simulation results for R600a are summarized in Figure 229, Table 51 and Table 52.
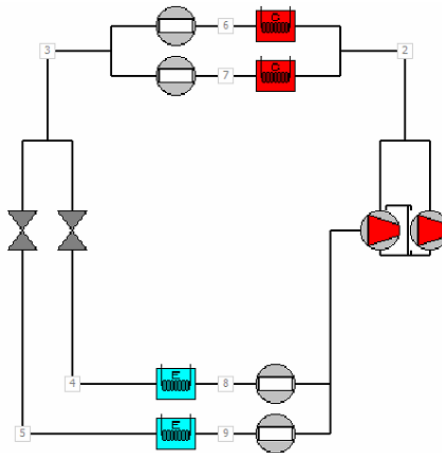
Figure 229 R600a HVRF system schematic

Table 51 Simulation results for R600a HVRF system

Junction	T [K]	P [kPa]	x	h [kJ/kg]	Delta T_{sat} [K]
1	280.1	167.9	1.1	565.2	5.0
2	337.8	696.2	1.1	650.0	13.9
3	309.6	559.3	-1.0	287.4	-5.5
4	275.1	167.9	0.2	287.4	0.0
5	275.1	167.9	0.2	287.4	0.0
6	309.6	559.3	-1.0	287.4	-5.5
7	309.6	559.3	-1.0	287.4	-5.5
8	280.1	167.9	1.1	565.2	5.0
9	280.1	167.9	1.1	565.2	5.0

Table 52 R600a HVRF system performance

Capacity	P_comp	P_con,fan	Refrigerant charge
[W]	[W]	[W]	[kg]
6868.58	2096.61	12.48	5.86

6.2.4. System performance comparison

Performances of all systems are summarized in Table 53. All five different VRF systems have similar capacities and the R410A systems have similar COPs. The biggest advantage of HVRF system is the refrigerant charge reduction. bBTHX is proved to have the potential to be applied as the indoor unit of VRF system. Besides having smaller pressure drop on both air and water side, bBTHX also reduces the weight of the coil by reducing material volume and internal water volume.

Table 53 System performance comparison

System	COP	Capacity	P_comp	P_con,fan	P_waterloop	P_eva,fan	P_total	Refrigerant charge
	[-]	[W]	[W]	[W]	[W]	[W]	[W]	[kg]
Baseline R410A VRF	3.14	6869.04	2153.71	12.48	-	20.38	2186.57	17.83
R410A HVRF-A	2.90	6862.17	2277.11	12.48	65.48	11	2366.07	10.51 (-41%)
R410A HVRF-B	2.91	6862.17	2277.11	12.48	60.22	4.36	2354.17	10.51 (-41%)
R290 HVRF-B	3.14	6869.13	2111.14	12.48	60.22	4.36	2188.2	5.66 (-68%)
R600a HVRF-B	3.16	6868.58	2096.61	12.48	60.22	4.36	2173.67	5.86 (-67%)

Chapter 7: Conclusions

This dissertation presents a novel compact air-to-fluid heat exchanger, bifurcated bare tube heat exchanger, that has the advantages of smaller volume, smaller material volume and lower pumping power. The key feature is the addition of bifurcation, which enhances airside heat transfer by creating 3D flow and improves waterside heat transfer by boundary layer interruption and redevelopment. This dissertation exploits the frontier of next generation compact heat exchanger design. This section summarizes the major contributions, publications and recommendations for future work.

7.1. *Summary of Contributions*

The contribution of the dissertation is broken down into three main parts and summarized as follows:

(1) Investigation of distinct types air-to-fluid heat exchanger performance:

- Experimentally investigated the thermal and hydraulic performance characteristics of slit fin-and-tube heat exchangers with diameter of 4 and 5 mm, louvered finned mini-channel heat exchanger, round bare tube heat exchanger (OD=0.8 mm) and shape optimized bare tube heat exchanger (D_h=0.87 mm) under both dry and dehumidifying conditions.

- Developed empirical correlations for Chilton – Colburn j and f factors based on experimental data for round bare tube and shape optimized bare tube heat exchangers.

- Analyzed the heat exchanger performance and gained the heat exchanger design fundamentals. The current airside heat transfer enhancement technology has the limitation of further improving heat transfer without pressure drop penalty.

(2) Novel heat exchanger design optimization:

- Reviewed nature inspired heat exchanger devices comprehensively and developed a nature-inspired heat exchanger design guideline.

- Developed two approaches of conducting Parallel Parameterized Computational Fluid Dynamics (PPCFD) technique using ANSYS® Workbench™ and coupled it with Approximation Assisted Optimization (AAO) HX design framework.

- Invented, investigated, 3d printed, validated and optimized a novel heat exchanger:
  - Invented a novel nature-inspired heat exchanger concept, bBTHX, that utilizes 3D flow at airside heat exchanger primary surface.
  - Investigated numerically the fundamental heat transfer and flow friction mechanisms for both airside and waterside.
  - Manufactured a prototype by 3D printing and experimentally validated the hydraulic performance of the novel heat exchanger numerical model.
  - Optimized a single phase HX that has 38% lower total power and 83% smaller volume and 87% smaller material volume than those of louvered fin mini-channel heat exchanger. Compared to round bare tube heat exchanger, the optimal design has 28% lower total power and 11% smaller volume and 10% smaller material volume.

(3) Analysis of bBTHX applicability:

- Investigated the potential applications for bBTHX as car radiator and indoor coil for hybrid VRF system.

- Optimized a car radiator that has 30% lower total pumping power, 68% smaller heat exchanger envelope volume, 87% smaller material volume and 67% smaller water weight than louvered fin-and-tube radiator.

- Optimized an indoor unit for HVRF system that has: 40~70% smaller refrigerant charge than traditional VRF system. The advantage of utilizing bBTHX design is that it provides the potential of fast onsite indoor unit manufacturing using 3d printing technology to lower logistics cost.

7.2. *Publications*

Based on this work, five journal papers, seven conference papers and one invention record were published as follows:

Journal papers:

- **Huang, Z.**, Li, Z., Hwang, Y. and Radermacher, R., Application of Entransy Dissipation Based Thermal Resistance to Design Optimization of a Novel Finless Evaporator. Sci China Tech Sci. (2016) 59: 1486. doi:10.1007/s11431-016-0312-3

- **Huang, Z.**, Hwang, Y., Radermacher, R., Review of Nature-inspired Heat Exchanger Technology, International Journal of Refrigeration, (2017) 78: 1-17, ISSN 0140-7007, https://doi.org/10.1016/j.ijrefrig.2017.03.006.

- **Huang, Z.**, Ling, J., Hwang, Y., Aute, V., Radermacher, R., Design and Numerical Parametric Study of Fractal Heat Exchanger, Science and Technology for the Built Environment. (2017), ISSN 2374-4731, DOI: 10.1080/23744731.2017.1335164

- Bacellar, D., Aute. V., **Huang, Z.**, Radermacher, R., Airside Friction and Heat Transfer Characteristics for Staggered Tube Bundle in Crossflow Configuration with Diameters from 0.5 mm to 2.0 mm, International Journal of Heat and Mass Transfer, (2016) 98: 448-454, ISSN 0017-9310.

- Bacellar, D., Aute, V., **Huang, Z.**, Radermacher, R., Design Optimization and Validation of High Performance Heat Exchangers using Multi-Scale Approximation Assisted Optimization and Additive Manufacturing, Science and Technology for the Built Environment. DOI: 10.1080/23744731.2017.1333877, DOI: 10.1080/23744731.2017.1333877

Conference papers:

- **Huang, Z.**, Hwang, Y., Aute, V., Radermacher, R., Review of Fractal Heat Exchangers, (2016), International Refrigeration and Air Conditioning Conference. Paper 1725

- **Huang, Z.**, Ling, J., Hwang, Y., Aute, V., Radermacher, R, Design and Numerical Parametric Study of Fractal Heat Exchanger, (2016), International Refrigeration and Air Conditioning Conference. Paper 1723

- **Huang, Z.**, Ling, J., Hwang, Y., Radermacher, R., Airside Thermal and Hydraulic Performance of a Bare Tube Heat Exchanger with Diameter of 0.8 mm under Dehumidifying Conditions, ASHRAE winter conference, Chicago, IL, Jan 20-24, 2018.

- Shabtay, Y., **Huang, Z.**, Aute, V., Sharma, V., Radermacher, R., Manufacturing & Testing of Air-to-refrigerant Heat Exchangers Based on 0.8mm Diameter Tubes, (2016), International Refrigeration and Air Conditioning Conference. Paper 1694

- Bacellar, D., Aute, V., **Huang, Z.**, Radermacher, R., Novel Airside Heat Transfer Surface Designs Using an Integrated Multi-Scale Analysis with Topology and Shape Optimization, (2016), International Refrigeration and Air Conditioning Conference. Paper 1610

- Bacellar, D., Aute, V., **Huang, Z.** Radermacher, R., High Performance Gas-to-fluid Crossflow Heat Exchangers using Micro Tubes with Round and Novel Shapes, Thermal Fluids Analysis Workshop (TFAWS16) at NASA-Ames Research Center, August 01-04, 2016

- Bacellar, D., **Huang, Z.**, Aute, V., Tancabel, J., Radermacher, R., Multi-scale Analysis, Shape Optimization and Experimental Validation of Novel Air-to-refrigerant Heat Exchangers, 9th World Conference on Experimental Heat Transfer, Fluid Mechanics and Thermodynamics, Foz do Iguaçu, Brazil, June 11-15, 2017.

Invention record:

- **Huang, Z.,** Bacellar, D., Ling, J., Hwang, Y., Aute, V., Hwang, Y., Radermacher, R., Finless air-to-refrigerant heat exchanger using novel micro fractal tube structure

7.3. *Recommendations for Future Work*

The focus of current dissertation is to enhance the heat transfer of air-to-fluid heat exchanger through novel geometry design to make it more compact and efficient. The key heat transfer mechanism utilized in current work is 3D flow caused by bifurcation. However, the bifurcation geometry is not the only one approach to generate 3D flow at primary heat transfer surface. Future work may be extended to investigate more novel geometries that can produce the same or better effect. Besides creating new geometries, other approaches, such as adding vortex

generators, novel fins should also be studied. Although it was found finless design with small diameter has an intrinsic advantage of improving heat transfer coefficient, it is still of significance to reconsider the design of secondary heat transfer area when cost and manufacturing easiness are taken into consideration.

In current multi-scale heat exchanger optimization design framework, the airside and waterside heat transfer and friction characteristics are simulated separately and then combined through a heat exchanger solver. It would be more meaningful to include both sides in the heat exchanger simulation domain in the future work. Current design framework is limited to geometry parameterization, which means geometry must be parameterized before being proceeded to numerical simulation and optimization. In the future, the design framework should be further improved and extended to have the capability of optimizing the heat exchanger through topology design without parameterization. And finally, this design framework should have the ability to learn from existing designs and generate innovative designs that meet the user requirements automatically.

In current study, the tube-side fluid used is water, however, two-phase flow simulation should be done in the future to widen the application of the new geometry. And the bifurcation geometry is not limited to hollow tubes, it can also be applied in other heat exchange device such as heat sink in electronic cooling to enhance heat transfer and reduce pumping power. This application has the advantage of easy manufacturing. There is a need to investigate more applications of current heat exchanger design. For instance, it can be applied as heat recovery heat exchanger in buildings, two-phase heat exchanger used as condenser/evaporator in heat pump/air conditioning systems, even air-to-air heat exchanger.

The main interest of developing the heat exchanger in current study is on the heat transfer improvement so that the stress analysis, vibration and noise, condensation, fouling/frosting and corrosion issues were not discussed thoroughly. In the future, such physics should be investigated to understand the new heat exchanger better. The consideration of these physics should also be added into the heat exchanger design framework.

One challenge in current study is mass production manufacturing method. The growing additive manufacturing technology makes it possible produce rapid prototypes for researchers. However, the tradeoff between the manufacturing cost, time, accuracy and reliability should be taken into consideration. Therefore, for mass production, the manufacturing method should be further investigated. And the manufacturing constraints should be added into the design framework. Another interesting research topic would be the onsite indoor unit 3D printing for HVRF system.

Appendices

Appendix A: Pictures of test facility
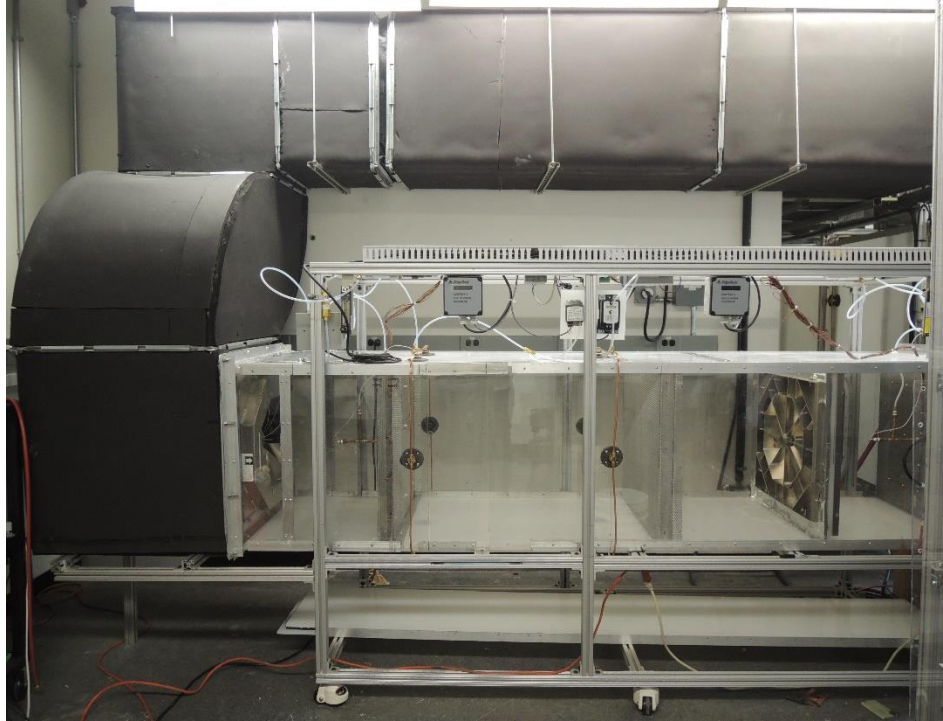
Figure A. 1 Test facility picture-test section

Figure A. 2 Test facility picture-flow rate measurement section
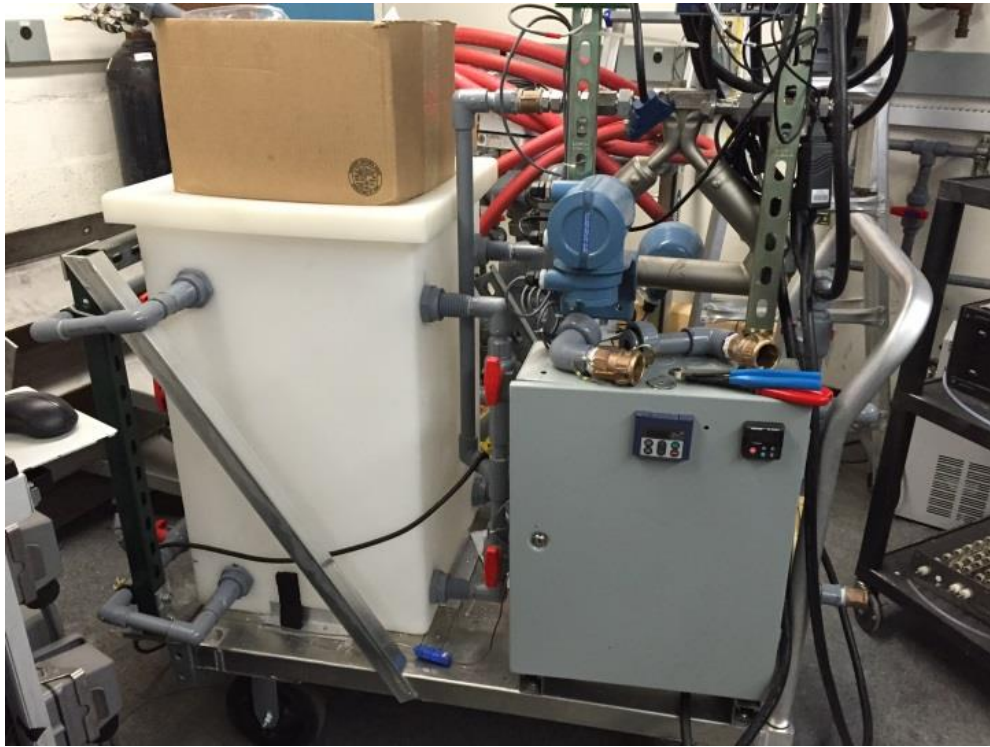
Figure A. 3 Test facility picture-water loop module

Figure A. 4 Test facility picture-refrigerant loop module

Here is the summary of heat exchanger blockage tests. Warm water was drawn through the heat exchanger and infrared pictures are on the right side. If the temperature of the whole heat exchanger is even, then the heat exchanger is not blocked. If the temperature of the whole heat exchanger is not even, then the heat exchanger is blocked where the temperature is lower. For all the heat exchangers tested, only 10kW copper BTHX has blockage issue.

10kW-Copper BTHX blockage test
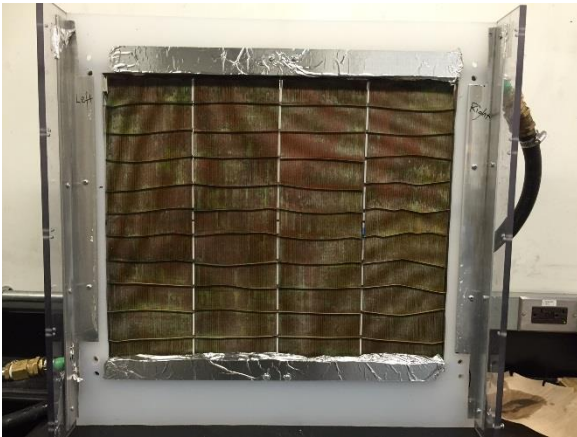
Figure B. 1 10 kW copper BTHX (front)
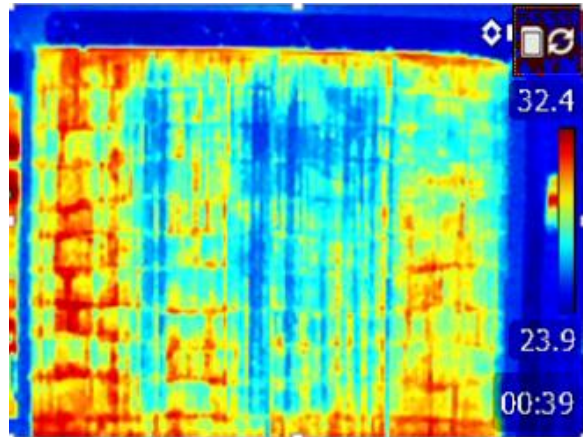
Figure B. 2 10 kW copper BTHX blockage test (front)

Figure B. 3 10 kW copper BTHX (back)
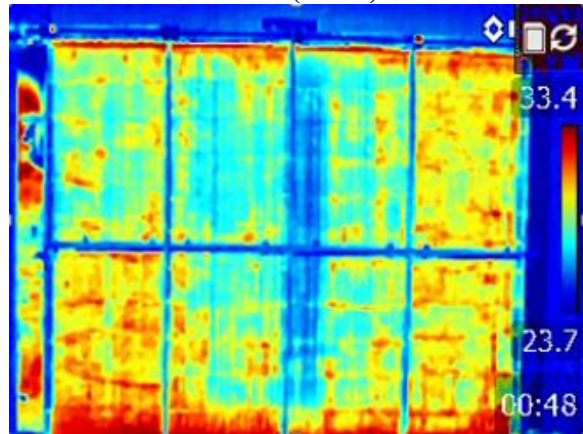
Figure B. 4 10 kW copper BTHX blockage test (back)

WTHX blockage test

Figure B. 5 WTHX (front)
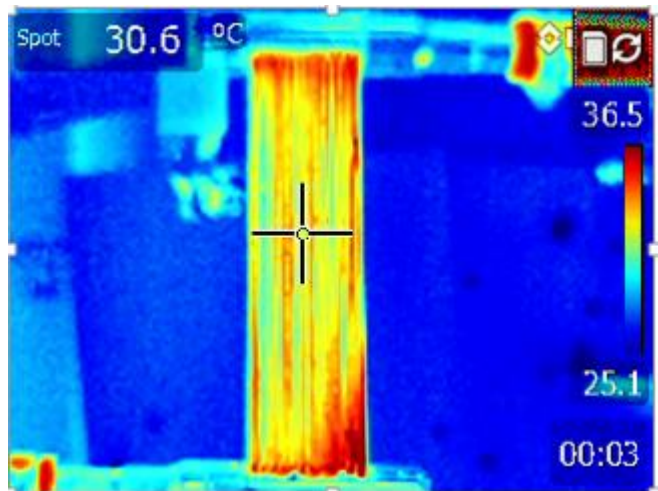
Figure B. 6 WTHX blockage test (front)
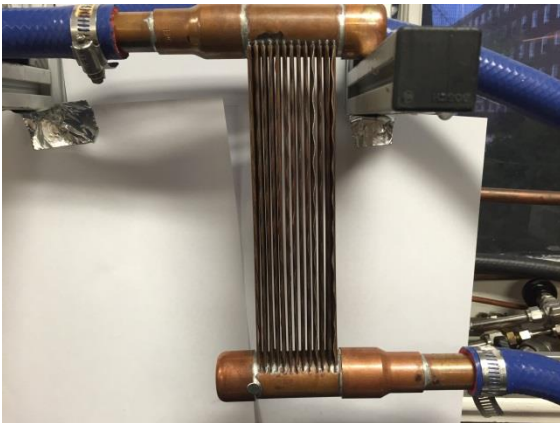
Figure B. 7 WTHX (back)
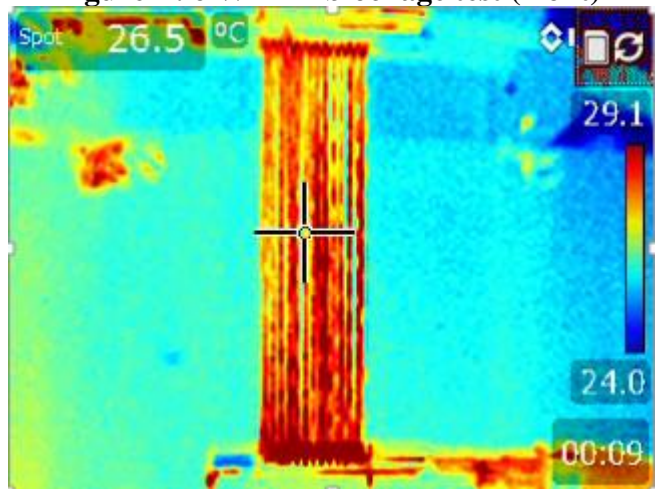
Figure B. 8 WTHX blockage test (back)

sBTHX blockage test

Figure B. 9 sBTHX (front)

Figure B. 10 sBTHX blockage test (front)

Figure B. 11 sBTHX (back)
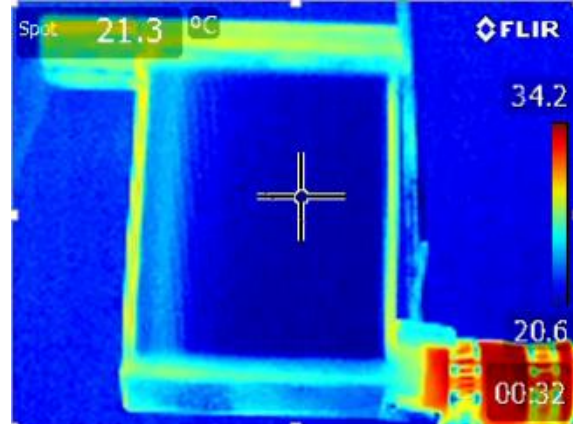
Figure B. 12 sBTHX blockage test (back)

BTHX blockage test

Figure B. 13 BTHX (front)
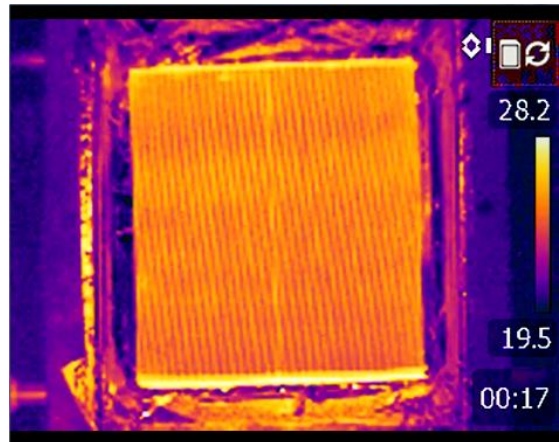
Figure B. 14 BTHX blockage test (front)
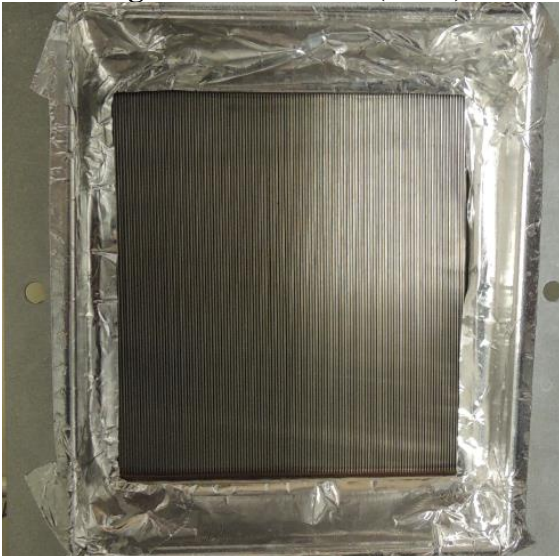
Figure B. 15 BTHX (back)
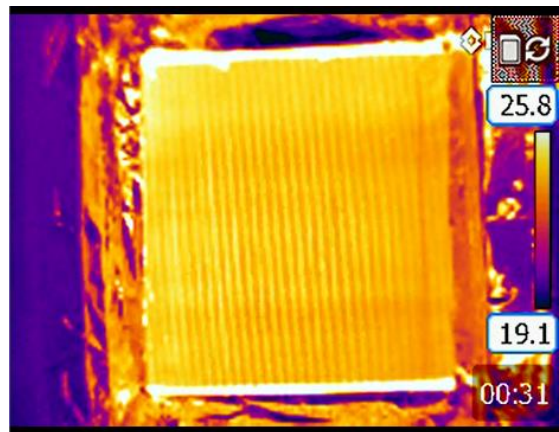
Figure B. 16 BTHX blockage test (back)

BTHX-copper blockage test

Figure B. 17 BTHX-copper (front)

Figure B. 18 BTHX-copper blockage test (front)

Figure B. 19 BTHX-copper (back)
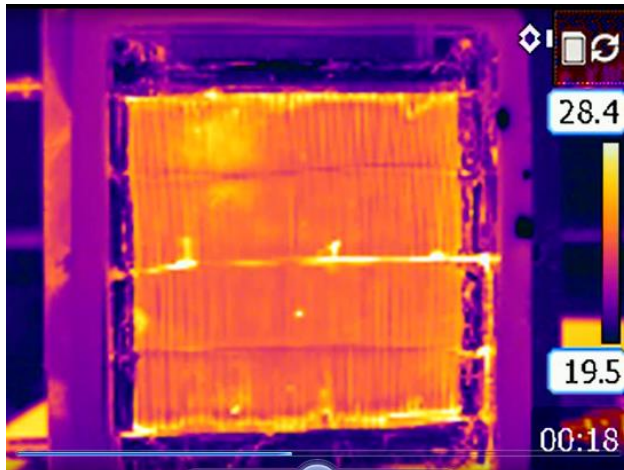
Figure B. 20 BTHX-copper blockage test (front)

Appendix C: Heat exchanger test data

In this section, all heat exchanger test data are summarized.

BTHX test data

Table C. 1 BTHX dry condition test data

Case #		1	2	3	4	5
T_air_in	[°C]	35.15	34.93	35.04	34.93	34.94
T_air_out	[°C]	51.64	50.28	49.21	48.20	47.14
RH_air_in	[%]	0.31	0.31	0.32	0.33	0.34
RH_air_out	[%]	0.14	0.15	0.16	0.17	0.19
P_air_in	[kPa]	100.86	100.88	100.94	101.06	101.10
DP_air	[Pa]	27.10	39.90	54.70	71.80	95.30
uncertainty_DP	[Pa]	1.10	1.30	1.50	1.80	2.00
MFR_air	[g/s]	36.21	46.39	56.45	66.84	79.09
VFR_air	[m³/s]	0.03	0.04	0.05	0.06	0.07
Capacity_air	[W]	601.63	717.20	805.79	893.61	971.92
Capacity_air_uncertainty	[W]	11.27	11.44	10.42	12.66	15.34
T_water_in	[°C]	60.01	59.99	59.96	59.98	60.08
T_water_out	[°C]	55.18	54.30	53.71	53.09	52.53
P_water in	[kPa]	98.50	98.53	98.70	98.81	98.85
DP_water	[kPa]	3.52	3.58	3.59	3.62	3.72
MFR_water	[g/s]	29.95	29.94	30.44	30.32	30.17
Water density	[kg/m³]	989.25	989.50	989.75	990.05	990.43
Capacity_water	[W]	605.40	712.40	795.20	873.20	952.60
Capacity_water_uncertainty	[W]	11.37	8.82	12.44	12.59	13.17
Energy balance	[%]	0.62	-0.67	-1.32	-2.31	-2.01
Average capacity	[W]	603.52	714.80	800.49	883.40	962.26
Capacity uncertainty	[W]	8.00	7.22	8.11	8.93	10.11
Case #		6	7	8	9	10
T_air_in	[°C]	35.18	35.03	35.10	34.93	35.11
T_air_out	[°C]	52.22	51.01	49.87	48.73	47.94
RH_air_in	[%]	30.4%	26.4%	26.5%	26.2%	29.0%
RH_air_out	[%]	13.8%	12.4%	13.4%	14.2%	15.5%
P_air_in	[kPa]	100.83	101.39	101.43	101.48	101.46
DP_air	[Pa]	27.10	38.70	55.90	74.80	95.70
uncertainty_DP	[Pa]	1.10	1.30	1.50	1.80	2.00
MFR_air	[g/s]	36.22	45.57	57.32	68.79	36.22
VFR_air	[m³/s]	0.03	0.04	0.05	0.06	0.03
Capacity_air	[W]	621.63	733.29	852.62	956.35	1029.80
Capacity_air_uncertainty	[W]	11.93	12.42	12.93	13.08	17.08
T_water_in	[°C]	59.97	59.95	60.01	59.99	59.94
T_water_out	[°C]	56.98	56.46	56.00	55.52	55.13
P_water in	[kPa]	102.71	103.34	103.38	103.40	103.26
DP_water	[kPa]	7.36	6.75	6.75	6.71	7.31
MFR_water	[g/s]	50.18	50.26	50.30	50.28	50.13
Water density	[kg/m³]	988.44	988.72	988.79	988.80	989.19
Capacity_water	[W]	626.80	733.60	845.00	940.60	1010.00
Capacity_water_uncertainty	[W]	15.46	14.09	22.38	15.54	15.81
Energy balance	[%]	0.83	0.04	-0.90	-1.66	-1.94

Average capacity	[W]	624.21	733.44	848.81	948.47	1019.90
capacity uncertainty	[W]	9.76	9.39	12.92	10.16	11.64
Case #		11	12	13	14	15
T_air_in	[°C]	34.95	34.90	34.92	35.15	35.00
T_air_out	[°C]	52.47	51.25	50.07	49.16	48.42
RH_air_in	[%]	30.8%	26.4%	26.6%	26.4%	29.2%
RH_air_out	[%]	13.8%	12.1%	12.8%	13.3%	15.3%
P_air_in	[kPa]	100.82	101.36	101.32	101.32	101.43
DP_air	[Pa]	27.10	38.70	56.10	75.30	93.50
uncertainty_DP	[Pa]	1.10	1.30	1.50	1.80	2.00
MFR_air	[g/s]	36.21	45.56	57.42	68.75	78.73
VFR_air	[m³/s]	0.03	0.04	0.05	0.06	0.07
Capacity_air	[W]	639.18	750.42	876.39	970.04	1064.23
Capacity_air_uncertainty	[W]	11.41	10.95	11.70	13.25	19.37
T_water_in	[°C]	60.01	59.91	59.95	60.00	60.01
T_water_out	[°C]	57.81	57.33	56.97	56.71	56.46
P_water in	[kPa]	108.44	108.93	108.88	108.92	108.90
DP_water	[kPa]	12.59	11.40	11.37	11.41	11.68
MFR_water	[g/s]	70.05	69.85	69.82	69.86	69.96
Water density	[kg/m³]	988.05	988.38	988.53	988.70	988.44
Capacity_water	[W]	646.50	752.70	871.20	961.20	1041.00
Capacity_water_uncertainty	[W]	23.95	21.50	23.89	23.92	31.14
Energy balance	[%]	1.14	0.30	-0.59	-0.91	-2.21
Average capacity	[W]	642.84	751.56	873.80	965.62	1052.61
capacity uncertainty	[W]	13.26	12.06	13.30	13.67	18.34

Table C. 2 BTHX wet condition data (Vertical orientation, inlet air condition 1)

Case #		1	2	3	4	5	6	7	8	9
T_air_in	[°C]	26.67	26.69	26.61	26.67	26.73	26.65	26.67	26.82	26.63
T_air_out	[°C]	17.55	20.26	21.57	16.93	19.30	20.63	16.73	19.11	20.32
RH_air_in	[%]	13.7%	14.1%	15.9%	14.0%	14.3%	21.9%	13.4%	15.0%	24.3%
RH_air_out	[%]	23.8%	20.8%	21.8%	25.4%	22.4%	30.9%	24.4%	23.9%	34.7%
P_air_in	[kPa]	102.08	101.63	101.73	102.00	101.65	101.18	102.13	101.70	100.95
DP_air	[Pa]	29.00	84.30	155.50	28.90	83.80	152.40	29.10	83.30	150.40
uncertainty_DP	[Pa]	1.20	1.90	1.80	1.20	1.90	1.80	1.10	1.90	1.90
correctionof DP	[Pa]	0.00	0.00	62.35	0.00	0.00	0.00	0.00	0.00	0.00
MFR_air	[g/s]	37.79	74.68	110.70	37.80	74.51	109.00	37.83	74.27	108.10
VFR_air	[m³/s]	0.03	0.06	0.09	0.03	0.06	0.09	0.03	0.06	0.09
Capacity_air	[W]	346.70	483.56	561.94	370.50	557.13	660.96	378.35	576.61	686.71
Capacity_air_uncertainty	[W]	8.48	10.50	15.49	8.01	9.32	16.25	8.02	8.61	18.80
T_water_in	[°C]	11.87	12.17	12.14	11.92	11.76	11.82	11.95	11.91	11.81
T_water_out	[°C]	15.99	17.86	18.62	14.41	15.44	16.13	13.70	14.56	14.96
P_water in	[kPa]	100.25	99.55	99.71	103.91	103.36	102.77	108.46	107.86	107.04
DP_water	[kPa]	2.46	2.18	2.18	6.11	5.57	6.19	9.88	9.77	10.56
MFR_water	[g/s]	20.11	20.34	20.70	34.89	35.34	35.18	50.16	50.27	50.32
Water density	[kg/m³]	996.94	997.16	997.54	996.76	996.85	996.36	996.75	996.86	995.93
Capacity_water	[W]	346.70	484.20	560.90	363.10	543.70	634.40	368.10	558.20	663.30
Capacity_water_uncertainty	[W]	7.08	16.21	16.77	9.76	7.56	7.92	12.02	12.37	15.26
Energy balance	[%]	0.00	0.13	-0.19	-2.02	-2.44	-4.10	-2.75	-3.24	-3.47
Average capacity	[W]	346.70	483.88	561.42	366.80	550.41	647.68	373.23	567.40	675.00
capacity uncertainty	[W]	5.52	9.66	11.41	6.31	6.00	9.04	7.22	7.54	12.11

Table C. 3 BTHX Wet condition data (Vertical orientation, inlet air condition 2)

Case #		1	2	3	4	5
T_air_in	[°C]	26.56	26.70	26.71	26.79	26.69
T_air_out	[°C]	17.90	20.30	21.27	16.95	19.41
RH_air_in	[%]	50.3%	51.2%	51.5%	50.6%	51.3%
RH_air_out	[%]	81.8%	74.8%	71.6%	86.8%	77.6%
P_air_in	[kPa]	100.40	100.93	102.13	100.30	100.81
DP_air	[Pa]	88.50	150.80	214.90	98.90	165.50
uncertainty_DP	[Pa]	2.70	2.60	2.60	3.70	3.60
SH	[W]	351.20	480.30	592.20	384.90	540.60
SH_un	[W]	7.70	10.30	23.30	9.00	11.60
LH	[W]	20.10	16.90	12.90	33.30	42.50
LH_un	[W]	25.40	48.00	96.30	24.90	55.60
MFR_air	[g/s]	40.28	74.62	108.20	38.88	73.83
VFR_air	[m³/s]	0.03	0.06	0.09	0.03	0.06
Capacity_air	[W]	369.42	492.45	599.75	416.40	578.44
Capacity_air_uncertainty	[W]	27.48	50.68	102.30	27.42	58.51
T_water_in	[°C]	12.00	12.07	12.00	12.04	12.06
T_water_out	[°C]	16.21	17.92	18.67	14.77	15.90
P_water in	[kPa]	98.22	98.76	99.98	101.83	102.26
DP_water	[kPa]	3.32	3.55	3.35	6.62	6.75
MFR_water	[g/s]	20.26	20.39	20.60	35.16	35.10
Water density	[kg/m³]	996.56	996.82	996.89	996.42	996.75
Capacity_water	[W]	356.90	498.50	574.80	402.20	563.50
Capacity_water_uncertainty	[W]	6.10	5.83	7.47	9.73	11.62
Energy balance	[%]	-3.45	1.22	-4.25	-3.47	-2.62
Average capacity	[W]	363.16	495.47	587.28	409.30	570.97
Capacity uncertainty	[W]	14.075	25.51	51.29	14.55	29.83
w_omega_in	[kg/kg]	0.0110330	0.0112635	0.0112021	0.0112627	0.0112768
w_omega_in_uncertainty	[kg/kg]	0.0002166	0.0002958	0.0002980	0.0002911	0.0003897
w_omega_out	[kg/kg]	0.0108312	0.0111719	0.0111539	0.0109163	0.0110439
w_omega_out_uncertainty	[kg/kg]	0.0000000	0.0000000	0.0000000	0.0000000	0.0000000
condensate	[g/s]	0.0081296	0.0068358	0.0052175	0.0134689	0.0171904
condenate_uncertainty	[g/s]	0.0000000	0.0000000	0.0000000	0.0000000	0.0000000
Case #		6	7	8	9	
T_air_in	[°C]	26.77	26.77	26.74	26.76	
T_air_out	[°C]	20.69	16.92	18.95	20.12	
RH_air_in	[%]	51.3%	50.7%	51.4%	51.0%	
RH_air_out	[%]	73.9%	87.3%	79.9%	75.7%	
P_air_in	[kPa]	102.09	100.51	100.74	102.11	
DP_air	[Pa]	234.00	104.70	180.00	243.10	
uncertainty_DP	[Pa]	3.90	3.10	3.90	4.50	
SH	[W]	672.20	379.90	576.00	721.80	
SH_un	[W]	15.90	9.60	10.60	22.20	
LH	[W]	22.20	59.00	48.80	30.90	
LH_un	[W]	97.50	18.90	47.50	95.10	
MFR_air	[g/s]	109.90	38.34	73.50	108.00	
VFR_air	[m³/s]	0.09	0.03	0.06	0.09	
Capacity_air	[W]	687.66	437.92	619.66	745.40	
Capacity_air_uncertainty	[W]	102.00	22.30	50.17	100.70	
T_water_in	[°C]	12.06	11.89	11.99	12.01	
T_water_out	[°C]	16.60	13.87	14.93	15.41	
P_water in	[kPa]	103.47	106.67	106.75	108.19	

216

DP_water	[kPa]	6.69	10.58	10.76	10.86	
MFR_water	[g/s]	34.80	50.38	50.32	50.43	
Water density	[kg/m³]	996.83	996.34	996.67	996.85	
Capacity_water	[W]	660.60	418.90	617.70	716.10	
Capacity_water_uncertainty	[W]	10.64	12.97	14.43	19.68	
Energy balance	[%]	-4.01	-4.44	-0.32	-4.01	
Average capacity	[W]	674.13	428.41	618.68	730.75	
Capacity uncertainty	[W]	51.28	12.90	26.10	51.30	
w_omega_in	[kg/kg]	0.0112065	0.0112394	0.0113600	0.0111313	
w_omega_in_uncertainty	[kg/kg]	0.0002963	0.0002895	0.0002925	0.0002910	
w_omega_out	[kg/kg]	0.0111248	0.0106170	0.0110915	0.0110155	
w_omega_out_uncertainty	[kg/kg]	0.0000000	0.0000000	0.0000000	0.0000000	
condensate	[g/s]	0.0089795	0.0238604	0.0197373	0.0124978	
condenate_uncertainty	[g/s]	0.0000000	0.0000000	0.0000000	0.0000000	

Table C. 4 BTHX Wet condition data (Vertical orientation, inlet air condition 3)

Case #		1	2	3	4	5
T_air_in	[°C]	26.68	26.70	26.77	26.68	26.74
T_air_out	[°C]	18.25	20.64	21.68	17.40	19.81
RH_air_in	[%]	70.6%	70.1%	71.1%	70.2%	70.4%
RH_air_out	[%]	98.0%	93.4%	93.3%	97.2%	93.6%
P_air_in	[kPa]	100.47	100.86	100.76	100.49	100.88
DP_air	[Pa]	95.30	213.40	301.90	93.10	222.10
uncertainty_DP	[Pa]	3.10	4.00	1.20	3.40	4.50
SH	[W]	323.80	445.20	551.70	359.00	505.70
SH_un	[W]	8.50	8.80	14.00	8.30	10.70
LH	[W]	221.10	212.90	168.20	283.50	339.30
LH_un	[W]	36.70	47.70	72.70	32.00	60.90
MFR_air	[g/s]	38.15	72.99	107.60	38.42	72.54
VFR_air	[m³/s]	0.03	0.06	0.09	0.03	0.06
Capacity_air	[W]	549.87	660.65	720.40	649.48	850.89
Capacity_air_uncertainty	[W]	39.57	50.21	76.86	35.17	64.04
T_water_in	[°C]	11.90	11.81	11.98	11.87	11.74
T_water_out	[°C]	18.24	19.62	20.47	16.09	17.45
P_water in	[kPa]	98.14	98.64	98.41	101.93	102.19
DP_water	[kPa]	3.55	2.26	2.66	6.57	5.77
MFR_water	[g/s]	20.18	20.16	20.59	35.19	35.15
Water density	[kg/m³]	996.80	996.70	996.91	996.58	996.74
Capacity_water	[W]	535.30	658.70	731.60	621.90	838.80
Capacity_water_uncertainty	[W]	8.21	8.54	7.22	9.72	10.45
Energy balance	[%]	-2.68	-0.30	1.54	-4.34	-1.43
Average capacity	[W]	542.58	659.68	726.00	635.69	844.84
Capacity uncertainty	[W]	20.206	25.47	38.60	18.24	32.44
w_omega_in	[kg/kg]	0.0156909	0.0155322	0.0158450	0.0155908	0.0156254
w_omega_in_uncertainty	[kg/kg]	0.0002972	0.0002958	0.0002980	0.0002956	0.0003897
w_omega_out	[kg/kg]	0.0133470	0.0143527	0.0152128	0.0126067	0.0137340
w_omega_out_uncertainty	[kg/kg]	0.0000000	0.0000000	0.0000000	0.0000000	0.0000000
condensate	[g/s]	0.0894168	0.0860932	0.0680283	0.1146492	0.1371981
condenate_uncertainty	[g/s]	0.0000000	0.0000000	0.0000000	0.0000000	0.0000000
Case #		6	7	8	9	
T_air_in	[°C]	26.61	26.76	26.67	26.77	
T_air_out	[°C]	20.73	16.78	19.40	20.31	
RH_air_in	[%]	71.4%	69.4%	70.2%	70.3%	

RH_air_out	[%]	93.7%	98.7%	93.4%	93.6%	
P_air_in	[kPa]	100.74	100.04	100.93	100.73	
DP_air	[Pa]	304.80	86.00	223.80	307.50	
uncertainty_DP	[Pa]	1.30	3.20	4.80	1.30	
SH	[W]	633.10	366.70	530.90	694.00	
SH_un	[W]	16.20	9.80	11.20	16.90	
LH	[W]	337.80	283.60	383.30	406.10	
LH_un	[W]	91.50	30.70	69.10	69.90	
MFR_air	[g/s]	107.00	36.51	72.56	106.80	
VFR_air	[m³/s]	0.09	0.03	0.06	0.09	
Capacity_air	[W]	976.61	656.52	921.30	1106.24	
Capacity_air_uncertainty	[W]	96.64	34.94	72.48	75.21	
T_water_in	[°C]	11.89	11.79	11.84	11.85	
T_water_out	[°C]	18.30	14.83	16.16	16.93	
P_water in	[kPa]	101.96	106.03	106.76	106.42	
DP_water	[kPa]	6.12	10.24	10.19	10.13	
MFR_water	[g/s]	35.19	50.18	50.22	50.02	
Water density	[kg/m³]	996.78	996.42	996.65	996.74	
Capacity_water	[W]	944.20	639.10	907.80	1064.00	
Capacity_water_uncertainty	[W]	11.76	16.88	19.96	14.74	
Energy balance	[%]	-3.37	-2.69	-1.48	-3.89	
Average capacity	[W]	960.40	647.81	914.55	1085.12	
Capacity uncertainty	[W]	48.68	19.40	37.59	38.32	
w_omega_in	[kg/kg]	0.0157473	0.0155629	0.0155203	0.0156499	
w_omega_in_uncertainty	[kg/kg]	0.0002963	0.0002954	0.0002925	0.0002910	
w_omega_out	[kg/kg]	0.0144706	0.0124219	0.0133841	0.0141122	
w_omega_out_uncertainty	[kg/kg]	0.0000000	0.0000000	0.0000000	0.0000000	
condensate	[g/s]	0.1366111	0.1146809	0.1550046	0.1642263	
condenate_uncertainty	[g/s]	0.0000000	0.0000000	0.0000000	0.0000000	

Table C. 5 BTHX Wet condition data (Horizontal orientation, inlet air condition 1)

Case #		1	2	3	4	5	6
T_air_in	[°C]	26.77	26.78	26.74	26.75	26.70	26.83
T_air_out	[°C]	17.50	21.07	16.98	20.34	16.59	20.14
RH_air_in	[%]	0.19	0.21	0.19	0.21	0.19	0.21
RH_air_out	[%]	0.36	0.30	0.36	0.32	0.37	0.32
P_air_in	[kPa]	101.17	100.81	101.10	100.87	101.08	100.76
DP_air	[Pa]	27.20	151.70	28.70	151.50	28.40	151.60
uncertainty_DP	[Pa]	1.1	1.8	1.1	1.9	1.1	1.9
MFR_air	[g/s]	37.70	110.20	38.84	110.10	38.61	110.20
VFR_air	[m³/s]	0.03	0.09	0.03	0.09	0.03	0.09
Capacity_air	[W]	344.36	580.08	368.62	657.72	385.04	695.42
Capacity_air_uncertainty	[W]	7.16	14.81	7.50	16.08	8.89	15.76
T_water_in	[°C]	11.89	11.92	11.93	11.92	11.75	11.97
T_water_out	[°C]	16.04	18.77	14.45	16.24	13.55	15.19
P_water in	[kPa]	100.76	100.12	105.99	105.83	113.07	112.67
DP_water	[kPa]	3.71	3.78	9.65	9.33	16.24	16.39
MFR_water	[g/s]	19.79	19.92	34.99	35.25	50.10	49.79
Water density	[kg/m³]	996.80	997.14	996.71	997.07	996.63	996.70
Capacity_water	[W]	343.90	570.30	368.50	637.20	376.00	670.90
Capacity_water_uncertainty	[W]	7.14	9.14	8.02	11.53	14.20	17.38
Energy balance	[%]	-0.13	-1.70	-0.03	-3.17	-2.38	-3.59

218

Average capacity	[W]	344.1	575.2	368.6	647.5	380.52	683.16
Capacity_uncertainty	[W]	5.1	8.7	5.5	9.9	8.4	11.7

Table C. 6 BTHX Wet condition data (Horizontal orientation, inlet air condition 2)

Case #		1	2	3	4	5	6
T_air_in	[°C]	26.76	26.82	26.76	26.68	26.76	26.64
T_air_out	[°C]	19.32	21.36	19.09	20.50	18.85	19.89
RH_air_in	[%]	0.51	0.52	0.51	0.51	0.51	0.52
RH_air_out	[%]	0.81	0.72	0.81	0.74	0.82	0.77
P_air_in	[kPa]	102.38	100.59	102.38	100.62	102.40	100.73
DP_air	[Pa]	123.20	253.80	133.40	263.00	135.90	279.90
uncertainty_DP	[Pa]	3.7	3.6	4.7	4.4	5	1.3
MFR_air	[g/s]	39.99	108.10	38.77	105.80	38.55	105.80
VFR_air	[m³/s]	0.03	0.09	0.03	0.09	0.03	0.09
Sensible capacity	[W]	291.9	526.6	276.7	591.3	284.6	653
Sensible capacity_uncertainty	[W]	7.7	20	8.6	20.3	9.4	24.2
Latent capacity	[W]	0	0	0	11.2	5.4	10.8
Latent capacity_uncertainty	[W]	0.385	1	0.43	1.015	0.47	1.21
Capacity_air	[W]	287.38	512.51	272.60	595.49	287.17	656.55
Capacity_air_uncertainty	[W]	3.9	10.0	4.3	10.2	4.7	12.1
T_water_in	[°C]	11.99	11.94	11.91	11.95	11.91	11.96
T_water_out	[°C]	14.83	18.00	13.53	15.81	13.06	14.84
P_water in	[kPa]	102.16	100.59	107.63	105.93	115.38	113.15
DP_water	[kPa]	4.68	4.01	9.74	10.17	16.90	16.81
MFR_water	[g/s]	19.96	19.80	35.05	34.98	50.92	50.17
Water density	[kg/m³]	996.60	997.02	996.45	996.94	996.36	996.86
Capacity_water	[W]	237.20	502.00	238.60	565.50	243.70	605.30
Capacity_water_uncertainty	[W]	6.56	9.14	16.95	12.67	27.12	26.17
Energy balance	[%]	-4.00	-2.07	-3.00	-5.17	-2.50	-4.00
Average capacity	[W]	262.29	507.26	255.6	580.5	265.4	630.93
Capacity_uncertainty	[W]	3.8	6.8	8.7	8.1	13.8	14.4

Table C. 7 BTHX Wet condition data (Horizontal orientation, inlet air condition 3)

Case #		1	2	3	4	5	6
T_air_in	[°C]	26.79	26.70	26.65	26.71	26.65	26.71
T_air_out	[°C]	20.29	21.64	20.06	20.99	20.32	20.66
RH_air_in	[%]	0.70	0.70	0.70	0.71	0.70	0.71
RH_air_out	[%]	1.00	0.92	1.00	0.93	0.98	0.94
P_air_in	[kPa]	101.45	101.30	101.39	101.19	101.38	101.19
DP_air	[Pa]	161.60	315.14	166.60	334.95	151.50	338.05
uncertainty_DP	[Pa]	6.1	3.1	3.9	3.1	5	3.1
MFR_air	[g/s]	37.65	108.40	37.26	109.30	37.13	108.70
VFR_air	[m³/s]	0.03	0.09	0.03	0.09	0.03	0.09
Sensible capacity	[W]	240.1	521.4	241.9	603.7	230.5	638.8
Sensible capacity_uncertainty	[W]	9.4	20.5	7.9	16.7	7.9	16.4
Latent capacity	[W]	50.8	125.5	58.5	243.3	66.9	315.3
Latent capacity_uncertainty	[W]	0.47	1.025	0.395	0.835	0.395	0.82
Capacity_air	[W]	290.72	648.19	300.69	850.83	298.10	959.80
Capacity_air_uncertainty	[W]	4.7	10.3	4.0	8.4	4.0	8.2
T_water_in	[°C]	11.87	11.98	11.85	11.96	11.96	11.94
T_water_out	[°C]	15.30	19.64	13.82	17.59	13.32	16.31

P_water in	[kPa]	102.07	101.96	106.69	105.98	113.77	113.21
DP_water	[Pa]	4.17	4.09	10.42	9.83	16.98	16.06
MFR_water	[g/s]	19.81	19.79	34.98	35.04	49.99	50.11
Water density	[kg/m^3]	996.21	996.46	996.07	996.47	996.02	996.36
Capacity_water	[W]	284.30	633.90	287.40	826.40	285.20	917.60
Capacity_water_uncertainty	[W]	8.27	8.07	13.38	9.35	18.63	14.67
Energy balance	[%]	-2.23	-2.23	-4.52	-2.91	-4.42	-4.50
Average capacity	[W]	287.51	641.04	294.05	838.61	291.65	938.70
Capacity_uncertainty	[W]	4.8	6.5	7.0	6.3	9.5	8.4

WTHX test data

WTHX (webbed tube heat exchanger) is one of the 1kW heat exchanger prototypes that

has been manufactured. Dimensions are shown below and the test data are summarized.
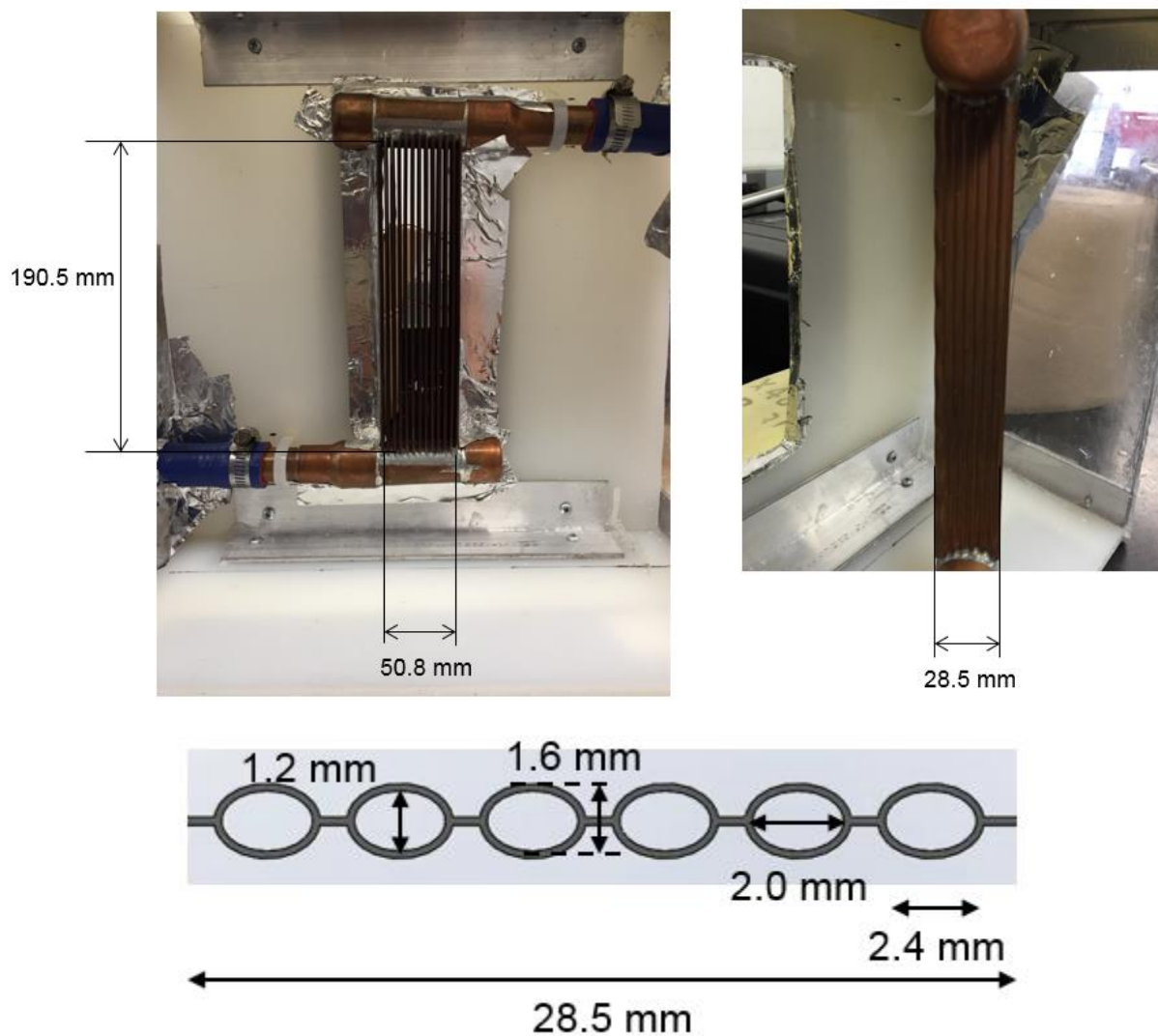
Figure C. 1 Geometry of Webbed Tube Heat Exchanger (WTHX)

Table C. 8 WTHX dimensions

Air cross section area	[m^2]	0.0097
Water cross section area	[m^2]	0.0001
Air heat transfer area	[m^2]	0.1647
Water heat transfer area	[m^2]	0.0759

Table C. 9 WTHX dry condition test data

Case #		1	2	3	4	5
T_air_in	[°C]	34.97	34.79	34.84	34.98	34.94
T_air_out	[°C]	41.14	41.27	41.42	41.52	41.46
RH_air_in	[%]	35.8%	35.7%	37.2%	35.8%	35.7%
RH_air_out	[%]	25.2%	24.9%	25.8%	24.5%	24.6%
P_air_in	[kPa]	100.9	100.5	100.6	100.7	100.7
DP_air	[Pa]	275.5	201.3	141.7	94.7	58.6
MFR_air	[g/s]	78.89	67.34	56.38	45.96	35.57
VFR_air	[m^3/s]	0.0702	0.0601	0.0503	0.0406	0.0314
Capacity_air	[W]	579.5	516.9	443.7	370.1	290.0
Capacity_air_uncertainty	[W]	13.3	15.4	10.1	9.1	7.6
T_water_in	[°C]	60.03	60.08	60.05	59.98	59.96
T_water_out	[°C]	57.90	58.15	58.32	58.46	58.69
P_water in	[kPa]	98.3	97.8	97.8	98.0	98.0
DP_water	[kPa]	95.3	94.6	94.6	94.7	94.6
MFR_water	[g/s]	3.7	3.8	3.8	3.8	3.8
Water density	[kg/m^3]	70.0	70.1	69.9	70.0	69.8
Capacity_water	[W]	988.1	987.9	987.8	987.9	987.7
Capacity_water_uncertainty	[W]	41.5	33.2	33.1	49.7	39.3
Energy balance	[%]	7.4%	0.7%	1.9%	3.6%	5.4%
Average capacity	[W]	601.6	541.5	474.7	407.5	330.2
Case #		6	7	8	9	10
T_air_in	[°C]	34.88	34.90	34.79	34.78	34.99

221

T_air_out	[°C]	40.90	41.11	41.23	41.14	41.43
RH_air_in	[%]	35.3%	36.0%	36.2%	37.4%	35.3%
RH_air_out	[%]	24.7%	25.1%	25.0%	25.8%	24.7%
P_air_in	[kPa]	100.6	100.5	100.7	100.7	100.6
DP_air	[Pa]	204.6	141.2	95.0	58.4	204.6
MFR_air	[g/s]	67.84	56.39	45.84	35.55	67.84
VFR_air	[m³/s]	0.0605	0.0503	0.0404	0.0314	0.0605
Capacity_air	[W]	500.9	434.8	362.2	284.9	500.9
Capacity_air_uncertainty	[W]	14.4	8.5	8.9	6.4	14.4
T_water_in	[°C]	59.85	59.97	60.00	59.94	59.85
T_water_out	[°C]	57.33	57.76	58.04	58.33	57.33
P_water in	[kPa]	96.8	96.7	96.8	96.8	96.8
DP_water	[kPa]	3.2	3.4	3.4	3.4	3.2
MFR_water	[g/s]	49.6	50.7	50.6	50.2	49.6
Water density	[kg/m³]	988.3	988.1	988.3	987.9	988.3
Capacity_water	[W]	522.2	468.3	414.5	337.7	522.2
Capacity_water_uncertainty	[W]	27.9	31.5	34.4	29.7	27.9
Energy balance	[%]	-2.5%	-1.6%	-0.6%	0.8%	-2.5%
Average capacity	[W]	511.6	451.6	388.3	311.3	511.6
Case #		11	12	13	14	15
T_air_in	[°C]	35.13	34.97	34.81	35.06	34.95
T_air_out	[°C]	40.84	40.94	40.95	41.36	41.33
RH_air_in	[%]	35.5%	35.6%	33.3%	34.8%	35.2%
RH_air_out	[%]	25.6%	25.5%	23.6%	24.6%	24.8%
P_air_in	[kPa]	100.7	100.7	100.6	100.6	100.6
DP_air	[Pa]	265.3	202.4	141.9	96.2	57.4
uncertainty_DP	[Pa]	3.7	3.0	2.4	1.9	1.5
MFR_air	[g/s]	77.43	67.48	56.49	46.23	35.15
VFR_air	[m3/s]	0.0690	0.0601	0.0502	0.0410	0.0311

Capacity_air	[W]	526.3	480.4	417.9	356.2	279.4
Capacity_air_uncertainty	[W]	12.9	16.8	9.2	7.7	7.1
T_water_in	[°C]	60.07	60.05	60.01	60.01	60.03
T_water_out	[°C]	55.95	56.27	56.61	57.05	57.63
P_water in	[kPa]	96.1	96.1	95.9	95.9	95.8
DP_water	[kPa]	2.9	2.9	3.0	3.0	2.9
MFR_water	[g/s]	30.1	30.2	29.9	30.0	30.0
Water density	[kg/m^3]	989.0	988.9	988.7	988.6	988.4
Capacity_water	[W]	518.0	476.6	424.6	370.9	301.4
Capacity_water_uncertainty	[W]	20.5	15.3	22.1	19.5	20.5
Energy balance	[%]	-5.8%	-5.3%	-5.1%	-4.4%	-3.6%
Average capacity	[W]	522.1	478.5	421.3	363.5	290.4

sBTHX test data

Table C. 10 sBTHX dry condition test data

Case #		1	2	3	4	5
T_air_in	[°C]	34.95	35.05	34.97	34.94	34.95
T_air_out	[°C]	49.25	48.21	46.58	45.47	44.80
RH_air_in	[%]	26.9%	27.1%	33.8%	31.6%	32.0%
RH_air_out	[%]	14.9%	15.8%	19.4%	19.5%	20.0%
P_air_in	[kPa]	101.62	101.34	101.19	101.45	101.14
DP_air	[Pa]	70.80	101.00	148.40	196.40	253.60
uncertainty_DP	[Pa]	0.00	0.00	0.00	0.00	0.00
MFR_air	[g/s]	36.27	45.38	56.86	68.65	79.26
VFR_air	[m^3/s]	0.03	0.04	0.05	0.06	0.07
Capacity_air	[W]	522.32	601.38	664.99	728.38	786.54
Capacity_air_uncertainty	[W]	9.15	10.15	19.48	11.89	12.8
T_water_in	[°C]	60.03	59.98	59.86	59.97	59.97

T_water_out	[°C]	55.90	55.31	54.70	54.31	53.91
P_water in	[kPa]	97.53	97.30	97.17	97.63	97.22
DP_water	[kPa]	3.01	3.85	2.89	3.16	3.1
MFR_water	[g/s]	30.02	29.81	30.20	30.19	30.21
Water density	[kg/m^3]	988.63	988.80	988.92	989.43	989.36
Capacity_water	[W]	518.90	587.20	652.50	713.80	766.50
Capacity_water_uncertainty	[W]	12.22	9.47	18.17	16.46	13.25
Energy balance	[%]	-0.66	-2.39	-1.90	-2.02	-2.58
Average capacity	[W]	520.61	594.29	658.75	721.09	776.52
capacity uncertainty	[W]	7.63	6.94	13.32	10.15	9.21
Case #		6	7	8	9	10
T_air_in	[°C]	34.92	34.99	35.06	34.87	34.95
T_air_out	[°C]	50.09	48.88	47.63	46.01	45.78
RH_air_in	[%]	26.9%	27.0%	35.9%	31.3%	32.4%
RH_air_out	[%]	14.0%	14.9%	20.3%	18.5%	19.9%
P_air_in	[kPa]	101.68	101.38	101.25	101.53	101.09
DP_air	[Pa]	71.20	99.30	141.20	202.70	243.00
uncertainty_DP	[Pa]	0.00	0.00	0.00	0.00	0.00
MFR_air	[g/s]	36.27	45.29	56.08	69.50	77.77
VFR_air	[m^3/s]	0.03	0.04	0.05	0.06	0.07
Capacity_air	[W]	554.02	633.71	710.10	780.01	848.34
Capacity_air_uncertainty	[W]	9.51	9.83	11.37	10.39	13.20
T_water_in	[°C]	59.94	59.94	59.88	59.87	59.90
T_water_out	[°C]	57.23	56.85	56.54	56.15	55.96
P_water in	[kPa]	99.39	99.17	99.19	99.55	99.06
DP_water	[kPa]	4.93	4.75	4.82	5.15	5.17
MFR_water	[g/s]	50.01	49.67	50.07	50.25	49.94
Water density	[kg/m^3]	988.09	988.25	988.22	988.58	988.63
Capacity_water	[W]	566.10	640.50	700.80	781.80	823.60

Capacity_water_uncertainty	[W]	18.82	23.51	22.00	14.15	15.42
Energy balance	[%]	2.16	1.07	-1.32	0.23	-2.96
Average capacity	[W]	560.06	637.11	705.45	780.90	835.97
capacity uncertainty	[W]	10.54	12.74	12.38	8.78	10.15
Case #		11	12	13	14	15
T_air_in	[°C]	35.03	34.97	35.05	35.05	35.17
T_air_out	[°C]	50.40	49.14	47.60	46.94	46.15
RH_air_in	[%]	27.5%	26.7%	27.1%	28.0%	29.5%
RH_air_out	[%]	14.0%	14.2%	15.1%	16.3%	17.0%
P_air_in	[kPa]	101.72	101.46	101.31	101.21	101.08
DP_air	[Pa]	70.20	100.70	149.50	193.50	247.40
uncertainty_DP	[Pa]	0.00	0.00	0.00	0.00	0.00
MFR_air	[g/s]	36.35	45.33	58.24	67.48	78.75
VFR_air	[m3/s]	0.03	0.04	0.05	0.06	0.07
Capacity_air	[W]	562.81	646.88	735.95	807.78	871.01
Capacity_air_uncertainty	[W]	10.12	9.54	13.41	13.86	13.38
T_water_in	[°C]	60.04	60.12	60.09	60.09	60.12
T_water_out	[°C]	58.02	57.80	57.51	57.32	57.15
P_water in	[kPa]	101.55	101.51	101.25	101.18	101.17
DP_water	[kPa]	6.09	6.16	6.25	6.09	6.24
MFR_water	[g/s]	69.98	70.00	70.43	70.36	70.67
Water density	[kg/m^3]	987.89	987.95	987.93	987.82	987.85
Capacity_water	[W]	591.20	678.20	760.00	815.10	876.80
Capacity_water_uncertainty	[W]	23.94	23.94	21.70	31.28	19.79
Energy balance	[%]	4.92	4.73	3.21	0.90	0.66
Average capacity	[W]	577.00	662.54	747.98	811.44	873.91
capacity uncertainty	[W]	13.00	12.88	12.75	17.11	11.94

Wet condition data (Inlet air condition 1):

Case #		1	2	3	4	5
T_air_in	[°C]	26.49	26.58	26.80	26.71	26.53
T_air_out	[°C]	17.96	20.66	22.07	17.59	20.47
RH_air_in	[%]	50.2%	49.0%	49.0%	49.9%	50.8%
RH_air_out	[%]	82.8%	74.4%	68.9%	83.6%	74.4%
P_air_in	[kPa]	101.45	101.60	102.24	101.38	102.28
DP_air	[Pa]	46.60	142.20	248.40	47.00	141.20
uncertainty_DP	[Pa]	1.50	2.90	2.70	1.40	2.70
SH	[W]	231.45	358.02	422.17	245.14	363.64
SH_un	[W]	6.05	13.10	11.22	6.58	16.75
LH	[W]	28.06	0.00	0.00	33.71	26.24
LH_un	[W]	0.51	0.00	0.00	0.19	0.10
MFR_air	[g/s]	26.96	60.10	88.71	26.71	59.57
VFR_air	[m³/s]	0.02	0.05	0.08	0.02	0.05
Capacity_air	[W]	259.50	358.02	422.17	278.85	389.88
Capacity_air_uncertainty	[W]	6.07	13.10	11.22	6.59	16.75
T_water_in	[°C]	11.93	11.90	11.93	11.97	11.93
T_water_out	[°C]	15.03	16.10	16.96	13.86	14.60
P_water in	[kPa]	98.75	98.25	98.82	100.24	100.94
DP_water	[kPa]	3.70	3.50	3.40	5.30	5.20
MFR_water	[g/s]	19.79	19.97	19.91	34.95	34.87
Water density	[kg/m³]	995.83	996.17	995.32	995.62	995.26
Capacity_water	[W]	257.00	350.70	418.50	276.90	389.60
Capacity_water_uncertainty	[W]	10.87	8.48	7.09	15.73	14.96
Energy balance	[%]	-0.97	-2.07	-0.87	-0.70	-0.07
Average capacity	[W]	258.25	354.36	420.34	277.88	389.74
Capacity uncertainty	[W]	6.225	7.80	6.64	8.53	11.23
w_omega_in	[kg/kg]	0.0108500	0.0106200	0.0106900	0.0109200	0.0109000
w_omega_in_uncertainty	[kg/kg]	0.0001423	0.0001395	0.0001403	0.0002143	0.0002136

		0.0104291	0.0106200	0.0106900	0.0104096	0.0107218
w_omega_out	[kg/kg]	0.0104291	0.0106200	0.0106900	0.0104096	0.0107218
w_omega_out_uncertainty	[kg/kg]	0.0000000	0.0000000	0.0000000	0.0000000	0.0000000
condensate	[g/s]	0.0113465	0.0000000	0.0000000	0.0136325	0.0106129
condenate_uncertainty	[g/s]	0.0002061	0.0000000	0.0000000	0.0000767	0.0000401
Case #		6	7	8	9	
T_air_in	[°C]	26.78	26.67	26.78	26.70	
T_air_out	[°C]	21.55	17.98	20.34	21.23	
RH_air_in	[%]	50.0%	50.0%	50.3%	51.2%	
RH_air_out	[%]	72.1%	83.7%	75.3%	74.4%	
P_air_in	[kPa]	102.46	101.40	102.21	100.89	
DP_air	[Pa]	257.10	48.00	145.50	265.30	
uncertainty_DP	[Pa]	4.20	1.60	3.20	3.10	
SH	[W]	476.75	231.57	383.60	486.61	
SH_un	[W]	11.26	6.00	11.76	11.66	
LH	[W]	14.30	44.47	43.01	15.40	
LH_un	[W]	0.09	0.51	0.41	0.03	
MFR_air	[g/s]	90.50	26.48	59.19	88.38	
VFR_air	[m^3/s]	0.08	0.02	0.05	0.08	
Capacity_air	[W]	491.05	276.05	426.61	502.01	
Capacity_air_uncertainty	[W]	11.26	6.02	11.77	11.66	
T_water_in	[°C]	11.90	11.89	11.92	11.86	
T_water_out	[°C]	15.11	13.24	13.90	14.26	
P_water in	[kPa]	101.04	102.52	103.16	101.30	
DP_water	[kPa]	5.10	7.10	7.10	6.60	
MFR_water	[g/s]	34.97	49.91	50.03	50.00	
Water density	[kg/m^3]	995.64	995.58	995.11	995.20	
Capacity_water	[W]	470.20	281.30	415.90	502.20	
Capacity_water_uncertainty	[W]	12.74	11.13	12.87	20.71	
Energy balance	[%]	-4.34	1.89	-2.54	0.04	

Average capacity	[W]	480.63	278.67	421.26	502.10
Capacity uncertainty	[W]	8.50	6.33	8.72	11.88
w_omega_in	[kg/kg]	0.0108700	0.0109200	0.0109800	0.0112700
w_omega_in_uncertainty	[kg/kg]	0.0001424	0.0002856	0.0002151	0.0002206
w_omega_out	[kg/kg]	0.0108061	0.0102408	0.0106861	0.0111995
w_omega_out_uncertainty	[kg/kg]	0.0000000	0.0000000	0.0000000	0.0000000
condensate	[g/s]	0.0057837	0.0179856	0.0173951	0.0062280
condenate_uncertainty	[g/s]	0.0000366	0.0002055	0.0001650	0.0000141

Table C. 11 sBTHX Wet condition data (Inlet air condition 2)

Case #		1	2	3	4	5
T_air_in	[°C]	26.60	26.80	26.74	26.53	26.63
T_air_out	[°C]	19.54	21.76	22.58	18.86	21.06
RH_air_in	[%]	71.0%	70.6%	71.7%	70.4%	70.4%
RH_air_out	[%]	92.2%	88.8%	87.9%	91.0%	88.6%
P_air_in	[kPa]	101.39	101.47	101.86	101.38	101.53
DP_air	[Pa]	50.80	155.70	263.80	51.10	156.80
uncertainty_DP	[Pa]	1.60	3.00	2.90	1.60	3.00
SH	[W]	189.49	300.33	372.27	205.11	332.46
SH_un	[W]	5.75	12.06	15.68	5.09	16.50
LH	[W]	179.58	207.00	217.36	202.94	257.69
LH_un	[W]	0.00	0.10	0.82	0.68	1.48
MFR_air	[g/s]	26.68	59.25	88.84	26.57	59.32
VFR_air	[m³/s]	0.02	0.05	0.08	0.02	0.05
Capacity_air	[W]	369.07	507.33	589.63	408.05	590.15
Capacity_air_uncertainty	[W]	5.75	12.06	15.70	5.14	16.57
T_water_in	[°C]	12.00	12.10	11.99	11.95	11.92
T_water_out	[°C]	16.60	18.05	18.80	14.81	15.87
P_water in	[kPa]	98.52	98.30	98.44	100.14	100.26

DP_water	[kPa]	3.50	3.50	3.50	5.30	5.30
MFR_water	[g/s]	19.92	19.96	20.10	34.99	35.06
Water density	[kg/m³]	995.83	995.91	996.00	995.68	995.81
Capacity_water	[W]	383.40	497.40	572.40	418.30	579.50
Capacity_water_uncertainty	[W]	9.50	12.98	10.97	12.07	13.41
Energy balance	[%]	3.81	-1.98	-2.97	2.48	-1.82
Average capacity	[W]	376.23	502.36	581.02	413.18	584.82
Capacity uncertainty	[W]	5.555	8.86	9.58	6.56	10.66
w_omega_in	[kg/kg]	0.0155400	0.0156300	0.0157600	0.0153500	0.0154300
w_omega_in_uncertainty	[kg/kg]	0.0003924	0.0002958	0.0002980	0.0002911	0.0003897
w_omega_out	[kg/kg]	0.0128176	0.0142168	0.0147704	0.0122609	0.0136732
w_omega_out_uncertainty	[kg/kg]	0.0000000	0.0000000	0.0000000	0.0000000	0.0000000
condensate	[g/s]	0.0726334	0.0837309	0.0879125	0.0820765	0.1042150
condenate_uncertainty	[g/s]	0.8108259	0.0966548	0.8189490	0.6820596	1.4835172

Case #		6	7	8	9
T_air_in	[°C]	26.60	26.50	26.51	26.80
T_air_out	[°C]	22.04	18.58	20.72	21.77
RH_air_in	[%]	71.8%	70.1%	70.9%	69.7%
RH_air_out	[%]	88.6%	90.7%	88.9%	87.7%
P_air_in	[kPa]	101.93	101.36	101.54	101.96
DP_air	[Pa]	279.10	51.00	158.80	279.90
uncertainty_DP	[Pa]	1.90	1.60	3.00	0.70
SH	[W]	418.88	210.96	344.82	459.09
SH_un	[W]	19.89	6.28	11.82	18.63
LH	[W]	301.76	218.87	294.30	314.11
LH_un	[W]	0.19	0.67	0.48	0.96
MFR_air	[g/s]	91.32	26.45	59.13	90.59
VFR_air	[m³/s]	0.08	0.02	0.05	0.08
Capacity_air	[W]	720.64	429.82	639.12	773.20

Capacity_air_uncertainty	[W]	19.89	6.32	11.83	18.65
T_water_in	[°C]	11.77	11.93	11.92	11.90
T_water_out	[°C]	16.60	13.98	14.84	15.46
P_water in	[kPa]	100.62	102.49	102.71	103.06
DP_water	[kPa]	5.20	7.20	7.20	7.20
MFR_water	[g/s]	34.85	50.51	50.47	50.53
Water density	[kg/m^3]	995.97	995.57	995.75	996.04
Capacity_water	[W]	703.30	434.70	618.10	754.10
Capacity_water_uncertainty	[W]	13.28	16.44	19.02	17.10
Energy balance	[%]	-2.43	1.13	-3.34	-2.50
Average capacity	[W]	711.97	432.26	628.61	763.65
Capacity uncertainty	[W]	11.96	8.81	11.20	12.65
w_omega_in	[kg/kg]	0.0156600	0.0152500	0.0154300	0.0153500
w_omega_in_uncertainty	[kg/kg]	0.0002963	0.0002895	0.0002925	0.0002910
w_omega_out	[kg/kg]	0.0143238	0.0119035	0.0134171	0.0139477
w_omega_out_uncertainty	[kg/kg]	0.0000000	0.0000000	0.0000000	0.0000000
condensate	[g/s]	0.1220219	0.0885162	0.1190218	0.1270322
condenate_uncertainty	[g/s]	0.1879926	0.6655276	0.4795712	0.9630440

1 kW-MCHX test data

Table C. 12 1 kW - MCHX dry condition test data

Case #		1	2	3	4	5
T_air_in	[°C]	35.02	34.94	34.89	34.92	34.88
T_air_out	[°C]	50.42	47.50	45.74	51.81	49.25
RH_air_in	[%]	37.1%	36.8%	39.5%	37.8%	35.8%
RH_air_out	[%]	16.0%	17.4%	20.3%	15.3%	16.2%
P_air_in	[kPa]	101.70	101.30	101.40	101.70	101.40
DP_air	[Pa]	17.60	32.50	52.00	17.50	32.80
uncertainty_DP	[Pa]	1.00	1.20	1.70	1.00	1.30

MFR_air	[g/s]	37.43	57.05	78.21	37.30	57.18
VFR_air	[m³/s]	0.03	0.05	0.07	0.03	0.05
Capacity_air	[W]	580.50	722.00	854.50	634.70	827.70
Capacity_air_uncertainty	[W]	11.50	12.70	12.30	11.40	13.20
T_water_in	[°C]	60.02	59.96	59.97	60.01	59.96
T_water_out	[°C]	55.54	54.19	53.13	57.08	55.99
P_water in	[kPa]	100.10	99.70	99.70	106.40	106.10
DP_water	[kPa]	5.20	5.30	5.20	11.00	11.00
MFR_water	[g/s]	30.10	30.40	30.20	50.10	49.90
Water density	[kg/m³]	988.90	989.10	989.70	988.20	988.40
Capacity_water	[W]	567.20	736.60	872.00	608.30	835.40
Capacity_water_uncertainty	[W]	10.90	12.60	9.60	21.50	25.60
Energy balance	[%]	-2.32	2.00	2.03	-4.25	0.93
Average capacity	[W]	573.85	729.30	863.25	621.50	831.55
capacity uncertainty	[W]	7.92	8.94	7.80	12.17	14.40
Case #		6	7	8	9	
T_air_in	[°C]	35.05	34.94	34.94	35.03	
T_air_out	[°C]	47.09	52.73	49.88	48.41	
RH_air_in	[%]	34.8%	37.7%	37.7%	36.9%	
RH_air_out	[%]	16.7%	14.7%	15.8%	16.8%	
P_air_in	[kPa]	101.70	101.70	101.80	101.80	
DP_air	[Pa]	53.80	17.70	32.90	53.70	
uncertainty_DP	[Pa]	1.70	1.00	1.20	1.80	
MFR_air	[g/s]	79.89	37.56	56.80	79.04	
VFR_air	[m³/s]	0.07	0.03	0.05	0.07	
Capacity_air	[W]	969.10	673.10	854.60	1065.10	
Capacity_air_uncertainty	[W]	17.50	12.90	12.90	15.90	
T_water_in	[°C]	59.94	60.10	60.04	60.03	
T_water_out	[°C]	55.16	57.90	57.07	56.38	

231

P_water in	[kPa]	106.70	115.90	116.00	116.00
DP_water	[kPa]	11.20	19.70	19.70	19.60
MFR_water	[g/s]	50.00	70.40	70.60	70.30
Water density	[kg/m^3]	989.20	987.80	988.10	988.40
Capacity_water	[W]	983.80	647.50	856.60	1059.00
Capacity_water_uncertainty	[W]	22.30	24.10	24.20	24.10
Energy balance	[%]	1.51	-3.88	0.23	-0.57
Average capacity	[W]	976.45	660.30	855.60	1062.05
capacity uncertainty	[W]	14.17	13.67	13.71	14.44

10 kW-Copper BTHX geometry and test data

Though the 10kW copper BTHX has blockage issues, it is still tested under dry condition.

The dimensions and test results are shown below.

Figure C. 2 10kW-copper BTHX geometry

Table C. 13 10kW-copper BTHX dimensions

Material	Copper	
Geometry	Length x width x depth	444 x 530 x 71 mm
	Frontal area	0.235 m^2
	Air heat transfer area	2.515 m^2
	Water heat transfer area	2.012 m^2

Table C. 14 10 kW-copper BTHX test matrix

Air	Inlet air temperature	30.0 ± 0.3	$^\circ$C
	Inlet air RH	6 ± 1	%
	Air flow rate	0.16 ± 0.0016	m^3/s
		0.31 ± 0.0031	m^3/s
		0.47 ± 0.0047	m^3/s
Water	Inlet water temperature	55.0 ± 0.6	$^\circ$C
	Water mass flow rate	71 ± 0.71	g/s
		95 ± 0.95	g/s
		118 ± 1.18	g/s
		141 ± 1.41	g/s
		165 ± 1.65	g/s
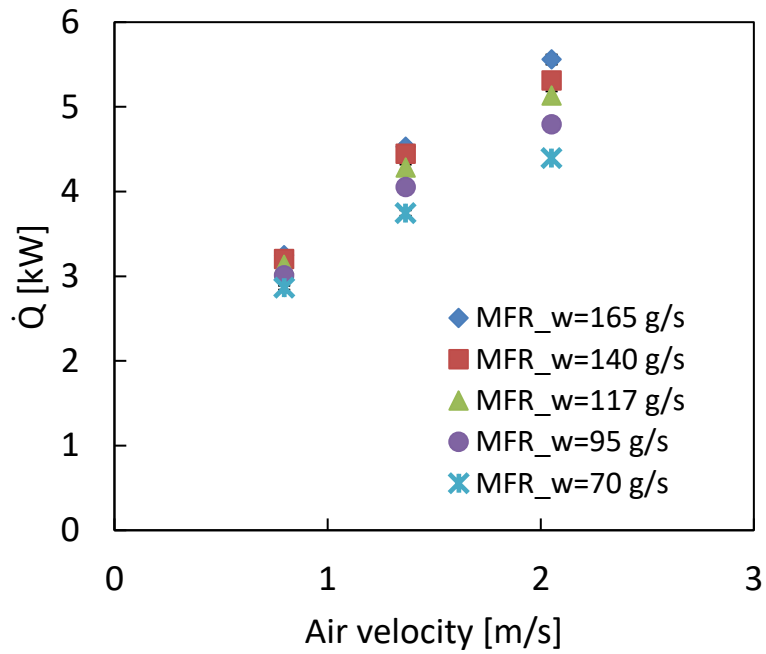
Figure C. 3 Capacity of 10 kW-copper BTHX
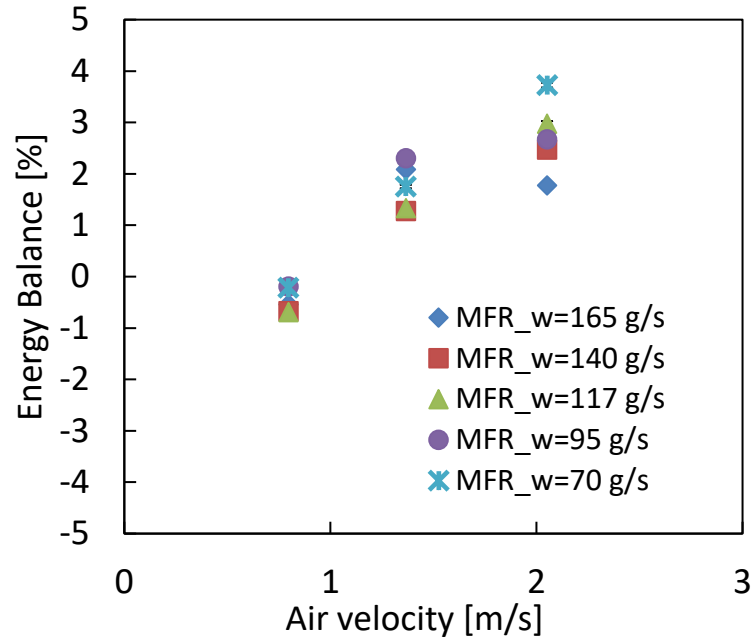
Figure C. 4 Energy balance of 10 kW-copper BTHX
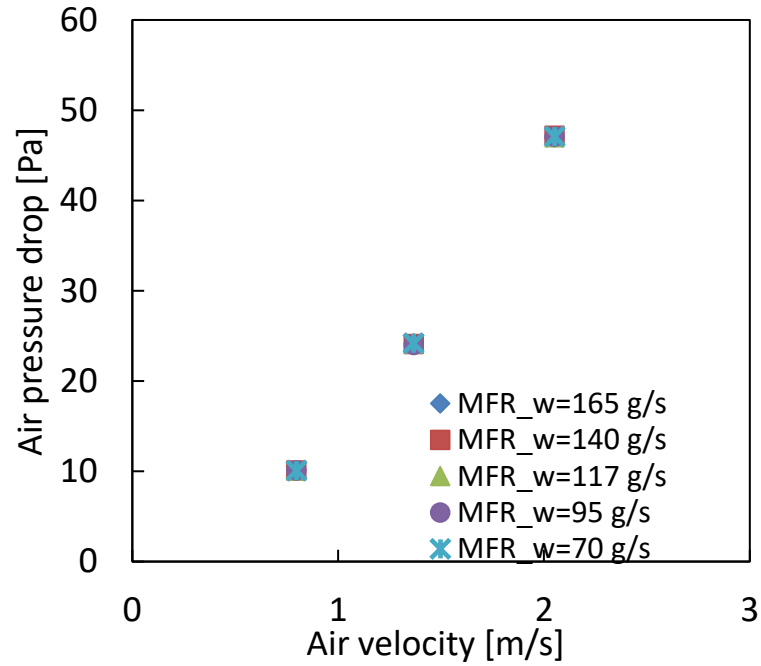
Figure C. 5 Airside pressure drop of 10 kW-copper BTHX

Table C. 15 10 kW-copper BTHX dry condition test data

Case #		1	2	3	4	5
T_air_in	[°C]	30.10	30.20	30.10	30.10	30.20
T_air_out	[°C]	43.77	44.63	45.16	45.47	45.79
RH_air_in	[%]	7.1%	7.3%	7.6%	8.0%	6.8%

RH_air_out	[%]	7.3%	7.3%	7.4%	7.5%	3.3%
P_air_in	[kPa]	101.6	101.5	101.5	101.5	101.4
DP_air	[Pa]	10.1	10.1	10.1	10.1	10.1
uncertainty_DP	[Pa]	0.7	0.7	0.7	0.7	0.7
MFR_air	[g/s]	208.30	207.40	207.30	207.50	207.50
VFR_air	[m^3/s]	0.1857	0.1856	0.1857	0.1863	0.1863
Capacity_air	[W]	2867.2	3013.8	3143.7	3212.5	3257.7
Capacity_air_uncertainty	[W]	41.5	42.5	39.2	44.0	44.2
T_water_in	[°C]	54.98	54.98	55.01	54.94	55.01
T_water_out	[°C]	45.29	47.36	48.67	49.54	50.31
P_water in	[kPa]	114.5	118.4	122.6	127.4	132.7
DP_water	[kPa]	10.0	10.0	10.0	10.0	10.0
MFR_water	[g/s]	70.6	94.5	117.8	141.4	164.9
Water density	[kg/m^3]	992.4	991.9	991.4	991.1	990.9
Capacity_water	[W]	2861.0	3008.0	3122.0	3191.0	3240.0
Capacity_water_uncertainty	[W]	22.3	33.7	42.1	49.0	50.0
Energy balance	[%]	(0.22)	(0.19)	(0.69)	(0.67)	(0.54)
Average capacity	[W]	2864.1	3010.9	3132.8	3201.8	3248.9
Capacity uncertainty	[W]	23.5	27.1	28.7	32.9	33.4
Case #		6	7	8	9	10
T_air_in	[°C]	30.10	30.00	30.10	30.00	30.20
T_air_out	[°C]	40.27	41.07	41.78	42.22	42.53
RH_air_in	[%]	6.5%	6.5%	6.5%	6.5%	6.6%
RH_air_out	[%]	7.3%	3.7%	6.0%	3.6%	4.8%
P_air_in	[kPa]	101.8	101.3	102.0	101.4	102.1
DP_air	[Pa]	24.2	24.0	24.2	24.1	24.2
uncertainty_DP	[Pa]	0.8	0.8	0.8	0.8	0.8
MFR_air	[g/s]	362.60	359.30	361.70	359.20	360.90
VFR_air	[m^3/s]	0.3199	0.3193	0.3198	0.3202	0.3197

235

Capacity_air	[W]	3713.4	4005.6	4253.9	4418.3	4480.6
Capacity_air_uncertainty	[W]	59.6	60.6	61.8	59.4	62.7
T_water_in	[°C]	54.89	54.95	54.97	55.10	54.97
T_water_out	[°C]	42.08	44.57	46.19	47.52	48.40
P_water in	[kPa]	114.9	118.5	123.3	127.7	133.9
DP_water	[kPa]	10.0	10.0	10.0	10.0	10.0
MFR_water	[g/s]	70.6	94.5	117.4	141.2	166.4
Water density	[kg/m^3]	993.3	992.5	992.4	991.8	991.9
Capacity_water	[W]	3779.0	4099.0	4311.0	4475.0	4575.0
Capacity_water_uncertainty	[W]	28.3	30.4	36.6	48.6	57.6
Energy balance	[%]	1.75	2.30	1.33	1.27	2.08
Average capacity	[W]	3746.2	4052.3	4282.5	4446.7	4527.8
Capacity uncertainty	[W]	33.0	33.9	35.9	38.4	42.6
Case #		11	12	13	14	15
T_air_in	[°C]	30.00	30.00	30.10	30.00	30.00
T_air_out	[°C]	37.81	38.62	39.27	39.56	40.00
RH_air_in	[%]	5.2%	6.4%	5.1%	6.4%	5.2%
RH_air_out	[%]	7.1%	4.2%	6.3%	4.1%	5.5%
P_air_in	[kPa]	102.4	101.3	102.4	101.3	102.3
DP_air	[Pa]	47.1	47.1	47.0	47.2	47.0
uncertainty_DP	[Pa]	0.9	0.9	0.9	0.9	0.9
MFR_air	[g/s]	548.80	545.20	547.60	544.70	547.00
VFR_air	[m^3/s]	0.4786	0.4814	0.4795	0.4819	0.4800
Capacity_air	[W]	4314.2	4731.0	5057.2	5245.6	5509.3
Capacity_air_uncertainty	[W]	87.4	94.1	90.5	97.5	99.5
T_water_in	[°C]	55.08	54.77	54.95	54.72	54.82
T_water_out	[°C]	39.99	42.49	44.38	45.60	46.76
P_water in	[kPa]	115.7	118.8	124.0	127.9	134.7
DP_water	[kPa]	10.0	10.0	10.0	10.0	10.0

MFR_water	[g/s]	70.9	94.7	117.9	141.0	166.3
Water density	[kg/m³]	993.6	993.0	992.6	992.3	991.9
Capacity_water	[W]	4478.0	4859.0	5210.0	5377.0	5608.0
Capacity_water_uncertainty	[W]	33.4	36.0	40.9	65.2	62.1
Energy balance	[%]	3.73	2.67	2.98	2.47	1.78
Average capacity	[W]	4396.1	4795.0	5133.6	5311.3	5558.6
Capacity uncertainty	[W]	46.8	50.4	49.6	58.6	58.6

10 kW-louvered fin radiator test data

This radiator is tested to compare with the 10kW copper BTHX. The dimensions and test results are shown below. However, since the 10kW copper BTHX has blockage issues, there is no comparison between these two heat exchangers.

Figure C. 6 10 kW-louvered fin radiator

Table C. 16 10 kW-louvered fin radiator dimensions

Material	Aluminum	
Geometry	Length x width x depth	457 x 419 x 35 mm
	Frontal area	0.192 m²
	Air heat transfer area	7.844 m²
	Water heat transfer area	1.147 m²

Table C. 17 10 kW-louvered fin radiator test matrix

Air	Inlet air temperature	35.0 ± 0.3	°C
	Inlet air RH	35 ± 1	%
	Air flow rate	0.192 ± 0.00192	m³/s
		0.479 ± 0.00479	m³/s
		0.766 ± 0.00766	m³/s
Water	Inlet water temperature	60.0 ± 0.6	°C
	Water mass flow rate	161 ± 1.61	g/s
		279 ± 2.79	g/s
		332 ± 3.32	g/s
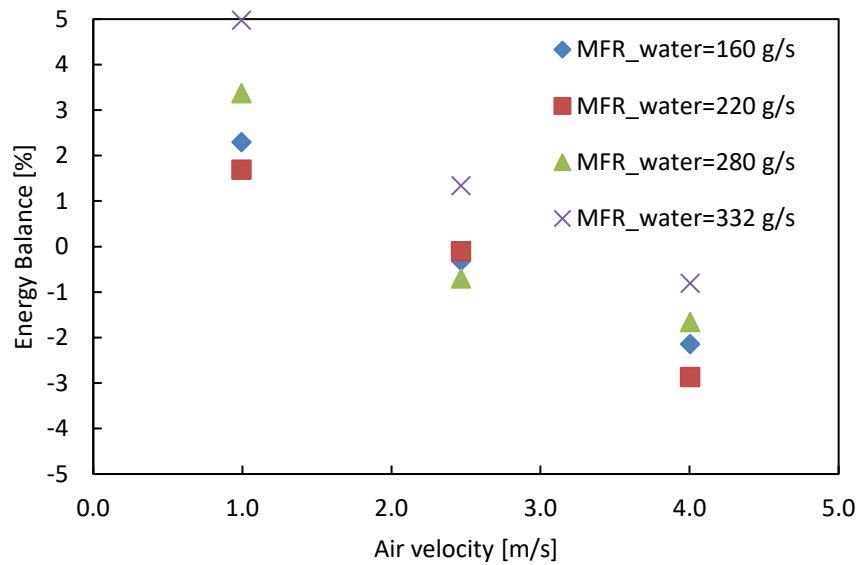
Figure C. 7 Energy balance of 10 kW-louvered fin radiator
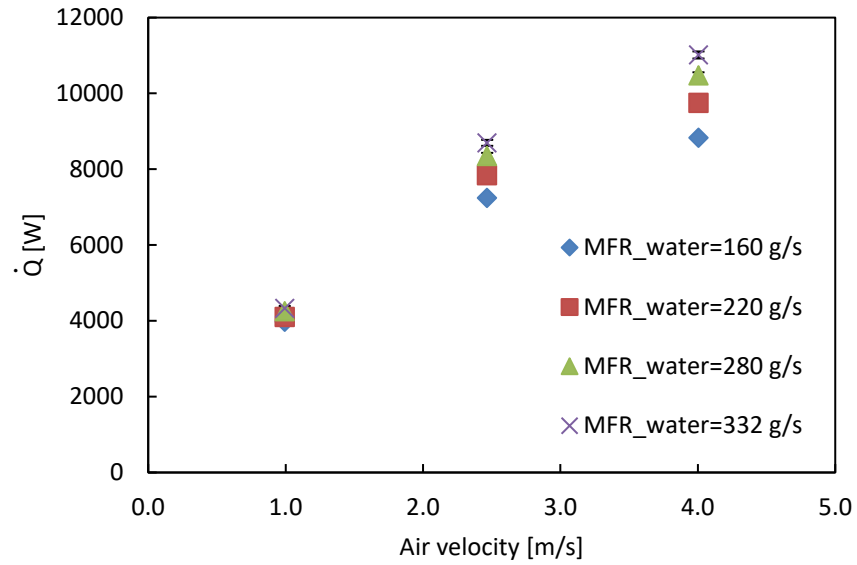
Figure C. 8 Capacity of 10 kW-louvered fin radiator
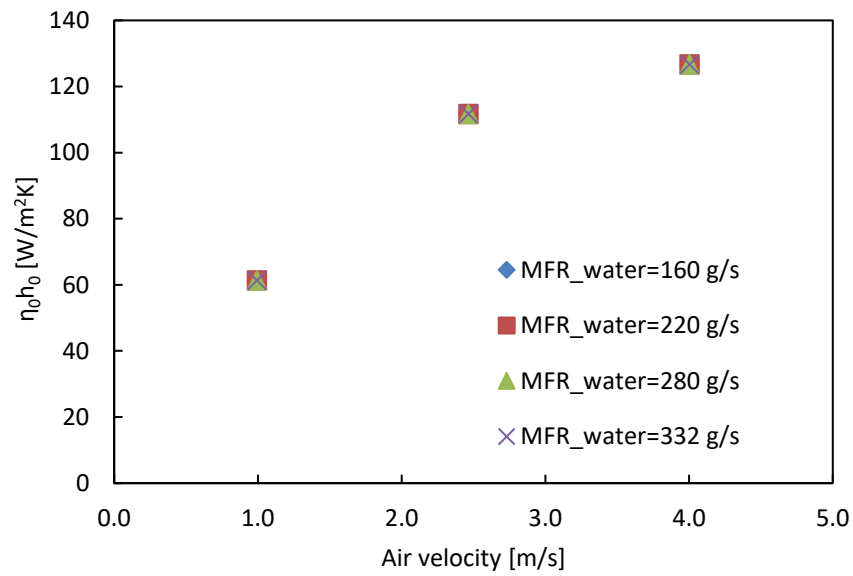
Figure C. 9 $\eta_0 h_0$ of 10 kW-louvered fin radiator
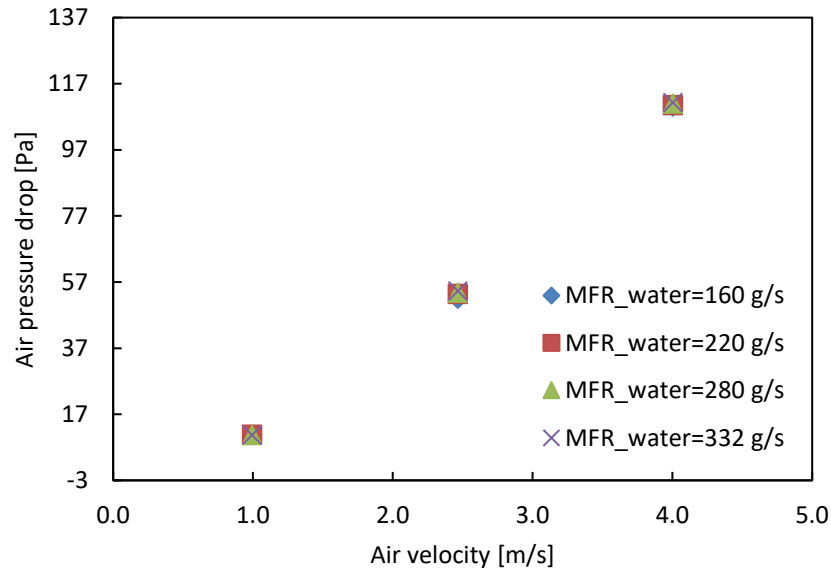
Figure C. 10 Airside pressure drop of 10 kW-louvered fin radiator

Table C. 18 10 kW-louvered fin radiator dry condition test data

Case #		1	2	3	4	5	6
T_air_in	[°C]	35.10	35.02	35.02	35.12	35.12	35.03
T_air_out	[°C]	54.04	49.02	45.54	54.78	49.98	46.68
RH_air_in	[%]	34.0%	38.3%	37.8%	33.1%	34.4%	37.8%
RH_air_out	[%]	13.6%	18.8%	21.8%	12.9%	16.6%	20.7%
P_air_in	[kPa]	101.27	100.84	100.86	101.23	101.30	100.88
DP_air	[Pa]	10.85	51.97	110.19	10.79	53.41	110.55
uncertainty_DP	[Pa]	0.77	1.01	1.28	0.76	1.04	1.34
MFR_air	[g/s]	206.13	514.72	842.95	205.58	524.72	842.61
VFR_air	[m³/s]	0.19	0.47	0.77	0.19	0.48	0.77
Capacity_air	[W]	3933.62	7256.42	8928.25	4071.29	7850.90	9886.64
Capacity_air_uncertainty	[W]	50.93	109.10	123.80	50.43	121.40	138.30
T_water_in	[°C]	59.90	59.91	59.91	60.00	60.03	59.94
T_water_out	[°C]	53.90	49.12	46.81	55.48	51.49	49.45
P_water in	[kPa]	114.98	112.58	112.57	122.77	121.12	121.11
DP_water	[kPa]	7064.67	6948.75	6905.76	8891.39	8856.38	8821.11

MFR_water	[g/s]	160.41	160.18	159.53	220.03	220.64	220.91
Water density	[kg/m^3]	988.36	990.16	990.87	987.34	989.75	990.10
Capacity_water	[W]	4024.98	7234.03	8738.80	4140.85	7842.69	9607.21
Capacity_water_uncertainty	[W]	66.65	59.28	64.58	113.90	77.38	92.15
Energy balance	[%]	2.30	-0.31	-2.14	1.69	-0.10	-2.87
Average capacity	[W]	3979.30	7245.23	8833.52	4106.07	7846.80	9746.93
capacity uncertainty	[W]	41.94	62.08	69.82	62.28	71.98	83.09
Case #		7	8	9	10	11	12
T_air_in	[°C]	35.10	35.01	35.03	35.09	35.13	34.96
T_air_out	[°C]	55.33	50.79	47.45	55.55	51.31	47.95
RH_air_in	[%]	31.3%	33.1%	35.9%	30.9%	33.5%	33.9%
RH_air_out	[%]	12.2%	15.1%	19.2%	12.1%	15.0%	17.8%
P_air_in	[kPa]	101.20	101.32	100.94	101.17	101.31	101.02
DP_air	[Pa]	10.75	53.79	111.03	10.74	54.31	111.34
uncertainty_DP	[Pa]	0.76	0.97	1.29	0.76	0.96	1.27
MFR_air	[g/s]	205.33	527.10	844.53	205.09	529.94	844.74
VFR_air	[m^3/s]	0.19	0.48	0.77	0.19	0.49	0.77
Capacity_air	[W]	4183.32	8378.80	10564.07	4227.02	8638.21	11058.59
Capacity_air_uncertainty	[W]	50.50	116.90	124.10	50.61	113.60	126.70
T_water_in	[°C]	60.07	60.04	59.92	59.98	59.96	59.90
T_water_out	[°C]	56.38	52.87	51.01	56.83	53.72	52.14
P_water in	[kPa]	133.04	131.56	131.68	143.87	142.26	144.17
DP_water	[kPa]	11154.61	11285.66	11269.44	13799.13	13866.52	14206.59
MFR_water	[g/s]	279.62	280.24	279.18	331.96	332.29	336.32
Water density	[kg/m^3]	986.63	988.77	989.81	985.21	987.75	989.59
Capacity_water	[W]	4326.86	8320.68	10390.34	4442.63	8754.52	10970.03
Capacity_water_uncertainty	[W]	86.42	115.70	101.30	102.50	109.20	136.90
Energy balance	[%]	3.37	-0.70	-1.66	4.97	1.34	-0.80
Average capacity	[W]	4255.09	8349.74	10477.21	4334.82	8696.36	11014.31

Capacity uncertainty	[W]	50.05	82.24	80.10	57.16	78.79	93.27

4 & 5mm slit fin-and-tube HX test matrix (air-water wet condition, condenser and evaporator condition)

Table C. 19 4 and 5 mm slit fin-and-tube HX wet condition test matrix

Test	Surface	Inlet Air Temperature	Inlet Air RH	Inlet Water Temperature	Air Velocity	Air Flow Rate	Water Flow Rate
		[°C]	[%]	[°C]	[m/s]	[m³/s]	[g/s]
1	Dry	26.7	50	7.2	1	0.15	50
2	Dry	26.7	50	7.2	1	0.15	100
3	Dry	26.7	50	7.2	1	0.15	150
4	Dry	26.7	50	7.2	2.5	0.375	50
5	Dry	26.7	50	7.2	2.5	0.375	100
6	Dry	26.7	50	7.2	2.5	0.375	150
7	Dry	26.7	50	7.2	4	0.6	50
8	Dry	26.7	50	7.2	4	0.6	100
9	Dry	26.7	50	7.2	4	0.6	150

5mm slit fin-and-tube HX test data

Table C. 20 5 mm slit fin-and-tube HX condenser test data (air and R410A)

Test No.		Tin [°C]			Tout [°C]			Pin_gage [kPa]			Pout_gage [kPa]			T_in_sat [°C]			T_out_sat [°C]			Volume Flow Rate [m3/s]
1	Air-Side	35.50	±	0.10	38.20	±	0.10		±			±			±			±		0.385 ± 5E-04
	Ref-side	90.28	±	1.11	46.53	±	0.10	2806.2	±	5.6	2800.5	±	5.8	47.8	±	0.1	47.7	±	0.1	2.562291805
2	Air-Side	35.50	±	0.10	38.10	±	0.10		±			±			±			±		0.384 ± 3E-04
	Ref-side	77.96	±	0.56	46.28	±	0.10	2784.8	±	6.7	2780.5	±	6.4	47.5	±	0.1	47.4	±	0.1	2.56095936
3	Air-Side	35.50	±	0.10	37.80	±	0.10		±			±			±			±		0.385 ± 1E-04
	Ref-side	68.11	±	0.21	45.51	±	0.10	2731.1	±	5.8	2728.2	±	5.8	46.6	±	0.1	46.6	±	0.1	2.561625583
4	Air-Side	35.50	±	0.10	37.40	±	0.10		±			±			±			±		0.385 ± 1E-04
	Ref-side	68.24	±	0.29	44.96	±	0.09	2687.7	±	4.8	2684.9	±	4.7	46.0	±	0.1	45.9	±	0.1	2.56362425
5	Air-Side	35.50	±	0.10	36.90	±	0.10		±			±			±			±		0.384 ± 1E-04
	Ref-side	47.15	±	0.17	43.61	±	0.08	2584.3	±	3.8	2581.8	±	3.7	44.4	±	0.1	44.3	±	0.1	2.56095936

Test No.		Mass Flow Rate [g/s]			Air/Ref Pressure Drop [Pa] / [kPa]			Capacity [W]			Heat Loss [W]	Adjusted Capacity [W]			Uncertainty [%]
1	Air-Side	441.6	±	3.0	27.4	±	0.9	1204	±	63.6	208.3	1412	±	63.62	4.50%
	Ref-side	8.3	±	0.2	5.7	±	8.0	1709.524742							
2	Air-Side	440.3	±	3.0	27.3	±	0.9	1156	±	63.4	195.3	1351	±	63.35	4.69%
	Ref-side	8.6	±	0.1	4.3	±	9.3	1645.941332							
3	Air-Side	440.1	±	3.0	27.3	±	0.8	1022	±	63.2	193.2	1215	±	63.22	5.20%

243

	Ref-side	8.4	±	0.1	2.9	±	8.2	1518.073233					
4	Air-Side	440.6	±	3.0	27.3	±	0.9	845.1	±	63.2	189.8	1035	±	63.17	6.10%
	Ref-side	7.2	±	0.1	2.9	±	6.7	1329.585558					
5	Air-Side	440.2	±	3.0	27.3	±	0.9	622.4	±	63.0	182.8	805.2	±	63.0	7.83%
	Ref-side	7.2	±	0.1	2.4	±	5.3	1123.213095					

Table C. 21 5 mm slit fin-and-tube HX evaporator test (air and R410A)

		Tin [°C]			Tout [°C]			Pin_gage [kPa]			Pout_gage [kPa]			T_in_sat [°C]			T_out_sat [°C]			Qualityin [-]			RHin [%]			RHout [%]		
1	Air	26.80	±	0.10	23.30	±	0.10		±			±			±			±			±		50.9%	±	1.7%	60.0%	±	1.6%
	Ref	9.17	±	0.40	22.22	±	0.29	962.5	±	15.8	951.6	±	14.4	9.4	±	0.5	9.0	±	0.5	0.28	±	0.05	-			-		
2	Air	26.70	±	0.10	23.60	±	0.20		±			±			±			±			±		70.5%	±	1.4%	79.3%	±	1.8%
	Ref	9.70	±	0.51	22.32	±	0.40	979.9	±	20.1	967.9	±	18.3	9.9	±	0.6	9.5	±	0.6	0.26	±	0.05	-			-		
3	Air	26.80	±	0.10	23.10	±	0.10		±			±			±			±			±		50.3%	±	1.3%	61.1%	±	1.6%
	Ref	10.32	±	0.30	21.23	±	0.33	998.7	±	12.0	985.6	±	11.3	10.5	±	0.4	10.1	±	0.4	0.35	±	0.02	-			-		
4	Air	26.90	±	0.10	23.90	±	0.10		±			±			±			±			±		70.2%	±	2.2%	79.3%	±	2.0%
	Ref	10.24	±	0.44	22.64	±	0.30	996.2	±	17.8	982.8	±	16.2	10.4	±	0.5	10.0	±	0.5	0.36	±	0.03	-			-		
5	Air	26.80	±	0.10	22.10	±	0.10		±			±			±			±			±		50.3%	±	1.3%	64.1%	±	1.7%
	Ref	10.61	±	0.12	16.62	±	0.70	1008.6	±	5.4	991.9	±	5.3	10.8	±	0.2	10.3	±	0.2	0.27	±	0.01	-			-		
6	Air	26.80	±	0.10	22.90	±	0.20		±			±			±			±			±		67.6%	±	3.4%	79.2%	±	3.1%
	Ref	10.65	±	0.29	20.63	±	0.47	1010.4	±	12.4	993.1	±	11.4	10.8	±	0.4	10.3	±	0.4	0.27	±	0.01						
7	Air	26.80	±	0.10	22.60	±	0.10		±			±			±			±			±		49.6%	±	1.3%	62.2%	±	1.6%
	Ref	10.64	±	0.10	17.92	±	0.60	1009.0	±	4.4	992.6	±	4.4	10.8	±	0.1	10.3	±	0.1	0.37	±	0.01						
8	Air	26.80	±	0.10	23.30	±	0.30		±			±			±			±			±		67.2%	±	5.0%	78.3%	±	4.6%
	Ref	10.65	±	0.22	21.49	±	0.64	1009.7	±	8.2	992.3	±	7.8	10.8	±	0.3	10.3	±	0.2	0.37	±	0.02						

Test No.		Volume Flow Rate	Mass Flow Rate	Air/Ref Pressure Drop	Capacity	Heat Loss	SH/LH	Adjusted Capacity	Uncertainty	Energy Balance

		[m3/s]			[g/s]			[Pa] / [kPa]			[W]			[W]	[W]/[W]			[W]			[%]	[%]
1	Air	0.387	±	1E-04	461.9	±	3.4	31.1	±	0.9	1657.0	±	68.1	-53.7	1603.3	±	68.1	1603.3	±	68.1	4.24%	1.0%
	Ref	2.581404735			9.7	±	1.9	10.9	±	21.3	1619.0	±	425.7	-	0.0	±	0.0	1619.0	±	425.7	26.29%	
2	Air	0.383	±	2E-04	454.9	±	3.0	34.4	±	1.0	1456.0	±	105.5	-46.9	1409.1	±	105.5	1736.1	±	105.5	6.08%	1.1%
	Ref	2.550591377			10.4	±	1.9	12.0	±	27.2	1755.0	±	415.9	-	327.0	±	1.2	1755.0	±	415.9	23.70%	
3	Air	0.384	±	2E-04	456.7	±	3.4	31.2	±	0.9	1732.0	±	67.5	-47.2	1684.8	±	67.5	1694.4	±	67.5	3.98%	-2.2%
	Ref	2.554993286			11.2	±	0.7	13.1	±	16.5	1658.0	±	160.8	-	9.6	±	0.2	1658.0	±	160.8	9.70%	
4	Air	0.384	±	1E-04	455.3	±	3.0	34.2	±	1.0	1411.0	±	67.2	-39.2	1371.8	±	67.2	1662.6	±	67.2	4.04%	-2.4%
	Ref	2.558137506			11.0	±	0.9	13.4	±	24.1	1623.0	±	212.8	-	290.8	±	2.9	1623.0	±	212.8	13.11%	
5	Air	0.381	±	3E-04	454.8	±	3.9	31.4	±	0.9	2191.0	±	68.5	-64.5	2126.5	±	68.5	2133.8	±	68.5	3.21%	0.2%
	Ref	2.538014497			13.4	±	0.4	16.7	±	7.5	2138.0	±	95.7	-	7.3	±	0.1	2138.0	±	95.7	4.47%	
6	Air	0.38	±	2E-04	450.7	±	3.1	35.7	±	1.1	1813.0	±	104.7	-49.4	1763.6	±	104.7	2238.5	±	105.0	4.69%	-2.4%
	Ref	2.532354901			13.4	±	0.6	17.3	±	16.9	2185.0	±	128.1	-	474.8	±	7.9	2185.0	±	128.1	5.86%	
7	Air	0.38	±	3E-04	452.0	±	3.1	31.6	±	0.9	1945.0	±	66.8	-64.6	1880.4	±	66.8	1888.9	±	66.8	3.54%	-3.3%
	Ref	2.534555855			13.0	±	0.4	16.4	±	6.3	1827.0	±	93.9	-	8.5	±	0.3	1827.0	±	93.9	5.14%	
8	Air	0.381	±	3E-04	451.2	±	3.1	35.3	±	1.1	1629.0	±	147.6	-47.3	1581.7	±	147.6	1925.8	±	147.9	7.68%	-2.5%
	Ref	2.538643341			13.1	±	0.5	17.4	±	11.3	1879.0	±	120.3		344.1	±	9.8	1879.0	±	120.3	6.40%	

246

Table C. 22 5 mm slit fin-and-tube HX dry condition (air and water)

Case #		1	2	3	4	5
T_air_in	[°C]	35.10	35.00	35.00	35.00	35.10
T_air_out	[°C]	46.56	41.17	39.34	49.82	43.96
RH_air_in	[%]	29.4%	26.3%	26.1%	29.7%	28.6%
RH_air_out	[%]	17.0%	19.0%	20.6%	14.9%	18.6%
P_air_in	[kPa]	102.24	102.13	102.13	102.23	101.54
DP_air	[Pa]	6.30	26.10	55.80	6.40	25.80
uncertainty_DP	[Pa]	0.70	0.90	1.50	0.70	0.90
MFR_air	[g/s]	176.20	431.50	679.40	175.40	423.30
VFR_air	[m^3/s]	0.16	0.38	0.60	0.16	0.38
Capacity_air	[W]	2034.56	2679.98	2967.05	2619.09	3775.76
Capacity_air_uncertainty	[W]	33.96	100.20	103.80	38.66	65.22
T_water_in	[°C]	60.01	60.01	60.01	59.92	59.88
T_water_out	[°C]	50.06	46.88	45.51	53.62	50.79
P_water in	[kPa]	118.20	118.10	118.19	160.31	159.36
DP_water	[kPa]	16090.00	15140.00	15930.00	56200.00	56800.00
MFR_water	[g/s]	50.29	50.35	50.25	100.20	100.40
Water density	[kg/m^3]	990.47	991.30	991.72	989.25	990.25
Capacity_water	[W]	2094.00	2764.00	3047.00	2640.00	3818.00

Capacity_water_uncertainty	[W]	28.12	23.03	18.41	41.50	35.20
Energy balance	[%]	2.88	3.09	2.66	0.80	1.11
Average capacity	[W]	2064.28	2721.99	3007.02	2629.54	3796.88
Capacity uncertainty	[W]	22.05	51.41	52.71	28.36	37.06
Case #		6	7	8	9	
T_air_in	[°C]	35.00	35.00	35.10	35.10	
T_air_out	[°C]	41.46	51.02	44.91	42.54	
RH_air_in	[%]	26.1%	29.9%	30.1%	25.8%	
RH_air_out	[%]	18.5%	14.2%	18.3%	17.5%	
P_air_in	[kPa]	102.20	102.22	102.12	102.26	
DP_air	[Pa]	56.30	6.40	25.80	56.50	
uncertainty_DP	[Pa]	1.10	0.70	0.90	1.10	
MFR_air	[g/s]	680.50	175.60	424.70	680.80	
VFR_air	[m³/s]	0.60	0.16	0.38	0.61	
Capacity_air	[W]	4428.96	2833.74	4198.14	5099.22	
Capacity_air_uncertainty	[W]	105.40	40.43	67.79	107.60	
T_water_in	[°C]	59.95	60.04	60.02	60.05	
T_water_out	[°C]	49.31	55.52	53.24	52.00	
P_water in	[kPa]	159.97	225.72	226.50	226.50	
DP_water	[Pa]	55680	119300	119800	119800	

248

MFR_water	[g/s]	99.87	149.90	150.40	150.00
Water density	[kg/m^3]	990.62	988.64	989.45	989.91
Capacity_water	[W]	4442.00	2831.00	4265.00	5050.00
Capacity_water_uncertainty	[W]	34.95	56.78	57.56	57.85
Energy balance	[%]	0.29	-0.10	1.58	-0.97
Average capacity	[W]	4435.48	2832.37	4231.57	5074.61
Capacity uncertainty	[W]	55.52	34.85	44.47	61.08

Table C. 23 5 mm slit fin-and-tube HX wet condition test data (air and water)

Case #		1	2	3	4	5
T_air_in	[°C]	26.70	26.70	26.70	26.80	26.70
T_air_out	[°C]	19.39	22.78	24.04	16.93	20.76
RH_air_in	[%]	50.3%	51.2%	50.6%	50.9%	51.2%
RH_air_out	[%]	75.3%	63.1%	57.9%	83.6%	69.9%
P_air_in	[kPa]	101.42	101.19	100.03	101.51	101.11
DP_air	[Pa]	7.00	27.90	57.60	8.50	29.60
uncertainty_DP	[Pa]	0.70	0.90	1.20	0.70	0.90
SH	[W]	1299.31	1744.03	1860.76	1790.39	2639.40
SH_un	[W]	33.07	51.77	75.05	26.17	54.42
LH	[W]	0.00	0.00	3.20	144.56	1.11
LH_un	[W]	0.00	0.00	0.06	0.26	0.05

MFR_air	[g/s]	176.70	441.80	695.90	180.20	441.10
VFR_air	[m^3/s]	0.15	0.37	0.60	0.15	0.37
Capacity_air	[W]	1299.31	1744.03	1863.96	1934.95	2640.51
Capacity_air_uncertainty	[W]	33.07	51.77	75.05	26.17	54.42
T_water_in	[°C]	7.16	7.17	7.13	7.19	7.11
T_water_out	[°C]	13.45	15.12	15.78	11.90	13.29
P_water in	[kPa]	119.01	118.70	117.19	165.11	163.19
DP_water	[kPa]	16270.00	16420.00	15650.00	59940.00	57960.00
MFR_water	[g/s]	50.11	50.00	49.96	100.10	100.00
Water density	[kg/m^3]	996.33	996.30	996.41	995.92	996.09
Capacity_water	[W]	1321.00	1664.00	1810.00	1978.00	2592.00
Capacity_water_uncertainty	[W]	18.23	15.50	19.26	37.05	37.34
Energy balance	[%]	1.66	-4.70	-2.94	2.20	-1.85
Average capacity	[W]	1310.16	1704.01	1836.98	1956.48	2616.25
Capacity uncertainty	[W]	18.881	27.02	38.74	22.68	33.00
w_omega_in	[kg/kg]	0.0109900	0.0112300	0.0112200	0.0112000	0.0112400
w_omega_in_uncertainty	[kg/kg]	0.0002156	0.0001468	0.0002932	0.0002192	0.0001470
w_omega_out	[kg/kg]	0.0109900	0.0112300	0.0112200	0.0108700	0.0112400
w_omega_out_uncertainty	[kg/kg]	0.0002156	0.0001468	0.0002932	0.0002192	0.0001470
condensate	[g/s]	0.0000000	0.0000000	0.0012986	0.0586831	0.0004491

250

condenate_uncertainty	[g/s]	0.0000000	0.0000000	0.0000247	0.0001050	0.0000203
Case #		6	7	8	9	
T_air_in	[°C]	26.70	26.70	26.90	26.70	
T_air_out	[°C]	22.44	15.97	19.92	21.47	
RH_air_in	[%]	50.3%	50.3%	50.6%	50.9%	
RH_air_out	[%]	62.6%	82.5%	72.5%	66.6%	
P_air_in	[kPa]	101.39	101.37	100.88	100.94	
DP_air	[Pa]	61.80	8.60	32.70	70.90	
uncertainty_DP	[Pa]	1.50	0.70	1.30	1.20	
SH	[W]	3041.82	1958.73	3126.66	3728.43	
SH_un	[W]	86.77	32.88	82.30	83.50	
LH	[W]	0.00	332.10	100.09	35.84	
LH_un	[W]	0.00	0.16	0.24	0.04	
MFR_air	[g/s]	708.70	181.30	444.80	708.70	
VFR_air	[m³/s]	0.60	0.15	0.37	0.60	
Capacity_air	[W]	3041.82	2290.83	3226.75	3764.12	
Capacity_air_uncertainty	[W]	86.77	32.88	82.30	83.50	
T_water_in	[°C]	7.31	7.32	7.16	7.17	
T_water_out	[°C]	14.31	11.05	12.27	13.03	
P_water in	[kPa]	176.13	239.20	239.94	240.85	

251

DP_water	[Pa]	59750	129800	126100	125900
MFR_water	[g/s]	100.20	150.40	149.70	149.90
Water density	[kg/m^3]	996.23	995.41	995.38	995.48
Capacity_water	[W]	2939.00	2353.00	3204.00	3679.00
Capacity_water_uncertainty	[W]	76.71	54.74	87.41	85.67
Energy balance	[%]	-3.44	2.68	-0.71	-2.29
Average capacity	[W]	2990.41	2321.92	3215.38	3721.56
Capacity uncertainty	[W]	57.91	31.93	60.03	59.82
w_omega_in	[kg/kg]	0.0109900	0.0109900	0.0112700	0.0111900
w_omega_in_uncertainty	[kg/kg]	0.0002156	0.0002156	0.0002206	0.0001464
w_omega_out	[kg/kg]	0.0109900	0.0102500	0.0111800	0.0111700
w_omega_out_uncertainty	[kg/kg]	0.0002156	0.0002159	0.0002206	0.0001464
condensate	[g/s]	0.0000370	0.1347732	0.0407849	0.0145460
condenate_uncertainty	[g/s]	0.0000523	0.0000636	0.0000980	0.0000166

5mm slit fin-and-tube HX airside heat transfer and pressure drop correlation validation

Correlations to be validated is from Sarpotdar et al. (2016). The following two graphs shows the prediction of the correlations against experiments. It can be seen that the heat transfer prediction is acceptable but the maximum pressure drop prediction deviation

is about 35%, thus correction factor is necessary to correct the correlation. Three correction factors 1.1, 1.35 and 1.55 are applied for three different inlet air velocity 1.05, 2.55 and 3.99 m/s, respectively. The corrected results are shown in the third graph.
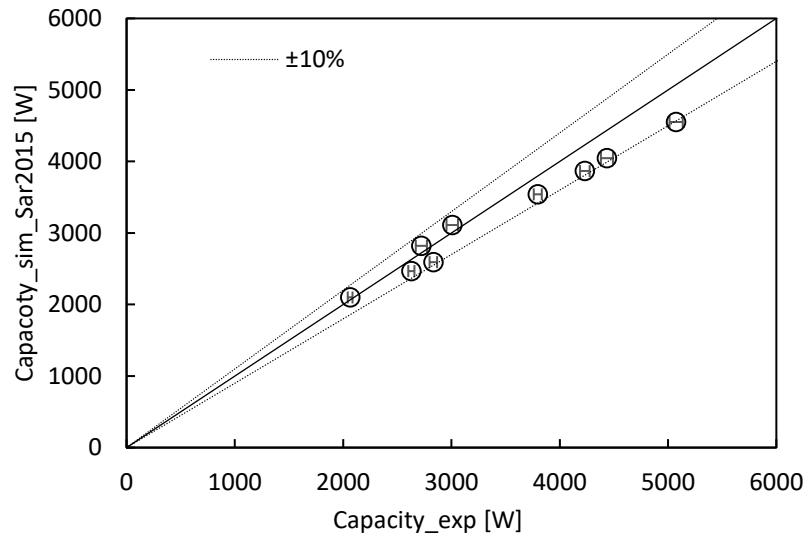
Figure C. 11 5 mm slit fin-and-tube HX capacity validation
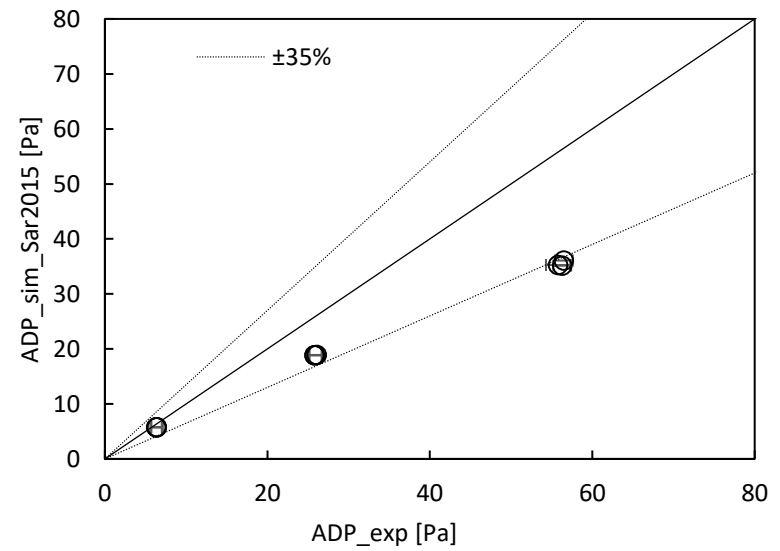
Figure C. 12 5 mm slit fin-and-tube HX ADP validation
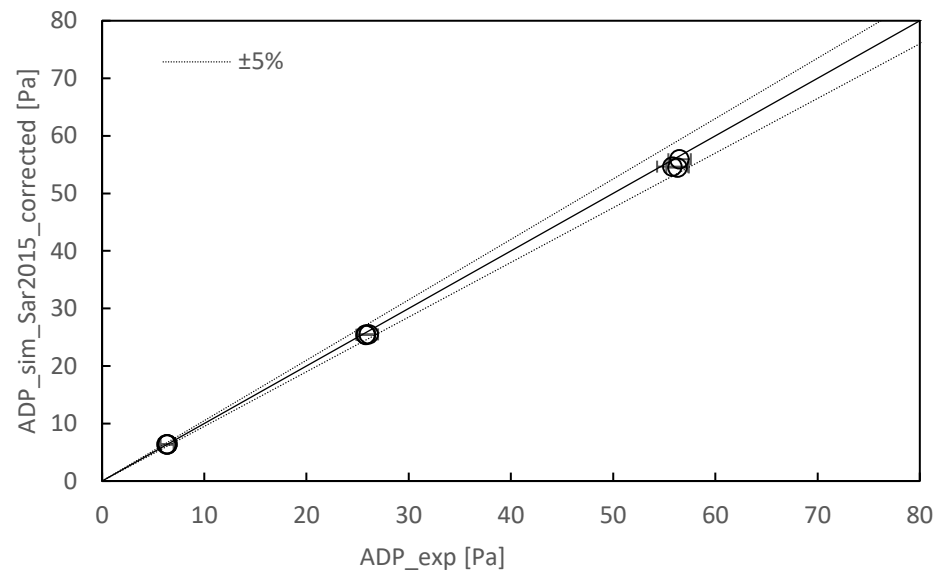
Figure C. 13 5 mm slit fin-and-tube HX corrected ADP

4 mm slit fin-and-tube HX test data

Table C. 24 4 mm slit fin-and-tube HX condenser test data (air and R410A)

Test No.		Tin			Tout			Pin_gage			Pout_gage			T_in_sat			T_out_sat			Volume Flow Rate			Mass Flow Rate		
		[°C]			[°C]			[kPa]			[kPa]			[°C]			[°C]			[m3/s]			[g/s]		
1	Air	28.00	±	0.10	31.70	±	0.10		±			±			±			±		0.389	±	2E-04	456.3	±	3.0
	Ref	55.78	±	0.48	38.55	±	0.10	2307.3	±	6.4	2303.2	±	6.3	39.8	±	0.1	39.9	±	0.1				9.8	±	0.1
2	Air	27.90	±	0.10	31.60	±	0.10		±			±			±			±		0.381	±	1E-04	447.3	±	3.1

254

Test No.										
	Ref	78.05 ± 0.22	38.22 ± 0.08	2301.9 ± 3.9	2301.9 ± 4.3	39.8 ± 0.1	39.8 ± 0.1			8.1 ± 0.1
3	Air	28.00 ± 0.10	31.50 ± 0.10	±	±	±	±	0.381 ± 4E-04	447.8 ± 3.1	
3	Ref	63.90 ± 0.80	37.81 ± 0.10	2271.2 ± 4.0	2270.4 ± 4.1	39.2 ± 0.1	39.2 ± 0.1			8.3 ± 0.1
4	Air	27.80 ± 0.10	31.10 ± 0.10	±	±	±	±	0.381 ± 8E-05	448.1 ± 3.1	
4	Ref	48.63 ± 0.17	36.91 ± 0.08	2210.4 ± 3.4	2207.5 ± 3.5	38.1 ± 0.1	38.2 ± 0.1			8.4 ± 0.1
5	Air	27.70 ± 0.10	30.40 ± 0.10	±	±	±	±	0.383 ± 8E-05	451.6 ± 3.0	
5	Ref	77.34 ± 0.16	36.08 ± 0.12	2185.5 ± 3.9	2186.9 ± 3.9	37.8 ± 0.1	37.7 ± 0.1			5.8 ± 0.1
6	Air	27.70 ± 0.10	30.30 ± 0.10	±	±	±	±	0.382 ± 1E-04	450.9 ± 3.0	
6	Ref	64.10 ± 0.26	35.73 ± 0.08	2145.6 ± 4.6	2145.5 ± 4.9	37.0 ± 0.1	37.0 ± 0.1			5.9 ± 0.1
7	Air	27.70 ± 0.10	30.10 ± 0.10	±	±	±	±	0.382 ± 2E-04	451.0 ± 3.0	
7	Ref	48.07 ± 0.35	35.13 ± 0.11	2108.9 ± 5.9	2108.0 ± 5.9	36.3 ± 0.1	36.4 ± 0.1			6.0 ± 0.1

Test No.		Mass Flow Rate [g/s]	Air/Ref Pressure Drop [Pa] / [kPa]	Capacity [W]	Heat Loss [W]	Adjusted Capacity [W]	Uncertainty [%]	Energy Balance [%]
1	Air	456.3 ± 3.0	21.9 ± 0.8	1707.0 ± 66.2	101.6	1808.6 ± 66.2	3.66%	-0.9%
1	Ref	9.8 ± 0.1	4.1 ± 8.9	1825.0 ± 13.4		1825.0 ± 13.4	0.73%	
2	Air	447.3 ± 3.1	21.2 ± 0.8	1673.0 ± 65.0	97.5	1770.5 ± 65.0	3.67%	1.2%
2	Ref	8.1 ± 0.1	0.0 ± 5.8	1750.0 ± 13.6		1750.0 ± 13.6	0.78%	
3	Air	447.8 ± 3.1	21.2 ± 0.8	1584.0 ± 64.9	91.5	1675.5 ± 64.9	3.87%	1.2%
3	Ref	8.3 ± 0.1	0.8 ± 5.7	1656.0 ± 16.2		1656.0 ± 16.2	0.98%	
4	Air	448.1 ± 3.1	21.1 ± 0.8	1496.0 ± 64.9	88.4	1584.4 ± 64.9	4.10%	3.2%

	Ref	8.4	±	0.1	2.9	±	4.9	1534.0	±	14.1		1534.0	±	14.1	0.92%	
5	Air	451.6	±	3.0	21.4	±	0.8	1232.0	±	65.1	81.9	1313.9	±	65.1	4.95%	3.1%
	Ref	5.8	±	0.1	-1.3	±	5.5	1274.0	±	15.4		1274.0	±	15.4	1.21%	
6	Air	450.9	±	3.0	21.3	±	0.8	1185.0	±	64.9	79.7	1264.7	±	64.9	5.13%	4.3%
	Ref	5.9	±	0.1	0.1	±	6.7	1212.0	±	16.4		1212.0	±	16.4	1.36%	
7	Air	451.0	±	3.0	21.3	±	0.8	1094.0	±	64.9	74.7	1168.7	±	64.9	5.55%	5.1%
	Ref	6.0	±	0.1	0.9	±	8.4	1111.0	±	15.9		1111.0	±	15.9	1.43%	

Table C. 25 4 mm slit fin-and-tube HX evaporator test data (air and R410A)

Test No.		Tin [°C]			Tout [°C]			Pin_gage [kPa]			Pout_gage [kPa]			T_in_sat [°C]			T_out_sat [°C]			Qualityin [-]			RHin [%]			RHout [%]		
1	Air	26.70	±	0.10	23.30	±	0.10		±			±			±			±					50.9%	±	1.7%	59.6%	±	1.6%
	Ref	10.15	±	0.33	16.30	±	1.50	992.7	±	13.2	974.7	±	11.7	10.3	±	0.4	9.8	±	0.4	0.27	±	0.03						
2	Air	26.80	±	0.10	24.10	±	0.20		±			±			±			±					68.8%	±	3.8%	75.0%	±	3.8%
	Ref	10.28	±	0.40	21.97	±	0.58	996.6	±	16.4	978.7	±	14.3	10.4	±	0.5	9.9	±	0.4	0.28	±	0.05						
3	Air	26.60	±	0.10	23.60	±	0.00		±			±			±			±					51.2%	±	1.3%	59.3%	±	1.5%
	Ref	10.75	±	1.49	13.64	±	0.26	1010.0	±	10.4	992.6	±	9.2	10.8	±	1.5	13.6	±	0.3	0.36	±	0.03						
4	Air	26.80	±	0.10	24.30	±	0.20		±			±			±			±					68.8%	±	3.8%	75.5%	±	3.9%
	Ref	10.58	±	0.37	22.05	±	0.80	1004.7	±	14.8	986.4	±	13.0	10.7	±	0.5	10.1	±	0.4	0.38	±	0.04						
5	Air	26.70	±	0.10	22.40	±	0.10		±			±			±			±					49.6%	±	1.3%	60.9%	±	1.2%
	Ref	11.57	±	0.22	11.71	±	0.60	1047.6	±	9.2	1018.8	±	7.6	12.0	±	0.3	11.1	±	0.2	0.26	±	0.02						
6	Air	26.80	±	0.10	23.40	±	0.10		±			±			±			±					68.8%	±	1.7%	78.3%	±	2.0%
	Ref	11.47	±	0.29	15.69	±	1.31	1044.3	±	12.7	1016.2	±	11.2	11.9	±	0.4	11.0	±	0.3	0.28	±	0.02						
7	Air	26.80	±	0.10	23.00	±	0.10		±			±			±			±					51.9%	±	0.7%	63.5%	±	0.9%
	Ref	11.67	±	0.10	11.15	*	0.09	1048.4	±	4.2	1019.2	±	3.8	12.0	±	0.1	11.1	±	0.1	0.34	±	0.02						
8	Air	26.80	±	0.10	23.70	±	0.10		±			±			±			±					69.3%	±	1.3%	77.8%	±	1.5%
	Ref	11.79	±	0.09	16.37	±	0.76	1052.3	±	5.5	1022.1	±	5.6	12.1	±	0.2	11.2	±	0.2	0.37	±	0.02						

Test No.		Volume Flow Rate [m3/s]	Mass Flow Rate [g/s]	Air/Ref Pressure Drop [Pa] / [kPa]	Capacity [W]	Heat Loss [W]	SH/LH [W]/[W]	Adjusted Capacity [W]	Uncertainty [%]	Energy Balance [%]

257

1	Air	0.38458997	±	0.00071028	458.7	±	3.0	25.2	±	0.9	1598.0	±	67.3	-65.5	1532.5	±	67.3	1532.5	±	68.0	4.44%	2.9%
	Ref	2.562224992			9.9	±	1.2	18.0	±	17.6	1577.0	±	256.9		0.0	±	9.9	1577.0	±	256.9	16.29%	
2	Air	0.38350449	±	0.00027231	455.9	±	3.4	30.7	±	1.4	1270.0	±	105.6	-47.2	1222.8	±	105.6	1442.6	±	105.6	7.32%	7.0%
	Ref	2.554993286			9.5	±	1.5	17.9	±	21.8	1547.0	±	336.1		219.8	±	2.9	1547.0	±	336.1	21.73%	
3	Air	0.38633618	±	0.00070179	461.6	±	3.4	25.5	±	0.8	1419.0	±	48.5	-56.0	1363.0	±	48.5	1395.6	±	48.5	3.48%	-3.2%
	Ref	2.573858607			9.5	±	0.8	17.8	±	13.9	1352.0	±	162.9		32.6	±	2.1	1352.0	±	162.9	12.05%	
4	Air	0.3846	±	0.0004	457.1	±	3.0	30.9	±	1.1	1179.0	±	105.8	-42.8	1136.2	±	105.8	1359.7	±	105.8	7.78%	0.5%
	Ref	2.562291805			9.6	±	1.1	18.3	±	19.6	1366.0	±	244.8	-	223.6	±	2.1	1366.0	±	244.8	17.92%	
5	Air	0.38062561	±	0.00028161	457.8	±	3.5	22.2	±	0.8	2016.0	±	68.0	-58.8	1957.2	±	68.0	1957.2	±	68.0	3.48%	4.9%
	Ref	2.535813543			13.4	±	0.9	28.8	±	12.0	2056.0	±	199.8		0.0	±	0.0	2056.0	±	199.8	9.72%	
6	Air	0.37954013	±	0.00061825	453.1	±	3.1	34.3	±	1.2	1590.0	±	67.0	-48.0	1542.0	±	67.0	2022.1	±	68.0	3.36%	1.2%
	Ref	2.528581837			13.2	±	0.6	28.1	±	17.0	2046.0	±	141.8		480.1	±	11.8	2046.0	±	141.8	6.93%	
7	Air	0.3825606	±	4.4387E-05	457.1	±	3.0	27.0	±	0.9	1781.0	±	67.3	-56.3	1724.7	±	67.3	1738.8	±	67.3	3.87%	5.3%
	Ref	2.548704845			13.4	±	0.5	29.2	±	5.7	1833.0	±	1067.0		14.1	±	0.4	1833.0	±	1067.0	58.21%	
8	Air	0.38048403	±	0.00036043	453.7	±	3.1	34.0	±	0.9	1451.0	±	66.9	-41.2	1409.8	±	66.9	1856.7	±	67.6	3.64%	-0.8%
	Ref	2.534870277			13.5	±	0.5	30.2	±	7.9	1842.0	±	114.0		446.9	±	9.2	1842.0	±	114.0	6.19%	

4 & 5 mm slit fin-and-tube HX test pictures
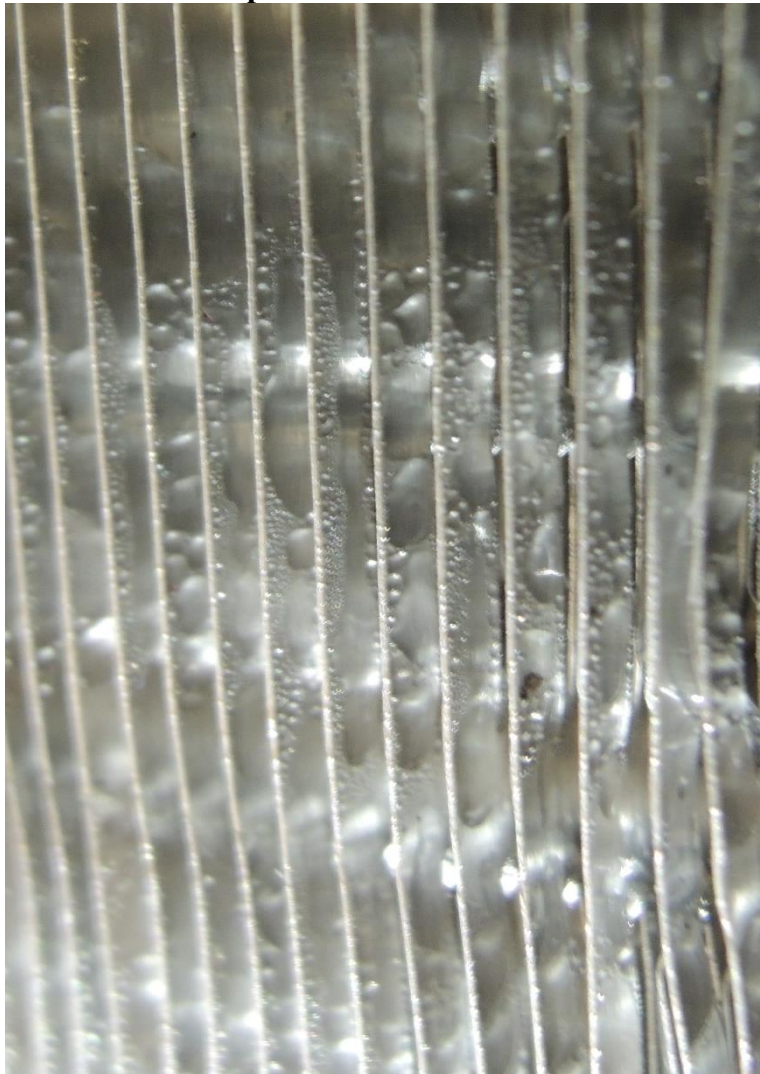
Figure C. 14 5 mm coil wet condition test picture

Figure C. 15 VFR_air=375 cfm, MFR_water= 150g/s
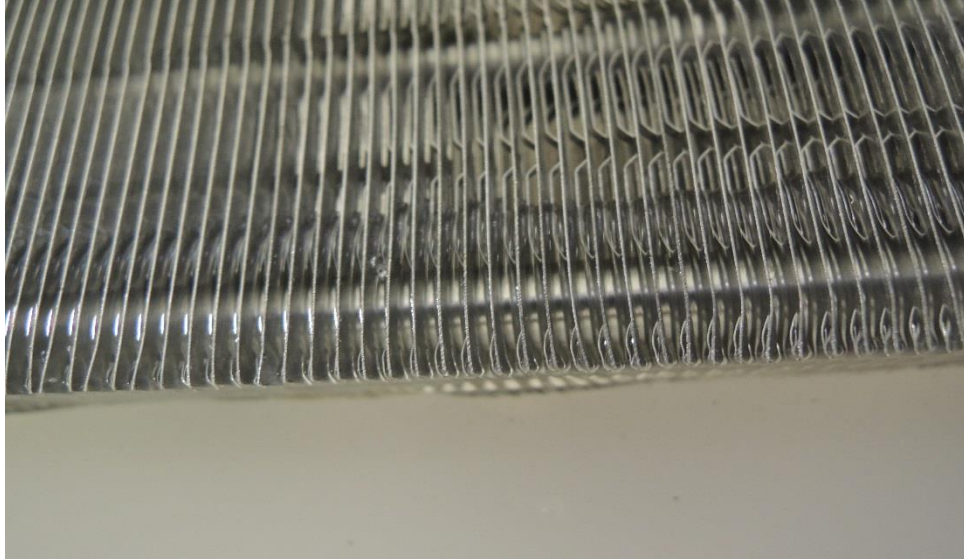
Figure C. 16 VFR_air=375 cfm, MFR_water= 100g/s

Appendix D: GCI calculation data

Table D. 1 Airside GCI calculation data

	Grid elements			Grid Ratio		HHTCTC			DP			HTC		ADP	
	Grid 1	Grid 2	Grid 3	r21	r32	HTC 1	HTC 2	HTC 3	DP 1	DP 2	DP 3	GCI 21	GCI 32	GCI 21	GCI 32
InC1	2531096	813194	266860	1.46006	1.44978	840.913	839.848	795.695	719.788	712.334	708.7279	0.14%	6.29%	1.16%	0.58%
InC2	1186452	330672	71996	1.53091	1.66225	923.183	921.545	907.427	787.866	772.257	758.6759	0.17%	1.10%	1.88%	1.27%
InC3	5831038	1981929	508845	1.43291	1.57338	805.149	804.489	746.098	438.922	434.661	439.0497	0.10%	6.63%	1.16%	0.85%
InC4	971569	342006	106026	1.41627	1.47754	805.199	807.28	781.209	413.371	408.15	417.6288	0.32%	3.53%	1.59%	2.40%
InC5	2800144	912378	285698	1.45323	1.47261	739.092	739.478	711.539	730.801	716.211	660.5554	0.06%	4.20%	2.29%	9.01%
InC6	651685	216051	75448	1.44486	1.42005	786.484	789.996	792.284	800.883	778.908	779.7605	1.15%	0.79%	7.29%	0.30%
InC7	6521896	2142880	557278	1.44919	1.56666	718.093	718.296	704.308	461.026	450.347	430.6212	0.03%	1.71%	2.69%	3.94%
InC8	1070725	367742	110469	1.42795	1.49314	724.448	726.35	717.93	441.682	431.027	427.5232	0.32%	1.19%	2.97%	0.83%
InC9	6640449	2114484	565489	1.46442	1.55213	553.326	557.84	553.582	95.5166	93.726	93.15457	4.81%	3.91%	11.37%	3.12%
InC10	1269633	405021	132656	1.46353	1.45072	601.431	604.051	603.712	90.0634	88.6098	87.03794	0.47%	0.06%	1.80%	2.04%
InC11	1.6E+07	6445999	2975095	1.353	1.29399	528.644	526.952	533.626	66.6594	66.624	65.56895	0.48%	2.32%	0.08%	2.98%
InC12	1763522	560612	166770	1.46523	1.49801	533.606	537.977	540.255	61.2543	60.3861	60.97759	1.15%	0.55%	2.04%	1.27%
InC13	7162884	2260219	592917	1.46886	1.56214	538.024	541.922	537.9	87.1149	85.2671	84.29393	4.24%	3.74%	12.78%	5.78%
InC14	1215879	370046	142156	1.48666	1.37561	572.469	576.79	580.99	88.5862	87.1142	85.86484	4.27%	5.23%	9.63%	10.52%
InC15	1.9E+07	6750233	2728367	1.40135	1.3525	510.09	512.632	516.052	59.084	58.8197	58.05584	1.89%	2.87%	1.71%	5.69%

InC16	2035375	624974	183639	1.48227	1.50418	513.207	517.862	519.304	55.0834	54.1299	54.65422	0.94%	0.27%	1.84%	0.95%
InC17	1497415	397580	218225	1.55587	1.22135	389.479	385.235	380.414	320.162	323.045	330.5782	5.57%	15.06%	4.51%	27.09%
InC18	1209160	334331	66568	1.53498	1.71253	307.854	304.998	301.007	498.943	487.207	473.6736	2.35%	2.51%	6.05%	5.41%
InC19	5813430	1522941	388518	1.56285	1.57673	344.294	293.703	286.044	306.088	292.857	287.7062	14.93%	2.25%	3.92%	1.51%
InC20	967656	344812	126149	1.41052	1.39819	258.89	260.951	257.367	278.774	271.481	274.5281	1.49%	2.71%	5.06%	2.16%
InC21	2802689	911053	281307	1.45438	1.47952	326.62	307.232	311.789	513.446	501.211	513.6211	7.07%	1.54%	2.74%	2.54%
InC22	654076	217564	68818	1.44327	1.46767	286.065	285.66	279.903	520.235	504.106	502.9947	0.16%	2.23%	3.69%	0.24%
InC23	6303207	2042656	530093	1.45587	1.56777	254.592	256.02	246.757	307.61	301.613	309.4478	0.62%	3.22%	2.22%	2.17%
InC24	1067456	370805	106442	1.42255	1.51592	249.698	248.354	243.848	285.338	278.336	290.6868	0.66%	1.78%	3.07%	4.09%
InC25	4696822	1233009	288087	1.56175	1.62361	364.276	357.626	351.202	72.7596	72.0456	70.75495	9.31%	8.34%	4.96%	8.32%
InC26	1257391	409346	131846	1.45365	1.45884	204.445	203.872	202.296	67.8354	65.0434	61.31714	0.32%	0.86%	4.82%	6.73%
InC27	1.6E+07	4976319	1380017	1.47492	1.53347	368.637	370.537	344.147	82.3682	81.0235	78.68922	0.55%	7.09%	1.76%	2.74%
InC28	1303620	345241	92114	1.55719	1.55334	215.009	203.709	199.672	30.2587	30.6907	34.74369	4.87%	1.79%	1.24%	10.32%
InC29	7360612	2257636	619188	1.48281	1.53914	185.376	184.914	183.581	63.7856	60.1065	60.08887	0.26%	0.66%	6.38%	0.03%
InC30	1210873	371373	138424	1.48285	1.38952	198.501	198.368	197.125	60.194	57.5606	55.60576	0.07%	0.85%	4.77%	4.72%
InC31	1.9E+07	1.1E+07	5234983	1.18495	1.28697	176.461	176.494	176.701	42.6811	42.0311	39.82754	0.06%	0.22%	4.78%	10.54%
InC32	2027063	623853	177840	1.48114	1.51944	178.102	178.24	175.348	39.4855	37.6538	36.65677	0.08%	1.58%	5.09%	2.60%

Table D. 2 Waterside GCI calculation data

	Grid			Grid Ratio		HTC			DP			HTC		ADP	
	Grid 1	Grid 2	Grid 3	r21	r32	HTC 1	HTC 2	HTC 3	DP 1	DP 2	DP 3	GCI 21	GCI 32	GCI 21	GCI 32
InC1	9386491	2391209	186964	1.57747	2.33859	6390.86	6131.88	6011.89	4362.631	4337.163	4258.9923	3.55%	0.56%	0.49%	0.51%
InC2	918190	134588	97254	1.8966	1.11438	56486.1	57737	57205.2	4284.45	4193.39	4117.724	1.04%	4.80%	1.05%	9.50%
InC3	3277121	1069894	149400	1.45228	1.92751	11173.6	10873.8	11377.1	23876.2	23477.8	23487.74	10.83%	8.83%	6.66%	0.08%
InC4	1062084	311250	107146	1.50551	1.42685	25860.3	25739.7	25530.8	5742.6	5618.93	5615.023	2.58%	5.26%	12.12%	0.45%
InC5	2238913	766666	159130	1.42937	1.68895	11223.2	11001.9	10965.2	15132.9	14933.8	14531.8	2.41%	0.23%	1.60%	1.87%
InC6	287294	271485	217697	1.01905	1.07638	33218.8	33227.3	33385.5	3417.78	3414.82	3424.177	0.84%	3.73%	2.82%	2.15%
InC7	2516418	896761	156693	1.41049	1.78872	10757.6	10464.3	11143.3	23494.9	23110.5	23440.38	7.15%	7.91%	4.24%	1.83%
InC8	2652950	88578	667167	3.10552	0.51015	22531.6	22365.1	22607.9	9389.43	9053.31	9366.006	1.08%	4.35%	5.38%	13.51%
InC9	1164051	374619	86774	1.45924	1.6283	5701.29	5576.57	5646.49	1370.03	1377.35	1303.053	2.48%	0.94%	0.59%	4.32%
InC10	892930	226542	105339	1.57963	1.29078	25157.4	24036.1	23148.3	3868.99	3901.04	3937.132	3.90%	7.20%	0.69%	1.72%
InC11	3826770	1125341	168300	1.50377	1.88394	5388.74	5195.58	5757.086	4591.27	4803.49	4838.318	5.79%	8.15%	6.88%	0.60%
InC12	1141300	285227	137992	1.58758	1.27383	11466.2	11229.7	11119.3	4273.16	4233.35	3908.09	1.73%	1.99%	0.77%	16.71%
InC13	1.5E+07	1.4E+07	8684757	1.01699	1.17626	6170	6168.59	6272.87	4364.82	4355.99	4192.583	0.84%	5.42%	7.40%	12.70%
InC14	2892046	534579	200781	1.75549	1.386	13347.4	13542.7	12828.9	1371.87	1421.36	1539.285	1.10%	9.22%	2.66%	12.69%
InC15	5260164	1847026	82385	1.41745	2.81973	6410.15	5754.88	9534.84	13337.1	13489.3	28739.92	14.10%	7.13%	1.40%	9.54%
InC16	1833962	438964	104716	1.6106	1.6124	9139.83	8599.88	8931.22	2316.39	2382.86	2362.27	4.92%	2.90%	2.19%	0.68%

Appendix E: Meta-model data

Table E. 1 Airside meta-model data

	Tube #	D0	Pl/D0	Pt/D0	LR=L0/L1	sita [deg]	air face velocity	j	f
1	0.008008	0.866667	0.969357	0.836333	0.158719	0.717750	0.135556	0.035890	0.835242
2	0.022022	0.562222	0.255890	0.535310	0.014757	0.538500	0.297778	0.014284	0.167818
3	0.023023	0.533333	0.416656	0.050745	0.200820	0.652625	0.011111	0.031217	0.264411
4	0.024024	0.148889	0.983322	0.168833	0.157757	0.351375	0.393333	0.034483	0.427176
5	0.034034	0.511111	0.544054	0.200042	0.194737	0.670625	0.402222	0.020778	0.232554
6	0.037037	0.851111	0.655208	0.541125	0.050043	0.189250	0.213333	0.028463	0.600552
7	0.042042	0.515556	0.714337	0.801557	0.529762	0.311250	0.155556	0.028376	0.335064
8	0.050050	0.164444	0.607798	0.934978	0.064815	0.770750	0.348889	0.023004	0.197962
9	0.051051	0.351111	0.163247	0.646935	0.607843	0.728750	0.013333	0.033143	0.222025
10	0.052052	0.146667	0.762200	0.434535	0.598485	0.701750	0.433333	0.029024	0.297190
11	0.041008	0.624444	0.008734	0.584982	0.955409	0.354625	0.788889	0.012470	0.172575
12	0.041208	0.033333	0.961599	0.926478	0.619048	0.668375	0.382222	0.045531	0.359882
13	0.042609	0.864444	0.800935	0.018355	0.577139	0.189250	0.006667	0.036245	0.433153
14	0.042809	0.066667	0.067884	0.670064	0.524775	0.676875	0.522222	0.019803	0.163549
15	0.043009	0.411111	0.276674	0.856379	0.545739	0.660375	0.115556	0.024862	0.221944
16	0.044009	0.111111	0.203957	0.791473	0.629310	0.098250	0.722222	0.022512	0.255326
17	0.044409	0.377778	0.633236	0.976729	0.703901	0.842625	0.220000	0.024675	0.243116
18	0.044809	0.662222	0.050316	0.841007	0.909420	0.983750	0.120000	0.014639	0.111271
19	0.045009	0.753333	0.706570	0.811217	0.607323	0.820000	0.526667	0.020739	0.408872
20	0.046209	0.944444	0.283232	0.212608	0.120833	0.841000	0.108889	0.012467	0.098307
21	0.008002	0.286667	0.752977	0.313185	0.658065	0.074250	0.593333	0.028713	0.291930
22	0.008202	0.604444	0.289192	0.977640	0.522242	0.358250	0.091111	0.031315	0.275098
23	0.008402	0.055556	0.036308	0.601331	0.450000	0.950000	0.255556	0.020450	0.094152
24	0.008802	0.455556	0.515931	0.614539	0.800388	0.072375	0.817778	0.019194	0.220610
25	0.009002	0.211111	0.037754	0.430126	0.341488	0.034250	0.231111	0.030155	0.268173

26	0.009402	0.635556	0.729994	0.809513	0.780303	0.477250	0.644444	0.018891	0.213257
27	0.009602	0.317778	0.665134	0.862737	0.880229	0.301875	0.233333	0.038221	0.342848
28	0.009802	0.206667	0.210256	0.840339	0.759662	0.804750	0.731111	0.018585	0.163469
29	0.010002	0.651111	0.361392	0.037289	0.541667	0.288625	0.415556	0.020034	0.226066
30	0.010202	0.526667	0.345861	0.947462	0.954710	0.227250	0.500000	0.020374	0.218216
31	0.010402	0.024444	0.196613	0.989875	0.686782	0.797500	0.360000	0.038993	0.283436
32	0.010602	0.837778	0.553603	0.188026	0.964721	0.028250	0.717778	0.015748	0.200469
33	0.010802	0.317778	0.636460	0.340052	0.237203	0.093875	0.104444	0.048602	0.447859
34	0.011002	0.068889	0.920716	0.469112	0.713312	0.206000	0.675556	0.041802	0.385319
35	0.011202	0.917778	0.122649	0.518207	0.832650	0.601125	0.893333	0.009781	0.130820
36	0.011402	0.231111	0.360580	0.577013	0.254464	0.493500	0.535556	0.023760	0.222423
37	0.011602	0.288889	0.851952	0.651227	0.641473	0.882000	0.086667	0.047015	0.344744
38	0.011802	0.484444	0.620354	0.167920	0.662381	0.793375	0.468889	0.021665	0.205453
39	0.012002	0.920000	0.010594	0.502494	0.734934	0.982375	0.346667	0.008273	0.067540
40	0.012202	0.066667	0.397725	0.486314	0.922101	0.275875	0.588889	0.038938	0.328778
41	0.012402	0.860000	0.877373	0.237991	0.459541	0.210250	0.611111	0.018376	0.230171
42	0.012803	0.877778	0.915791	0.866192	0.987730	0.925375	0.300000	0.021444	0.199080
43	0.013003	0.620000	0.504400	0.411864	0.499597	0.735125	0.717778	0.014990	0.161217
44	0.013203	0.306667	0.746197	0.695740	0.071029	0.631125	0.933333	0.018385	0.198648
45	0.013603	0.122222	0.965812	0.982215	0.036822	0.739750	0.300000	0.038452	0.309184
46	0.013803	0.097778	0.594247	0.725123	0.101852	0.488125	0.166667	0.051040	0.411322
47	0.014003	0.277778	0.457627	0.717860	0.191581	0.927000	0.886667	0.013197	0.104026
48	0.014203	0.277778	0.153674	0.338558	0.095118	0.559250	0.746667	0.012598	0.117607
49	0.014603	0.044444	0.953441	0.358137	0.647436	0.967375	0.351111	0.049561	0.346678
50	0.015003	0.126667	0.007246	0.007045	0.127637	0.320625	0.333333	0.022666	0.179442
51	0.015203	0.393333	0.727577	0.678475	0.325848	0.710500	0.948889	0.017185	0.183289
52	0.015603	0.177778	0.906881	0.024718	0.433642	0.676375	0.464444	0.035757	0.337841
53	0.015803	0.573333	0.846319	0.857321	0.771870	0.871625	0.680000	0.018112	0.179511
54	0.016603	0.482222	0.568581	0.105987	0.154122	0.660500	0.931111	0.014488	0.171530

55	0.016803	0.335556	0.039060	0.597861	0.758333	0.584125	0.077778	0.031667	0.234151
56	0.017003	0.566667	0.642672	0.347367	0.759477	0.047250	0.148889	0.035645	0.331938
57	0.017203	0.235556	0.622520	0.930593	0.344502	0.926750	0.353333	0.026285	0.196683
58	-0.046731	0.515556	0.957833	0.233154	0.445152	0.548500	0.255556	0.028464	0.292511
59	-0.045730	0.206667	0.976329	0.519096	0.762897	0.427375	0.935556	0.024751	0.259128
60	-0.043728	0.506667	0.558675	0.474477	0.343063	0.630625	0.180000	0.026555	0.256704
61	-0.042727	0.646667	0.930880	0.642599	0.933486	0.551500	0.017778	0.043269	0.365969
62	-0.041726	0.148889	0.335670	0.532063	0.314000	0.286250	0.784444	0.022796	0.258965
63	-0.039724	0.077778	0.091033	0.108984	0.638889	0.626625	0.935556	0.018422	0.186939
64	-0.038723	0.382222	0.240125	0.380026	0.221235	0.333375	0.542222	0.016912	0.219831
65	-0.021706	0.040000	0.443826	0.398769	0.899123	0.297250	0.184444	0.056176	0.411714
66	-0.016701	0.288889	0.712140	0.750121	0.501589	0.167125	0.208889	0.031445	0.341533
67	-0.015700	0.071111	0.126027	0.771053	0.982510	0.253250	0.906667	0.021213	0.242979
68	-0.014699	0.206667	0.845170	0.104503	0.036195	0.992000	0.242222	0.025106	0.132763
69	-0.012697	0.908889	0.031061	0.783565	0.583333	0.707750	0.611111	0.010420	0.154849
70	-0.006691	0.815556	0.237585	0.022309	0.467874	0.364375	0.360000	0.023216	0.497174
71	-0.001686	0.691111	0.332635	0.977942	0.099794	0.268250	0.002222	0.029597	0.303308
72	-0.052527	0.266667	0.588262	0.740087	0.134428	0.532250	0.977778	0.017583	0.212972
73	-0.052327	0.488889	0.380393	0.332904	0.179858	0.345625	0.982222	0.013221	0.217599
74	-0.052127	0.806667	0.829758	0.553455	0.084758	0.403500	0.006667	0.038752	0.378707
75	-0.051727	0.326667	0.471017	0.278068	0.425439	0.836750	0.997778	0.014263	0.155475
76	-0.051527	0.351111	0.946686	0.672213	0.584773	0.176875	0.766667	0.022891	0.249103
77	-0.051326	0.315556	0.200053	0.205448	0.922101	0.816000	0.535556	0.017286	0.166983
78	-0.051126	0.280000	0.727253	0.235093	0.332339	0.134625	0.428889	0.029858	0.319486
79	-0.050926	0.826667	0.399525	0.974824	0.838394	0.735750	0.657778	0.012734	0.158465
80	-0.050726	0.371111	0.647665	0.003057	0.620098	0.950375	0.262222	0.025721	0.220245
81	-0.050326	0.695556	0.807020	0.599280	0.781994	0.096000	0.175556	0.029547	0.290018
82	-0.050126	0.051111	0.633667	0.282684	0.271739	0.911625	0.580000	0.027902	0.210588
83	-0.049926	0.020000	0.534343	0.617340	0.530142	0.520500	0.993333	0.031120	0.290700

266

84	-0.049726	0.686667	0.169938	0.100518	0.310041	0.917125	0.175556	0.011980	0.086655
85	-0.049526	0.766667	0.619915	0.379898	0.119707	0.225000	0.968889	0.013141	0.223436
86	-0.049326	0.295556	0.582519	0.419245	0.971311	0.728375	0.704444	0.020966	0.214164
87	-0.048926	0.260000	0.420615	0.257711	0.315000	0.716750	0.755556	0.017145	0.183030
88	-0.048526	0.762222	0.614624	0.735811	0.174567	0.521500	0.944444	0.012230	0.189229
89	0.068068	0.060000	0.593403	0.328508	0.164352	0.434375	0.508889	0.033093	0.345918
90	0.069069	0.304444	0.955996	0.265880	0.776848	0.146125	0.071111	0.048936	0.471479
91	0.070070	0.202222	0.979853	0.780667	0.303459	0.944000	0.706667	0.021106	0.226001
92	0.074074	0.062222	0.052080	0.158088	0.390625	0.853875	0.566667	0.014296	0.092095
93	0.078078	0.331111	0.198795	0.405104	0.093750	0.796750	0.064444	0.018651	0.105527
94	0.079079	0.644444	0.066936	0.992881	0.405754	0.613625	0.786667	0.010343	0.155209
95	0.092092	0.002222	0.068371	0.584414	0.706284	0.184125	0.388889	0.038159	0.292244
96	0.094094	0.242222	0.063123	0.683779	0.272727	0.856875	0.246667	0.011372	0.065362
97	0.095095	0.208889	0.733465	0.483966	0.464080	0.612625	0.791111	0.023234	0.302654
98	0.097097	0.433333	0.735862	0.756848	0.716117	0.705750	0.040000	0.039721	0.324364
99	0.101101	0.500000	0.952354	0.841334	0.091592	0.753750	0.455556	0.019350	0.241314
100	0.102102	0.053333	0.839860	0.186358	0.371795	0.961000	0.235556	0.044963	0.302679
101	0.105105	0.104444	0.273159	0.622575	0.597953	0.611625	0.446667	0.026358	0.246368
102	0.052811	0.284444	0.574972	0.111369	0.473389	0.265250	0.731111	0.024573	0.276880
103	0.053011	0.497778	0.082609	0.519410	0.168651	0.454875	0.471111	0.012926	0.138976
104	0.053211	0.773333	0.509279	0.739783	0.663450	0.591750	0.946667	0.013325	0.175257
105	0.053411	0.040000	0.029296	0.247662	0.490741	0.849000	0.013333	0.050058	0.266471
106	0.053611	0.062222	0.788318	0.209968	0.175926	0.859000	0.311111	0.039958	0.280492
107	0.053811	0.177778	0.717906	0.192025	0.442460	0.992375	0.977778	0.019985	0.163051
108	0.054211	0.357778	0.330628	0.081447	0.128788	0.598750	0.695556	0.015107	0.152343
109	0.054411	0.973333	0.431311	0.027905	0.855357	0.806750	0.353333	0.017466	0.181302
110	0.054611	0.731111	0.265106	0.737820	0.570175	0.117875	0.691111	0.014928	0.202525
111	0.054811	0.617778	0.253388	0.642958	0.602543	0.011250	0.180000	0.027717	0.278669
112	0.055211	0.268889	0.764330	0.028427	0.223621	0.621875	0.875556	0.021174	0.229642

113	0.058012	0.644444	0.902605	0.416940	0.528220	0.871375	0.180000	0.028419	0.255468
114	0.058212	0.815556	0.226520	0.924416	0.003652	0.560125	0.100000	0.016075	0.150803
115	0.058412	0.375556	0.814917	0.982254	0.671053	0.931000	0.757778	0.019764	0.187292
116	0.058812	0.566667	0.576827	0.548445	0.134780	0.381125	0.395556	0.022265	0.252230
117	0.059012	0.873333	0.340685	0.387744	0.684080	0.641500	0.900000	0.011868	0.154728
118	0.059412	0.586667	0.754678	0.300555	0.226763	0.988625	0.213333	0.021812	0.166492
119	0.059812	0.426667	0.468609	0.438658	0.823506	0.093000	0.964444	0.018085	0.220522
120	0.060412	0.635556	0.411362	0.458607	0.847733	0.176000	0.524444	0.019560	0.225528
121	0.060612	0.586667	0.867174	0.095585	0.882427	0.457500	0.315556	0.027902	0.303479
122	0.060812	0.360000	0.485213	0.833378	0.471557	0.500875	0.393333	0.026008	0.247834
123	0.061012	0.744444	0.732171	0.727166	0.457612	0.686375	0.095556	0.031797	0.283122
124	0.061412	0.480000	0.863518	0.622240	0.195445	0.361625	0.824444	0.019958	0.256731
125	0.061612	0.326667	0.764362	0.849696	0.493590	0.764125	0.424444	0.026968	0.243732
126	0.061812	0.513333	0.537508	0.220556	0.023990	0.411250	0.860000	0.015837	0.221112
127	0.062012	0.977778	0.291767	0.377539	0.568519	0.453750	0.088889	0.025609	0.231223
128	0.062212	0.533333	0.937107	0.459231	0.942569	0.044000	0.926667	0.019379	0.240755
129	0.146146	0.115556	0.546539	0.793305	0.040323	0.837875	0.780000	0.016223	0.140742
130	0.148148	0.048889	0.142283	0.436872	0.939038	0.087125	0.066667	0.070031	0.442732
131	0.152152	0.568889	0.443886	0.565129	0.993827	0.219250	0.120000	0.028936	0.314396
132	0.154154	0.071111	0.487161	0.286004	0.567901	0.658625	0.706667	0.027631	0.290666
133	0.156156	0.235556	0.969826	0.829411	0.533936	0.139125	0.175556	0.040803	0.406783
134	0.105421	0.011111	0.035752	0.526012	0.448925	0.491125	0.264444	0.035099	0.235436
135	0.105621	0.100000	0.233249	0.410995	0.414319	0.416875	0.260000	0.033337	0.282083
136	0.106221	0.213333	0.314884	0.988415	0.688406	0.581375	0.384444	0.023985	0.243869
137	0.106421	0.315556	0.217290	0.742619	0.073970	0.917625	0.262222	0.008302	0.038085
138	0.106821	0.115556	0.369235	0.608308	0.935185	0.911750	0.768889	0.021510	0.206564
139	0.109222	0.364444	0.784861	0.014166	0.960884	0.302500	0.820000	0.025240	0.431991
140	0.110422	0.791111	0.977944	0.022151	0.296899	0.492750	0.035556	0.035493	0.455846
141	0.111022	0.457778	0.490443	0.038345	0.814706	0.364250	0.208889	0.029070	0.362154

142	0.111622	0.200000	0.410369	0.649201	0.472222	0.826625	0.480000	0.021119	0.205518
143	0.112623	0.884444	0.021951	0.065983	0.054630	0.847000	0.106667	0.000547	0.000233
144	0.113023	0.140000	0.563543	0.306279	0.605000	0.457875	0.835556	0.024984	0.320574
145	0.113223	0.037778	0.307167	0.466671	0.993386	0.126625	0.317778	0.044493	0.358006
146	0.114623	0.171111	0.992855	0.480493	0.492938	0.609875	0.284444	0.036665	0.369472
147	0.115223	0.075556	0.079083	0.062727	0.260057	0.150875	0.153333	0.039503	0.336174
148	0.115423	0.020000	0.764764	0.466639	0.054348	0.365250	0.277778	0.055262	0.474856
149	0.116223	0.146667	0.992413	0.718224	0.621930	0.277625	0.868889	0.027014	0.374380
150	0.117023	0.104444	0.664256	0.145973	0.283129	0.070875	0.562222	0.033338	0.429983
151	0.117223	0.351111	0.422789	0.963117	0.895358	0.317500	0.308889	0.025146	0.281431
152	0.117423	0.431111	0.080569	0.267460	0.733498	0.922750	0.393333	0.013693	0.120289
153	0.118224	0.577778	0.086488	0.703997	0.638889	0.846375	0.240000	0.013968	0.123725
154	0.118824	0.031111	0.819745	0.915765	0.477891	0.733125	0.824444	0.030257	0.291090
155	0.119224	0.855556	0.584030	0.042962	0.010305	0.487750	0.220000	0.020662	0.320641
156	0.119424	0.466667	0.492916	0.903443	0.639937	0.768125	0.260000	0.021794	0.232574
157	0.119624	0.093333	0.971581	0.603478	0.521386	0.401500	0.748889	0.030414	0.379736
158	0.120224	0.064444	0.157568	0.955302	0.073529	0.989375	0.828889	0.003264	0.006157
159	0.120824	0.175556	0.493627	0.664071	0.083333	0.294625	0.148889	0.038647	0.352536
160	0.121024	0.175556	0.804679	0.118390	0.468519	0.899375	0.395556	0.028640	0.292838
161	0.121224	0.362222	0.668978	0.039518	0.166058	0.889125	0.011111	0.039253	0.268657
162	0.121624	0.244444	0.030677	0.747817	0.015537	0.193000	0.126667	0.021480	0.199416
163	0.123625	0.133333	0.293217	0.539161	0.898148	0.934375	0.382222	0.025341	0.208183
164	0.123825	0.566667	0.730555	0.024373	0.012483	0.603500	0.960000	0.016836	0.293585
165	0.124225	0.017778	0.165665	0.306172	0.685897	0.881375	0.357778	0.032051	0.208914
166	0.124625	0.173333	0.026127	0.868010	0.728311	0.183375	0.255556	0.025982	0.242825
167	0.125025	0.560000	0.204000	0.793192	0.685146	0.042000	0.582222	0.017526	0.272774
168	0.125425	0.691111	0.508224	0.913815	0.904047	0.340250	0.202222	0.023252	0.284726
169	0.127626	0.437778	0.856418	0.564595	0.030702	0.256625	0.573333	0.023905	0.387605
170	0.127826	0.055556	0.188144	0.959171	0.127451	0.905375	0.886667	0.009815	0.053908

171	0.128026	0.940000	0.446247	0.232528	0.143894	0.568500	0.822222	0.014502	0.301706
172	0.128426	0.264444	0.165838	0.288000	0.088442	0.143375	0.680000	0.018692	0.244273
173	0.198198	0.102222	0.481648	0.624710	0.227169	0.003000	0.293333	0.038382	0.373624
174	0.199199	0.162222	0.319183	0.383996	0.040870	0.223250	0.788889	0.021106	0.289665
175	0.206206	0.831111	0.264889	0.848299	0.810099	0.543500	0.262222	0.019091	0.270723
176	0.210210	0.542222	0.193778	0.513254	0.289506	0.898875	0.453333	0.010796	0.098122
177	0.170234	0.453333	0.197667	0.156590	0.882924	0.492125	0.811111	0.017258	0.286636
178	0.174035	0.268889	0.795825	0.973925	0.883947	0.501500	0.926667	0.021788	0.308944
179	0.174235	0.137778	0.518313	0.991378	0.129487	0.941750	0.528889	0.017081	0.123707
180	0.174435	0.566667	0.397400	0.942268	0.011947	0.142875	0.164444	0.023258	0.298723
181	0.175035	0.960000	0.266953	0.356421	0.769540	0.589750	0.013333	0.026919	0.262460
182	0.175235	0.195556	0.709521	0.181127	0.756024	0.339250	0.706667	0.027882	0.392168
183	0.176035	0.084444	0.267875	0.963716	0.850000	0.657750	0.011111	0.072207	0.403775
184	0.176435	0.020000	0.902425	0.675482	0.875000	0.614750	0.906667	0.033342	0.346014
185	0.176635	0.040000	0.967860	0.913761	0.148455	0.180000	0.797778	0.034194	0.407142
186	0.176835	0.244444	0.521831	0.133644	0.852657	0.457250	0.473333	0.027328	0.342553
187	0.178436	0.540000	0.906620	0.555754	0.868421	0.410250	0.108889	0.033498	0.376280
188	0.180236	0.066667	0.206230	0.675409	0.263514	0.881000	0.795556	0.017125	0.114556
189	0.180436	0.900000	0.928453	0.224831	0.531604	0.140625	0.822222	0.016854	0.256689
190	0.180636	0.733333	0.508137	0.065167	0.423554	0.722500	0.591111	0.015979	0.186784
191	0.180836	0.215556	0.115271	0.062144	0.292328	0.890750	0.453333	0.013887	0.077826
192	0.181036	0.068889	0.066535	0.387377	0.882576	0.534875	0.122222	0.056029	0.385397
193	0.181236	0.086667	0.766057	0.254935	0.588710	0.853125	0.417778	0.040771	0.331983
194	0.181436	0.646667	0.579896	0.028705	0.290340	0.438125	0.960000	0.015636	0.238943
195	0.181636	0.340000	0.006534	0.132802	0.982932	0.777750	0.164444	0.025173	0.166730
196	0.181836	0.768889	0.521016	0.781288	0.404487	0.690500	0.675556	0.014504	0.176190
197	0.182036	0.882222	0.492430	0.510633	0.376029	0.570375	0.753333	0.013614	0.183918
198	0.182436	0.711111	0.505659	0.698564	0.755236	0.016000	0.677778	0.017557	0.229424
199	0.182637	0.831111	0.681461	0.262798	0.838130	0.199625	0.646667	0.018042	0.241521

200	0.182837	0.622222	0.783863	0.450878	0.758638	0.466125	0.706667	0.019424	0.240306
201	0.183037	0.546667	0.252806	0.065984	0.130952	0.686750	0.722222	0.011261	0.115804
202	0.183237	0.277778	0.612127	0.902290	0.989411	0.384875	0.708889	0.025548	0.262163
203	0.183437	0.513333	0.219228	0.166105	0.286285	0.290875	0.802222	0.014872	0.194327
204	0.183637	0.348889	0.884038	0.853473	0.608918	0.435500	0.691111	0.025049	0.274253
205	0.183837	0.060000	0.275258	0.720810	0.162281	0.924750	0.573333	0.017766	0.098304
206	0.184037	0.262222	0.315577	0.157764	0.681944	0.485875	0.593333	0.024404	0.234541
207	0.184437	0.673333	0.987694	0.055344	0.945152	0.854625	0.495556	0.021796	0.257814
208	0.185037	0.977778	0.546302	0.094839	0.131492	0.607875	0.506667	0.014695	0.189816
209	0.185237	0.637778	0.106164	0.717791	0.138112	0.908750	0.664444	0.004103	0.021944
210	0.186237	0.086667	0.435829	0.464282	0.955882	0.165625	0.462222	0.043790	0.367314
211	0.186437	0.691111	0.280738	0.883979	0.426083	0.914750	0.488889	0.012311	0.114622
212	0.186637	0.220000	0.069716	0.024638	0.784314	0.716375	0.711111	0.017663	0.148245
213	0.187037	0.393333	0.429964	0.649297	0.848101	0.566875	0.140000	0.038143	0.317801
214	0.187237	0.235556	0.336677	0.945856	0.420068	0.596125	0.337778	0.028570	0.253913
215	0.188038	0.986667	0.053968	0.779470	0.137640	0.353875	0.313333	0.011162	0.140198
216	0.188238	0.513333	0.992138	0.895893	0.039831	0.504500	0.055556	0.044895	0.423843
217	0.188838	0.366667	0.281986	0.869080	0.461111	0.944000	0.915556	0.012181	0.110692
218	0.189038	0.431111	0.754726	0.914574	0.474044	0.334250	0.288889	0.031918	0.318368
219	0.189238	0.742222	0.973835	0.553683	0.918750	0.504125	0.497778	0.021663	0.255882
220	0.189638	0.728889	0.755016	0.705638	0.003623	0.933000	0.024444	0.024190	0.150466
221	0.190238	0.357778	0.248831	0.932245	0.173077	0.556875	0.877778	0.013504	0.189568
222	0.190638	0.242222	0.858106	0.610279	0.909292	0.928625	0.557778	0.028531	0.311451
223	0.191038	0.800000	0.661859	0.969507	0.330513	0.584750	0.188889	0.025165	0.308037
224	0.191238	0.411111	0.625522	0.282748	0.983333	0.938375	0.762222	0.019926	0.275976
225	0.191438	0.006667	0.973384	0.414248	0.637597	0.772125	0.726667	0.045247	0.459219
226	0.191638	0.364444	0.157359	0.423764	0.787634	0.984375	0.173333	0.024723	0.195819
227	0.191838	0.891111	0.205483	0.314199	0.154762	0.393875	0.417778	0.013729	0.209439
228	0.192038	0.477778	0.740887	0.824949	0.932870	0.070625	0.328889	0.030323	0.368775

229	0.192238	0.466667	0.124620	0.998545	0.057163	0.748500	0.573333	0.006451	0.057956
230	0.192639	0.397778	0.721412	0.987814	0.097756	0.197875	0.775556	0.021620	0.335034
231	0.192839	0.386667	0.607335	0.727554	0.845716	0.347125	0.068889	0.051090	0.578960
232	0.193239	0.342222	0.250521	0.094081	0.262027	0.929375	0.411111	0.014931	0.116438
233	0.193439	0.293333	0.601050	0.209021	0.382132	0.941375	0.468889	0.023063	0.230509
234	0.193839	0.086667	0.583722	0.673609	0.297222	0.715500	0.077778	0.065364	0.532095
235	0.219219	0.655556	0.216961	0.390382	0.249077	0.260250	0.037778	0.035262	0.325299
236	0.221221	0.155556	0.101447	0.427283	0.241870	0.403375	0.448889	0.024169	0.206632
237	0.222222	0.402222	0.168299	0.214271	0.988562	0.999000	0.626667	0.015482	0.134388
238	0.223223	0.253333	0.138889	0.782391	0.990964	0.656625	0.182222	0.033250	0.267097
239	0.224224	0.546667	0.641835	0.719016	0.325472	0.677625	0.537778	0.019520	0.213394
240	0.225225	0.184444	0.372164	0.837220	0.268116	0.542500	0.742222	0.022264	0.220208
241	0.227227	0.486667	0.185810	0.766186	0.655568	0.133125	0.020000	0.045229	0.388031
242	0.228228	0.002222	0.860242	0.253815	0.397059	0.489500	0.548889	0.054096	0.482855
243	0.229229	0.282222	0.584844	0.589863	0.670910	0.092125	0.633333	0.027223	0.290461
244	0.230230	0.455556	0.431702	0.720449	0.757317	0.461500	0.328889	0.026568	0.258226
245	0.231231	0.124444	0.529934	0.523910	0.863757	0.870875	0.980000	0.025064	0.226601
246	0.233233	0.171111	0.560399	0.869867	0.636640	0.156125	0.124444	0.058583	0.482313
247	0.234234	0.995556	0.107548	0.680348	0.543899	0.781750	0.164444	0.014477	0.131521
248	0.235235	0.340000	0.668926	0.029805	0.236111	0.867875	0.342222	0.025347	0.221939
249	0.236236	0.493333	0.073580	0.272502	0.801146	0.148125	0.411111	0.019701	0.213448
250	0.237237	0.833333	0.033580	0.852833	0.347368	0.689750	0.477778	0.008381	0.087269
251	0.238238	0.302222	0.059696	0.701905	0.035211	0.328375	0.271111	0.018281	0.174430
252	0.240240	0.975556	0.884613	0.133572	0.532018	0.269250	0.171111	0.028714	0.338887
253	0.241241	0.028889	0.642283	0.356712	0.769841	0.775750	0.142222	0.077608	0.514939
254	0.242242	0.237778	0.325070	0.779122	0.076765	0.076125	0.788889	0.020948	0.260657
255	0.244244	0.142222	0.934652	0.468182	0.799383	0.562625	0.255556	0.050073	0.433447
256	0.245245	0.831111	0.727046	0.681966	0.847113	0.514500	0.757778	0.016340	0.214841
257	0.246246	0.482222	0.417038	0.066534	0.931507	0.885875	0.375556	0.022970	0.212957

258	0.247247	0.508889	-0.000614	0.217471	0.483918	0.766750	0.640000	0.008923	0.081520
259	0.248248	0.651111	0.449574	0.356537	0.138889	0.785750	0.126667	0.022733	0.180367
260	0.249249	0.613333	0.388926	0.115547	0.754318	0.708750	0.662222	0.016570	0.191156
261	0.250250	0.782222	0.744838	0.009642	0.574040	0.905875	0.906667	0.014251	0.187900
262	0.251251	0.553333	0.427901	0.651198	0.602028	0.159125	0.922222	0.016416	0.222724
263	0.252252	0.431111	0.391212	0.207920	0.915072	0.407375	0.106667	0.041096	0.337750
264	0.254254	0.160000	0.638605	0.972135	0.178082	0.322375	0.315556	0.041316	0.396013
265	0.255255	0.993333	0.156848	0.915059	0.263228	0.477500	0.195556	0.015651	0.170209
266	0.257257	0.660000	0.864459	0.274364	0.608724	0.829875	0.708889	0.017683	0.210114
267	0.258258	0.397778	0.400104	0.510348	0.429431	0.128125	0.128889	0.039944	0.361569
268	0.259259	0.606667	0.720176	0.119464	0.163171	0.084125	0.895556	0.018318	0.283275
269	0.261261	0.235556	0.772135	0.073082	0.785826	0.875875	0.844444	0.024285	0.254487
270	0.262262	0.373333	0.341214	0.717396	0.016667	0.850875	0.306667	0.011907	0.073554
271	0.210642	0.226667	0.683234	0.692613	0.988095	0.672875	0.128889	0.051600	0.410693
272	0.210842	0.435556	0.713217	0.919530	0.261561	0.762750	0.733333	0.018107	0.194775
273	0.211042	0.082222	0.965912	0.397969	0.179952	0.801750	0.895556	0.029409	0.269285
274	0.211242	0.700000	0.841723	0.921094	0.284038	0.722125	0.840000	0.015279	0.189923
275	0.211442	0.560000	0.580638	0.278707	0.215313	0.755375	0.697778	0.015722	0.174714
276	0.211642	0.100000	0.313910	0.260142	0.198357	0.178625	0.524444	0.034501	0.322750
277	0.211842	0.615556	0.553301	0.714703	0.844884	0.818125	0.200000	0.027351	0.245005
278	0.212042	0.282222	0.172349	0.184322	0.776389	0.030625	0.740000	0.021476	0.231779
279	0.212242	0.088889	0.151411	0.243163	0.466049	0.510125	0.542222	0.029877	0.233346
280	0.212442	0.195556	0.789298	0.864128	0.717120	0.423875	0.371111	0.039586	0.365135
281	0.213243	0.451111	0.358587	0.109770	0.531457	0.253625	0.522222	0.022427	0.251003
282	0.213443	0.526667	0.253746	0.055881	0.038440	0.275000	0.275556	0.021804	0.239513
283	0.213643	0.975556	0.041254	0.433875	0.399916	0.858375	0.271111	0.008540	0.066902
284	0.214243	0.242222	0.149360	0.027334	0.514678	0.078000	0.475556	0.026466	0.245484
285	0.214443	0.068889	0.476036	0.448472	0.112434	0.500750	0.448889	0.038898	0.344409
286	0.214643	0.926667	0.276693	0.145401	0.826634	0.095875	0.268889	0.021017	0.237887

287	0.214843	0.486667	0.422157	0.851065	0.665535	0.443875	0.915556	0.016502	0.206722
288	0.215043	0.073333	0.343815	0.519697	0.221491	0.357500	0.660000	0.032471	0.295600
289	0.215243	0.917778	0.352867	0.913509	0.153997	0.315250	0.966667	0.011617	0.184381
290	0.215643	0.460000	0.289457	0.381162	0.188328	0.216500	0.511111	0.019949	0.235513
291	0.215843	0.540000	0.827551	0.481105	0.997126	0.566375	0.631111	0.021864	0.251217
292	0.216043	0.466667	0.630307	0.427268	0.452273	0.111875	0.395556	0.027542	0.303034
293	0.216243	1.000000	0.492292	0.092428	0.675970	0.182875	0.944444	0.014188	0.221285
294	0.216443	0.773333	0.142546	0.745563	0.109010	0.052000	0.053333	0.026140	0.272564
295	0.216643	0.162222	0.467874	0.165223	0.852941	0.987375	0.826667	0.023593	0.202374
296	0.216843	0.808889	0.963521	0.803711	0.974858	0.379625	0.715556	0.018241	0.237171
297	0.271271	0.031111	0.081473	0.069468	0.551802	0.490500	0.664444	0.025424	0.245749
298	0.272272	0.068889	0.163838	0.234585	0.876984	0.642625	0.353333	0.031906	0.272527
299	0.274274	0.795556	0.342698	0.970492	0.120011	0.458500	0.415556	0.015239	0.220293
300	0.275275	0.082222	0.624820	0.266877	0.932471	0.277250	0.022222	0.095834	0.632987
301	0.276276	0.722222	0.694677	0.149459	0.477969	0.760750	0.140000	0.025918	0.313858
302	0.277277	0.060000	0.133871	0.957146	0.735294	0.882875	0.077778	0.045570	0.242027
303	0.280280	0.835556	0.012242	0.198286	0.401341	0.795750	0.151111	0.010471	0.082497
304	0.281281	0.528889	0.403614	0.651722	0.014192	0.455500	0.051111	0.028014	0.274785
305	0.283283	0.084444	0.624628	0.650606	0.747685	0.537500	0.471111	0.034575	0.337771
306	0.287287	0.946667	0.315419	0.166372	0.953401	0.852875	0.131111	0.020905	0.239154
307	0.289289	0.182222	0.859606	0.802557	0.996599	0.805750	0.413333	0.030276	0.317639
308	0.293293	0.917778	0.939317	0.520248	0.029981	0.842875	0.326667	0.016218	0.199990
309	0.296296	0.573333	0.409904	0.090473	0.174390	0.594625	0.653333	0.016592	0.245160
310	0.297297	0.264444	0.663287	0.400452	0.088164	0.218250	0.215556	0.034461	0.409548
311	0.301301	0.862222	0.576994	0.885188	0.660394	0.792750	0.246667	0.019410	0.240641
312	0.302302	0.384444	0.091751	0.657105	0.628713	0.273250	0.966667	0.014139	0.205650
313	0.312312	0.144444	0.773619	0.306877	0.298780	0.793750	0.748889	0.024503	0.289602
314	0.263253	0.733333	0.732542	0.525844	0.424383	0.558875	0.402222	0.021610	0.247680
315	0.263453	0.580000	0.462715	0.761338	0.579268	0.392875	0.108889	0.035327	0.320594

316	0.263653	0.242222	0.459600	0.448197	0.411364	0.080250	0.904444	0.023255	0.268621
317	0.263853	0.973333	0.657046	0.670260	0.304603	0.329125	0.566667	0.016836	0.235905
318	0.264053	0.751111	0.867025	0.255817	0.622329	0.694000	0.040000	0.040420	0.371943
319	0.264253	0.655556	0.786100	0.688284	0.521277	0.411875	0.966667	0.016615	0.232082
320	0.264453	0.306667	0.014244	0.714981	0.428419	0.279000	0.100000	0.031133	0.267119
321	0.264653	0.953333	0.802596	0.918047	0.329840	0.222875	0.551111	0.018167	0.249551
322	0.264853	0.240000	0.130189	0.378779	0.681442	0.109375	0.506667	0.025324	0.245959
323	0.265053	0.802222	0.831045	0.580138	0.248153	0.580125	0.142222	0.029392	0.299452
324	0.265253	0.848889	0.191945	0.772626	0.090752	0.374875	0.233333	0.016264	0.187021
325	0.265653	0.488889	0.983026	0.072430	0.655340	0.897125	0.335556	0.027707	0.288381
326	0.265853	0.168889	0.724662	0.963378	0.400407	0.979625	0.666667	0.024645	0.200429
327	0.266053	0.448889	0.298451	0.598433	0.429654	0.599750	0.666667	0.016659	0.183744
328	0.266253	0.506667	0.594458	0.592060	0.088745	0.346500	1.000000	0.016348	0.238950
329	0.266453	0.411111	0.389601	0.044551	0.241870	0.993000	0.262222	0.018342	0.117297
330	0.267053	0.615556	0.763244	0.993006	0.489651	0.499750	0.575556	0.020488	0.241874
331	0.267253	0.440000	0.064555	0.831387	0.664667	0.594500	0.924444	0.011551	0.142465
332	0.267453	0.182222	0.371191	0.706159	0.397287	0.040625	0.786667	0.025488	0.276537
333	0.267854	0.222222	0.651608	0.453799	0.311869	0.495500	0.397778	0.033942	0.327115
334	0.268454	0.084444	0.292998	0.023506	0.632576	0.299875	0.524444	0.038228	0.320447
335	0.268654	0.820000	0.589880	0.849089	0.386022	0.609750	0.044444	0.034483	0.306234
336	0.268854	0.857778	0.658690	0.748982	0.157566	0.381500	0.551111	0.017359	0.240641
337	0.269054	0.073333	0.390491	0.408379	0.913522	0.618875	0.151111	0.065289	0.458933
338	0.269254	0.040000	0.788107	0.424380	0.701977	0.576750	0.148889	0.076513	0.541008
339	0.269454	0.935556	0.222712	0.085012	0.643880	0.249500	0.113333	0.025964	0.248529
340	0.269654	0.648889	0.196762	0.526993	0.215262	0.060000	0.006667	0.039733	0.360664
341	0.269854	0.735556	0.018875	0.247626	0.271545	0.197500	0.173333	0.018157	0.188687
342	0.270054	0.033333	0.323503	0.388059	0.816667	0.233500	0.315556	0.059645	0.450719
343	0.270254	0.851111	0.364937	0.233240	0.408590	0.913125	0.133333	0.020230	0.157928
344	0.270454	0.617778	0.424422	0.299777	0.834590	0.709375	0.297778	0.023535	0.228142

275

345	0.270654	0.280000	0.016942	0.990959	0.261905	0.841750	0.086667	0.013773	0.066298
346	0.270854	0.795556	0.655197	0.304616	0.116102	0.678500	0.733333	0.013983	0.181095
347	0.271054	0.586667	0.233275	0.101552	0.230507	0.663500	0.864444	0.011291	0.132328
348	0.271654	0.148889	0.898686	0.476023	0.274138	0.375875	0.791111	0.031678	0.346724
349	0.271854	0.475556	0.456341	0.179714	0.524250	0.559500	0.533333	0.021204	0.231681
350	0.272054	0.415556	0.517208	0.605645	0.555457	0.296000	0.200000	0.035365	0.329690
351	0.400400	0.093333	0.029844	0.508093	0.147436	0.747750	0.068889	0.018937	0.076238
352	0.410410	0.055556	0.480910	0.790144	0.817460	0.952000	0.088889	0.060097	0.348175
353	0.371274	0.551111	0.385164	0.674658	0.588710	0.642375	0.528889	0.017649	0.236475
354	0.372474	0.155556	0.315480	0.798860	0.865741	0.626375	0.637778	0.022581	0.243879
355	0.376075	0.613333	0.817141	0.561812	0.104815	0.952000	0.175556	0.019747	0.173070
356	0.376875	0.528889	0.383841	1.000751	0.315177	0.647875	0.144444	0.022499	0.227495
357	0.377475	0.637778	0.082010	0.151675	0.071478	0.374250	0.562222	0.012868	0.178802
358	0.379076	0.946667	0.837675	0.598309	0.308853	0.897000	0.266667	0.018602	0.240728
359	0.379676	0.268889	0.764334	0.366142	0.324219	0.711125	0.882222	0.020984	0.305254
360	0.381276	0.040000	0.115038	0.227418	0.088095	0.623375	0.575556	0.017024	0.122660
361	0.381876	0.346667	0.985941	0.049957	0.089662	0.891750	0.702222	0.018679	0.238976
362	0.382476	0.057778	0.786534	0.098835	0.370219	0.644500	0.942222	0.029373	0.379485
363	0.384077	0.428889	0.599511	0.398072	0.402412	0.855750	0.175556	0.026049	0.252829
364	0.384477	0.440000	0.979075	0.982873	0.466088	0.380625	0.284444	0.028227	0.363238
365	0.385877	0.417778	0.775767	0.609626	0.190341	0.740500	0.264444	0.024691	0.276214
366	0.386277	0.024444	0.990804	0.047983	0.677536	0.989750	0.755556	0.034924	0.371419
367	0.386677	0.782222	0.467971	0.937545	0.326296	0.929125	0.160000	0.017252	0.164753
368	0.387277	0.026667	0.990010	0.893476	0.354938	0.677125	0.800000	0.033379	0.332456
369	0.388078	0.342222	0.921084	0.442962	0.663448	0.426250	0.188889	0.035463	0.406238
370	0.388878	0.753333	0.665438	0.630670	0.700711	0.534250	0.584444	0.018872	0.306643
371	0.389078	0.700000	0.668950	0.699316	0.022599	0.880125	0.735556	0.010830	0.124915
372	0.389478	0.415556	0.365922	0.645152	0.798906	0.286500	0.237778	0.025760	0.293548
373	0.389878	0.104444	0.398428	0.796294	0.017974	0.966375	0.106667	0.018614	0.058954

276

374	0.390478	0.033333	0.052134	0.051329	0.714286	0.753000	0.235556	0.034126	0.241840
375	0.390878	0.191111	0.730434	0.066742	0.465686	0.680750	0.615556	0.027020	0.369431
376	0.391278	0.080000	0.240446	0.692750	0.087398	0.910750	0.495556	0.011731	0.056057
377	0.392278	0.642222	0.883542	0.006610	0.675595	0.673125	0.346667	0.025288	0.442896
378	0.392679	0.673333	0.584931	0.285041	0.254902	0.569750	0.040000	0.032027	0.331000
379	0.392879	0.326667	0.933754	0.710022	0.333333	0.682500	0.926667	0.020362	0.305105
380	0.393279	0.320000	0.128082	0.450191	0.896032	0.579875	0.311111	0.021076	0.215467
381	0.394279	0.775556	0.655022	0.268396	0.854575	0.894375	0.413333	0.019687	0.286878
382	0.395079	0.413333	0.716740	0.272586	0.919326	0.612500	0.728889	0.024333	0.483782
383	0.396679	0.315556	0.391632	0.368579	0.905556	0.643375	0.533333	0.022493	0.278656
384	0.397479	0.208889	0.495209	0.109426	0.952381	0.861375	0.597778	0.024554	0.293682
385	0.398680	0.124444	0.857939	0.118774	0.653409	0.652500	0.922222	0.027461	0.396248
386	0.398880	0.402222	0.847139	0.815354	0.689024	0.895625	0.711111	0.020000	0.271280
387	0.399080	0.488889	0.321719	0.758430	0.774476	0.286250	0.182222	0.025252	0.278725
388	0.399480	0.015556	0.316359	0.314549	0.278736	0.917750	0.673333	0.022494	0.151066
389	0.399680	0.951111	0.673882	0.853562	0.086048	0.909625	0.073333	0.018443	0.156295
390	0.400880	0.368889	0.013854	0.022837	0.450893	0.529750	0.451111	0.014809	0.163516
391	0.401480	0.171111	0.391013	0.687840	0.688272	0.304250	0.635556	0.024422	0.290195
392	0.403881	0.611111	0.414870	0.506992	0.613465	0.905000	0.728889	0.014489	0.190904
393	0.338268	0.582222	0.824613	0.885233	0.799645	0.756750	0.137778	0.034667	0.364872
394	0.338468	0.273333	0.098104	0.134029	0.008258	0.438250	0.197778	0.017454	0.188047
395	0.339068	0.042222	0.125991	0.580033	0.216667	0.896750	0.300000	0.017346	0.089872
396	0.340868	0.324444	0.547760	0.182405	0.220370	0.653125	0.553333	0.021043	0.332375
397	0.341268	0.491111	0.545505	0.776762	0.253205	0.401125	0.051111	0.035453	0.402348
398	0.341868	0.373333	0.273226	0.993980	0.989255	0.154625	0.920000	0.017490	0.309899
399	0.342068	0.024444	0.474365	0.690699	0.826023	0.394250	1.000000	0.028877	0.361578
400	0.342268	0.691111	0.692081	0.384102	0.784335	0.926625	0.020000	0.034633	0.356999
401	0.342669	0.011111	0.026376	0.897046	0.810284	0.273000	0.437778	0.033217	0.321287
402	0.343269	0.693333	0.367180	0.866703	0.542535	0.883000	0.477778	0.017039	0.240207

403	0.343869	0.595556	0.366054	0.429792	0.656818	0.535875	0.120000	0.026174	0.330801
404	0.346069	0.260000	0.374159	0.791021	0.908879	0.604750	0.057778	0.042043	0.365207
405	0.346269	0.855556	0.044810	0.322612	0.217372	0.744500	0.273333	0.008422	0.080714
406	0.346469	0.480000	0.350432	0.210429	0.562652	0.939625	0.337778	0.018181	0.221663
407	0.346869	0.022222	0.590683	0.421153	0.186782	0.411500	0.840000	0.031965	0.413464
408	0.348070	0.386667	0.282084	0.503533	0.505848	0.823125	0.842222	0.014254	0.196744
409	0.348870	0.444444	0.518809	0.624190	0.589080	0.622375	0.253333	0.024719	0.323115
410	0.349270	0.835556	0.808729	0.102933	0.598291	0.785125	0.428889	0.020368	0.392470
411	0.349670	0.782222	0.008797	0.044961	0.185897	0.898125	0.520000	0.002824	0.012790
412	0.351270	0.526667	0.405366	0.749456	0.595029	0.714375	0.033333	0.032133	0.299542
413	0.351470	0.591111	0.523954	0.919950	0.234167	0.744000	0.255556	0.018974	0.243812
414	0.356271	0.691111	0.022984	0.189981	0.131609	0.846125	0.111111	0.004704	0.016801
415	0.357271	0.544444	0.741050	0.759661	0.511281	0.652125	0.002222	0.042830	0.394317
416	0.358072	0.831111	0.278459	0.942490	0.916667	0.864750	0.040000	0.023512	0.236062
417	0.358872	0.664444	0.354975	0.589509	0.824266	0.774125	0.297778	0.019054	0.252430
418	0.360072	0.215556	0.456390	0.190628	0.028589	0.385625	0.982222	0.019719	0.357341
419	0.360272	0.362222	0.481376	0.867107	0.550000	0.619750	0.175556	0.027862	0.307262
420	0.362472	0.142222	0.784601	0.731389	0.162602	0.794750	0.977778	0.020511	0.270726
421	0.367073	0.600000	0.396892	0.184235	0.737624	0.639750	0.044444	0.032528	0.354710
422	0.317263	0.428889	0.227673	0.849902	0.974099	0.550750	0.415556	0.019484	0.230063
423	0.317463	0.586667	0.922422	0.642706	0.677165	0.726125	0.211111	0.026706	0.328567
424	0.318064	0.757778	0.801749	0.368577	0.279902	0.575875	0.457778	0.020795	0.334892
425	0.318264	0.713333	0.447803	0.560172	0.532407	0.798750	0.166667	0.021254	0.231188
426	0.319064	0.086667	0.335507	0.859153	0.641667	0.533500	0.484444	0.028777	0.271360
427	0.319864	0.537778	0.545111	0.834670	0.083333	0.442875	0.144444	0.025571	0.295699
428	0.320064	0.377778	0.718167	0.854542	0.254444	0.133250	0.031111	0.046062	0.414449
429	0.320264	0.462222	0.338496	0.932515	0.333333	0.482875	0.215556	0.022197	0.247809
430	0.320664	0.248889	0.138403	0.384814	0.144097	0.201250	0.326667	0.021490	0.243847
431	0.429429	0.311111	0.228811	0.196763	0.386612	0.513500	0.782222	0.017870	0.191815

432	0.430430	0.146667	0.613613	0.282667	0.678839	0.590625	0.953333	0.027053	0.278639
433	0.431431	0.446667	0.245754	0.914159	0.495169	0.660625	0.951111	0.013291	0.163108
434	0.432432	0.031111	0.139463	0.710706	0.642857	0.983000	0.404444	0.030275	0.181101
435	0.433433	0.602222	0.522198	0.384180	0.779557	0.742750	0.062222	0.039465	0.337318
436	0.434434	0.564444	0.787104	0.511780	0.334354	0.640625	0.680000	0.019184	0.232302
437	0.435435	0.848889	0.246492	0.289578	0.056187	0.561500	0.524444	0.011240	0.137050
438	0.436436	0.266667	0.164930	0.335920	0.711765	0.261250	0.060000	0.052920	0.400013
439	0.437437	0.551111	0.771949	0.411348	0.303962	0.615625	0.046667	0.044448	0.411588
440	0.439439	0.337778	0.167022	0.948037	0.530142	0.132125	0.488889	0.021301	0.236426
441	0.441441	0.044444	0.220075	0.306938	0.206250	0.232250	0.131111	0.065396	0.510650
442	0.443443	0.217778	0.655832	0.864684	0.364780	0.692750	0.586667	0.026863	0.256408
443	0.445445	0.755556	0.718131	0.931147	0.832185	0.485500	0.326667	0.023976	0.264141
444	0.446446	0.902222	0.527045	0.860273	0.985192	0.754750	0.100000	0.028732	0.260775
445	0.447447	0.344444	0.647897	0.698046	0.338923	0.221250	0.184444	0.040431	0.391383
446	0.448448	0.504444	0.182298	0.903089	0.125661	0.444500	0.926667	0.011379	0.153957
447	0.449449	0.982222	0.594702	0.557640	0.249563	0.568625	0.853333	0.013145	0.192371
448	0.450450	0.522222	0.329960	0.275880	0.696219	0.275250	0.633333	0.019334	0.234596
449	0.453453	0.688889	0.732463	0.988976	0.151593	0.600625	0.706667	0.016194	0.210536
450	0.454454	0.928889	0.668335	0.181362	0.330502	0.503500	0.924444	0.014370	0.225676
451	0.455455	0.542222	0.045956	0.914920	0.356061	0.833875	0.226667	0.011327	0.082010
452	0.456456	0.391111	0.762745	0.641556	0.998391	0.147125	0.635556	0.025740	0.291911
453	0.457457	0.784444	0.087500	0.926658	0.676941	0.544500	0.673333	0.011273	0.152672
454	0.458458	0.075556	0.802811	0.425385	0.150000	0.819875	0.464444	0.037048	0.305325
455	0.459459	0.175556	0.376549	0.732433	0.839041	0.758750	0.455556	0.030628	0.257677
456	0.460460	0.240000	0.926242	0.992353	0.061198	0.724750	0.506667	0.027334	0.265704
457	0.461461	0.828889	0.095859	0.436815	0.981707	0.663625	0.235556	0.017657	0.177887
458	0.463463	0.942222	0.620189	0.060779	0.266849	0.586625	0.311111	0.020316	0.250904
459	0.465465	0.095556	0.272434	0.724877	0.492647	0.450500	0.093333	0.062480	0.464004
460	0.466466	0.511111	0.059741	0.184946	0.449468	0.391375	0.417778	0.016795	0.179442

461	0.467467	0.044444	0.436958	0.256082	0.591463	0.767750	0.313333	0.050239	0.367702
462	0.468468	0.571111	0.813377	0.832381	0.894543	0.412375	0.848889	0.018951	0.243595
463	0.469469	0.153333	0.959625	0.630520	0.524401	0.299250	0.640000	0.035700	0.367572
464	0.470470	0.131111	0.594118	0.862297	0.174242	0.950000	0.097778	0.042946	0.256965
465	0.471471	0.097778	0.685263	0.758448	0.482323	0.400375	0.344444	0.048188	0.423293
466	0.421284	0.162222	0.538655	0.163873	0.787778	0.829375	0.960000	0.024290	0.239164
467	0.421484	0.808889	0.707877	0.236545	0.413435	0.528875	0.071111	0.035192	0.348457
468	0.421684	0.015556	1.005934	0.172830	0.476908	0.327875	0.035556	0.134847	0.941836
469	0.422084	0.711111	0.875246	0.580176	0.154130	0.219625	0.382222	0.024564	0.314966
470	0.422284	0.697778	0.382919	0.705366	0.008185	0.655875	0.491111	0.012376	0.140434
471	0.422484	0.371111	0.187454	0.062890	0.668465	0.488500	0.428889	0.022976	0.220062
472	0.422885	0.331111	0.974911	0.571419	0.519892	0.836375	0.097778	0.046196	0.383418
473	0.423085	0.277778	0.660899	0.694061	0.334314	0.436500	0.873333	0.022837	0.266785
474	0.423485	0.500000	0.260494	0.062228	0.322917	0.531125	0.804444	0.014898	0.185341
475	0.423685	0.571111	0.825311	0.340644	0.387705	0.482250	0.040000	0.046596	0.435081
476	0.423885	0.708889	0.183913	0.188914	0.343567	0.851750	0.900000	0.008802	0.093120
477	0.424085	0.255556	0.842052	0.654463	0.380288	0.379125	0.164444	0.048150	0.445506
478	0.424285	0.542222	0.244915	0.875288	0.753425	0.809750	0.342222	0.018899	0.180327
479	0.425085	0.304444	0.714636	0.778882	0.283991	0.593125	0.526667	0.026267	0.269887
480	0.425285	0.304444	0.725529	0.169928	0.603509	0.432250	0.720000	0.025812	0.303853
481	0.425685	0.455556	0.892231	0.051574	0.232008	0.324500	0.826667	0.022033	0.326230
482	0.475295	0.253333	0.848282	0.764270	0.723829	0.815625	0.324444	0.029480	0.308745
483	0.475695	0.093333	0.022624	0.766495	0.555556	0.911375	0.362222	0.016262	0.098043
484	0.475895	0.028889	0.430207	0.953788	0.297619	0.863625	0.557778	0.026888	0.199672
485	0.480896	0.328889	0.234982	0.134567	0.216967	0.632500	0.088889	0.027098	0.231976
486	0.481096	0.113333	0.249038	0.131400	0.159314	0.486125	0.595556	0.022575	0.250603
487	0.481296	0.288889	0.309174	0.479534	0.956522	0.850625	0.282222	0.024519	0.237246
488	0.482897	0.091111	0.545256	0.491484	0.241935	0.668500	0.235556	0.039075	0.311332
489	0.483097	0.522222	0.457860	0.972317	0.831579	0.626500	0.348889	0.021004	0.260103

490	0.485897	0.108889	0.025955	0.901253	0.305556	0.881750	0.406667	0.010909	0.055985
491	0.488098	0.060000	0.506677	0.445604	0.214103	0.467250	0.946667	0.025978	0.310174
492	0.488698	0.000000	0.788543	0.492165	0.231481	0.811000	0.742222	0.034748	0.289664
493	0.491898	0.157778	0.295223	0.677521	0.992424	0.342500	0.788889	0.022492	0.266432
494	0.492298	0.831111	0.448159	0.404567	0.057270	0.831125	0.813333	0.009189	0.113104
495	0.501900	0.071111	0.955558	0.885925	0.174731	0.889000	0.773333	0.026001	0.241708
496	0.504501	0.208889	0.049399	0.637862	0.947031	0.103375	0.344444	0.023552	0.239803
497	0.506501	0.620000	0.976649	0.397952	0.297799	0.774000	0.993333	0.017163	0.290311
498	0.506901	0.315556	0.068471	0.360580	0.317511	0.886750	0.362222	0.010440	0.069065
499	0.508702	0.257778	0.593945	0.188487	0.766150	0.220500	0.397778	0.030358	0.396035
500	0.509302	0.540000	0.184106	0.412249	0.595960	0.942750	0.233333	0.015862	0.141285
501	0.509502	0.062222	0.269465	0.678671	0.192308	0.292000	0.373333	0.031967	0.300217
502	0.510302	0.388889	0.594030	0.475019	0.645833	0.802375	0.746667	0.019277	0.268201
503	0.510502	0.080000	0.882179	0.802022	0.052469	0.546875	0.411111	0.037103	0.361143
504	0.510902	0.835556	0.112295	0.006962	0.609776	0.670750	0.748889	0.011429	0.188290
505	0.512302	0.077778	0.344359	0.498384	0.952899	0.418250	0.557778	0.030862	0.308702
506	0.512703	0.753333	0.892863	0.749365	0.741784	0.891625	0.573333	0.018318	0.274624
507	0.514303	0.842222	0.520222	0.881694	0.579032	0.589125	0.811111	0.017208	0.394747
508	0.514703	0.086667	0.493214	0.638060	0.567610	0.811750	0.408889	0.031312	0.266611
509	0.514903	0.106667	0.670511	0.530171	0.268750	0.567375	0.617778	0.028815	0.324864
510	0.516103	0.200000	0.214313	0.730606	0.914141	0.888125	0.191111	0.027319	0.209394
511	0.517103	0.231111	0.432977	0.769383	0.797814	0.472500	0.431111	0.025425	0.284241
512	0.517303	0.428889	0.354567	0.125067	0.983568	0.694750	0.324444	0.023919	0.290629
513	0.519304	0.126667	0.468305	0.902245	0.610215	0.217000	0.662222	0.026168	0.303237
514	0.521304	0.393333	0.743451	0.135154	0.672555	0.169000	0.804444	0.027706	0.639616
515	0.535536	0.151111	0.145320	0.058220	0.080846	0.557500	0.426667	0.020720	0.150673
516	0.536537	0.048889	0.508547	0.888920	0.602713	0.818875	0.948889	0.029881	0.258363
517	0.537538	0.080000	0.298596	0.763674	0.688306	0.105125	0.182222	0.059741	0.485291
518	0.538539	0.613333	0.135006	0.173006	0.278287	0.430375	0.744444	0.012542	0.166300

519	0.539540	0.960000	0.245361	0.947692	0.471774	0.749750	0.813333	0.010116	0.130207
520	0.541542	0.268889	0.191382	0.413826	0.383333	0.662625	0.300000	0.024852	0.198782
521	0.542543	0.322222	0.807384	0.152069	0.920509	0.217250	0.228889	0.041781	0.421213
522	0.544545	0.544444	0.051814	0.558168	0.595139	0.300250	0.597778	0.014214	0.184414
523	0.545546	0.626667	0.702610	0.446368	0.896636	0.296250	0.862222	0.018305	0.252864
524	0.546547	0.875556	0.405862	0.031366	0.205840	0.459500	0.686667	0.014425	0.214090
525	0.547548	0.211111	0.440888	0.977591	0.619565	0.475500	0.555556	0.028184	0.276045
526	0.548549	0.524444	0.977332	0.694569	0.039593	0.855875	0.660000	0.016828	0.171477
527	0.550551	0.595556	0.697191	0.139815	0.514977	0.801750	0.908889	0.016071	0.207800
528	0.552553	0.677778	0.003146	0.525263	0.095411	0.888875	0.395556	0.000097	0.000012
529	0.553554	0.904444	0.150672	0.502182	0.981481	0.523500	0.902222	0.011604	0.165350
530	0.554555	0.428889	0.490980	0.961922	0.456758	0.285250	0.337778	0.027685	0.289710
531	0.555556	0.166667	0.590448	0.509221	0.278509	0.928875	0.946667	0.019612	0.169627
532	0.556557	0.166667	0.377893	0.018182	0.666667	0.637625	0.666667	0.027546	0.258835
533	0.557558	0.273333	0.850364	0.248293	0.028736	0.125125	0.726667	0.027665	0.373188
534	0.558559	0.700000	0.146722	0.214765	0.694779	0.830875	0.840000	0.010788	0.125399
535	0.560561	0.726667	0.533643	0.436539	0.046099	0.565625	0.357778	0.018732	0.219326
536	0.561562	0.602222	0.980034	0.417172	0.411847	0.375375	0.488889	0.024504	0.308812
537	0.562563	0.986667	0.706203	0.093412	0.777006	0.524500	0.037778	0.037363	0.374646
538	0.565566	0.955556	0.936847	0.333583	0.231085	0.541500	0.617778	0.017226	0.252295
539	0.567568	0.080000	0.435035	0.796548	0.154255	0.967000	0.677778	0.019193	0.119980
540	0.570571	0.788889	0.432273	0.074956	0.551515	0.962000	0.806667	0.012444	0.144017
541	0.572573	0.495556	0.465320	0.393255	0.826667	0.399375	0.077778	0.043263	0.370968
542	0.573574	0.860000	0.428222	0.922645	0.256790	0.686625	0.217778	0.019218	0.198759
543	0.577578	0.171111	0.084460	0.029589	0.239247	0.180125	0.384444	0.028049	0.244652
544	0.526705	0.322222	0.945282	0.887545	0.048246	0.542125	0.280000	0.034879	0.357031
545	0.527105	0.680000	0.273996	0.047254	0.931895	0.684375	0.211111	0.024448	0.227634
546	0.527906	0.380000	0.043320	0.956300	0.044985	0.564750	0.013333	0.019538	0.122887
547	0.528706	0.288889	0.340703	0.290247	0.773603	0.127000	0.057778	0.057782	0.450219

548	0.528906	0.184444	0.390843	0.891730	0.100000	0.569375	0.520000	0.024138	0.232381
549	0.529106	0.726667	0.398943	0.275566	0.508357	0.143250	0.882222	0.015419	0.232388
550	0.529706	0.962222	0.921615	0.358727	0.330940	0.755500	0.951111	0.013686	0.196953
551	0.530106	0.155556	0.974657	0.193143	0.817061	0.335125	0.635556	0.036413	0.395481
552	0.530306	0.942222	0.293480	0.733703	0.459834	0.099250	0.133333	0.024682	0.269021
553	0.530506	0.257778	0.863755	0.384103	0.943182	0.711375	0.140000	0.049401	0.424006
554	0.530706	0.995556	0.371536	0.199020	0.979021	0.731750	0.280000	0.019551	0.211661
555	0.530906	0.448889	0.846864	0.007198	0.891638	0.394625	0.166667	0.040328	0.435699
556	0.531106	0.848889	0.451899	0.087176	0.183099	0.636125	0.104444	0.025419	0.241525
557	0.531506	0.780000	0.159333	0.799854	0.631966	0.337875	0.613333	0.013735	0.189215
558	0.531706	1.000000	0.728946	0.438088	0.877589	0.765125	0.662222	0.015662	0.210526
559	0.531906	0.842222	0.016385	0.023391	0.229003	0.255250	0.188889	0.016216	0.172753
560	0.532106	0.406667	0.164115	0.876153	0.750000	0.953625	0.342222	0.017663	0.145129
561	0.532907	0.397778	0.771394	0.194884	0.869919	0.792000	0.620000	0.023897	0.265598
562	0.533107	0.262222	0.144769	0.396578	0.479630	0.605500	0.724444	0.017495	0.174510
563	0.591592	1.000000	0.933192	0.091108	0.465818	0.890875	0.837778	0.015429	0.304341
564	0.593594	0.108889	0.461922	0.209418	0.092424	0.972000	0.462222	0.017617	0.102084
565	0.597598	0.184444	0.920718	0.883588	0.290498	0.729750	0.835556	0.023236	0.296692
566	0.600601	0.117778	0.359376	0.403485	0.862745	0.569625	0.560000	0.027804	0.296105
567	0.603604	0.744444	0.827468	0.529065	0.553591	0.722750	0.404444	0.020762	0.315982
568	0.607608	0.642222	0.408193	0.900960	0.198517	0.810750	0.517778	0.012867	0.153603
569	0.611612	0.208889	0.257580	0.694086	0.717687	0.483500	0.937778	0.018771	0.243410
570	0.620621	0.195556	0.770458	0.053247	0.627451	0.736750	0.482222	0.029783	0.388980
571	0.622623	0.404444	0.303669	0.278694	0.358696	0.939000	0.442222	0.015047	0.144239
572	0.579116	0.475556	0.683488	0.264164	0.002427	0.613500	0.600000	0.018468	0.282333
573	0.579316	0.157778	0.653061	0.546218	0.115462	0.743125	0.826667	0.020940	0.243274
574	0.579516	0.068889	0.475815	0.196840	0.596405	0.702375	0.997778	0.025492	0.298370
575	0.579716	0.717778	0.991710	0.555368	0.644309	0.889625	0.473333	0.020334	0.305817
576	0.582917	0.117778	0.902163	0.686643	0.831633	0.544250	0.715556	0.030151	0.368711

577	0.591718	0.588889	0.341988	0.589365	0.332064	0.604875	0.264444	0.019446	0.231472
578	0.592118	0.291111	0.182214	0.720987	0.568519	0.721125	0.160000	0.024529	0.207027
579	0.593519	0.360000	0.115320	0.826269	0.555085	0.547750	0.235556	0.020124	0.199185
580	0.593919	0.566667	0.371948	0.118979	0.435417	0.917000	0.684444	0.014084	0.182763
581	0.594719	0.035556	0.029326	0.184561	0.355263	0.270875	0.342222	0.030445	0.267514
582	0.594919	0.462222	0.861449	0.223221	0.383880	0.940625	0.562222	0.021055	0.319878
583	0.596319	0.397778	0.798645	0.875828	0.231151	0.769375	0.228889	0.025918	0.270032
584	0.596919	0.377778	0.298510	0.914311	0.656728	0.938625	0.093333	0.025821	0.192147
585	0.597119	0.808889	0.272848	0.609649	0.177171	0.640875	0.026667	0.021954	0.198059
586	0.597319	0.353333	0.849928	0.926368	0.447065	0.764000	0.257778	0.027615	0.294195
587	0.597720	0.686667	0.788268	0.260248	0.350949	0.910625	0.366667	0.019653	0.261487
588	0.597920	0.586667	0.729947	0.639192	0.088095	0.883625	0.193333	0.019892	0.187883
589	0.599720	0.217778	0.147442	0.888536	0.380208	0.971375	0.060000	0.023040	0.115159
590	0.600920	0.024444	0.619210	0.876077	0.461934	0.277000	0.046667	0.094438	0.592048
591	0.602120	0.148889	0.354082	0.041170	0.834699	0.902125	0.668889	0.023406	0.256953
592	0.602320	0.077778	0.617047	0.021409	0.184426	0.662125	0.973333	0.025030	0.324644
593	0.602521	0.648889	0.868413	0.908770	0.820281	0.862375	0.188889	0.025247	0.291464
594	0.603521	0.320000	0.181960	0.324475	0.120031	0.591875	0.104444	0.022939	0.186721
595	0.604521	0.577778	0.224555	0.792676	0.781532	0.864000	0.240000	0.017768	0.181017
596	0.605521	0.524444	0.999247	0.501387	0.896288	0.809125	0.015556	0.045222	0.395005
597	0.606321	0.373333	0.529390	0.369442	0.841146	0.901750	0.988889	0.017654	0.257000
598	0.606721	0.180000	0.014728	0.354438	0.606250	0.417125	0.471111	0.019797	0.199920
599	0.610122	0.713333	0.569653	0.701008	0.373624	0.450125	0.346667	0.021189	0.312188
600	0.612122	0.122222	0.249532	0.820340	0.378415	0.605125	0.326667	0.026825	0.238091
601	0.612322	0.242222	0.394393	0.125871	0.041971	0.403250	0.684444	0.020578	0.311225
602	0.612723	0.244444	0.462733	0.250569	0.725962	0.655500	0.437778	0.026269	0.307114
603	0.615123	0.111111	0.066561	0.332107	0.945652	0.686500	0.015556	0.058461	0.351527
604	0.643644	0.313333	0.989896	0.338275	0.585632	0.922875	0.622222	0.025350	0.261738
605	0.644645	0.611111	0.315225	0.899213	0.532986	0.644625	0.662222	0.014981	0.182144

606	0.645646	0.106667	0.614452	0.088283	0.391975	0.529500	0.171111	0.056709	0.484882
607	0.646647	0.064444	0.217502	1.005061	0.127104	0.203250	0.262222	0.042852	0.406570
608	0.647648	0.295556	0.502541	0.225441	0.861337	0.089125	0.860000	0.023803	0.283695
609	0.648649	0.355556	0.709977	0.020583	0.959163	0.343375	0.951111	0.022810	0.307828
610	0.650651	0.935556	0.281522	0.729704	0.279540	0.308250	0.102222	0.024851	0.261163
611	0.651652	0.284444	0.026201	0.238864	0.498792	0.948000	0.144444	0.018383	0.090704
612	0.652653	0.991111	0.462303	0.260123	0.463941	0.366375	0.797778	0.014324	0.220182
613	0.653654	0.093333	0.658709	0.184792	0.768315	0.425375	0.464444	0.044351	0.412129
614	0.654655	0.593333	0.923633	0.862550	0.575581	0.266250	0.642222	0.021969	0.277182
615	0.657658	0.317778	0.921337	0.455285	0.936620	0.908875	0.900000	0.022356	0.247173
616	0.658659	0.724444	0.203166	0.465202	0.610990	0.533500	0.786667	0.012984	0.175896
617	0.660661	0.957778	0.308304	0.078250	0.827206	0.690750	0.122222	0.024781	0.232027
618	0.662663	0.408889	0.908816	0.547093	0.057832	0.765750	0.035556	0.045488	0.370064
619	0.663664	0.282222	0.777519	0.412029	0.003501	0.960000	0.813333	0.013814	0.101574
620	0.668669	0.317778	0.190912	0.075921	0.250000	0.774750	0.228889	0.021142	0.142592
621	0.670671	0.197778	0.347812	0.947284	0.212025	0.718750	0.917778	0.016977	0.171210
622	0.671672	0.933333	0.137702	0.181729	0.841975	0.210250	0.604444	0.014017	0.199980
623	0.672673	0.344444	0.673306	0.199936	0.048826	0.068125	0.204444	0.038267	0.437484
624	0.675676	0.217778	0.716009	0.753095	0.354938	0.499500	0.088889	0.056628	0.477557
625	0.676677	0.951111	0.750487	0.963668	0.433117	0.620625	0.382222	0.019352	0.231937
626	0.677678	0.448889	0.303278	0.842394	0.243659	0.462500	0.215556	0.026053	0.253151
627	0.678679	0.115556	0.855428	0.961797	0.665000	0.197250	0.533333	0.041528	0.401395
628	0.679680	0.480000	0.521756	0.019847	0.498555	0.263250	0.762222	0.020467	0.280842
629	0.680681	0.806667	0.977279	0.515747	0.986472	0.982000	0.337778	0.022925	0.244526
630	0.681682	0.015556	0.430307	0.317676	0.481061	0.481500	0.515556	0.049510	0.412835
631	0.682683	0.302222	0.254524	0.240473	0.032780	0.243250	0.251111	0.028355	0.287994
632	0.683684	0.397778	0.166295	0.361344	0.054207	0.889875	0.113333	0.009142	0.028737
633	0.631726	0.753333	0.088595	0.211307	0.259306	0.606500	0.655556	0.009729	0.116048
634	0.631926	0.571111	0.684767	0.772282	0.013248	0.986250	0.180000	0.015800	0.093748

285

635	0.632126	0.368889	0.440039	0.756619	0.717681	0.266000	0.451111	0.026706	0.281298
636	0.632326	0.757778	0.219809	0.737693	0.697415	0.844750	0.126667	0.021810	0.185560
637	0.632527	0.473333	0.322637	0.285769	0.948198	0.496500	0.248889	0.029089	0.268933
638	0.632727	0.160000	0.603142	0.916179	0.702941	0.685875	0.617778	0.030635	0.283206
639	0.632927	0.235556	0.841131	0.938894	0.529614	0.718375	0.640000	0.027913	0.279400
640	0.633127	0.168889	0.822870	0.400383	0.278907	0.106250	0.097778	0.063740	0.568438
641	0.633327	0.386667	0.432092	0.070867	0.871212	0.651125	0.864444	0.019518	0.231599
642	0.633527	0.226667	0.073311	0.470930	0.129781	0.992750	0.017778	0.005538	0.005923
643	0.633727	0.724444	0.900954	0.371511	0.510763	0.199000	0.735556	0.019325	0.281344
644	0.633927	0.953333	0.417759	0.986423	0.236010	0.790000	0.357778	0.013983	0.149389
645	0.634327	0.588889	0.175612	0.796806	0.221655	0.824125	0.388889	0.011041	0.091111
646	0.634527	0.075556	0.961316	0.209121	0.234375	0.894000	0.302222	0.045191	0.366809
647	0.634727	0.331111	0.606831	0.428494	0.724462	0.873125	0.997778	0.018755	0.206089
648	0.634927	0.340000	0.963347	0.239535	0.873620	0.953750	0.526667	0.027074	0.280626
649	0.635327	0.742222	0.899996	0.774063	0.995455	0.995000	0.588889	0.018460	0.207486
650	0.635527	0.742222	0.925019	0.985825	0.671725	0.717000	0.466667	0.021107	0.241858
651	0.635727	0.466667	0.731627	0.082892	0.618896	0.344125	0.037778	0.052556	0.502117
652	0.635927	0.324444	0.260645	0.992633	0.838685	0.661375	0.293333	0.027158	0.247133
653	0.636127	0.455556	0.449701	0.479083	0.141870	0.470750	0.488889	0.020898	0.238222
654	0.636327	0.251111	0.476378	0.756367	0.176011	0.086375	0.582222	0.026527	0.311113
655	0.636527	0.951111	0.026108	0.852912	0.317493	0.556500	0.537778	0.008682	0.108280
656	0.637327	0.208889	0.719649	0.865512	0.314565	0.648500	0.375556	0.034327	0.316642
657	0.637728	0.884444	0.131149	0.361980	0.931973	0.880750	0.386667	0.013437	0.142301
658	0.638128	0.740000	0.528734	0.876936	0.090256	0.194250	0.417778	0.019910	0.272937
659	0.638328	0.135556	0.424901	0.502623	0.552564	0.764750	0.075556	0.059859	0.410856
660	0.638528	0.573333	0.121521	0.015072	0.210276	0.464500	0.675556	0.012514	0.156585
661	0.638928	0.884444	0.166124	0.555166	0.544393	0.407625	0.017778	0.032290	0.283072
662	0.714743	0.468889	0.572033	0.760397	0.419919	0.547125	0.337778	0.026329	0.269863
663	0.716343	0.055556	0.732534	0.498772	0.079932	0.994375	0.653333	0.022311	0.145571

664	0.716943	0.222222	0.976095	0.507008	0.584596	0.657125	0.208889	0.038719	0.385519
665	0.718344	0.473333	0.470276	0.779188	0.264840	0.983250	0.853333	0.011627	0.127414
666	0.718944	0.195556	0.603712	0.875863	0.759091	0.550875	0.282222	0.032573	0.318959
667	0.720144	0.044444	0.834304	0.574177	0.923469	0.965000	0.155556	0.064192	0.408086
668	0.720744	0.711111	0.109924	0.853139	0.409184	0.425250	0.508889	0.013410	0.199944
669	0.720944	0.260000	0.606680	0.751651	0.007310	0.706375	0.626667	0.018137	0.215324
670	0.721744	0.153333	0.628810	0.834191	0.754016	0.707000	0.680000	0.024922	0.284061
671	0.721944	0.051111	0.095783	0.355352	0.443548	0.890375	0.431111	0.019509	0.122805
672	0.722344	0.786667	0.863315	0.687580	0.070847	0.775000	0.131111	0.023102	0.254588
673	0.722545	0.317778	0.198640	0.786178	0.852041	0.711500	0.144444	0.026993	0.234790
674	0.723145	0.337778	0.630126	0.348539	0.107323	0.799375	0.253333	0.023638	0.230081
675	0.724945	0.380000	0.256268	0.007978	0.333634	0.213875	0.177778	0.028371	0.350949
676	0.725145	0.348889	0.959413	0.398036	0.390504	0.712125	0.731111	0.022575	0.351294
677	0.725545	0.568889	0.370106	0.922823	0.138686	0.375125	0.564444	0.016460	0.256015
678	0.726745	0.008889	0.941931	0.013771	0.344203	0.678750	0.237778	0.062822	0.558555
679	0.727145	0.273333	0.210882	0.370931	0.824297	0.831375	0.595556	0.018181	0.201366
680	0.727546	0.402222	0.203181	0.208589	0.350295	0.780125	0.640000	0.013720	0.157587
681	0.729546	0.084444	0.466373	0.493257	0.278205	0.544750	0.560000	0.028812	0.295516
682	0.729946	0.875556	0.938026	0.016824	0.844810	0.877375	0.375556	0.022036	0.410242
683	0.730146	0.344444	0.300070	0.277115	0.471905	0.373500	0.062222	0.036894	0.341023
684	0.730546	0.340000	0.419545	0.636539	0.063725	0.756125	0.057778	0.028054	0.194136
685	0.731346	0.964444	0.368389	0.730375	0.069600	0.792500	0.368889	0.010612	0.118986
686	0.706707	0.191111	0.712484	0.465990	0.498428	0.633625	0.275556	0.034460	0.350951
687	0.723724	0.333333	0.529530	0.296296	0.131356	0.887875	0.015556	0.035630	0.216273
688	0.725726	0.426667	0.572792	0.317176	0.941419	0.500500	0.722222	0.021244	0.343209
689	0.731732	0.988889	0.114227	0.687373	0.165978	0.672625	0.351111	0.009209	0.109205
690	0.732733	0.502222	0.727516	0.381011	0.151802	0.872875	0.411111	0.018588	0.215578
691	0.684737	0.417778	0.834660	0.978645	0.569444	0.898375	0.282222	0.024598	0.267115
692	0.685937	0.602222	0.146187	0.155590	0.781346	0.427500	0.384444	0.018452	0.258099

693	0.688938	0.746667	0.956867	0.995861	0.149729	0.564375	0.226667	0.023979	0.330649
694	0.689338	0.328889	0.098155	0.717370	0.356410	0.423500	0.440000	0.017040	0.194390
695	0.710711	0.742222	0.697732	0.656666	0.198029	0.703750	0.060000	0.037722	0.517060
696	0.713714	0.191111	0.001266	0.560974	0.680303	0.800750	0.426667	0.015127	0.120330
697	0.684337	0.126667	0.638895	0.076703	0.792793	0.712750	0.608889	0.030319	0.379444
698	0.686337	0.382222	0.937336	0.868003	0.238506	0.784750	0.931111	0.018229	0.265510
699	0.003003	0.224444	0.045360	0.300447	0.101852	0.803750	0.402222	0.005692	0.023482
700	0.046409	0.135556	0.895051	0.553781	0.134259	0.351875	0.493333	0.030692	0.377364
701	0.059212	0.688889	0.147926	0.370472	0.576176	0.837625	0.840000	0.009600	0.102815
702	0.125125	0.113333	0.487028	0.735033	0.843220	0.854875	0.362222	0.030556	0.251821
703	0.195239	0.273333	0.945191	0.231794	0.924048	0.151375	0.771111	0.028003	0.390159
704	0.188638	0.840000	0.884317	0.568731	0.414843	0.096875	0.862222	0.016656	0.245928
705	0.217043	0.180000	0.712199	0.007740	0.240637	0.816625	0.877778	0.023048	0.230201
706	0.528106	0.128889	0.621197	0.416268	0.220149	0.921625	0.553333	0.022981	0.219937
707	0.531532	0.691111	0.855196	0.528633	0.162242	0.359375	0.280000	0.027038	0.325083
708	0.534535	0.584444	0.563628	0.388670	0.805556	0.892875	0.424444	0.021166	0.213357
709	0.495495	0.435556	0.006624	0.460809	0.742938	0.585625	0.817778	0.012462	0.143031
710	0.323065	0.286667	0.485518	0.688043	0.406627	0.399500	0.302222	0.026944	0.301478
711	0.425425	0.333333	0.411229	0.192503	0.133333	0.336375	0.000000	0.059491	0.491138
712	0.426426	0.566667	0.113304	0.066333	0.915692	0.539500	0.880000	0.013485	0.173962
713	0.427427	0.875556	0.891587	0.307406	0.619478	0.554500	0.931111	0.015664	0.234522
714	0.428428	0.348889	0.842677	0.311770	0.327909	0.659625	0.484444	0.027108	0.289951
715	0.521504	0.022222	0.224946	0.674521	0.190476	0.917375	0.731111	0.015501	0.089886
716	0.522505	0.797778	0.039473	0.140558	0.287341	0.695750	0.360000	0.009660	0.097492
717	0.522705	0.664444	0.301550	0.457559	0.933333	0.475500	0.295556	0.020904	0.270351
718	0.524505	0.675556	0.336129	0.134438	0.432249	0.514500	0.848889	0.016650	0.346890
719	0.530531	0.773333	0.881690	0.545566	0.414444	0.804750	0.980000	0.014355	0.191468
720	0.531532	0.984444	0.575914	0.792039	0.104182	0.094125	0.231111	0.022688	0.296183
721	0.532533	0.628889	0.399908	0.013657	0.884409	0.497500	0.055556	0.040292	0.347414

722	0.713343	0.671111	0.113971	0.303766	0.522331	0.862125	0.195556	0.014352	0.132537
723	0.686687	0.444444	0.105105	0.143143	0.883648	0.904875	0.400000	0.015927	0.166398
724	0.693694	0.024444	0.519796	0.084713	0.042398	0.405375	0.728889	0.032377	0.392808
725	0.616923	0.100000	0.979455	0.489863	0.170091	0.874125	0.962222	0.023609	0.261459
726	0.617323	0.344444	0.116611	0.435471	0.063953	0.993375	0.573333	0.000455	0.000180
727	0.642643	0.204444	0.108265	0.893452	0.768519	0.619625	0.006667	0.056376	0.418440
728	0.687337	0.717778	0.744013	0.263685	0.019588	0.892000	0.513333	0.012995	0.149334
729	0.692739	0.006667	0.912827	0.158668	0.030488	0.781375	0.140000	0.070739	0.446739
730	0.194639	0.764444	0.415951	0.767385	0.365385	0.562875	0.604444	0.014889	0.224634
731	0.194839	0.813333	0.405404	0.891190	0.021368	0.807000	0.740000	0.007862	0.096757
732	0.215215	0.326667	0.939860	0.535848	0.015915	0.093125	0.395556	0.033950	0.403061
733	-0.049734	0.157778	0.004422	0.427442	0.384409	0.527500	0.108889	0.028299	0.225920
734	-0.048733	0.811111	0.817226	0.352913	0.818525	0.936875	0.637778	0.014825	0.166482
735	0.144144	0.368889	0.589866	0.183900	0.594398	0.340375	0.317778	0.027780	0.365626
736	0.194039	0.926667	0.151627	0.406855	0.683579	0.538875	0.793333	0.011122	0.181952
737	0.583584	0.073333	0.723611	0.621099	0.899718	0.764750	0.222222	0.049617	0.372045
738	0.272855	0.026667	0.809609	0.938537	0.138889	0.817375	0.688889	0.034965	0.281050
739	0.273455	0.471111	0.977296	0.016472	0.180969	0.098000	0.568889	0.026626	0.375948
740	0.387387	0.640000	0.365528	0.945602	0.558712	0.938000	0.320000	0.016111	0.169527
741	0.388388	0.022222	0.674159	0.742125	0.843333	0.314375	0.186667	0.067875	0.470019
742	0.639640	0.595556	0.535623	0.893000	0.997053	0.388375	0.520000	0.021501	0.250399
743	0.128826	0.226667	0.123419	0.399820	0.311983	0.336625	0.717778	0.017803	0.209217
744	0.129226	0.435556	0.113511	0.251923	0.170168	0.685500	0.173333	0.014445	0.115209
745	0.114114	0.131111	0.859012	0.561691	0.977273	0.943000	0.820000	0.025127	0.286389
746	0.063013	0.222222	0.017449	0.614891	0.111502	0.602875	0.168889	0.015643	0.094042
747	0.128128	0.066667	0.076493	0.933273	0.231013	0.240250	0.542222	0.022267	0.218198
748	0.043043	0.733333	0.307927	0.002477	0.727954	0.306250	0.066667	0.027338	0.322551
749	-0.048126	0.146667	0.876959	0.412573	0.093602	0.221875	0.642222	0.031639	0.350189
750	-0.047726	0.122222	0.356019	0.273286	0.555556	0.539125	0.268889	0.036109	0.325793

751	0.378378	0.111111	0.966079	0.466836	0.865530	0.654625	0.988889	0.027520	0.363816
752	0.384384	0.457778	0.922841	0.971862	0.328483	0.914875	0.677778	0.017826	0.226604
753	0.427886	0.228889	0.534214	0.965900	0.709064	0.567500	0.131111	0.049043	0.407043
754	0.486486	0.364444	0.625352	0.223017	0.348485	0.954000	0.162222	0.026900	0.232619
755	0.694539	0.208889	0.487062	0.468627	0.039683	0.861000	0.315556	0.018888	0.136016
756	0.017403	0.248889	0.097334	0.378984	0.771127	0.801500	0.177778	0.028156	0.193278
757	0.321264	0.417778	0.737722	0.288253	0.680723	0.805750	0.484444	0.023017	0.309666
758	-0.050735	0.168889	0.553105	0.204408	0.377637	0.283250	0.960000	0.023027	0.270504
759	0.634635	0.408889	0.875143	0.044079	0.818352	0.779750	0.975556	0.020378	0.272107
760	-0.046125	0.337778	0.284595	0.007255	0.878662	0.104375	0.677778	0.019351	0.227739
761	0.214214	0.151111	0.707453	0.588866	0.521667	0.552500	0.108889	0.060382	0.468958
762	0.426885	0.548889	0.361528	0.674695	0.637550	0.763000	0.042222	0.037977	0.294404
763	0.507508	0.453333	0.548878	0.176426	0.522464	0.436375	0.268889	0.027046	0.361995
764	0.515516	0.500000	0.465664	0.347449	0.517521	0.573625	0.877778	0.019009	0.384412
765	0.516517	0.222222	0.474039	0.289410	0.363126	0.255250	0.368889	0.029319	0.361360
766	0.686937	0.531111	0.928569	0.930773	0.714674	0.369875	0.917778	0.019451	0.340968
767	0.195039	0.271111	0.446431	0.056607	0.627252	0.167250	0.455556	0.030585	0.368509
768	0.404081	0.822222	0.562540	0.514784	0.480820	0.909375	0.351111	0.017034	0.213169
769	0.427085	0.197778	0.743097	0.907563	0.951031	0.810750	0.075556	0.060573	0.443579
770	0.425885	0.051111	0.543810	0.625273	0.936047	0.975375	0.491111	0.041401	0.305299
771	0.494494	0.393333	0.686888	0.040164	0.904321	0.555500	0.273333	0.030344	0.415869
772	0.194239	0.084444	0.430405	0.514181	0.209459	0.435250	0.837778	0.028635	0.329603
773	0.534307	0.448889	0.734447	0.352453	0.306061	0.540500	0.002222	0.056650	0.479570
774	0.533907	0.308889	0.519206	0.447596	0.218680	0.516750	0.224444	0.034580	0.319847
775	0.426485	0.206667	0.520744	0.455701	0.884085	0.085000	0.313333	0.041466	0.374881
776	0.018004	0.104444	0.219905	0.678466	0.169540	0.558250	0.906667	0.018656	0.170121
777	0.615723	0.371111	0.032583	0.885596	0.361684	0.692125	0.340000	0.012556	0.112539
778	0.640641	0.664444	0.112428	0.800311	0.987374	0.233250	0.562222	0.015310	0.200988
779	0.641642	0.215556	0.259947	0.918920	0.111111	0.721750	0.322222	0.020108	0.159760

780	0.687738	0.673333	0.925279	0.662759	0.766026	0.925625	0.544444	0.019379	0.286633
781	0.686737	0.780000	0.687654	0.609442	0.158382	0.537250	0.926667	0.015046	0.279644
782	0.357471	0.848889	0.837322	0.908743	0.184821	0.579125	0.162222	0.023558	0.348296
783	0.616123	0.962222	0.997854	0.838145	0.516816	0.616375	0.406667	0.019993	0.326147

Table E. 2 Waterside meta-model data

Case#	D1	Pl/D1	LR	θ	Velocity	Nu_CFD	ADP/Segment_CFD
	[-]	[-]	[-]	[-]	[-]	[-]	[Pa]
1	0.53106	0.29259	0.69138	0.36874	0.56713	27.13	346.79
2	0.58517	0.45892	0.05411	0.29259	0.90381	44.05	438.37
3	0.98196	0.75752	0.41683	0.05411	0.81162	40.87	1257.90
4	0.06012	0.63327	0.41884	0.59118	0.40882	13.20	414.32
5	0.60321	0.07816	0.96393	0.84168	0.11824	15.27	28.91
6	0.72946	0.21242	0.21643	0.50701	0.22846	24.28	44.99
7	0.22846	0.56914	0.94389	0.51303	0.77355	22.45	913.34
8	0.18437	0.92585	0.85772	0.57515	0.13828	7.73	110.35
9	0.53908	0.72144	0.61924	0.71343	0.44088	28.34	239.58
10	0.40882	0.60120	0.01002	0.15030	0.69739	25.01	461.39
11	0.65731	0.68136	0.20240	0.71743	0.47695	39.67	188.03
12	0.60922	0.08617	0.75752	0.60521	0.57315	37.21	299.43
13	0.59519	0.81964	0.55511	0.23046	0.32064	16.43	214.50
14	0.54509	0.84770	0.89780	0.14429	0.22044	10.50	235.74
15	0.65331	0.76353	0.28858	0.82565	0.15230	20.32	32.23
16	0.72745	0.43888	0.03808	0.52305	0.41483	37.09	106.11
17	0.39880	0.11824	0.27455	0.71142	0.36473	29.12	135.53
18	0.55912	0.22244	0.48697	0.96192	0.70140	55.83	519.28
19	0.60721	0.88577	0.27054	0.73547	0.80361	51.24	501.79
20	0.59920	0.42485	0.49699	0.77956	0.03607	8.02	1.92
21	0.69739	0.80160	0.35872	0.19439	0.54910	26.98	395.78

22	0.07214	0.28056	0.19238	0.51102	0.24649	11.26	138.89
23	0.06413	0.09018	0.89980	0.79559	0.62325	18.10	746.80
24	0.32265	0.36072	0.65531	0.57315	0.67735	28.03	502.25
25	0.41884	0.12625	0.23447	0.27255	0.09218	8.63	18.84
26	0.54108	0.98998	0.38277	0.22645	0.18838	11.20	102.70
27	0.43287	0.62725	0.07615	0.83768	0.67936	47.31	360.84
28	0.95792	0.87375	0.92786	0.63727	0.05210	8.22	6.78
29	0.76553	0.86373	0.34469	0.55711	0.02204	5.42	3.34
30	0.39479	0.04810	0.95391	0.85371	0.89178	45.98	984.45
31	0.89379	0.62525	0.76152	0.94790	0.82164	62.53	599.05
32	0.44890	0.53307	0.02806	0.54108	0.38878	28.46	121.95
33	0.66533	0.95792	0.31062	0.59920	0.48898	34.52	229.12
34	0.08417	0.26453	0.71944	0.50301	0.82365	18.38	1037.48
35	0.81563	0.60321	0.26052	0.37475	0.10822	13.09	18.52
36	0.88778	0.83166	0.80561	0.44088	0.84369	48.30	695.54
37	0.01403	0.59519	0.63928	0.41483	0.18236	6.19	267.23
38	0.49699	0.67936	0.44489	0.98798	0.83768	53.15	683.25
39	0.57715	0.35471	0.67535	0.91583	0.33667	30.16	151.42
40	0.89178	0.50100	0.97796	0.89780	0.60321	47.75	367.34
41	0.80962	0.82365	0.07816	0.38076	0.05611	9.78	4.69
42	0.92184	0.89980	0.32465	0.32665	0.90180	51.69	610.81
43	0.57315	0.76754	0.31864	0.63928	0.30261	24.71	105.98
44	0.58116	0.86974	0.52705	0.49900	0.49900	28.22	295.26
45	0.74749	0.07615	0.00601	0.57114	0.05812	14.56	0.99
46	0.06814	0.40281	0.88978	0.34469	0.84569	14.47	1607.03
47	0.17234	0.38477	0.47695	0.48096	0.17435	9.55	88.31
48	0.84770	0.38677	0.26253	0.15631	0.76553	40.92	494.91
49	0.19038	0.68737	0.75150	0.91182	0.08417	7.34	36.72
50	0.07615	0.93387	0.12826	0.47495	0.33467	12.05	266.42

51	0.88176	0.58517	0.43888	0.84569	0.44689	44.11	181.05
52	0.80561	0.54509	0.39078	0.72144	0.14830	20.51	28.70
53	0.36473	0.16232	0.52906	0.51503	0.76954	33.96	502.04
54	0.75150	0.02405	0.64930	0.39078	0.12425	12.18	21.32
55	0.11222	0.51102	0.04810	0.45892	0.73948	22.94	544.25
56	0.05611	0.42685	0.88377	0.94589	0.64529	18.35	918.43
57	0.09218	0.48697	0.70541	0.56313	0.69339	17.33	868.57
58	0.89980	0.30661	0.43487	0.03607	0.23647	14.70	188.45
59	0.54309	0.02204	0.13627	0.64729	0.96192	70.14	615.96
60	0.65932	0.16032	0.36473	0.69940	0.76353	57.86	443.82
61	0.22044	0.74749	0.67335	0.68537	0.76152	25.67	801.52
62	0.74148	0.27455	0.54509	0.13828	0.71543	34.24	619.32
63	0.85571	0.95992	0.45090	0.80160	0.72545	55.40	442.79
64	0.96192	0.23647	0.81964	0.44489	0.86172	53.82	535.72
65	0.02605	0.47896	0.30261	0.33467	0.64128	12.33	902.89
66	0.97595	0.20842	0.68337	0.47695	0.06613	10.45	7.03
67	0.64529	0.40481	0.05010	0.13226	0.25251	15.51	85.50
68	0.17836	0.08417	0.14429	0.56513	0.20641	14.47	66.45
69	0.31463	0.81162	0.07415	0.63126	0.78758	38.34	491.57
70	0.95591	0.52705	0.72946	0.70541	0.88377	60.95	604.29
71	0.56313	0.47495	0.03006	0.34870	0.10621	12.52	16.43
72	0.50701	0.06012	0.50301	0.70341	0.55912	40.26	306.53
73	0.25251	0.17836	0.66533	0.32265	0.83166	23.57	783.48
74	0.57916	0.40882	0.07014	0.91784	0.94389	75.16	607.88
75	0.95391	0.82966	0.59920	0.62926	0.11623	15.91	24.67
76	0.35271	0.58317	0.19038	0.72345	0.86974	43.77	588.88
77	0.42285	0.40681	0.28657	0.10020	0.09619	6.45	55.02
78	0.47094	0.99599	0.08818	0.66733	0.66333	40.22	344.01
79	0.48096	0.79559	0.81363	0.81764	0.61122	32.16	468.02

80	0.75952	0.99198	0.55711	0.87174	0.34269	30.75	147.92
81	0.50301	0.98397	0.22244	0.92585	0.98397	58.79	747.15
82	0.61323	0.25651	0.82966	0.77355	0.40281	30.75	197.59
83	0.37876	0.39078	0.20040	0.73747	0.50301	33.25	231.79
84	0.92585	0.00401	0.59719	0.91984	0.20040	34.05	68.54
85	0.94790	0.31263	0.55912	0.27856	0.86373	49.39	547.86
86	0.93387	0.79158	0.88577	0.73948	0.74749	52.52	542.90
87	0.69138	0.73747	0.72144	0.22846	0.16633	11.13	89.10
88	0.29459	0.34669	0.78958	0.69138	0.50701	23.54	361.76
89	0.39078	0.44689	0.70741	0.07615	0.54309	16.71	938.23
90	0.84970	0.33267	0.85371	0.33267	0.15832	13.40	49.33
91	0.73747	0.34469	0.18236	0.89579	0.52305	55.29	223.29
92	0.82766	0.60721	0.31463	0.80561	0.75752	61.79	406.50
93	0.21844	0.63126	0.71343	0.93186	0.99800	35.11	1222.45
94	0.79960	0.33667	0.50902	0.27455	0.40681	25.78	178.27
95	0.67335	0.29659	0.33467	0.53307	0.03006	5.75	4.35
96	0.96994	0.96994	0.24449	0.30661	0.03407	5.70	0.66
97	0.97996	0.39279	0.86974	0.56914	0.13427	15.61	26.96
98	0.66132	0.64529	0.83367	0.15832	0.87174	35.77	1274.50
99	0.70541	0.43086	0.74749	0.25651	0.47896	25.04	315.76
100	0.87776	0.87575	0.65932	0.69539	0.55110	41.81	306.33
101	0.19439	0.73146	0.25251	0.81964	0.39479	21.70	236.96
102	0.16834	0.13627	0.58918	0.98397	0.77956	35.07	980.77
103	0.56112	0.37675	0.76754	0.88978	0.04208	7.42	3.38
104	0.49900	0.31062	0.22044	0.90982	0.02605	8.22	4.11
105	0.84569	0.88176	0.45491	0.29860	0.20240	15.81	73.44
106	0.66333	0.55511	0.30461	0.98998	0.35471	39.19	136.14
107	0.87575	0.85571	0.41082	0.67936	0.32866	31.60	113.83
108	0.13226	0.89579	0.87174	0.92986	0.37675	15.34	405.44

109	0.81764	0.30862	0.42685	0.87575	0.86774	70.82	574.63
110	0.87174	0.73347	0.49900	0.58317	0.70942	50.27	403.43
111	0.96593	0.83367	0.13828	0.74549	0.57114	56.25	218.15
112	0.87976	0.72745	0.99800	0.90782	0.98798	61.74	895.34
113	0.94990	0.80962	0.29259	0.97194	0.46693	52.73	191.63
114	0.18036	0.51503	0.53707	0.51703	0.93186	26.67	1017.45
115	0.67735	0.52305	0.57114	0.60321	0.70741	44.34	429.33
116	0.47896	0.00000	0.95190	0.58717	0.06012	7.39	9.51
117	0.31263	0.45291	0.37475	0.81563	0.80160	39.61	610.37
118	0.30862	0.56513	0.98397	0.87776	0.75952	31.06	793.19
119	0.62926	0.71743	0.42084	0.84369	0.66533	46.90	396.73
120	0.65130	0.72345	0.89379	0.60922	0.92385	47.22	844.53
121	0.79760	0.51703	0.47896	0.09018	0.68537	33.05	777.19
122	0.78557	0.19439	0.66132	0.79960	0.26653	30.03	91.52
123	0.21242	0.69940	0.24248	0.40481	0.12224	8.41	51.19
124	0.63327	0.24048	0.51102	0.44890	0.80561	44.86	466.82
125	0.24048	0.25451	0.20441	0.57715	0.47495	24.13	222.92
126	0.93788	0.03407	0.87375	0.16433	0.46493	28.03	275.22
127	0.45691	0.49900	0.46092	0.54709	0.60120	31.53	347.07
128	0.34469	0.64128	0.62525	0.16633	0.73547	21.23	1078.27
129	0.36273	0.41283	0.07214	0.25251	0.24850	14.32	88.56
130	0.46293	0.47094	0.13026	0.19038	0.46894	20.85	244.97
131	0.61122	0.71944	0.80962	0.75351	0.01202	4.13	2.28
132	0.80762	0.48497	0.29659	0.35271	0.30461	23.74	88.99
133	0.64128	0.64729	0.01403	0.14830	0.43687	22.93	197.97
134	0.41283	0.35070	0.27655	0.63327	0.24048	20.43	71.91
135	0.14429	0.43487	0.45291	0.62325	0.59920	20.96	504.51
136	0.86974	0.03808	0.63527	0.39279	0.52705	37.72	204.79
137	0.71543	0.30060	0.42886	0.65130	0.36874	33.01	126.47

138	0.85772	0.44489	0.64529	0.84970	0.29058	31.46	98.68
139	0.73948	0.79359	0.04008	0.51904	0.96994	62.60	479.82
140	0.76152	0.30461	0.78557	0.61924	0.24449	22.07	74.77
141	0.84369	0.18236	0.41283	0.47295	0.12024	15.38	16.66
142	0.31663	0.42084	0.30661	0.53507	0.71343	31.06	436.89
143	0.10621	0.93788	0.36273	0.68938	0.62725	20.24	669.27
144	0.37675	0.49299	0.74950	0.11022	0.21844	8.86	250.43
145	0.36072	0.90581	0.08617	0.78758	0.18637	18.67	53.95
146	0.28457	0.09619	0.91984	0.57916	0.78958	29.18	689.69
147	0.67936	0.05411	0.09419	0.66934	0.57715	59.07	247.03
148	0.68537	0.10020	0.82766	0.31463	0.41884	23.83	199.12
149	0.74349	0.38277	0.81563	0.97996	0.97996	66.32	887.32
150	0.63727	0.32265	0.94589	0.94389	0.57515	41.54	388.94
151	0.23447	0.95591	0.21443	0.98597	0.39279	25.61	242.72
152	0.42485	0.46293	0.58116	0.96994	0.78557	46.82	657.65
153	0.45892	0.67335	0.67735	0.82766	0.94990	46.72	880.26
154	0.52906	0.09820	0.98196	0.74950	0.40481	28.44	216.76
155	0.24248	0.89178	0.17635	0.10421	0.55311	14.31	755.80
156	0.31062	0.42886	0.73347	0.43888	0.84770	28.15	827.72
157	0.33267	0.25852	0.84168	0.25451	0.60521	19.52	602.00
158	0.29058	0.44289	0.12024	0.53106	0.17034	14.30	46.15
159	0.70942	0.42285	0.54108	0.65932	0.91984	57.12	625.33
160	0.49299	0.18838	0.10220	0.49299	0.26052	23.30	59.04
161	0.75551	0.31864	0.70942	0.63527	0.78357	51.26	487.97
162	0.28056	0.96794	0.88778	0.29459	0.82565	21.68	1421.19
163	0.85170	0.21443	0.25451	0.47896	0.51303	43.20	162.57
164	0.51303	0.39880	0.84770	0.67335	0.25050	18.72	102.22
165	0.33868	0.78557	0.53106	0.90180	0.49499	28.58	334.46
166	0.28257	0.71543	0.40080	0.46894	0.87976	30.03	807.46

167	0.83367	0.48096	0.03206	0.71543	0.17836	28.37	27.48
168	0.61924	0.59920	0.87976	0.87375	0.88778	50.37	768.73
169	0.10822	0.24449	0.60922	0.73146	0.65531	21.38	625.33
170	0.68337	0.70341	0.26453	0.37074	0.41283	27.08	165.89
171	0.11623	0.57916	0.34870	0.22445	0.88978	16.98	1334.61
172	0.31864	0.52505	0.86573	0.50501	0.12826	8.70	62.68
173	0.72144	0.94188	0.00000	0.80962	0.28858	35.93	76.54
174	0.30060	0.99399	0.50501	0.73347	0.29459	17.93	172.99
175	0.74950	0.03006	0.00401	0.32866	0.74549	58.08	235.27
176	0.13828	0.00200	0.79760	0.34068	0.77756	18.03	840.67
177	0.44489	0.02605	0.23046	0.75752	0.58717	54.13	407.75
178	0.70140	0.43687	0.15230	0.86974	0.07214	15.44	4.90
179	0.29659	0.08818	0.01804	0.38677	0.35872	22.07	108.96
180	0.24449	0.94990	0.64329	0.27655	0.92184	22.43	1514.86
181	0.67535	0.66533	0.46293	0.79359	0.94589	59.62	695.05
182	0.90581	0.36874	0.03407	0.08216	0.08818	8.68	18.71
183	0.67134	0.66934	0.83768	0.40681	0.64729	33.35	499.38
184	0.53507	0.69539	0.59118	0.35872	0.69539	30.90	551.89
185	0.82365	0.73948	0.91383	0.37275	0.34469	21.98	190.13
186	0.38277	0.55110	0.46493	0.82966	0.30661	23.11	135.37
187	0.60521	0.59719	0.37876	0.14028	0.24248	12.96	141.77
188	0.82565	0.92385	0.97996	0.68737	0.51904	35.51	341.75
189	0.52705	0.74950	0.72345	0.54509	0.14429	10.02	50.37
190	0.25651	0.70140	0.48096	0.64529	0.57916	24.32	436.52
191	0.07014	0.13026	0.35471	0.16834	0.36273	8.57	434.33
192	0.03808	0.99800	0.75351	0.45090	0.65331	11.81	1387.81
193	0.40281	0.35671	0.73747	0.35671	0.29659	14.71	168.47
194	0.81363	0.26052	0.70341	0.66333	0.47295	38.94	208.83
195	0.21042	0.91383	0.38878	0.52505	0.41082	17.20	309.26

196	0.33066	0.53507	0.24048	0.99198	0.51703	39.12	330.40
197	0.24850	0.67134	0.29058	0.69739	0.16834	13.42	63.80
198	0.16032	0.61323	0.96794	0.68337	0.37475	14.19	359.85
199	0.62124	0.66132	0.46894	0.18036	0.91383	36.92	969.57
200	0.77555	0.09218	0.80160	0.28056	0.68337	37.29	412.81
201	0.90381	0.70942	0.11824	0.30461	0.32265	26.19	89.29
202	0.71743	0.89379	0.09619	0.67535	0.60721	48.45	258.22
203	0.46894	0.02806	0.40481	0.08016	0.75551	26.38	787.68
204	0.32665	0.22846	0.31663	0.67735	0.79960	40.64	542.98
205	0.40681	0.90982	0.43086	0.56112	0.73747	32.98	576.20
206	0.22645	0.79960	0.74549	0.26854	0.68136	17.21	1027.60
207	0.35671	0.98196	0.19439	0.22244	0.77154	24.97	743.46
208	0.16433	0.68537	0.43687	0.92385	0.95190	33.87	1070.39
209	0.69940	0.74549	0.14228	0.46693	0.71142	45.58	327.26
210	0.30261	0.89780	0.64729	0.24048	0.31062	11.41	321.96
211	0.92385	0.67735	0.68737	0.07415	0.65932	34.26	993.89
212	0.77154	0.56313	0.13226	0.20842	0.62525	34.92	304.21
213	0.57515	0.65731	0.94188	0.26453	0.09419	6.66	43.84
214	0.93186	0.85371	0.65731	0.33667	0.49098	31.70	293.37
215	0.66733	0.28457	0.02605	0.76353	0.67134	65.73	313.81
216	0.99399	0.26854	0.36874	0.58517	0.28657	33.01	68.71
217	0.98597	0.34068	0.44689	0.93587	0.52104	58.13	232.00
218	0.78156	0.10822	0.21042	0.80361	0.29259	41.05	86.44
219	0.50100	0.79760	0.25050	0.22044	0.37074	17.82	216.28
220	0.09018	0.49098	0.14028	0.35471	0.17635	8.65	108.93
221	0.09820	0.10421	0.90982	0.53908	0.09820	6.33	62.17
222	0.15431	0.24649	0.39479	0.45691	0.39078	15.63	244.86
223	0.63126	0.76152	0.01202	0.49699	0.32665	28.17	85.12
224	0.71343	0.18437	0.06413	0.45491	0.59319	46.02	180.68

225	0.91984	0.21042	0.41483	0.58116	0.71743	58.77	330.58
226	0.85972	0.05812	0.99599	0.36072	0.85571	48.74	574.31
227	0.27856	0.61122	0.63327	0.46293	0.67335	22.93	604.27
228	0.74549	0.66733	0.35271	0.50100	0.93387	54.60	578.42
229	0.48297	0.57114	0.93186	0.20641	0.42084	16.80	432.43
230	0.73547	0.65531	0.80361	0.86172	0.28257	25.89	112.93
231	0.95190	0.53908	0.29860	0.93988	0.04409	11.74	4.90
232	0.60120	0.50902	0.38477	0.60120	0.25451	22.20	74.97
233	0.97796	0.37275	0.44088	0.81363	0.21643	30.40	51.42
234	0.94188	0.17034	0.94990	0.97796	0.27655	34.59	115.99
235	0.89579	0.11623	0.51303	0.71944	0.06814	13.93	5.24
236	0.88577	0.93186	0.28457	0.13427	0.27856	17.61	156.73
237	0.21443	0.83768	0.38677	0.72946	0.02405	5.03	2.09
238	0.94389	0.84369	0.44890	0.90381	0.10421	18.54	15.40
239	0.41683	0.97996	0.53307	0.06814	0.85371	24.28	2136.04
240	0.04609	0.85170	0.61122	0.70140	0.13226	6.59	124.86
241	0.15230	0.50701	0.24850	0.77555	0.61523	26.61	494.28
242	0.77956	0.58116	0.73547	0.60721	0.16433	16.62	43.14
243	0.81162	0.55311	0.72745	0.55511	0.48297	34.08	234.84
244	0.99599	0.19639	0.09820	0.18437	0.43888	32.36	126.40
245	0.58717	0.46493	0.30060	0.88577	0.75150	55.52	447.82
246	0.78758	0.81764	0.99198	0.20441	0.82766	38.83	1163.25
247	0.43687	0.97395	0.09018	0.65731	0.99198	50.37	670.69
248	0.49098	0.15631	0.48297	0.38277	0.25651	16.83	87.02
249	0.77355	0.58717	0.98798	0.58918	0.20842	17.95	77.06
250	0.16633	0.40080	0.34669	0.74148	0.14629	11.37	59.24
251	0.18637	0.32064	0.42285	0.04208	0.36673	9.16	729.33
252	0.46693	0.82565	0.94790	0.75551	0.20441	15.09	97.96
253	0.23046	0.38076	0.33868	0.83166	0.42485	24.60	232.49

254	0.37374	0.57576	0.68687	0.84848	0.17172	15.29	65.72
255	0.06212	0.34870	0.83567	0.82365	0.18437	8.38	149.79
256	0.52305	0.96593	0.21242	0.40080	0.36072	22.15	158.69
257	0.51515	0.73737	0.30303	0.69697	0.34343	26.55	130.85
258	0.66667	0.25253	0.48485	0.29293	0.52525	28.95	258.29
259	0.54910	0.54709	0.37675	0.05010	0.73146	25.89	1168.65
260	0.96794	0.44088	0.27856	0.61523	0.79559	65.31	376.08
261	0.33667	0.77355	0.95591	0.30862	0.08016	5.69	55.46
262	0.83567	0.04008	0.90782	0.61122	0.38277	32.94	149.60
263	0.75351	0.06613	0.79559	0.89379	0.43287	43.88	280.75

Appendix F: Design optimization results

Table F. 1 Design problem I results

N_r	OD	Pl/OD	Pt/OD	LR	θ	V_a	V_w	N_tpr	Volume	material volume	Power	Q_total'	Afr_air	A_air	A_water	Height	Length	AHTC	ADP	WHTC	WDP
-	-	-	-	-	°	m/s	m/s	-	cm³	cm3	W	W	m²	m²	m²	m	m	W/ m²K	Pa	W/ m²K	kPa
4	0.8	1.6	1.5	6.4	46	2.8	0.4	108	85.41	10.12	2.41	849.18	0.02	0.14	0.11	0.13	0.14	430.02	52.47	9787	4.44
4	0.8	1.6	1.5	6.5	46	2.8	0.4	108	85.70	10.16	2.40	850.77	0.02	0.15	0.11	0.13	0.14	429.71	52.15	9775	4.45
4	0.8	1.6	1.5	6.5	47	2.8	0.4	109	85.99	10.20	2.39	850.96	0.02	0.15	0.11	0.13	0.14	429.23	51.88	9752	4.38
4	0.8	1.6	1.5	6.4	46	2.8	0.4	109	86.15	10.20	2.39	851.33	0.02	0.15	0.11	0.13	0.14	429.64	51.93	9741	4.38
4	0.8	1.6	1.5	6.4	46	2.8	0.4	109	86.21	10.21	2.38	850.26	0.02	0.15	0.11	0.13	0.14	428.67	51.61	9734	4.38
4	0.8	1.6	1.5	6.5	46	2.8	0.4	109	86.29	10.23	2.38	851.56	0.02	0.15	0.11	0.13	0.14	428.99	51.61	9733	4.39
4	0.8	1.6	1.5	6.5	46	2.8	0.4	109	86.37	10.24	2.37	852.89	0.02	0.15	0.11	0.13	0.14	429.30	51.61	9730	4.39
4	0.8	1.6	1.5	6.5	46	2.8	0.4	109	86.49	10.25	2.37	854.39	0.02	0.15	0.11	0.13	0.14	429.74	51.64	9723	4.40
4	0.8	1.6	1.5	6.5	46	2.8	0.4	109	86.56	10.25	2.37	854.39	0.02	0.15	0.11	0.13	0.14	429.74	51.63	9723	4.40
4	0.8	1.6	1.5	6.5	46	2.8	0.4	109	86.97	10.24	2.37	852.78	0.02	0.15	0.11	0.13	0.14	429.15	51.54	9726	4.39
4	0.8	1.6	1.5	6.5	46	2.8	0.4	109	87.04	10.25	2.37	854.11	0.02	0.15	0.11	0.13	0.14	429.46	51.54	9723	4.40
4	0.8	1.6	1.5	6.6	47	2.7	0.4	109	87.47	10.35	2.33	855.61	0.02	0.15	0.11	0.13	0.14	427.91	50.34	9710	4.46
4	0.8	1.6	1.5	6.6	46	2.7	0.4	108	87.67	10.37	2.33	858.95	0.02	0.15	0.11	0.13	0.14	428.86	50.37	9705	4.54
4	0.8	1.6	1.5	6.6	47	2.7	0.4	109	87.75	10.38	2.32	858.64	0.02	0.15	0.11	0.13	0.14	428.93	50.41	9700	4.47
4	0.8	1.6	1.5	6.6	47	2.7	0.4	109	88.13	10.42	2.31	857.64	0.02	0.15	0.11	0.13	0.14	427.22	49.77	9680	4.48
4	0.8	1.6	1.5	6.6	46	2.7	0.4	109	88.35	10.45	2.30	860.59	0.02	0.15	0.11	0.13	0.14	428.06	49.82	9661	4.48
4	0.8	1.6	1.5	6.6	46	2.7	0.4	109	88.48	10.46	2.29	859.28	0.02	0.15	0.11	0.13	0.14	426.91	49.49	9654	4.48
4	0.8	1.6	1.5	6.6	46	2.7	0.4	109	88.76	10.49	2.28	859.49	0.02	0.15	0.11	0.13	0.14	426.34	49.20	9645	4.49
4	0.8	1.6	1.5	6.6	47	2.7	0.4	109	90.32	10.51	2.12	853.15	0.02	0.15	0.11	0.13	0.14	419.79	46.09	9643	4.49
4	0.8	1.6	1.5	6.6	46	2.6	0.4	109	90.93	10.58	2.10	854.46	0.02	0.15	0.11	0.13	0.14	418.37	45.48	9604	4.50
4	0.8	1.6	1.5	6.6	46	2.6	0.4	109	91.36	10.62	2.08	855.91	0.02	0.15	0.11	0.13	0.14	418.02	45.22	9588	4.51

N_r	OD	Pl/OD	Pt/OD	LR	θ	V_a	V_w	N_tpr	Volume	material volume	Power	Q_total'	Afr_air	A_air	A_water	Height	Length	AHTC	ADP	WHTC	WDP
4	0.8	1.6	1.5	7.2	46	2.5	0.4	109	95.15	11.18	2.06	874.13	0.02	0.16	0.12	0.14	0.14	412.91	43.68	9506	4.72
4	0.8	1.6	1.5	7.2	46	2.5	0.4	109	95.57	11.23	2.04	875.67	0.02	0.16	0.12	0.14	0.14	411.90	43.33	9497	4.73
4	0.8	1.6	1.5	7.2	47	2.5	0.4	108	96.08	11.11	1.93	864.70	0.02	0.16	0.12	0.14	0.14	406.04	41.24	9534	4.78
4	0.8	1.6	1.5	7.2	47	2.5	0.4	109	96.97	11.21	1.90	865.71	0.02	0.16	0.12	0.14	0.14	403.88	40.60	9487	4.72
4	0.8	1.6	1.5	7.4	46	2.4	0.4	109	100.41	11.58	1.78	867.37	0.02	0.17	0.12	0.15	0.14	392.62	37.63	9422	4.82
4	0.8	1.6	1.5	7.4	46	2.4	0.4	109	100.71	11.61	1.73	855.15	0.02	0.17	0.12	0.15	0.14	381.02	36.17	9421	4.83
4	0.8	1.6	1.5	7.2	46	2.3	0.4	113	103.52	11.87	1.72	870.11	0.02	0.17	0.13	0.14	0.15	385.17	36.17	9222	4.55

Table F. 2 Design problem II results

N_r	OD	Pl/OD	Pt/OD	LR	θ	V_a	V_w	N_tpr	Volume	material volume	Power	Q_total'	Afr_air	A_air	A_water	Height	Length	AHTC	ADP	WHTC	WDP
-	-	-	-	-	°	m/s	m/s	-	cm³	cm3	W	W	m²	m²	m²	m	m	W/ m²K	Pa	W/ m²K	kPa
4	0.5	1.9	1.5	6.7	63	2.3	0.5	200	62	7.28	1.51	839.87	0.02	0.15	0.12	0.11	0.20	386.38	20.91	14346	9.20
4	0.5	1.9	1.5	6.7	63	2.3	0.5	200	62	7.28	1.51	839.87	0.02	0.15	0.12	0.11	0.20	386.38	20.91	14346	9.20
4	0.5	1.9	1.5	6.1	63	2.4	0.4	200	63	7.48	1.50	835.53	0.02	0.15	0.12	0.10	0.20	384.91	21.84	14255	8.03
4	0.5	1.9	1.5	6.1	63	2.4	0.4	200	63	7.48	1.50	835.74	0.02	0.15	0.12	0.10	0.20	384.80	21.81	14249	8.03
4	0.5	1.9	1.5	6.2	63	2.3	0.4	200	64	7.53	1.48	835.85	0.02	0.16	0.12	0.11	0.20	382.48	21.32	14194	8.06
4	0.5	1.9	1.5	6.2	63	2.3	0.4	200	64	7.57	1.47	837.62	0.02	0.16	0.12	0.11	0.20	381.97	21.20	14136	8.08
4	0.5	1.9	1.5	6.2	63	2.3	0.4	200	64	7.58	1.46	837.00	0.02	0.16	0.12	0.11	0.20	381.12	21.02	14134	8.08
4	0.5	1.9	1.5	6.3	63	2.3	0.4	200	65	7.66	1.44	839.74	0.02	0.16	0.13	0.11	0.20	379.43	20.64	14026	8.12
4	0.5	1.9	1.5	6.3	63	2.3	0.4	200	65	7.68	1.43	839.76	0.02	0.16	0.13	0.11	0.20	378.26	20.37	14002	8.13
4	0.5	1.9	1.5	6.7	63	2.3	0.4	200	65	7.62	1.43	843.06	0.02	0.16	0.13	0.11	0.20	377.63	19.71	14011	8.78
4	0.5	1.9	1.5	6.4	63	2.3	0.4	200	65	7.73	1.42	840.83	0.02	0.16	0.13	0.11	0.20	376.88	20.09	13944	8.16
4	0.5	1.9	1.5	6.1	63	2.3	0.4	200	66	7.82	1.42	837.82	0.02	0.16	0.13	0.11	0.21	376.08	20.53	13913	7.65
4	0.5	1.9	1.5	6.5	63	2.3	0.4	200	66	7.81	1.40	843.47	0.02	0.16	0.13	0.11	0.20	375.22	19.74	13840	8.20
4	0.5	1.9	1.5	6.5	63	2.2	0.4	200	66	7.82	1.40	843.37	0.02	0.16	0.13	0.11	0.20	374.78	19.67	13838	8.22
4	0.5	1.9	1.5	6.5	63	2.2	0.4	200	66	7.84	1.40	844.11	0.02	0.16	0.13	0.11	0.20	374.37	19.58	13806	8.22

4	0.5	1.9	1.5	6.5	63	2.2	0.4	200	66	7.84	1.40	844.32	0.02	0.16	0.13	0.11	0.20	374.28	19.55	13798	8.22
4	0.5	1.9	1.5	6.5	63	2.2	0.4	200	66	7.84	1.39	844.11	0.02	0.16	0.13	0.11	0.20	374.09	19.53	13798	8.22
4	0.5	1.9	1.5	6.5	63	2.2	0.4	200	67	7.85	1.39	843.38	0.02	0.16	0.13	0.11	0.20	373.14	19.37	13796	8.22
4	0.5	1.9	1.5	6.5	63	2.2	0.4	200	67	7.86	1.39	843.59	0.02	0.16	0.13	0.11	0.20	373.04	19.34	13789	8.23
4	0.5	1.9	1.5	6.6	63	2.2	0.4	200	67	7.90	1.38	845.30	0.02	0.16	0.13	0.11	0.20	372.61	19.26	13737	8.25
4	0.5	1.9	1.5	6.6	63	2.2	0.4	200	68	7.96	1.36	845.85	0.02	0.16	0.13	0.11	0.20	370.00	18.79	13666	8.30
4	0.5	1.9	1.5	6.6	63	2.2	0.4	200	68	7.96	1.36	845.85	0.02	0.16	0.13	0.11	0.20	370.00	18.79	13666	8.30
4	0.6	1.9	1.5	6.0	63	2.2	0.4	200	68	8.14	1.36	840.90	0.02	0.16	0.13	0.11	0.21	369.77	19.79	13561	7.23
4	0.5	1.9	1.5	6.7	63	2.2	0.4	200	68	8.05	1.34	848.01	0.02	0.17	0.13	0.11	0.20	367.78	18.36	13567	8.36
4	0.5	1.9	1.5	6.7	63	2.2	0.4	200	69	8.05	1.34	847.80	0.02	0.17	0.13	0.11	0.20	367.60	18.34	13567	8.36
4	0.5	1.9	1.5	6.7	63	2.2	0.4	200	69	8.05	1.34	847.80	0.02	0.17	0.13	0.11	0.20	367.60	18.34	13567	8.36
4	0.6	1.9	1.5	6.1	63	2.2	0.4	200	69	8.22	1.34	842.73	0.02	0.16	0.13	0.11	0.21	367.54	19.38	13469	7.28
4	0.6	1.9	1.5	6.1	63	2.2	0.4	200	69	8.22	1.34	842.73	0.02	0.16	0.13	0.11	0.21	367.54	19.38	13469	7.28
4	0.6	1.9	1.5	6.1	63	2.2	0.4	200	69	8.24	1.33	842.41	0.02	0.16	0.13	0.11	0.21	366.39	19.15	13453	7.29
4	0.6	1.9	1.5	6.1	63	2.2	0.4	200	69	8.25	1.33	842.51	0.02	0.16	0.13	0.11	0.21	366.19	19.11	13445	7.29
4	0.6	1.9	1.5	6.1	63	2.2	0.4	200	69	8.25	1.33	842.51	0.02	0.16	0.13	0.11	0.21	366.19	19.11	13445	7.29
4	0.6	1.9	1.5	6.1	63	2.2	0.4	200	69	8.25	1.33	842.61	0.02	0.16	0.13	0.11	0.21	365.98	19.08	13439	7.30
4	0.6	1.9	1.5	6.2	63	2.2	0.4	200	70	8.34	1.31	845.37	0.02	0.17	0.13	0.11	0.21	364.34	18.73	13335	7.34
4	0.6	1.9	1.5	6.2	63	2.2	0.4	200	70	8.33	1.30	844.32	0.02	0.17	0.13	0.11	0.21	363.72	18.64	13347	7.33
4	0.6	1.9	1.5	6.2	63	2.2	0.4	200	70	8.35	1.30	844.85	0.02	0.17	0.13	0.11	0.21	363.31	18.55	13326	7.34
4	0.6	1.9	1.5	6.2	63	2.2	0.4	200	70	8.35	1.30	844.74	0.02	0.17	0.13	0.11	0.21	363.22	18.54	13326	7.34
4	0.6	1.9	1.5	6.2	63	2.2	0.4	200	71	8.35	1.30	844.64	0.02	0.17	0.13	0.11	0.21	363.13	18.53	13326	7.34
4	0.5	1.9	1.5	6.6	63	2.1	0.4	200	71	8.34	1.29	850.04	0.02	0.17	0.14	0.11	0.21	362.52	17.87	13294	7.88
4	0.5	1.9	1.5	6.6	63	2.1	0.4	200	71	8.36	1.28	849.71	0.02	0.17	0.14	0.11	0.21	361.39	17.67	13279	7.89
4	0.6	1.9	1.5	6.3	63	2.2	0.4	200	71	8.44	1.28	846.68	0.02	0.17	0.13	0.11	0.21	360.94	18.10	13229	7.38
4	0.6	1.9	1.5	6.5	63	2.1	0.4	200	72	8.58	1.26	850.21	0.02	0.17	0.14	0.11	0.21	358.16	17.60	13081	7.44

303

N_r	OD	Pl/OD	Pt/OD	LR	θ	V_a	V_w	N_tpr	Volume	material volume	Power	Q_total'	Afr_air	A_air	A_water	Height	Length	AHTC	ADP	WHTC	WDP
4	0.6	1.9	1.5	6.4	63	2.1	0.4	200	73	8.55	1.26	848.72	0.02	0.17	0.14	0.11	0.21	357.98	17.58	13112	7.42
4	0.6	1.9	1.5	6.1	63	2.1	0.4	200	73	8.63	1.26	845.79	0.02	0.17	0.14	0.11	0.21	357.87	18.04	13061	6.97
4	0.6	1.9	1.5	6.5	63	2.1	0.4	200	73	8.58	1.26	850.20	0.02	0.17	0.14	0.11	0.21	357.88	17.55	13075	7.44
4	0.6	1.9	1.5	6.5	63	2.1	0.4	200	73	8.65	1.24	850.80	0.02	0.17	0.14	0.11	0.21	355.66	17.14	13012	7.47
4	0.6	1.9	1.5	6.5	63	2.1	0.4	200	73	8.65	1.24	850.80	0.02	0.17	0.14	0.11	0.21	355.66	17.14	13012	7.47
4	0.6	1.9	1.5	6.5	63	2.1	0.4	200	73	8.65	1.24	850.80	0.02	0.17	0.14	0.11	0.21	355.66	17.14	13012	7.47
4	0.6	1.9	1.5	6.6	63	2.1	0.4	200	74	8.75	1.22	852.67	0.02	0.17	0.14	0.12	0.21	352.97	16.66	12908	7.52
4	0.6	1.9	1.5	6.0	63	2.1	0.4	200	75	8.95	1.21	847.08	0.02	0.17	0.14	0.11	0.22	351.90	17.46	12773	6.62
4	0.6	1.9	1.5	6.7	63	2.0	0.4	200	75	8.86	1.20	854.57	0.02	0.18	0.14	0.12	0.21	350.37	16.21	12807	7.59
4	0.6	1.9	1.5	6.2	63	2.1	0.4	200	77	9.11	1.18	850.22	0.02	0.18	0.14	0.11	0.22	347.82	16.69	12612	6.69
4	0.6	1.9	1.5	6.2	63	2.1	0.4	200	77	9.11	1.18	850.22	0.02	0.18	0.14	0.11	0.22	347.82	16.69	12612	6.69
4	0.6	1.9	1.5	6.5	63	2.0	0.4	200	77	9.06	1.17	853.83	0.02	0.18	0.14	0.12	0.21	347.38	16.13	12639	7.14
4	0.6	1.9	1.5	6.3	63	2.0	0.4	200	78	9.25	1.15	853.63	0.02	0.18	0.14	0.11	0.22	345.22	16.21	12477	6.74

Table F. 3 Automotive radiator optimization results

N_r	OD	Pl/OD	Pt/OD	LR	θ	V_a	V_w	N_tpr	Volume	material volume	Power	Q_total'	Afr_air	A_air	A_water	Height	Length	AHTC	ADP	WHTC	WDP
-	-	-	-	-	°	m/s	m/s	-	cm³	cm3	W	W	m²	m²	m²	m	m	W/ m²K	Pa	W/ m²K	kPa
9	0.9	2.8	1.5	5.5	35	4.2	0.5	183	2112	155.7	63.6	10345.2	0.19	2.06	1.54	0.44	0.44	389.0	72.7	8868	15.8
9	0.9	2.8	1.5	5.5	35	4.2	0.5	183	2112	155.7	63.6	10345.2	0.19	2.06	1.54	0.44	0.44	389.0	72.7	8868	15.8
9	0.9	2.8	1.5	5.5	35	4.2	0.5	186	2126	157.6	62.3	10435.9	0.20	2.08	1.56	0.44	0.45	389.1	71.3	8816	15.4
9	0.9	2.8	1.5	5.5	35	4.2	0.5	186	2137	157.6	62.2	10431.6	0.20	2.08	1.56	0.44	0.45	388.7	71.2	8816	15.4
9	0.9	2.8	1.5	5.5	35	4.2	0.5	186	2137	157.6	62.2	10431.6	0.20	2.08	1.56	0.44	0.45	388.7	71.2	8816	15.4
9	0.9	2.8	1.5	5.5	35	4.2	0.5	186	2137	157.6	62.2	10431.6	0.20	2.08	1.56	0.44	0.45	388.7	71.2	8816	15.4
9	0.9	2.8	1.5	5.5	35	4.2	0.5	186	2141	157.6	62.1	10428.7	0.20	2.08	1.56	0.44	0.45	388.5	71.1	8816	15.4
9	0.9	2.8	1.5	5.5	35	4.2	0.5	186	2141	157.6	62.1	10428.7	0.20	2.08	1.56	0.44	0.45	388.5	71.1	8816	15.4
9	0.9	2.8	1.5	5.5	35	4.2	0.5	186	2141	157.6	62.1	10428.7	0.20	2.08	1.56	0.44	0.45	388.5	71.1	8816	15.4

9	0.9	2.8	1.5	5.5	35	4.2	0.5	186	2141	157.6	62.1	10428.7	0.20	2.08	1.56	0.44	0.45	388.5	71.1	8816	15.4
9	0.9	2.8	1.5	5.5	35	4.2	0.5	186	2141	157.6	62.1	10428.7	0.20	2.08	1.56	0.44	0.45	388.5	71.1	8816	15.4
9	0.9	2.8	1.5	5.5	35	4.2	0.5	186	2141	157.6	62.1	10428.7	0.20	2.08	1.56	0.44	0.45	388.5	71.1	8816	15.4
9	0.9	2.8	1.5	5.5	35	4.2	0.5	186	2141	157.6	62.1	10428.7	0.20	2.08	1.56	0.44	0.45	388.5	71.1	8816	15.4
9	0.9	2.8	1.5	5.5	35	4.2	0.5	186	2141	157.6	62.1	10428.7	0.20	2.08	1.56	0.44	0.45	388.5	71.1	8816	15.4
9	0.9	2.8	1.5	5.5	35	4.2	0.5	186	2141	157.6	62.1	10428.7	0.20	2.08	1.56	0.44	0.45	388.5	71.1	8816	15.4
9	0.9	2.8	1.5	5.5	35	4.2	0.5	186	2141	157.6	62.1	10428.7	0.20	2.08	1.56	0.44	0.45	388.5	71.1	8816	15.4
9	0.9	3.0	1.5	5.5	40	4.1	0.5	186	2147	150.4	58.5	9985.8	0.20	1.99	1.49	0.42	0.48	371.8	66.4	9511	16.0
9	0.9	3.0	1.5	5.5	40	4.1	0.5	186	2147	150.4	58.5	9985.8	0.20	1.99	1.49	0.42	0.48	371.8	66.4	9511	16.0
9	0.9	3.0	1.5	5.5	40	4.1	0.5	186	2147	150.4	58.5	9985.8	0.20	1.99	1.49	0.42	0.48	371.8	66.4	9511	16.0
9	0.9	3.0	1.5	5.5	40	4.1	0.5	186	2147	150.4	58.5	9985.8	0.20	1.99	1.49	0.42	0.48	371.8	66.4	9511	16.0
9	0.9	3.0	1.5	5.5	40	4.0	0.5	186	2181	151.5	53.8	10089.6	0.20	2.00	1.50	0.42	0.48	377.0	60.6	9562	16.3
9	0.9	3.0	1.5	5.5	40	4.0	0.5	186	2181	151.5	53.8	10089.6	0.20	2.00	1.50	0.42	0.48	377.0	60.6	9562	16.3

Table F. 4 HVRF system indoor coil optimization results

N_r	OD	Pl/OD	Pt/OD	LR	θ	V_a	V_w	N_tpr	Volume	material volume	Power	Q_total'	Afr_air	A_air	A_water	Height	Length	AHTC	ADP	WHTC	WDP
-	-	-	-	-	°	m/s	m/s	-	cm³	cm3	W	W	m²	m²	m²	m	m	W/ m²K	Pa	W/ m²K	kPa
5	0.5	2.9	1.5	3.8	19.9	1.9	0.4	556	575.5	40.86	3.65	3173	0.15	0.85	0.68	0.17	0.88	327.6	9.58	8322	8.46
5	0.5	2.9	1.5	3.9	19.9	1.8	0.4	548	584.2	41.36	3.61	3170	0.16	0.86	0.69	0.18	0.86	324.0	9.22	8420	8.70
5	0.5	2.9	1.5	3.8	19.8	1.8	0.4	548	585.9	41.68	3.61	3180	0.15	0.86	0.69	0.18	0.87	324.5	9.37	8246	8.46
5	0.5	2.9	1.5	3.9	19.9	1.8	0.4	556	587.0	41.57	3.58	3192	0.16	0.86	0.69	0.18	0.88	324.6	9.25	8353	8.55
5	0.5	2.9	1.5	3.8	19.9	1.8	0.4	556	592.8	42.13	3.54	3183	0.16	0.87	0.69	0.18	0.89	322.3	9.17	8219	8.36
5	0.5	2.9	1.5	3.8	19.8	1.8	0.4	556	594.4	42.29	3.54	3196	0.16	0.87	0.70	0.18	0.89	322.6	9.19	8196	8.37
5	0.5	2.9	1.5	3.8	19.9	1.8	0.4	556	595.7	42.37	3.53	3188	0.16	0.87	0.70	0.18	0.89	321.1	9.07	8227	8.38
5	0.5	2.9	1.5	3.8	19.8	1.8	0.4	556	597.4	42.45	3.52	3195	0.16	0.87	0.70	0.18	0.89	321.5	9.09	8204	8.39

5	0.5	2.9	1.5	4.0	19.9	1.8	0.4	548	606.9	43.05	3.49	3207	0.16	0.89	0.71	0.18	0.87	317.9	8.78	8318	8.65
5	0.5	2.9	1.5	4.0	19.9	1.7	0.4	556	618.7	43.84	3.41	3220	0.16	0.90	0.72	0.18	0.89	314.9	8.54	8278	8.57
5	0.6	2.9	1.5	3.9	19.9	1.7	0.4	548	638.9	45.39	3.32	3212	0.16	0.91	0.73	0.18	0.89	310.4	8.39	7990	8.19
5	0.6	2.9	1.5	3.8	19.9	1.7	0.4	548	640.1	45.44	3.32	3191	0.16	0.91	0.72	0.18	0.90	310.5	8.50	7874	7.97
5	0.6	2.9	1.5	3.9	19.9	1.7	0.4	548	640.6	45.47	3.32	3217	0.17	0.91	0.73	0.18	0.89	310.4	8.38	8006	8.20
5	0.6	2.9	1.5	3.9	19.9	1.7	0.4	548	640.6	45.47	3.32	3217	0.17	0.91	0.73	0.18	0.89	310.4	8.38	8006	8.20
5	0.6	2.9	1.5	3.8	19.9	1.7	0.4	548	641.9	45.62	3.31	3204	0.16	0.91	0.73	0.18	0.90	310.7	8.49	7874	7.97
5	0.6	2.9	1.5	3.9	19.9	1.7	0.4	548	646.2	45.82	3.29	3213	0.17	0.92	0.74	0.19	0.89	307.9	8.20	8006	8.24
5	0.6	2.9	1.5	3.8	19.8	1.7	0.4	548	648.3	45.97	3.28	3201	0.17	0.92	0.73	0.18	0.90	308.5	8.32	7868	8.02
5	0.6	2.9	1.5	3.9	19.9	1.7	0.4	548	652.9	46.23	3.26	3207	0.17	0.92	0.74	0.19	0.90	307.5	8.21	7906	8.06
5	0.6	2.9	1.5	3.9	19.9	1.7	0.4	548	652.9	46.23	3.26	3207	0.17	0.92	0.74	0.19	0.90	307.5	8.21	7906	8.06
5	0.6	2.9	1.5	3.9	19.9	1.7	0.4	548	652.9	46.23	3.26	3207	0.17	0.92	0.74	0.19	0.90	307.5	8.21	7906	8.06
5	0.6	2.9	1.5	3.9	19.9	1.7	0.4	548	656.1	46.50	3.24	3211	0.17	0.93	0.74	0.19	0.90	306.3	8.12	7914	8.08
5	0.6	2.9	1.5	3.9	19.9	1.7	0.4	548	656.1	46.50	3.24	3211	0.17	0.93	0.74	0.19	0.90	306.3	8.12	7914	8.08
5	0.6	2.9	1.5	3.9	19.9	1.7	0.4	548	658.6	46.68	3.23	3209	0.17	0.93	0.74	0.19	0.90	305.0	8.03	7907	8.10
5	0.6	2.9	1.5	4.0	19.9	1.7	0.4	548	665.6	47.11	3.20	3227	0.17	0.94	0.75	0.19	0.90	304.4	7.93	7939	8.15
5	0.6	2.9	1.5	4.0	19.9	1.7	0.4	548	668.8	47.29	3.19	3225	0.17	0.94	0.75	0.19	0.90	303.2	7.84	7947	8.18
5	0.6	2.9	1.5	4.0	19.9	1.7	0.4	548	668.8	47.29	3.19	3225	0.17	0.94	0.75	0.19	0.90	303.2	7.84	7947	8.18
5	0.6	2.9	1.5	4.0	19.9	1.7	0.4	548	671.3	47.47	3.18	3222	0.17	0.95	0.76	0.19	0.90	301.8	7.75	7948	8.20
5	0.6	2.9	1.5	4.0	19.9	1.7	0.4	548	671.4	47.47	3.18	3222	0.17	0.95	0.76	0.19	0.90	301.9	7.76	7940	8.20
5	0.6	2.9	1.5	4.0	19.9	1.7	0.4	548	671.4	47.47	3.18	3222	0.17	0.95	0.76	0.19	0.90	301.9	7.76	7940	8.20
5	0.6	2.9	1.5	4.0	19.9	1.7	0.4	548	671.4	47.47	3.18	3222	0.17	0.95	0.76	0.19	0.90	301.9	7.76	7940	8.20
5	0.6	2.9	1.5	4.0	19.9	1.7	0.4	548	671.4	47.47	3.18	3222	0.17	0.95	0.76	0.19	0.90	301.9	7.76	7940	8.20
5	0.6	2.9	1.5	4.0	19.9	1.6	0.4	548	675.2	47.73	3.16	3226	0.17	0.95	0.76	0.19	0.90	300.8	7.66	7964	8.23
5	0.6	2.9	1.5	4.0	19.9	1.6	0.4	548	675.2	47.73	3.16	3226	0.17	0.95	0.76	0.19	0.90	300.8	7.66	7964	8.23
5	0.6	2.9	1.5	4.1	19.9	1.6	0.4	548	678.4	47.90	3.15	3240	0.17	0.96	0.76	0.19	0.90	301.4	7.66	7973	8.25

306

5	0.6	2.9	1.5	4.1	19.9	1.6	0.4	548	678.4	47.90	3.15	3240	0.17	0.96	0.76	0.19	0.90	301.4	7.66	7973	8.25
5	0.6	2.9	1.5	4.1	19.9	1.6	0.4	548	678.4	47.90	3.15	3240	0.17	0.96	0.76	0.19	0.90	301.4	7.66	7973	8.25
5	0.6	2.9	1.5	4.1	19.9	1.6	0.4	548	678.4	47.90	3.15	3240	0.17	0.96	0.76	0.19	0.90	301.4	7.66	7973	8.25
5	0.6	2.9	1.5	4.1	19.9	1.6	0.4	548	681.6	48.08	3.14	3238	0.17	0.96	0.77	0.19	0.90	300.1	7.57	7981	8.28
5	0.6	2.9	1.5	4.1	19.9	1.6	0.4	548	681.6	48.08	3.14	3238	0.17	0.96	0.77	0.19	0.90	300.1	7.57	7981	8.28
5	0.6	2.9	1.5	4.1	19.8	1.6	0.4	548	683.6	48.28	3.13	3234	0.17	0.96	0.77	0.19	0.90	298.7	7.49	7960	8.29
5	0.6	2.9	1.5	4.1	19.9	1.6	0.4	548	684.2	48.27	3.13	3234	0.17	0.96	0.77	0.19	0.90	298.8	7.49	7975	8.29
5	0.6	2.9	1.5	4.1	19.9	1.6	0.4	548	684.2	48.27	3.13	3234	0.17	0.96	0.77	0.19	0.90	298.8	7.49	7975	8.29
5	0.6	2.9	1.5	4.1	19.9	1.6	0.4	548	684.2	48.27	3.13	3234	0.17	0.96	0.77	0.19	0.90	298.8	7.49	7975	8.29
5	0.6	2.9	1.5	4.1	19.9	1.6	0.4	548	684.7	48.34	3.13	3240	0.17	0.96	0.77	0.19	0.90	298.9	7.48	7990	8.30
5	0.6	2.9	1.5	4.1	19.7	1.6	0.4	548	686.3	48.46	3.12	3248	0.18	0.97	0.77	0.19	0.90	299.2	7.50	7953	8.30
5	0.6	2.9	1.5	4.1	19.8	1.6	0.4	548	686.9	48.45	3.12	3248	0.18	0.97	0.77	0.19	0.90	299.3	7.50	7969	8.31
5	0.6	2.9	1.5	4.1	19.8	1.6	0.4	548	686.9	48.45	3.12	3248	0.18	0.97	0.77	0.19	0.90	299.3	7.50	7969	8.31
5	0.6	2.9	1.5	4.1	19.9	1.6	0.4	548	687.9	48.52	3.12	3237	0.18	0.97	0.77	0.20	0.90	297.6	7.39	7999	8.32
5	0.6	2.9	1.5	4.1	19.9	1.6	0.4	548	687.9	48.52	3.12	3237	0.18	0.97	0.77	0.20	0.90	297.6	7.39	7999	8.32
5	0.6	2.9	1.5	4.1	19.9	1.6	0.4	548	687.9	48.52	3.12	3237	0.18	0.97	0.77	0.20	0.90	297.6	7.39	7999	8.32
5	0.6	2.9	1.5	4.1	19.9	1.6	0.4	548	687.9	48.52	3.12	3237	0.18	0.97	0.77	0.20	0.90	297.6	7.39	7999	8.32
5	0.6	2.9	1.5	4.4	19.9	1.6	0.4	548	705.6	49.70	3.06	3281	0.18	1.00	0.80	0.20	0.89	293.3	6.94	8178	8.70
5	0.5	2.9	1.5	5.5	19.9	1.4	0.4	548	773.7	53.64	2.96	3384	0.21	1.11	0.89	0.24	0.86	277.9	5.44	9211	10.28
5	0.5	2.9	1.5	5.3	19.9	1.4	0.4	556	777.9	54.15	2.90	3380	0.21	1.12	0.89	0.23	0.89	276.8	5.46	8919	9.85
5	0.5	2.9	1.5	5.5	19.9	1.3	0.4	556	801.4	55.69	2.85	3407	0.21	1.15	0.92	0.24	0.89	272.8	5.16	9060	10.00
5	0.5	2.9	1.5	5.3	19.9	1.3	0.4	556	816.6	56.67	2.78	3403	0.21	1.15	0.92	0.24	0.90	271.9	5.18	8727	9.58
5	0.5	2.9	1.5	5.3	19.9	1.3	0.4	556	819.6	56.84	2.78	3394	0.21	1.15	0.92	0.24	0.90	270.4	5.11	8743	9.59
5	0.6	2.9	1.5	5.3	19.9	1.3	0.4	548	844.2	58.63	2.72	3394	0.22	1.17	0.94	0.24	0.90	267.1	4.97	8568	9.42
5	0.6	2.9	1.5	5.3	19.9	1.3	0.4	548	845.8	58.86	2.72	3407	0.22	1.17	0.94	0.24	0.90	267.3	4.97	8552	9.43
5	0.6	2.9	1.5	5.4	19.9	1.3	0.4	548	856.9	59.51	2.70	3409	0.22	1.19	0.95	0.24	0.90	265.0	4.82	8635	9.49

307

5	0.6	2.9	1.5	5.4	19.9	1.3	0.4	548	858.7	59.69	2.69	3421	0.22	1.19	0.95	0.24	0.90	265.5	4.82	8653	9.51
5	0.6	2.9	1.5	5.4	19.9	1.3	0.4	548	858.7	59.69	2.69	3421	0.22	1.19	0.95	0.24	0.90	265.5	4.82	8653	9.51
5	0.6	2.9	1.5	5.4	19.9	1.3	0.4	548	858.7	59.69	2.69	3421	0.22	1.19	0.95	0.24	0.90	265.5	4.82	8653	9.51
5	0.6	2.9	1.5	5.4	19.9	1.3	0.4	548	860.1	59.69	2.69	3421	0.22	1.19	0.95	0.24	0.90	265.5	4.82	8653	9.51
5	0.6	2.9	1.5	5.4	19.9	1.3	0.4	548	860.1	59.69	2.69	3421	0.22	1.19	0.95	0.24	0.90	265.5	4.82	8653	9.51
5	0.6	2.9	1.5	5.4	19.9	1.3	0.4	548	860.1	59.69	2.69	3421	0.22	1.19	0.95	0.24	0.90	265.5	4.82	8653	9.51
5	0.6	2.9	1.5	5.4	19.9	1.3	0.4	548	860.1	59.69	2.69	3421	0.22	1.19	0.95	0.24	0.90	265.5	4.82	8653	9.51
5	0.6	2.9	1.5	5.4	19.9	1.3	0.4	548	860.1	59.69	2.69	3421	0.22	1.19	0.95	0.24	0.90	265.5	4.82	8653	9.51
5	0.6	2.9	1.5	5.4	19.9	1.3	0.4	548	860.1	59.69	2.69	3421	0.22	1.19	0.95	0.24	0.90	265.5	4.82	8653	9.51
5	0.6	2.9	1.5	5.4	19.9	1.3	0.4	548	863.4	59.92	2.69	3413	0.22	1.19	0.96	0.24	0.90	263.9	4.75	8650	9.53
5	0.6	2.9	1.5	5.5	19.9	1.3	0.4	548	869.7	60.30	2.68	3440	0.22	1.20	0.96	0.25	0.90	264.9	4.75	8707	9.57
5	0.6	2.9	1.5	5.5	19.9	1.3	0.4	548	869.7	60.30	2.68	3440	0.22	1.20	0.96	0.25	0.90	264.9	4.75	8707	9.57
5	0.6	2.9	1.5	5.5	19.9	1.3	0.4	548	869.7	60.30	2.68	3440	0.22	1.20	0.96	0.25	0.90	264.9	4.75	8707	9.57
5	0.6	2.9	1.5	5.5	19.9	1.3	0.4	548	869.7	60.30	2.68	3440	0.22	1.20	0.96	0.25	0.90	264.9	4.75	8707	9.57
5	0.6	2.9	1.5	5.5	19.9	1.3	0.4	548	869.7	60.30	2.68	3440	0.22	1.20	0.96	0.25	0.90	264.9	4.75	8707	9.57
5	0.6	2.9	1.5	5.5	19.9	1.3	0.4	548	872.9	60.48	2.67	3429	0.22	1.21	0.96	0.25	0.90	263.3	4.68	8726	9.59
5	0.6	2.9	1.5	5.5	19.9	1.3	0.4	548	872.9	60.48	2.67	3429	0.22	1.21	0.96	0.25	0.90	263.3	4.68	8726	9.59
5	0.6	2.9	1.5	5.5	19.9	1.3	0.4	548	872.9	60.48	2.67	3429	0.22	1.21	0.96	0.25	0.90	263.3	4.68	8726	9.59
5	0.6	2.9	1.5	5.5	19.9	1.3	0.4	548	872.9	60.48	2.67	3429	0.22	1.21	0.96	0.25	0.90	263.3	4.68	8726	9.59
5	0.6	2.9	1.5	5.5	19.9	1.3	0.4	548	873.0	60.54	2.67	3432	0.22	1.21	0.97	0.25	0.90	263.3	4.68	8705	9.59
5	0.6	2.9	1.5	5.5	19.9	1.3	0.4	548	876.2	60.71	2.67	3444	0.22	1.21	0.97	0.25	0.90	263.8	4.68	8724	9.61
5	0.6	2.9	1.5	5.5	19.9	1.3	0.4	548	876.2	60.71	2.67	3444	0.22	1.21	0.97	0.25	0.90	263.8	4.68	8724	9.61
5	0.6	2.9	1.5	5.5	19.7	1.3	0.4	548	882.2	61.19	2.66	3450	0.23	1.22	0.98	0.25	0.90	262.6	4.62	8715	9.64
5	0.6	2.9	1.5	5.6	19.9	1.3	0.4	548	885.6	61.36	2.66	3440	0.23	1.22	0.98	0.25	0.90	261.0	4.54	8804	9.68
5	0.6	2.9	1.5	5.6	19.9	1.3	0.4	548	885.8	61.33	2.66	3438	0.23	1.22	0.98	0.25	0.90	261.0	4.54	8782	9.68
5	0.6	2.9	1.5	5.6	19.9	1.2	0.4	548	887.5	61.60	2.65	3455	0.23	1.23	0.98	0.25	0.90	261.6	4.54	8803	9.70

308

5	0.6	2.9	1.5	5.6	19.9	1.2	0.4	548	887.5	61.60	2.65	3455	0.23	1.23	0.98	0.25	0.90	261.6	4.54	8803	9.70
5	0.6	2.9	1.5	5.6	19.9	1.2	0.4	548	889.0	61.60	2.65	3455	0.23	1.23	0.98	0.25	0.90	261.5	4.54	8803	9.70
5	0.6	2.9	1.5	5.6	19.9	1.2	0.4	548	889.0	61.60	2.65	3455	0.23	1.23	0.98	0.25	0.90	261.5	4.54	8803	9.70
5	0.6	2.9	1.5	5.6	19.9	1.2	0.4	548	889.0	61.60	2.65	3455	0.23	1.23	0.98	0.25	0.90	261.5	4.54	8803	9.70
5	0.6	2.9	1.5	5.6	19.9	1.2	0.4	548	889.0	61.60	2.65	3455	0.23	1.23	0.98	0.25	0.90	261.5	4.54	8803	9.70
5	0.6	2.9	1.5	5.6	19.8	1.2	0.4	548	889.3	61.57	2.65	3453	0.23	1.23	0.98	0.25	0.90	261.5	4.54	8780	9.70
5	0.6	2.9	1.5	5.6	19.8	1.2	0.4	548	891.0	61.84	2.65	3447	0.23	1.23	0.99	0.25	0.90	259.9	4.48	8800	9.72
5	0.6	2.9	1.5	5.6	19.8	1.2	0.4	548	891.0	61.84	2.65	3447	0.23	1.23	0.99	0.25	0.90	259.9	4.48	8800	9.72
5	0.6	2.9	1.5	5.6	19.8	1.2	0.4	548	892.5	61.84	2.65	3446	0.23	1.23	0.99	0.25	0.90	259.9	4.47	8800	9.72
5	0.6	2.9	1.5	5.6	19.8	1.2	0.4	548	892.5	61.84	2.65	3446	0.23	1.23	0.99	0.25	0.90	259.9	4.47	8800	9.72
5	0.6	2.9	1.5	5.6	19.8	1.2	0.4	548	892.5	61.84	2.65	3446	0.23	1.23	0.99	0.25	0.90	259.9	4.47	8800	9.72
5	0.6	2.9	1.5	5.6	19.8	1.2	0.4	548	892.5	61.84	2.65	3446	0.23	1.23	0.99	0.25	0.90	259.9	4.47	8800	9.72
5	0.6	2.9	1.5	5.6	19.8	1.2	0.4	548	892.5	61.84	2.65	3446	0.23	1.23	0.99	0.25	0.90	259.9	4.47	8800	9.72
5	0.6	2.9	1.5	5.6	19.8	1.2	0.4	548	892.5	61.84	2.65	3446	0.23	1.23	0.99	0.25	0.90	259.9	4.47	8800	9.72
5	0.6	2.9	1.5	5.6	19.7	1.2	0.4	548	895.9	62.08	2.65	3461	0.23	1.24	0.99	0.25	0.90	260.3	4.48	8799	9.74
5	0.6	2.9	1.5	5.6	19.7	1.2	0.4	548	895.9	62.08	2.65	3461	0.23	1.24	0.99	0.25	0.90	260.3	4.48	8799	9.74
5	0.6	2.9	1.5	5.6	19.7	1.2	0.4	548	895.9	62.08	2.65	3461	0.23	1.24	0.99	0.25	0.90	260.3	4.48	8799	9.74
5	0.6	2.9	1.5	5.6	19.2	1.2	0.4	548	921.0	63.79	2.62	3469	0.24	1.27	1.02	0.26	0.90	255.2	4.23	8785	9.89
5	0.6	2.9	1.5	5.6	19.2	1.2	0.4	548	921.0	63.79	2.62	3469	0.24	1.27	1.02	0.26	0.90	255.2	4.23	8785	9.89

Bibliography

Abdelaziz, O. (2009). Development of Multi-scale, Multi-physics, Analysis Capability and its Application to Novel Heat Exchanger Design and Optimization. University of Maryland college park.

Abdelaziz, O., Aute, V., Azarm, S. and Radermacher, R. Approximation-Assisted Optimization for novel compact heat exchangers," HVAC&R Research, vol. 16, no. 5, pp. 707-728, 2010.

Abdelaziz, O., Development of multi-scale, multi-physics, analysis capability and its application to novel heat exchanger design and optimization, College Park, MD: PhD Thesis presented to the Department of Mechanical Engineering at the University of Maryland, 2009.

AHRI 2008, Performance Rating of Unitary Air-Conditioning & Air-Source Heat Pump Equipment, ANSI/AHRI Standard 210/240.

AHRI, 2010. Standard for Performance Rating of Variable Refrigerant Flow (VRF) Multi-Split Air-Conditioning and Heat Pump Equipment, AHRI Standard 1230.

ANSYS® Academic Research, Release 14.5, 2012, ANSYS FLUENT® User's Guide, ANSYS, Inc.

ASHRAE Standard 41.2, Standard methods for laboratory air-flow measurement, American Society of Heating, Refrigeration and Air Conditioning Engineers, Atlanta, GA, USA, 1987.

ASHRAE, ANSI/ASHRAE Standard 33-2000, Method of Testing Forced Circulation Air Cooling and Air Heating Coils.

ASHRAE, ANSI/ASHRAE Standard 41.1-2013, Standard Method for Temperature Measurement.

ASHRAE, ANSI/ASHRAE Standard 41.2-1987, Standard Methods for Laboratory Airflow Measurement.

ASHRAE, ANSI/ASHRAE Standard 41.3-1987, Standard Method for pressure Measurement.

ASHRAE, ANSI/ASHRAE Standard 41.6-1987, Method for Measurement of Moist Air Properties.

ASME, Standard for verification and validation in Computational Fluid Dynamics and heat transfer - ASME V&V 20-2009, New York: ASME, 2009.

Aute, V. (2008) Single and Multi-Response Adaptive Design of Experiments with Application to Design Optimization of Novel Heat Exchangers, Working Dissertation, University of Maryland, College Park, MD, June 20th 2008.

Bacellar D. (2016). Airside Passive Heat Transfer Enhancement, Using Multi-Scale Analysis and Shape Optimization, For Compact Heat Exchangers with Small Characteristic Lengths (doctoral dissertation). Retrieved from UMD Theses and Dissertations. doi:10.13016/M26R84

Bacellar D., Aute, V., Radermacher R. (2014). CFD-Based Correlation Development for Air Side Performance of Finned and Finless Tube Heat Exchangers with Small Diameter Tubes, *Int. Refrig. Air Cond. Conf.* Paper 1410.

Bacellar. D., Airside passive heat transfer enhancement, using multi-scale analysis and shape optimization, for compact heat exchangers with small characteristic lengths, College Park, MD: PhD Thesis presented to the Department of Mechanical Engineering at the University of Maryland, 2016.

Bourdin, X., Trosseille, X. (2007). Comparison of tetrahedral and hexahedral meshes for organ finite element modeling: an application to kidney impact, in 20th Century Enhanced Safety of Vehicles Conference: Innovations for Safety: Applications and Challenges (Lyon, France)

Box, G., and Draper, N., (1986), Empirical Model-Building and Response Surface, Wiley Series in Probability and Mathematical Statistics, Wiley, New York.

Brognaux, L.J., Webb, R.L., Chamra, L.M. and Chung, B.Y. (1997). Single-phase heat transfer in micro-fin tubes. Int. J Heat Mass Transfer, 40:4345-4357.

Bump, T.R., Average temperatures in simple heat exchangers, ASME J. Heat Transfer 85 (2) (1963) 182–183.

Celata, G.P., Cumo, M., Guglielmi, M., Zummo, G., Experimental investigation of hydraulic and single phase heat transfer in 0.130 mm capillary tube, Microscale Thermophysical Engineering 6 (2002) 85– 97.

Chen, Y., and Cheng, P. (2002). Heat transfer and pressure drop in fractal tree-like microchannel nets. *International Journal of Heat and Mass Transfer*, 45(13), 2643–2648. http://doi.org/10.1016/S0017-9310(02)00013-3.

Cifuentes, A.O., Kalbag, A. (1992). A performance study of tetrahedral and hexahedral elements in 3D finite element structural analysis, Finite Elements in Analysis and Design, 12(3)313-318, ISSN 0168-874X, http://dx.doi.org/10.1016/0168-874X(92)90040-J.

Deb, K. (2001) Multi-objective optimization using evolutionary algorithms, 1st ed., Chichester; New York: John Wiley & Sons.

Deb, K., Genetic algorithms for optimization, KanGAL Report No. 2001002, Kanpur, India, 2001.

Dittus, F.W., Boelter, L.M.K. (1985) Heat Transfer in Automobile Radiators of the Tubular Type, International Communications in Heat and Mass Transfer 12 (1) 3-22.

Dittus, F.W., Boelter, L.M.K., Heat Transfer in Automobile Radiators of the Tubular Type, International Communications in Heat and Mass Transfer 12 (1) (1985) 3-22. Originally published in the University of California Publications in Engineering 2 (13) (1930) 443-461.

Du, Y.J., Wang C.C. (2000). An experimental study of the air side performance of the superslit fin-and-tube heat exchangers, *International Journal of Heat and Mass Transfer.* 43: 4475–4482.

Fernández-Seara, J., Uhía, F.J., Sieres, J. Campo, A., (2007).A general review of the Wilson plot method and its modifications to determine convection coefficients in heat exchange devices, Appl. Therm. Eng. 27: 2745–2757. doi:10.1016/j.applthermaleng.2007.04.004.

Fluent Inc., FLUENT® 6.1 User's Guide, Lebanon, New Hampshire, 2003.

Fonseca, DJ, Navaresse, DO, Moynihan GP Simulation metamodeling through artificial neural networks. Engineering applications of artificial intelligence 2003; 16:177-183.

Gnielinski, V., New equation for heat and mass transfer in turbulent pipe and channel flow, Int. Chem. Eng. 16 (1976)359–368.

Hamad, H. (2006). A new metric for measuring metamodels quality-of-fit for deterministic simulations, in Proceedings of the 38th conference on Winter simulation, Monterey, California, Winter Simulation Conference.

Hu, H., Ding, G., Wang, K. (2008). Heat transfer characteristics of R410A–oil mixture flow boiling inside a 7mm straight microfin tube. International Journal of Refrigeration. 31. 1081-1093. 10.1016/j.ijrefrig.2007.12.004.

Huang, L., Aute, V. and Radermacher, R. A survey of optimization formulations and techniques for the design of heat exchangers using lower GWP refrigerants, in ASHRAE Winter Conference, Chicago, IL, 2015.

Incropera, F.P., DeWitt, D.P. (1996). Introduction to heat transfer. (3rd ed.), John Wiley & Sons, New York.

Jacobi, A. and Shah, R., "Heat transfer surface enhancement through the use of longitudinal vortices," Experimental Thermal and Fluid Sciences, vol. 11, no. 3, pp. 295-309, 1995.

Jin, R., Chen, W., and Sudjianto, A., 2002, "On Sequential Sampling for Global Metamodeling in Engineering Design", CD-ROM Proceedings of ASME IDETC, Design Automation Conference, Montreal, Canada.

Jin, R., Chen, W., Simpson, T. W., 2001, "Comparative Studies of Metamodeling Techniques Under Multiple Modeling Criteria," Structural and Multidisciplinary Optimization, Vol. 23, No. 1. pp, 1-13.

Joardar A., Jacobi A. M. (2008). Heat transfer enhancement by winglet-type vortex generator arrays in compact plain-fin-and-tube heat exchangers, *International Journal of Refrigeration.* 31: 87–97. doi:10.1016/j.ijrefrig.2007.04.011.

Johnson, M. E., Moore, L. M., and Ylvisaker, D., 1990, "Minimax and Maximin Distance Designs," Journal of Statistics Planning and Inference, Vol. 26, No. 2, pp. 131-148.

Jones, D. R., Schonlau, M., and Welch, W. J., 1998, "Efficient Global Optimization of Expensive Black-Box Functions," Journal of Global Optimization, Vol. 13, pp. 455-492.

Kalagnanam, J. R., and Diwekar, U. M., 1997, "An Efficient Sampling Technique for Off-Line Quality Control," Technometrics, Vol. 39, No. 3, pp.308-319.

Kandlikar, S.G., (2002). Fundamental issues related to flow boiling in minichannels and microchannels, In Experimental Thermal and Fluid Science, 26(2–4): 389-407, ISSN 0894-1777, https://doi.org/10.1016/S0894-1777(02)00150-4.

Keywords: Multichannel evaporation; Compact evaporators; Flow patterns; Heat transfer; Pressure drop; Microchannels; Minichannels

Kwak K., Torii K., Nishino K. (2002). Heat transfer and flow characteristics of fin-tube bundles with and without winglet-type vortex generators, *Exp. Fluids.* 33: 696–702. doi:10.1007/s00348-002-0528-2.

Langley, P., Simon, H.A. (1995) Applications of machine learning and rule induction. Communications of the ACM, 38(11), 55–64.

Lelea, D., Nishio, S., Yakano, K., The experimental research on microtube heat transfer and fluid flow of distilled water, International Journal of Heat and Mass Transfer 47 (2004) 2817–2830.

Li, Z.X., Du, D.X., Guo, Z.Y., Experimental study on flow characteristics of liquid in circular microtubes, Microscale Thermophysical Engineering 7 (2003) 253–265.

Mancin, S., Zilio, C., Righetti, G., Doretti, L., and Longo, G.A., (2016). R134a Flow Boiling inside a 4.3 mm ID Microfin Tube. International Refrigeration and Air Conditioning Conference. Paper 1675. http://docs.lib.purdue.edu/iracc/1675

McKay, M., Beckman, R., and Conover, W. A comparison of three methods for selecting values of input variables in the analysis of output from a computer code, Technometrics, vol. 21, pp. 239-245, 1979.

McKay, M., Beckman, R., and Conover, W., (2000), "A Comparison of Three Methods for Selecting Values of Input Variables in the Analysis of Output From a Computer Code," Technometrics, 42, pp. 55–61.

Mitsubishi, 2012. Mitsubishi electric data book for model PURY-WP-YJM-A, CMB-WP-V-G and PEFY-WP-VMA-E. https://www.mitsubishi-les.info/database/servicemanual/files/DATABOOK_MEE11K026_HYBRID_CITY_MULTI_PURY_WP_YJM_A.pdf

Munson, B.R., Young, D.F., Okiishi, T.H. (2006). Fundamentals of fluid mechanics. Hoboken, NJ: J. Wiley & Sons.

Myers R.J., The effect of dehumidification on the air-side heat transfer coefficient for a finned-tube coil, M.S. Thesis, University of Minnesota, Minneapolis, 1967.

Otto, J. C., Landman, D. and Patera, A. T., 1996, "A Surrogate Approach to the Experimental Optimization of Multi-Element Airfoils," Proceedings of the 6th AIAA/NASA/ISSMO Symposium on Multidisciplinary Analysis and Optimization, Bellevue Wa, September 4–6, AIAA 96-4138 CP.

Owen, A., 1992, "Orthogonal Arrays for Computer Experiments, Integration and Visualization," Statistica Sinica, Vol. 2, pp.439-452.

Paitoonsurikarn, S., Kasagi, N., Suzuki, Y., 2000, Optimal design of micro bare-tube heat exchanger, *Proceedings of the Symposium on Energy Engineering (SEE2000)*, vol. 3, pp. 972-979

Petukhov, B. S., in T. F. Irvine and J. P. Hartnett, Eds., (1970). Advances in Heat Transfer, Vol. 6, Academic Press, New York.

Petukhov, B. S.; and Popov, V. N.: Theoretical Calculation of Heat Exchange and Frictional Resistance in Turbulent Flow in Tubes of an Incompressible Fluid with Variable Physical Properties. High Temp., Engl. Transl., vol. 1, no. 1, July/Aug. 1963, pp.69-83.

Procedure for Estimation and Reporting of Uncertainty Due to Discretization in CFD Applications. ASME. J. Fluids Eng. 2008; 130(7):078001-078001-4. doi:10.1115/1.2960953.

Ranut, P., Janiga, G., Nobile, E., Thévenin., D, 2014, "Multi-objective shape optimization of a tube bundle in cross-flow, International Journal of Heat and Mass Transfer", Volume 68, January 2014, Pages 585-598, ISSN 0017-9310, http://dx.doi.org/10.1016/j.ijheatmasstransfer.2013.09.062.

Richardson, L. F., 1910, "The Approximate Arithmetical Solution by Finite Differences of Physical Problems Involving Differential Equations, With an Application to the Stresses in a Masonary Dam," Philos. Trans. R. Soc. London, Ser. A, 210, pp. 307–357.

Roache, P. J., 1993, "A Method for Uniform Reporting of Grid Refinement Studies," Proceedings of Quantification of Uncertainty in Computation Fluid Dynamics, Edited by Celik, et al., ASME Fluids Engineering Division Spring Meeting, Washington, D.C., June 23–24, ASME Publ. No. FED-Vol. 158.

Roy C. J. and Oberkampf W. L., 2011, "A comprehensive framework for verification, validation, and uncertainty quantification in scientific computing," Computational Methods Applied to Mechanical Engineering, vol. 200, p. 2131–2144.

Sacks, J., Welch, W. J., Mitchell, T. J., and Wynn, H. P., 1989, "Design and Analysis of Computer Experiments," Statistical Science, Vol.4, No.4, pp. 409–435.

Saleh, K. (2010). Online approximation assisted multiobjective optimization with heat exchanger design applications. University of Maryland college park.

Sarpotdar, S.; Nasuta, D.; Aute, V. (2016). CFD-Baseed Air Side Correlation for Slit Fin-and-tube Heat Exchangers with Small Diameter Tubes. International Refrigeration and Air Conditioning Conference. Paper 1714. http://docs.lib.purdue.edu/iracc/1714

Schmidt, Th.E., Heat transfer calculations for extended surfaces, Refrigerating Engineering (1949) 351.

Shewry and H. Wynn, "Maximum entropy sampling," Journal of Applied Statistics, vol. 14, no. 2, pp. 165-170, 1987.

Shewry, M. and Wynn, H. Maximum entropy sampling, Journal of Applied Statistics, vol. 14, no. 2, pp. 165-170, 1987.

Shih., T. andZhu, J., A new Reynolds stress algebraic equation model, NASA Lewis Research Center, Cleveland, OH, 1994.

Simpson T. W., Peplinski, J. D., Koch, P. N., and Allen, J. K., 2001, "Metamodels for computer-based engineering design: Survey and recommendations", Engineering with Computers, Vol. 17, No. 2, pp. 129- 150.

Simpson, T. W., Peplinski, J. D., Koch, P. N. and Allen, J. K. (2001) 'Metamodels for computer-based engineering design: Survey and recommendations', Engineering with Computers, 17(2), 129-150.

Singh, V., Abdelaziz, O., Aute, V., Radermacher, R. (2011). Simulation of air-to-refrigerant fin-and-tube heat exchanger with CFD-based air propagation, *International Journal of Refrigeration*, 34, pp. 1883-1897.

Singh, V., Aute, V., Radermacher, R. (2009). A heat exchanger model for air-to-refrigerant fin-and-tube heat exchanger with arbitrary fin sheet, *International Journal of Refrigeration,* 32, pp. 1724-1735.

Sobieski, I.P., Manning, V.M. and Kroo, I. M., 1998, "Response Surface Estimation and Refinement in Collaborative Optimization," Proceedings of the 6th AIAA/NASA/ISSMO Symposium on Multidisciplinary Analysis and Optimization, St. Louis, MS, AIAA-98-4753, pp. 359-370.

Taguchi, G., (1987), System of Experimental Design, Edited by Don Clausing, American Supplier Institute, Dearborn, MI, 1987.

Tang L.H., Zeng M., Wang Q.W. (2009). Experimental and numerical investigation on air-side performance of fin-and-tube heat exchangers with various fin patterns, *Exp. Therm. Fluid Sci.* 33: 818–827. doi:10.1016/j.expthermflusci.2009.02.008.

Threlkeld, J.L., Thermal Environmental Engineering, Prentice-Hall, Inc., New-York, NY, 1970.

Torii K., Kwak K.M., Nishino K. (2002). Heat transfer enhancement accompanying pressure-loss reduction with winglet-type vortex generators for fin-tube heat exchangers, *International Journal of Heat and Mass Transfer*. 45: 3795–3801. doi:10.1016/S0017-9310(02)00080-7.

Tuckerman, D. and Pease, R., (1981) "High-performance heat sinking for VLSI," IEEE Electron Device Letters, vol. 2, no. 5, pp. 126-129.

Wang, C.C., Chi., K.Y., Chang, C.J. (2000). Heat transfer and friction characteristics of plain fin-and-tube heat exchangers, part I: New experimental data, *International Journal of Heat and Mass Transfer*, 43, pp. 2681-2691.

Wang, C.C., Hsieh, Y.C., Lin, Y.T., (1997). Performance of plate finned tube heat exchangers under dehumidifying conditions, J. Heat Transfer 119: 109–117.

Wang, C.C., Lee, C.J., Chang, C.T., Lin, S.P. (1999) Heat transfer and friction correlation for compact louvered fin-and-tube heat exchangers, International Journal of Heat and Mass Transfer 42: 1945-1956.

Wang, C.C., Lee, W.S., Sheu, W.J., (2001) A comparative study of compact enhanced fin-and-tube heat exchangers, International Journal of Heat and Mass Transfer 44 (2001) 3565-3573.

Wang, C.C., Tao W.H., Chang C.J., Investigation of the airside performance of the slit fin-and-tube heat exchangers, *International Journal of Refrigeration.* 22 (1999) 595–603. doi:10.1016/S0140-7007(99)00031-6.

Wang, E., Nelson, T. and Rauch, R. (2004). "Back to elements – tetrahedral verses hexahedral elements", Proceedings of the 2004 International ANSYS Conference, Pittsburgh, PA, USA, 24–26 May 2004.

Wang, G. G. and Shan, S. (2007) 'Review of metamodeling techniques in support of engineering design optimization', Journal of Mechanical Design, Transactions of the ASME, 129(4), 370-380.

Wang, Q., Liang, H., Xie, G., Zeng, M., Luo, L. and Feng, Z. (2007) 'Genetic algorithm optimization for primary surfaces recuperator of microturbine', ASME Journal of Engineering for Gas Turbines and Power, 129(2), 436-442.

Wang, X. Q., Mujumdar, A. S., and Yap, C., 2007, "Effect of Bifurcation Angle in TreeShaped Microchannel Networks," Journal of Applied Physics, 102, 073530 doi: 10.1063/1.2794379

Wang, X. Q., Xu, P., Mujumdar, A. S., and Yap, C. (2010). Flow and thermal characteristics of offset branch network. *International Journal of Thermal Sciences,* 49(2), 272–280. http://doi.org/10.1016/j.ijthermalsci.2009.07.019.

Wilson, E.E., A basis of rational design of heat transfer apparatus, ASME J. Heat Transf. 37 (1915) 47–70.

Winkler, J., Aute, V., Radermacher, R., (2008) Comprehensive investigation of numerical methods in simulating a steady-state vapor compression system, International Journal of Refrigeration, Volume 31, Issue 5, Pages 930-942, ISSN 0140-7007, http://dx.doi.org/10.1016/j.ijrefrig.2007.08.008.

Yang, C.Y. , Wu, J.C., Chien, H.T., Lu, S.R., Friction characteristics of water, R-134a, and air in small tubes, Microscale Thermophysical Engineering 7 (2003) 335–348.

Yang, C.Y., Lin, T.Y., Heat transfer characteristics of water flow in microtubes, Experimental Thermal and Fluid Science, Volume 32, Issue 2, 2007, Pages 432-439, ISSN 0894-1777, http://dx.doi.org/10.1016/j.expthermflusci.2007.05.006.

Yu, X. F., Zhang, C. P., Teng, J. T., Huang, S. Y., et al. (2012). A study on the hydraulic and thermal characteristics in fractal tree-like microchannels by numerical and experimental methods. *International Journal of Heat and Mass Transfer*, *55*(25-26), 7499–7507. http://doi.org/10.1016/j.ijheatmasstransfer.2012.07.050.

Zhang Y. H., Wu X., Wang L.B., Song K.W., Dong Y.X., Liu S. (2008). Comparison of heat transfer performance of tube bank fin with mounted vortex generators to

tube bank fin with punched vortex generators, *Exp. Therm. Fluid Sci.* 33: 58–66. doi: http://dx.doi.org/10.1016/j.expthermflusci.2008.07.002.